Nanocellulose as building block for novel materials

Koon-Yang Lee

November 2011

A dissertation submitted in partial fulfilment of the requirements for the degree of
Doctor of Philosophy of Imperial College London

Department of Chemical Engineering
Imperial College London
South Kensington Campus
SW7 2AZ London UK

Declaration

This dissertation is a description of the work carried out by the author in the Department of Chemical Engineering, Imperial College London between September 2008 and November 2011 under the supervision of Prof. Alexander Bismarck and Prof. Sakis Mantalaris. I herewith certify that all material in this dissertation, which is not my own work, has been properly acknowledged. The material presented is the original work of the author and has not been submitted for a degree at this or any other university.

Abstract

This thesis describes the fabrication of novel green materials using nanocellulose as the building block. Bacterial cellulose (BC) was used as the nanocellulose predominantly in this work. BC is highly crystalline pure cellulose with an inherent fibre diameter in the nano-scale. A single BC nanofibre was found to possess a Young's modulus of 114 GPa. All these properties are highly favourable for using BC as a nanofiller/reinforcement in green nanocomposite materials.

In this work, the *surface* of BC was rendered hydrophobic by grafting organic acids with various aliphatic chain lengths. These *surface*-modified BC was used as nano-filler for poly(L-lactide) (PLLA). Direct wetting measurements showed that the BC nanofibre-PLLA interface was improved due to the hydrophobisation of BC with organic acids. This led to the production of BC reinforced PLLA nanocomposites with improved tensile properties. Nanocellulose can also be obtained by grinding of wood pulp, producing nanofibrillated cellulose (NFC). The surface and bulk properties of one type of NFC and BC were compared in this work. Furthermore, the reinforcing ability of NFC and BC was also studied and it was observed that there is no significant difference in the mechanical performance of NFC or BC reinforced nanocomposites.

A novel method based on slurry dipping to coat sisal fibres with BC was developed to modify the surface of natural fibres. This method can produce either (i) a densely BC coating layer or (ii) "hairy" BC coated sisal fibres. Randomly oriented short BC coated sisal fibre reinforced hierarchical composites were manufactured. It was found that hierarchical (nano)composites containing BC coated sisal fibres and BC dispersed in the matrix were required to produce composites with improved mechanical properties. This slurry dipping method was also extended to produce robust short sisal fibre preforms. By infusing this preform with a bio-based thermosetting resin followed by curing, green composites with significantly improved mechanical properties were produced. BC was also used as stabiliser and nano-filler for the production of macroporous polymers made by frothing of acrylated epoxidised soybean oil followed by microwave curing.

Contents

Acknowledgements

First and foremost, I would like to express my gratitude to my PhD supervisors, Prof. Alexander Bismarck and Prof. Sakis Mantalaris, for their constant guidance throughout the course of my PhD degree. Both of them have shared their experience and expertise with me. I deeply appreciate the time and effort that they have spent with me on both research and non-research related work, which has proven to be highly stimulating. A special thank goes to Prof. Alexander Bismarck. The enthusiasm that he possesses for research has been extremely motivational and contagious to me, even throughout the time in my pursuit of the PhD degree.

The members of Polymers and Composite Engineering (PaCE) group have contributed significantly to my personal and professional time at Imperial College London. They have been a group of good friends for support and advice whenever I needed them. I am especially grateful to Dr. Jonny Blaker for helping me to start my PhD work at Imperial College London, Dr. Kingsley Ho for his constant jokes and his insights to composite materials and Dr. Juntaro Julasak for passing the knowledge of hierarchical composites to me. I would also like to thank Dr. John

List of Publications

Invited book chapters

1. Shamsuddin, S.-R., Ho, K. K. C., <u>Lee, K.-Y.</u>, Hodgkinson, J. M. and Bismarck, A., "Carbon Fibres: Properties, Testing and Analysis" in "Wiley Encyclopedia of Composites". Edited by Nicolais, L, John Wiley & Sons (Germany), 2011. *submitted*.

2. <u>Lee, K.-Y.</u>, Delille, A. and Bismarck, A., "Greener Surface Treatments of Natural Fibres for Production of Renewable Composite Materials" in "Cellulose Fibers: Bio- and Nano-Polymer Composites". Edited by Kalia, S., Kaith, B. S., Kaur, I., Springer-Verlag, Berlin (Germany), 2011.

3. <u>Lee, K.-Y.</u> and Bismarck, A., "Assessing the Moisture Uptake Behaviour of Natural Fibres" in "Interface Engineering of Natural Fibre Composites for Maximum Performance". Edited by Zafeiropoulos, N. E., Woodhead Publishing Ltd, Cambridge (UK), 2011.

Invited Refereed Journal Papers

1. Shamsuddin, S.-R., Ho, K. K. C., <u>Lee, K.-Y.</u>, and Bismarck, A., "Plasma Treatment of Carbon Fibres: Effect on Fibre Properties, Adhesion and Composite Performance", (2011) *submitted*.

2. Blaker, J. J., <u>Lee, K.-Y.</u> and Bismarck, A., "Hierarchical Composites Made Entirely from Renewable Resources", *J. Biobased Mater. Bioenergy* **5** (2011), 1-16.

3. Blaker, J. J., <u>Lee, K.-Y.</u>, Mantalaris, A. and Bismarck, A., "Ice Microsphere Templating to Produce Highly Porous Nanocomposite PLA Matrix Scaffolds with Pores Selectively Lined by Bacterial Cellulose Nano-Whiskers", *Comp. Sci. Tech.* **70** (2010), 1879-1888.

Peer-reviewed Journal Papers

1. <u>Lee, K.-Y.</u>, Bharadia, P., Blaker, J.J., and Bismarck, A., "Creating Hierarchical Structures in Short Sisal Fibre Reinforced Polylactide; Short Hairy Fibre Reinforced Bacterial Cellulose Nanocomposites", (2011) *submitted*.

2. <u>Lee, K.-Y.</u>, Wong, L. L. C., Blaker, J. J., Hodgkinson, J. M., and Bismarck, A., "Bio-based Macroporous Polymer Nanocomposites Made By Mechanical Frothing of Acrylated Epoxidised Soybean Oil", *Green. Chem.* **13** (2011), 3117-3123.

3. <u>Lee, K.-Y.</u>, Quero, F., Blaker, J. J., Hill, C. A. S., Eichhorn, S. J. and Bismarck, A., "Surface Only Modification of Bacterial Cellulose Nanofibres with Organic Acids", *Cellulose* **18** (2011), 595-605.

4. Quero, F., Nogi, M., <u>Lee, K.-Y.</u>, van den Poel, G., Bismarck, A., Mantalaris, A., Yano, H. and Eichhorn, S. J., "Cross-Linked Bacterial Cellulose Networks Using Glyoxalization", *ACS Appl. Mater. Interfaces* **3** (2011), 490-499.

5. Chrzanowski, W., Abou Neel, E. A., <u>Lee, K.-Y.</u>, Bismarck, A., Young, A. M., Hart, A. D., Dalby, M. J. and Knowles, J. C., "Tailoring Cell Behaviour of Polymers by the Incorporation of Titanium Doped Phosphate Glass Filler", *Adv. Eng. Mater. (Adv. Biomater.)* **12** (2010), B298-B308.

6. <u>Lee, K.-Y.</u>, Blaker, J. J. and Bismarck, A., "Surface Functionalisation of Bacterial Cellulose as the Route to Produce Green Polylactide Nanocomposites with Improved Properties", *Comp. Sci. Tech.* **69** (2009), 2724-2733.

7. Blaker, J. J., <u>Lee, K.-Y.</u>, Li, X., Menner, A. and Bismarck, A., "Renewable Nanocomposite Polymer Foams Synthesized from Pickering Emulsion Templates", *Green Chem.* **11** (2009), 1321-1326.

Conference Proceedings

1. <u>Lee, K.-Y.</u>, Blaker, J. J. and Bismarck, A., "Single Step Functionalisation of Cellulose to Produce All-Cellulose Nanocomposites", *Proceedings of the 14th European Conference on Composite Materials*, 7th - 10th June 2010, Budapest, Hungary.

2. Quero, F., <u>Lee, K.-Y.</u>, Blaker, J. J., Bismarck, A. and Eichhorn, S. J., "Characterisation of Functionalised Bacterial Cellulose for Green

Nanocomposite Reinforcement Applications", *Proceedings of the 14th European Conference on Composite Materials*, 7th - 10th June 2010, Budapest, Hungary.

3. Blaker, J. J., Lee, K.-Y. and Bismarck, A., "Bio-based Nanocomposite Foams from Bacterial Cellulose Whiskers and PLA via Cryogenic in situ Porosification Techniques", *Proceedings of the 14th European Conference on Composite Materials*, 7th - 10th June 2010, Budapest, Hungary.

4. Lee, K.-Y., Juntaro, J., Blaker, J. J., Abbott, A., Mantalaris, A. and Bismarck, A., "Green Hierarchical Composites: The Bottom-Up Approach", *Proceedings of the 17th International Conference on Composite Materials*, 27th – 31st July 2009, Edinburgh, UK.

5. Lee, K.-Y., Blaker, J. J. and Bismarck, A., "Improving the Properties of Nanocellulose/Polylactide Composites by Esterification of Nanocellulose. Can It Be Done?", *Proceedings of the 17th International Conference on Composite Materials*, 27th – 31st July 2009, Edinburgh, UK.

6. Blaker, J. J., Lee, K.-Y., Mantalaris, A. and Bismarck, A., "Nanocomposite Scaffolds based on Bacterial Cellulose and Polylactide Towards the 3D Culture of Haemopoietic Stem Cells?" *Proceedings of the 17th International Conference on Composite Materials*, 27th – 31st July 2009, Edinburgh, UK.

Oral Presentations at Conferences

1. Lee, K.-Y., Tammelin, T., Kiiskinen, H., Samela, J., Schlufter, K., Bismarck, A., "Nano-fibrillated cellulose vs bacterial cellulose: Reinforcing ability of nanocellulose obtained top-down or bottom-up", 19th Annual BioEnvironmental Polymer Society (BEPS) meeting, 28th-30th September 2011, Vienna.

2. Lee, K.-Y., Blaker, J. J., Murakami, R., Bismarck, A., "Time dependent behaviour of water-in-oil emulsions stabilized by hydrophobised bacterial cellulose nanofibrils", 19th Annual BioEnvironmental Polymer Society (BEPS) meeting, 28th-30th September 2011, Vienna.

3. Lee, K.-Y., Wong, L. L. C., Blaker, J. J., Hodgkinson, J. M., Bismarck, A., "Air templated bio-based polymer nanocomposite foams", 19th Annual BioEnvironmental Polymer Society (BEPS) meeting, 28th-30th September 2011, Vienna.

4. <u>Lee, K.-Y.</u>, Ho, K. C. C., Schlufter, K., Hodgkinson, J. M., Bismarck, A., "Bacterial cellulose as the binder for sisal fibres to produce green bio-based nanocomposites with improved properties", 19th Annual BioEnvironmental Polymer Society (BEPS) meeting, 28th-30th September 2011, Vienna.

5. <u>Lee, K.-Y.</u>, Bharadia, P., Blaker, J.J., Bismarck, A., "Towards green hierarchical composites with improved properties", 4th International Conference on Sustainable Materials, Polymers and Composites, 6th-7th July 2011, Birmingham, UK

6. <u>Lee, K.-Y.</u>, Bharadia, P., Blaker, J.J., Bismarck, A., "Towards green hierarchical composites with improved properties", 241st ACS National Meeting & Exposition, 27th-31st March 2011, Anaheim, California, USA.

7. <u>Lee, K.-Y.</u>, Blaker, J.J., Bismarck, A., "Why do cellulose nanofibrils behave differently when modifying freeze-dried or never-dried bacterial cellulose?", 241st ACS National Meeting & Exposition, 27th-31st March 2011, Anaheim, California, USA.

8. <u>Lee, K.-Y.</u>, Blaker, J.J., Bismarck, A., "Single step functionalisation of cellulose to produce all-cellulose nanocomposites", 2010 AIChE Annual Meeting, 7th - 12th November, Salt Lake City, Utah, USA.

9. <u>Lee, K.-Y.</u>, Bharadia, P., Blaker, J.J., Bismarck, A., "A simpler process to coat natural fibres with cellulose nanofibrils: towards green hierarchical composites with improved properties", 18th Annual BEPS Meeting, 13th - 16th October 2010, Toronto, Canada.

10. <u>Lee, K.-Y.</u>, Tay, F.H., Blaker, J.J., Kazarian, S.G., Bismarck, A., "Bacterial cellulose as a greener and novel activated carbon source for electric double layer capacitors", 18th Annual BEPS Meeting, 13th - 16th October 2010, Toronto, Canada.

11. <u>Lee, K.-Y.</u>, Delille, A., Blaker, J.J., Mantalaris, A., Bismarck, A., "Single step functionalisation of cellulose to produce all-cellulose nanocomposites", 2010 TAPPI International Conference on nano for the Forest Product Industry, 27th - 29th September, Espoo, Finland.

12. <u>Lee, K.-Y.</u>, Blaker, J.J., Bismarck, A., "Surface modification of bacterial cellulose nanofibrils: Why do cellulose nanofibrils behave differently when modifying freeze-dried or never-dried bacterial cellulose?", 2010 TAPPI

International Conference on nano for the Forest Product Industry, 27th - 29th September, Espoo, Finland.

13. <u>Lee, K.-Y.</u>, Delille, A., Blaker, J.J., Mantalaris, A., Bismarck, A., "Single step functionalisation of cellulose to produce all-cellulose nanocomposites", 14th European Conference on Composite Materials, 7th - 10th June 2010, Budapest, Hungary.

14. <u>Lee, K.-Y.</u>, Blaker, J.J., Bismarck, A., "Surface functionalisation of bacterial cellulose nanofibrils as the route to produce green polylactide nanocomposites with improved properties, 2009 AIChE Annual Meeting, 8th – 13th Nov 2009, Nashville TN, USA.

15. <u>Lee, K.-Y.</u>, Blaker, J.J., Murakami, R., Bismarck, A., "Time dependent behaviour of water-in-oil emulsions stabilised by hydrophobised bacterial cellulose nanofibrils", 14th UK Polymer and Colloids Forum, 14th – 16th September 2009, Hull, UK.

16. <u>Lee, K.-Y.</u>, Juntaro, J., Blaker, J.J., Abbott, A., Mantalaris, S., Bismarck, A., "Green hierarchical composites: the bottom-up approach", at 17th International Conference on Composite Materials, 27th – 31st July 2009, Edinburgh, UK.

17. <u>Lee, K.-Y.</u>, Blaker, J.J., Bismarck, A., "Improving the properties of bacterial cellulose/poly(L-lactic acid) nanocomposites by heterogeneous modification of bacterial cellulose. Is it the way forward?" at 16th Annual BioEnvironmental Polymer Society (BEPS) meeting, 16th – 19th June 2009, Chicago IL, USA.

Poster Presentations at Conferences

1. <u>Lee, K.-Y.</u>, Blaker, J. J., Bismarck, A., "Improving the properties of bacterial cellulose/poly(L-lactic acid) nanocomposites by heterogeneous modification of bacterial cellulose. Is it the way forward?" 19th Annual BioEnvironmental Polymer Society (BEPS) meeting, 28th-30th September 2011, Vienna.

Awards

1. Student Achievement Awards, 19th BioEnvironmental Polymer Society (BEPS) annual meeting, 28-30th September 2011, Vienna University of Technology, Vienna, Austria.

Patents

1. <u>Lee, K.-Y.</u>, Bharadia, P. and Bismarck, A., "Reinforcement", P53102GB/JLH

List of Figures

List of Tables

Chapter 1 – Introduction

Steadily increasing oil prices, the reduced availability of landfill sites, and the greater attention paid to end-of-life problems associated with traditional petroleum-derived materials and conventional composites have all triggered fresh interest in renewable and sustainable resources as well as biodegradable materials. Public demands for more environmentally friendly consumer goods and an intensifying legislative pressure for greener and carbon neutral technologies are forcing materials suppliers and manufacturers to consider the environmental impact of their product at all stages of their life cycle, including processing, recycling and final disposal. Three recent European Union directives on landfill of waste,[1] end-of-life of vehicle[2] and waste of electrical and electronic equipments[3] are asserting legislative pressure. As a result, industry, end users and local authorities will need to move away from traditional waste management methods and will require new strategies for reuse and recycling. This shift represents a significant technical challenge to those involved in the composites industry since economically feasible recycling of the vast majority of plastic waste and polymer matrix composite materials is relatively difficult to achieve. Consequently, industry is confronted with a major challenge to move to greener materials that match the physical performance of traditional materials. Renewable polymers often have inferior properties to their synthetic counterparts against which they have to compete. In order to maintain the environmental credentials of the matrix, synthetic fillers such as glass or carbon fibres and even nanotubes/nanofibres should be replaced by renewable biodegradable ones.

Alternative fillers such as natural fibres are already considered for a multitude of applications. Advantages of natural fibres are their low cost, low density, renewability and biodegradability. Their drawbacks are mainly the variability in their mechanical properties, their anisotropy, their relatively limited processing temperature and their low tensile strength compared to synthetic fibres.[4] Simple fibre reinforcement is thus not sufficient to achieve the performance of the conventional non-biodegradable composite materials.[5] Bacterial cellulose appears to be an interesting alternative to synthetic fillers for the design of green recyclable

and biodegradable composites. A single nanofibre of bacterial cellulose have a diameter range from 10 to 100 nm and a Young's modulus of 114 GPa.[6] Bacterial cellulose (BC) has also low density (1.5 g cm^{-3}), low toxicity, and is renewable and biodegradable. It also has valuable intrinsic properties as a result of its small size and can influence the behaviour of the surrounding matrix due to its high surface area to volume ratio. The addition of nanocellulose to renewable polymers can provide improved mechanical and other physical properties.

1.1 Objectives of this project

It can be anticipated that truly green hierarchical composites (i.e.: fibre reinforced nanocomposites) will be the next major step forward in the area of green composite materials for non-critical structural applications. The main aim of this project is to produce truly green, natural fibre-reinforced nanocellulose renewable polymer composites and to demonstrate the scale of the resulting performance improvements. The specific objectives in this project are:

(i)   Derive optimal process parameters for the manufacturing of cellulose nanocomposites using laboratory facilities.

(ii)   Manufacture natural fibre reinforced nanocellulose renewable polymer composites in a reproducible bioprocess at laboratory scale.

(iii)   Produce and characterise the mechanical properties of nanocellulose reinforced polymer foams

1.2 Structure of this thesis

This thesis is divided into 11 chapters, whereby each chapter is an independent publication. The introduction (chapter 1) includes the motivation and objectives of the research, as well as the overview of the thesis. Chapter 2 discusses the state-of-the-art of greener surface treatments of natural fibres for the production of renewable composites. Following this chapter, this thesis is split into 3 sections due to the multiple directions taken in this research. The first section (chapters 3-7) of this thesis is dedicated to nanocellulose modification and polymer nanocomposites. The *surface-only* modification of BC with organic acids is discussed in chapter 3 In chapter 4, attempts were made to simplify the laborious *surface-only* modification of BC nanofibres discussed in chapter 3 by modifying freeze-dried BC directly as

opposed to solvent exchanging BC from water through methanol into the pyridine. By doing so, significant bulk modification of BC was observed. Since modifying freeze-dried BC resulted in significant loss of crystallinity of BC, the reinforcing ability of the *surface-modified* BC for poly(L-lactic acid) was investigated in chapter 5. In addition to the chemical modification of BC to improve the mechanical performance of the PLLA nanocomposites, a carbohydrate derived copolymer of PLA was used as the compatibiliser to produce BC reinforced PLLA nanocomposites. This approach is reported in chapter 6. Chapter 7 compares nanocellulose obtained using the top-down (nanofibrillated cellulose) and bottom-up (bacterial cellulose) approach.

The second section of this thesis describes the manufacturing and properties of sisal fibre reinforced hierarchical (nano)composites. This section starts with chapter 8; a novel method based on slurry dipping to produce "hairy sisal fibres" and the mechanical performance of the resulting randomly oriented short "hairy fibres" reinforced PLLA hierarchical composites are discussed. This slurry dipping method is extended to produce natural fibre preforms by using BC as binder. This allows for the production of composites using vacuum assisted resin infusion. The properties of the natural fibre preform and the fibre preform reinforced acrylated epoxidised soybean oil (AESO) composites are discussed in chapter 9. The third section of this thesis discusses the use of BC as stabiliser and nano-filler simultaneously to produce macroporous polyAESO (chapter 10). The conclusions of this research and future work are summarised in chapter 11.

Chapter 2 – Greener surface treatments of natural fibres for the use in the production of composite materials

Summary

Natural fibres have been the prime candidate to replace man-made glass fibres in the production of composite materials. Major advantages associated with natural fibres include low cost, low density, high toughness and biodegradability. However, these intriguing properties of natural fibres do come at a price. The hydrophilic nature of natural fibres often results in poor compatibility with hydrophobic polymer matrices. Various surface treatments of natural fibres using chemicals have been developed to improve the compatibility between the fibres and the matrix but large amount of solvents are usually involved. In this chapter, greener surface treatments without the use of hazardous chemicals are introduced. These include plasma treatment, the use of enzyme and fungal for the extractions and surface treatment of natural fibres and the deposition of bacterial cellulose onto natural fibres. These treatments are aimed at improving the interfacial adhesion between the fibres and the matrix, thereby improving the stress transfer efficiency from the matrix to the fibre. The effects of these treatments on the properties of natural fibres are discussed. In addition to this, the overall impact of these treatments on the mechanical properties of the resulting natural fibre reinforced composites is also addressed in this chapter.

2.1 Introduction

Public's growing demand for more environmentally friendlier products, the search for greener sustainable technology, the ever growing problem of global waste, environmental legislative pressure such as the end-of-life vehicle regulations,[2] the landfill of waste products,[1] electrical and electronic equipments waste[3] and the depletion of fossil resources have initiated the interest of using renewable sources in the polymer industry.[7, 8] Polymer manufacturers are forced to consider the life-cycle

of their products and evaluate the environmental impact of these products throughout the products' lifetime. These include the selection of raw materials, polymer processing, recycling and disposal. Combining all these factors and the worldwide availability of plant based natural fibres,[9] research interest of using natural fillers to reinforce polymers is emerging in the field of composites engineering. The use of natural fibres in the production of composite materials is well developed.[4, 10-19] Such extensive use of natural fibres as reinforcement for polymers is not surprising as natural fibres offer several advantages over conventional reinforcing fibres, such as lower cost, low density, high toughness and biodegradability.[20, 21] A big step towards the application of natural fibre reinforced composites can be found in door panels of *Mercedes-Benz E-class*.[22] Daimler Chrysler replaced the door panels of *Mercedes-Benz E-class* with flax/sisal fibre mat embedded epoxy resin. A remarkable weight reduction of 20% and an improvement in the mechanical properties of the door panels were achieved. This further improves the protection of the passengers in an event of an accident. In addition to this, Rieter Automotive won the JEC Composites Award 2005 for their development in natural fibre reinforced thermoplastic composites for an under-floor module with integrated aerodynamic, thermal and acoustic functions.[23]

2.1.1 A brief introduction to natural fibres

Natural fibres can be derived either from plants (such as flax or hemp), produced by animals (such as silk or spider silk) or from minerals (such as asbestos). Table 1 shows the comparison of selected physical properties between natural fibres and synthetic fibres. Although the mechanical properties of natural fibres are very much lower than those of conventional synthetic fibres such as glass or carbon fibres, significant research effort is still poured into the field of plant based natural fibre reinforced composite materials due to its low cost and low environmental impact. On a "per weight" basis, flax, jute and hemp fibres have higher tensile moduli than E-glass fibres[24, 25] due to the low density of natural fibres ($\sim$1.4 g cm^{-3}) compared to E-glass ($\sim$2.5 g cm^{-3}). This is particularly important in applications where weight reduction is a priority. Therefore, it is not surprising that natural fibres are used as reinforcement for polymer matrices to replace conventional glass fibres.

Table 1: A comparison between the physical properties of selected natural fibres and man-made fibres.

Fibre	Density (g cm^{-3})	Tensile Strength (MPa)	Young's Modulus (GPa)	Elongation at break (%)
Flax	1.5	345-1500	27.6	2.7-3.2
Hemp	1.47	690	70	1.6
Jute	1.3-1.49	393-800	13-26.5	1.16-1.5
Ramie	1.55	400-938	61.4-128	1.2-3.8
Sisal	1.45	468-700	9.4-22	3-7
Cotton	1.5-1.6	287-800	5.5-12.6	7-8
Silk[*]		600	10	20
Spider silk[§]		800-1000	7.2-9.2	30-60
Basalt[$]	2.66	3050	92.5	
Asbestos[$]		550-750	1.0-3.5	
E-glass	2.55	3400	73	2.5
Kevlar	1.44	3000	60	2.5-3.7
Carbon	1.78	3400[a]-4800[b]	240[b]-425[a]	1.4-1.8

[*] Natural fibre derived animal sources (silkworm).
[$] Natural fibre derived from mineral sources.
[§] Natural fibre derived from spider (*Argiope trifasciata*)
[a] Ultra high modulus carbon fibre.
[b] Ultra high tenacity carbon fibre.
Source: Adapted from Bismarck et al. Plant fibers as reinforcement for green composites. In Mohanty et al. Natural fibers, biopolymers and biocomposites (CRC Press 2005). Further developed with Craven et al. *Compos Part A-Appl S 2000* (31), 653, Brant. Cement-based composites: materials, mechanical properties and performance (Routledge Ltd), Perez-Rigueiro et al. *J Exp. Biol. 2006* **(209)**, 320 and Martiny et al. *J Pres. Ves. Tech. 2009* (131), 061407-1.

2.1.2 Structure of plant based natural fibres

Plant based natural fibres are rigid and they are composed of cellulose, hemicellulose, lignin, pectin, waxes and water soluble compounds, with cotton being the exception. Cotton is made up of nearly 90wt% cellulose, 5.7wt% hemicellulose, 1wt% pectin and 0.6wt% waxes.[4] Cellulose is the major constituent in plant based natural fibres. It is a linear molecule consisting of repeating β-D-glucopyranose units linked together by 1→4 glycosidic bonds (Figure 1). It has a degree of polymerisation of approximately 10,000.[26] Strong hydrogen bonds exist between cellulose molecules due to the presence of hydroxyl groups, which governs the physical properties of cellulose. It has a semi-crystalline structure, consisting of crystalline and amorphous regions. Cellulose in natural fibres (such as cotton, flax

and ramie) typically has a degree of crystallinity of between 65% and 70%.[27] The amorphous regions can be hydrolysed by acids to create short cellulose nanocrystals.[28] In addition to this, cellulose is stable in most common organic solvents. It can only be dissolved in strong acidic solutions such as concentrated phosphoric acids and concentrated sulphuric acid[29] or ionic liquids such as N-ethylpyridinium[30] and lithium chloride/N,N-dimethylacetamide.[31]
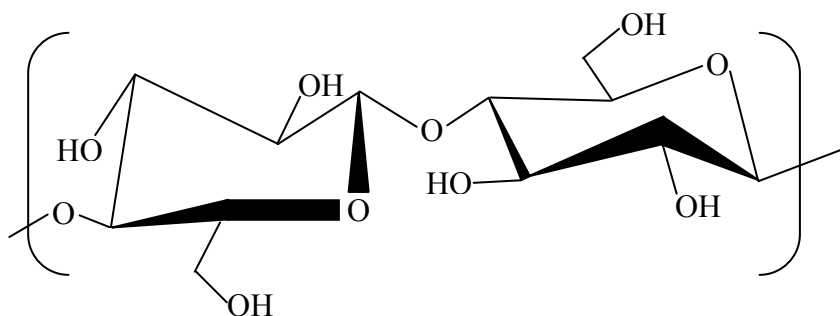
Figure 1: Schematic diagram showing the structure of cellulose.

Hemicellulose is the other major constituent of plant based natural fibres and it is made up of a combination of 5- and 6-ring carbon polysaccharides.[5] It is a branched polymer and has much shorter polymer chains (degree of polymerisation of between 50 and 300) compared to native cellulose. In addition to this, hemicellulose is very hydrophilic in nature,[32] easily hydrolysed by acids and soluble in alkali. The role of hemicellulose in natural fibres is to form the supporting matrix for cellulose microfibrils.

Lignin is a phenolic compound that acts as a binder to consolidate the polysaccharide, holding cellulose and hemicellulose fibres together.[33] It was found that lignin has high carbon low hydrogen content and this implies that it is highly unsaturated or aromatic. Lignin can be produced by the dehydrogenation polymerisation of p-coumaryl, coniferyl and sinapyl alcohols.[34] It contains hydroxyl (-OH), methoxyl (-O-CH$_3$) and carbonyl (C=O) groups. Ethylenic and sulphur containing groups have also been identified in lignin.[4] Lignin is amorphous and hydrophobic in nature. It has been shown that lignin possesses a softening temperature of about 90°C and a melt temperature of 170°C.[32]

2.2 Green modifications of plant based natural fibres

Although natural fibres are highly comparable to conventional glass fibres on a "per weight" basis, the major drawback arise from the inherent variability of natural fibres.[5] Natural fibres can vary in terms of their dimensions and mechanical properties, even within the same cultivation. This situation is different from synthetic fibres, which can be manufactured uniformly (for example: Toray's T700S carbon fibre has only a variability of ±10% in its tensile strength and modulus,[35] ±3% in its diameter). All natural fibres are hydrophilic in nature due to the presence of large amounts of hydroxyl groups; their absorbed moisture content can be as high as 30% at 95% relative humidity.[36] This extremely hydrophilic nature of natural fibres often results in poor compatibility between natural fibres and hydrophobic polymer matrices such as polypropylene or polylactide.[13] Another factor that limits the use of natural fibres is its low thermal stability. To avoid degradation of natural fibres during thermal processing, the temperature at which natural fibres are exposed to is usually limited to 200°C (shorter processing time is preferable).[37] This further limits the choices of polymer that can be used as potential matrix for natural fibres reinforced composites. Figure 2 shows the reduction in the tensile strength of natural fibres with increasing processing temperature and time of the natural fibres.
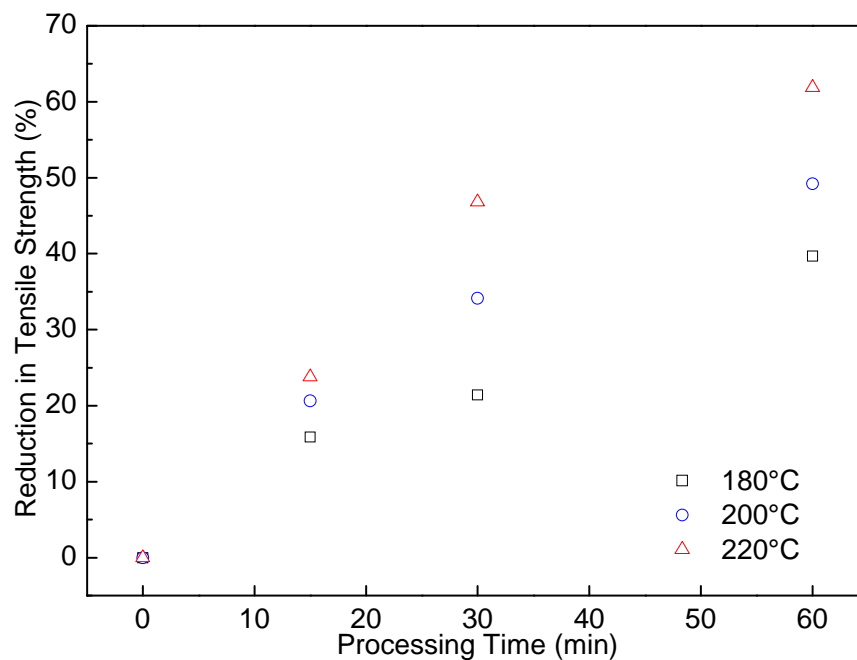
Figure 2: Temperature and time dependency of natural fibre's tensile strength. Adapted from reference.[37]

To improve the compatibility between natural fibres and hydrophobic polymer matrices, various methods have been explored to increase the hydrophobicity of natural fibres.[38-40] Most of the surface chemical treatments of natural fibres involve silylation,[41-44] acetylation,[45] benzoylation,[46] maleated coupling agents,[47] isocyanate treatment[48] and graft copolymers of natural fibres.[49] Although these methods alter the wettability of natural fibres, large quantities of hazardous chemicals were or are usually involved in the process of hydrophobising the natural fibres and the chemical waste must be handled and disposed of appropriately. This adds extra cost to the production of natural fibre reinforced composites, making the chemical treatments less attractive as a viable solution. Moreover, chemical treatments of natural fibres do not always result in improved composite performance. The main reason is the anisotropicity of natural fibres. The transverse modulus of natural fibres is orders of magnitude lower than its axial modulus.[50, 51] Cichocki Jr et al.[50] showed that the axial modulus of jute fibres is 38.4 GPa but its transverse modulus is only 5.5 GPa. Baley et al.[51] also showed that the axial modulus of flax fibres is 7 times larger than its transverse modulus (axial modulus: 59 GPa, transverse modulus: 8 GPa). In addition to this, Thomason[52] also attributed the failure of natural fibres to deliver good performance in composites to the high linear thermal coefficient of expansion (LTCE) of natural fibres. The interfacial shear stress between the fibre and the matrix is the product of residual compressive stress (σ_r) and the static friction coefficient at the fibre-matrix interface. Due to the high LTCE of natural fibres, σ_r will be lowered, leading to poor interfacial shear strength between the fibres and the matrix. Therefore, chemical modification of natural fibres might not be the next step forward. Instead, efforts should be focussed on environmental friendlier processes to increase the hydrophobicity of natural fibres and to avoid the shrinkage problem of natural fibres during thermal processing.

2.2.1 Plasma – a brief introduction

Plasma is known as the fourth state of matter. It is defined as a gaseous environment composed of charged and neutral species with an overall zero charge density. Plasma has been shown to modify the tribology of thermoplastics and synthetic fibres (such as carbon fibres).[53-56] Further details regarding plasma treatments of various materials can be found in literature.[57-59] Plasma treatments has the ability to change

the surface properties of the fibres through the formation of free radicals, ions and electrons in the plasma stream.[60] During plasma treatment, the substrate is bombarded with high-energy particles travelling in the stream of plasma or vacuum UV (in low pressure plasma). As a result, the surface properties such as the wettability, surface chemistry and surface roughness of the substrate can be altered without the need for any hazardous chemicals or solvents. Usually, plasma treatments modify the surface of natural fibres by[59] (i) removing weakly attached surface layers (ie: cleaning and abrasion) and (ii) forming new functional groups (functionalisation and crosslinking). The functional groups formed on the surface of natural fibres depend on the nature of the plasma feed gas. Therefore, plasma treatment minimises the environmental impact of natural fibres surface treatment. Different types of plasma sources are available[61] and they are summarised in Table 2.

Table 2: Comparison between different plasma sources. Adapted from literature.[61]

Plasma Source	Gas Temp (°C)	Electron Temp (eV)	Applied Voltage (kV)	Charge Density (cm^{-3})
Arc and torches	7000-65000	2.5-6.8	10-50	10^{16}-10^{19}
Corona	50-400	4-6	10-50	10^{9}-10^{13}
Dielectric barriers	50-400	2-10	5-25	10^{12}-10^{15}
Low pressure discharge	10-500	1-10	0.2-0.8	10^{8}-10^{13}
Atmospheric pressure discharge	25-200	1-2	0.05-0.2	10^{11}-10^{12}

2.2.1.1 Low pressure (cold) plasma treatment of natural fibres

The plasma discharge can be generated at atmospheric (see next section) or under vacuum conditions (cold plasma).[40] Essentially, the two types of plasmas generated are the same. The plasma produced can be used to modify the surface energy of natural fibres,[62, 63] crosslink the fibres,[62] create free radicals to initiate polymerisation[49] or introduce functional groups onto the surface of the fibres.[59] A major advantage of employing cold plasma treatment is that such plasma can be generated at low power output. Atmospheric plasma treatments are usually carried out at a maximum power of 10 kW.[62, 64] Cold plasma treatments, on the other hand,

are carried out at much lower power output of about 60 W.[65, 66] As aforementioned, the mechanical properties of natural fibres are highly dependent on the temperature at which the natural fibres are exposed to. By using a smaller power output, it is possible to minimise the thermal damage caused by plasma treatment on the natural fibres, thereby preserving the properties of natural fibres. However, there are disadvantages associated with cold plasma treatment. A well-designed plasma reactor system is required along with vacuum pumps and seals. In addition to this, cold plasma is also often used in small batch process only due to the limitation in the size of the vacuum chamber as a result of capital and operating costs.

Table 3: A comparison between untreated and plasma treated wood fibre and sisal fibre reinforced PP composites. All composites contains 20 wt% fibres . Adapted from literature. [65, 66]

Composites	Wood Fibre		Sisal Fibre	
	σ (MPa)	E (GPa)	σ (MPa)	E (GPa)
Neat PP	23	1.5	23	1.5
Untreated fibre	22	2.6	22	2.6
Argon plasma	25	3.0	24	3.2
Air plasma	27	3.4	27	2.9

Various researchers have investigated the use of cold plasma to modify the surface of natural fibres.[65-72] Cold plasma has been used to treat wood fibres and sisal fibres, using argon and air as the plasma feed gas.[65, 66] Table 3 summarises the untreated and plasma treated natural fibres reinforced polypropylene (PP) composites. The plasma treatment of the fibres had a positive impact on the mechanical properties of the resulting wood fibre and sisal fibre reinforced PP composites when compared to untreated natural fibres. The tensile strength was found to increase by as much as 16% for both wood fibres and sisal fibres reinforced PP composites. The tensile modulus improved by as much as 127% (wood fibre) and 93% (sisal fibre), respectively. When comparing neat PP to plasma treated wood fibre or sisal fibre reinforced PP composites, the tensile modulus improved by as much as 127% (wood fibre) and 113% (sisal fibre), respectively and the tensile strength improved by as much as 17% (for both wood and sisal fibre). This is an indication of improved interfacial adhesion between the fibres and the matrix as a result of plasma treatment.

Jute fibres were also treated with cold argon plasma.[72] The fibres were treated for 5 min, 10 min and 15 min, respectively in argon plasma. With longer plasma treatment, the fibres became rougher and the formation of pits on the fibre surface was observed when the fibres were plasma treated for 15 min. This is a result of plasma etching, which results in the degradation of the jute fibres.[73] The wettability of the plasma treated jute fibres decreased with increasing treatment time (Table 4). This is also accompanied by an increase in the flexural strength of the plasma treated jute fibre reinforced polyester composites. It was found that the flexural strength of the composites improved by 14% (10 min plasma treated jute fibres) compared to neat jute fibre reinforced polyester. This improvement was attributed to the increased roughness and hydrophobicity of the plasma treated fibres, which results in better interfacial adhesion between the fibres and the matrix. However, composites reinforced with fibres treated with plasma for 15 min resulted showed a 10% decrease in the flexural strength. This is a direct result of heavy degradation of the treated fibres during the prolonged plasma treatment.[70]

Table 4: A comparison between neat and plasma treated jute fibres and the flexural strength of jute fibre reinforced polyester composites. Adapted from literature.[72] The composites contain 15 wt% fibres loading fraction.

Jute fibre treatment	Water/air contact angle	Polar surface energy (mJ m^{-2})	Flexural strength of polyester composites (MPa)
Neat jute fibres	81.6°	21.9	158.8
5 min plasma treated	84.1°	17.5	152.4
10 min plasma treated	86.9°	11.6	181.6
15 min plasma treated	90.0°	8.5	143.2

2.2.1.2 Atmospheric Air Pressure Plasma (AAPP) treatment of natural fibres

To improve the wettability and interfacial adhesion between natural fibres and a polymer matrix, AAPP treatment can be applied to natural fibres to remove non-cellulosic substances from the surface of these fibres. The advantages of using AAPP treatment for composite production are its low operating cost, short treatment time

and greater flexibility, as no vacuum system is required.[74-76] The critical surface tension of a solid substrate corresponds to the surface tension of an imaginary liquid that will wet the substrate completely.[77] It was reported that oxygen and nitrogen plasma led to a reduction of the critical surface tension of lignocellulosic fibres as a result of etching effect.[62] Compressed air can be used as an alternative feed gas to overcome this negative impact generated by oxygen and nitrogen feed gases on lignocellulosic fibres.

As a general rule, good adhesion can be achieved when the surface tension of the substrate (natural fibres) is larger than that of the matrix. Baltazar-Y-Jimenez et al.[62] have shown that the critical surface tension can be modified through AAPP treatment (Figure 3). Different lignocellulosic fibres can be seen behaving differently if exposed to the same AAPP treatment. The critical surface tension of abaca fibres reduced with increasing treatment time. However, hemp and sisal fibres showed otherwise. With increasing AAPP treatment time, the critical surface tension increased. The authors hypothesised that longer treatment times of hemp and sisal fibres led to the crosslinking of the fibres surfaces (hemp fibres) and decomposition of hydrophobic groups. This might have led to the observed increase in the critical surface tension.

The effect of AAPP treatment on the properties of natural fibre reinforced cellulose acetate butyrate (CAB) composites was then further studied.[64] At a fibre loading fraction of 30wt%, the storage modulus of the composites produced improved by as much as 370% (Figure 4). This is due to the enhanced interfacial adhesion between the fibres and the matrix as a result of AAPP treatment (as measured by single fibre pull-out test).[78] In addition to this, the increment in the mechanical glass transition temperature and a reduction in the height of tan δ showed better fibre-matrix bonding and fibre-in-matrix distribution. It is evident that AAPP treatment is able to improve the fibre-matrix interface, resulting in composites with improved mechanical properties.
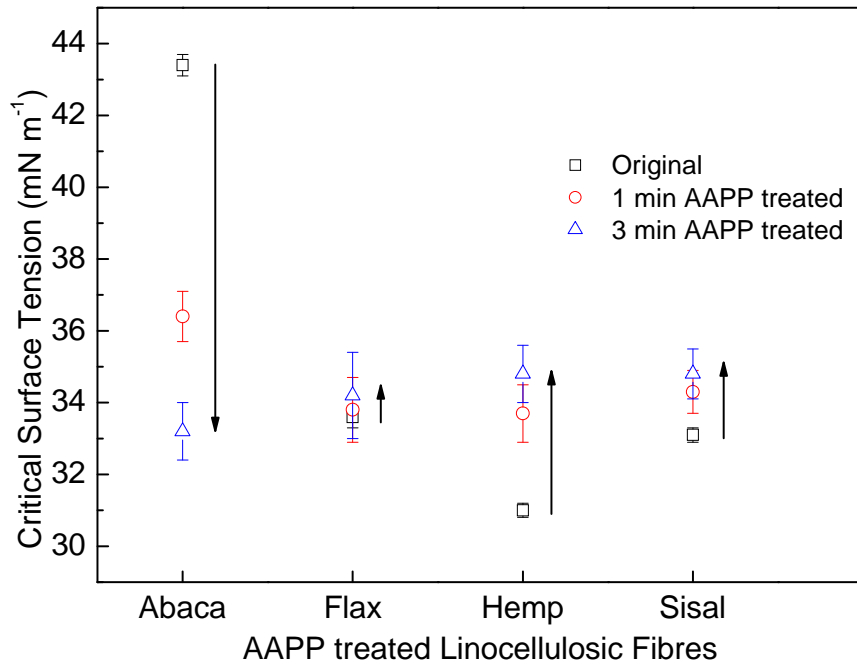
Figure 3: Critical surface tension of lignocellulosic fibres after AAPP treatment at various times. Adapted from literature.[62]
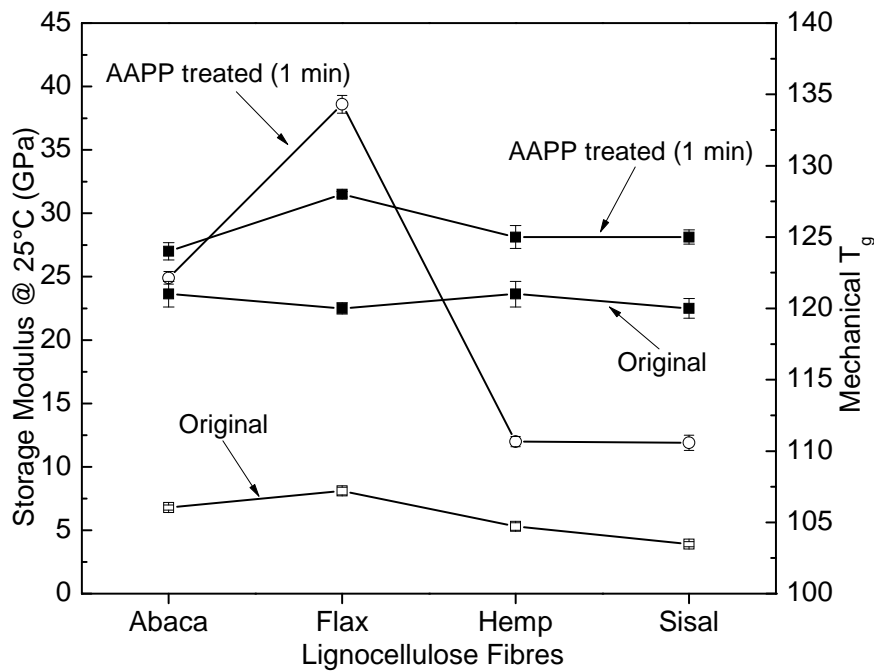
Figure 4: Viscoelastic behaviour of AAPP treated lignocellulosic fibres reinforced CAB composites. Hollow icon indicates storage modulus, solid icon indicates mechanical T_g. Adapted from literature.[64]

2.2.2 The use of enzyme in natural fibres extractions and surface treatments

Retting is a process of the separation or loosening of bast fibres from its non-fibrous components.[79] Water-retting is performed by immersing the fibres stalk in water for a certain period of time. Water will penetrate to the central stalk, swells the inner

cells and bursts the outer most layers of the plant materials. This increases the absorption of moisture and decay-producing bacteria. Water-retting is able to produce high quality fibres but it also produces large amount of waste[80] and therefore, this process was discontinued in many countries (apart from China and Hungary).[81] Dew-retting, on the other hand, relies on aerobic fungi to colonise plant fibres in the fields. A combination of bacteria, air, sun and dew produces fermentation, which dissolves much of the stem materials surrounding the fibre bundles.[79] However, this method suffers from several disadvantages. Appropriate moisture and temperature conditions during dew-retting are needed.[79] This is a parameter that is very difficult to control as it is highly dependent on the region and the weather. In addition to this, the fibres extracted through dew-retting method have lower quality compared to water-retted fibres.[79, 82]

Enzyme retting is a natural fibre extraction method which refers to the separation of fibres from its non-fibre components through the use of enzymes.[83] This process generally uses pectin-degrading enzymes such as the commercially available Viscozyme L or Flaxzyme from Novozyme (Bagsvaerd, Denmark). The use of pectin-degrading enzymes promotes the selective degradation of pectinaceous substances.[5] Apart from this, the use of different types of enzymes such as cellulase, hemicellulase, laccase and peroxidase have also been reported.[84, 85] There are many advantages associated with enzyme retting over conventional water-retting and dew-retting. Enzyme retting is able to overcome the problems associated with dew- and water-retting as the fibres are treated in a well-controlled environment and the produced fibres possess the quality of water-retted fibres without large amount of fermentation waste. However, high cost associated with enzymes and equipment have limited this technology to pilot scale only.[86]

Foulk et al.[87, 88] compared dew-retted flax fibre reinforced high density polyethylene (HDPE) composites with enzyme retted flax fibre reinforced HDPE composites. Flax fibres were extracted with commercially available Viscozyme L (Novozymes, Bagsvaerd, Denmark) and a chelator, Mayoquest 200 (Callaway Chemical Co. Smyrna, GA). Mayoquest 200 is a chelator that contains about 36% to 38% sodium EDTA and 40% total dissolved salts.[79] The chelator is often used to improve the efficiency of enzyme retting by sequestering calcium from the

solution.[89] Figure 5 shows the effect of different flax fibre extractions (dew-retted, enzyme retted at different enzyme/chelator concentration) on the mechanical properties of the randomly oriented flax fibre reinforced HDPE composites. The flax fibres treated with enzymes and chelators showed significant improvements in terms of tensile properties compared to raw flax fibre reinforced composites. Enzyme and chelators modified the surface of flax fibres by removing pectin and calcium, therefore enhancing the interfacial adhesion between the fibres and the matrix. The composites reinforced with dew-retted flax fibres showed worse properties compared to enzyme retted flax fibres. This is most probably due to poor surface properties of dew-retted fibres (contains high level of calcium and the inability of dew-retting to remove specific components such as pectin) compared to enzyme-retted fibres.
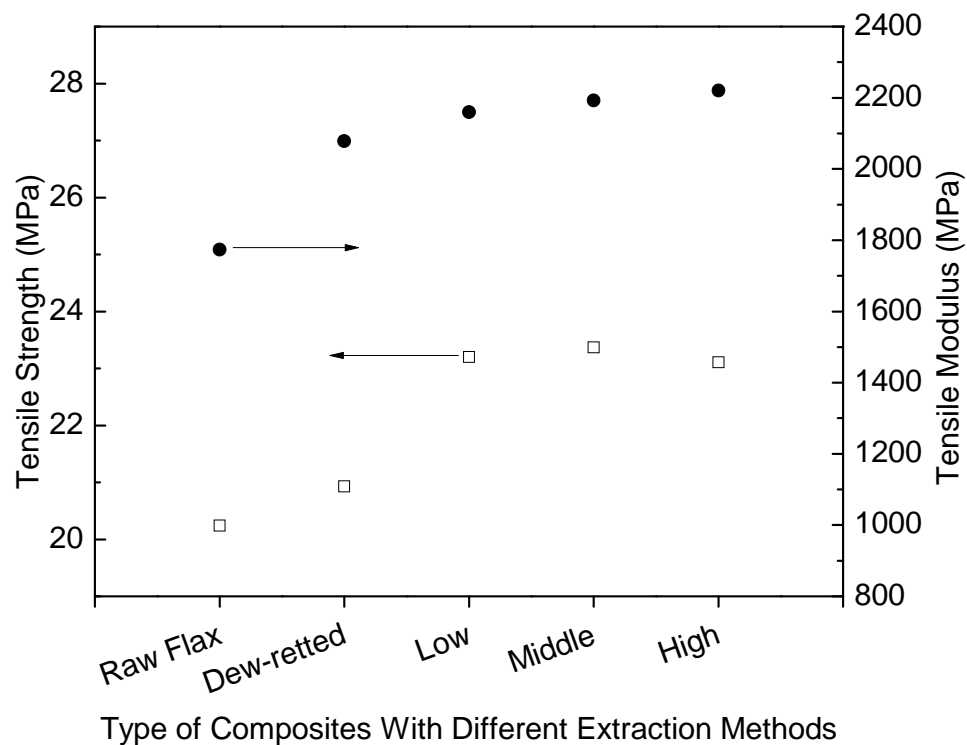
Figure 5: A comparison between not-treated flax fibre, dew retted flax fibre and enzyme retted flax fibre reinforced HDPE composites. Adapted from literature.[87] Low indicates 0.05% enzyme and 5 mM chelator), Medium indicates 0.1% enzyme and 10 mM chelator, High indicates 0.3% enzyme and 25 mM chelator.

In addition to using enzyme for the extraction of natural fibres, it can also be used to treat post-extracted natural fibres. Enzyme treatments of natural fibres also have advantages over conventional alkaline treated natural fibres. Ouajai et al.[90] compared the viscoelastic properties of neat, alkali treated and enzyme treated hemp

fibres reinforced CAB composites. Hemp fibres were treated with Scourzyme L (Novozymes, Bagsvaerd, Denmark). Scourzyme is an alkaline pectinase that removes pectin without significant degradation of cellulose.[91] The enzyme scoured hemp fibres reinforced CAB composites showed improvements over neat CAB, neat hemp fibres reinforced CAB and most of the alkaline treated hemp fibres reinforced CAB. The composites reinforced with alkaline treated hemp fibres (fibre length of 45 μm), however, possessed the highest storage modulus. Single fibre tensile tests indicated that the neat, alkaline treated and enzyme scoured hemp fibre possess Young's moduli of 42.8 GPa, 29.0 GPa and 91.4 GPa, respectively,[92, 93] with alkaline treated fibres possessing the worst mechanical properties. Therefore, the observed better storage modulus of alkaline treated hemp fibres reinforced composites (fibre length of 45 μm, Figure 6) observed might be due to the greater control of fibre suspension in the polymer solvent prior to composite consolidation (solution casting method).[90] Nonetheless, composites reinforced with enzyme scoured hemp fibres possessed a toughness (area under the stress-strain curve) of 40% higher than that of untreated hemp fibre reinforced composites. This is an indication of the potential of enzyme treatment on natural fibre reinforced composites.
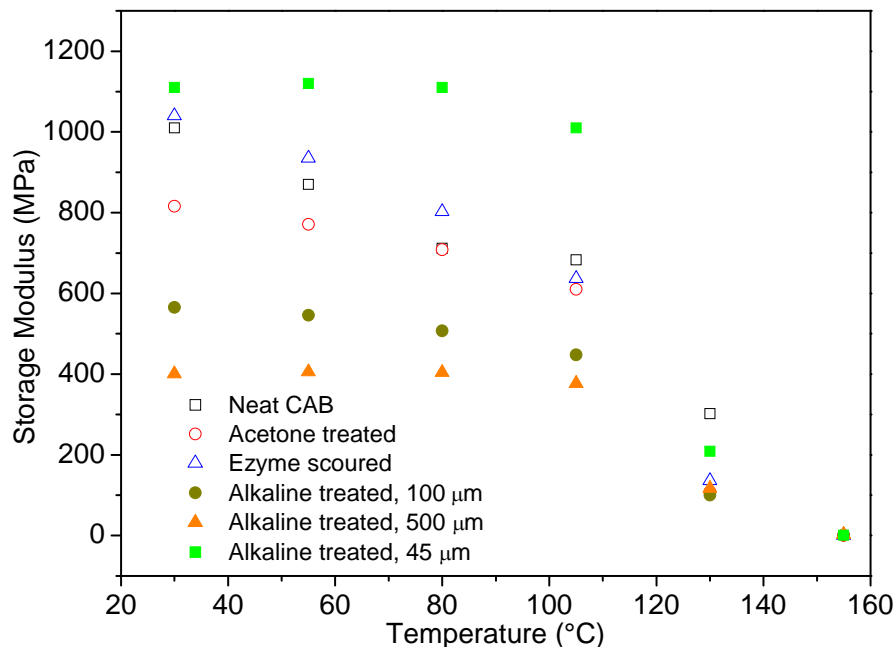
Figure 6: Viscoelastic behaviour of flax fibre reinforced CAB composites. Adapted from literature.[90]

2.2.3 The use of fungi in the surface treatments and extractions of natural fibres

Enzyme retting and treatments have been shown to be an effective method of treating natural fibres to improve the interface between the fibres and the matrix, leading to improved mechanical properties of the composites. However, it is expensive and limited to pilot scale only. Another underexplored method of natural fibre surface treatment involves the use of fungi. The use of fungi can provide low cost, highly efficient and environmentally friendly alternatives to natural fibre surface treatment.[94] Unlike dew-retting, fungal treatment is performed in a more controlled environment. The controlled parameters include the type of fungi, the temperature and the period of treatment.

Fungi can be classified into four categories; basidiomycetes, ascomycetes, zygomycetes and deuteromycetes, respectively. White rot fungus (basidiomycetes) is the only fungus that has been shown to degrade lignin, exposing cellulose and hemicellulose.[94] It has also been shown that white rot fungus can degrade the hydrophobic constituents of natural fibres such as triglycerides and fatty acids. In addition to this, white rot fungus can also degrade sitosterol, sitosterol esters and resin acid.[95] These compounds are known to be resistant towards microbial degradation.[96-98] Therefore, it is not surprising that white rot fungus is used to remove non-cellulosic compounds in order to improve the mechanical properties of the resulting natural fibre reinforced composites.

Table 5: Tensile strength of hemp fibre and its PP composites treated with white rot fungi. Adapted from literature.[94]

Treatment type	Lignin removal	Single Fibre tensile strength (MPa)	Composites tensile strength (MPa)
Control	-	683	36.7
Phanerochaete sordida	Yes	576	41.5
Pycnoporus species	Yes	470	44.6
Schizophyllum Commune	Yes	354	45.0
Alkali	Yes	621	43.3
Alkali + *Phanerochaete sordida*	Yes	579	48.3
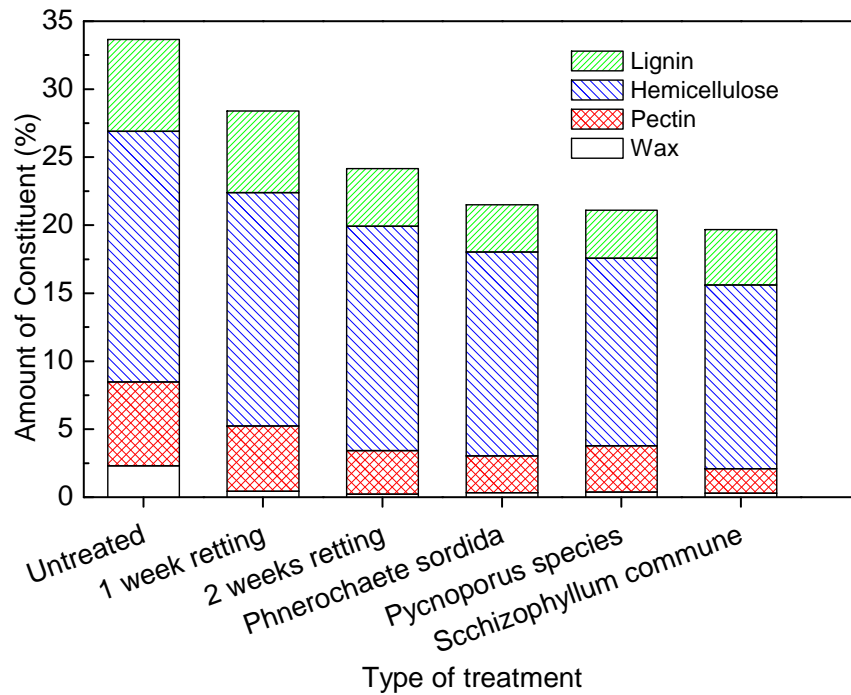
Figure 7: A comparison between natural retting and white rot fungi treatment on the amount of non-cellulosic compound in hemp fibres. Adapted from literature.[99]

The use of white-rot fungus in the treatment of natural fibres can be found in literature.[94, 99-101] White rot fungi treated hemp fibres have higher crystallinity index as measured by X-ray diffraction when compared to untreated fibres.[94] This is a direct result of the fungi's ability to remove non-cellulosic compounds such as amorphous lignin, thereby increased the crystallinity index. Zeta-potential measurements have also shown that non-cellulosic compounds were removed by the fungal treatment. A more negative zeta potential was obtained and this was due to the exposed hydroxyl groups from cellulose as a result of fungal treatment. Table 5 shows the tensile strengths of hemp fibres and randomly oriented hemp fibre reinforced polypropylene (PP) composites. The fibres were treated with white rot fungi and/or alkali. The tensile strength of the composites improved by as much as 32% (combination of alkali and white rot fungi treatments) when compared to neat hemp fibre reinforced composites. Fungi treatments can provide extra benefits in addition to alkali treatment alone. This improvement seen in the composites is a result of improved fibre morphology and mechanical interlocking between the fibre and the matrix.
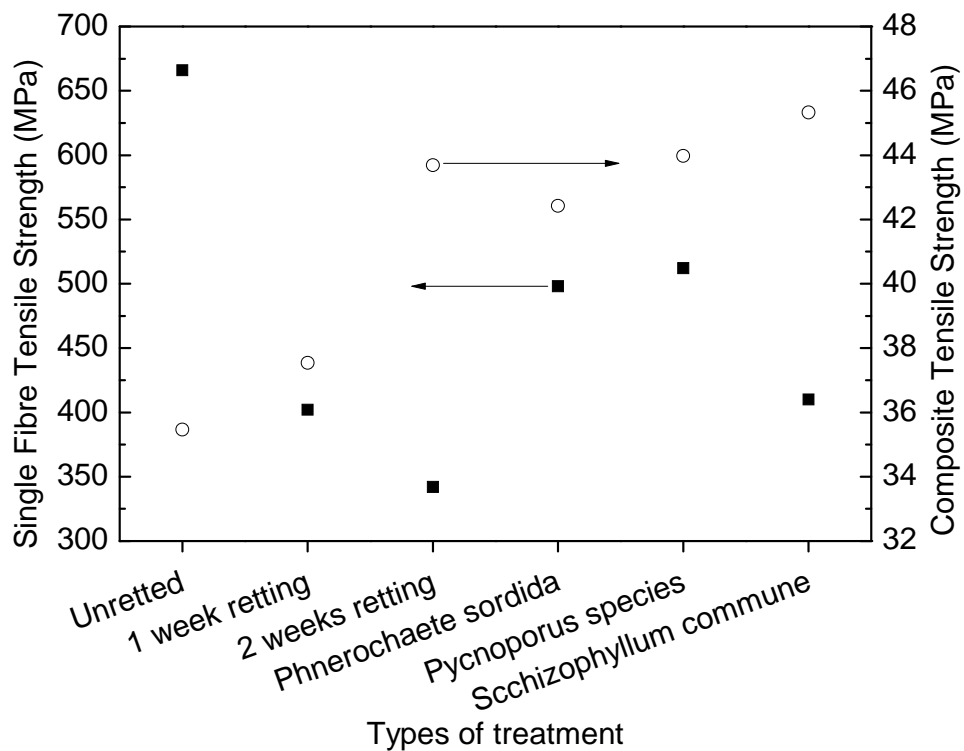
Figure 8: Tensile properties of hemp fibres and hemp fibres reinforced PP composites treated with different methods. Adapted from literature.[99]

White rot fungi have also been used to extract natural fibres.[99] Clarke et al.[102] reported a method for natural retting in which the hemp fibre bundles are separated from the plant by sealing the fibres in a bag for a fixed period of time. The microorganism present in the fibres will produce enzymes to remove non-cellulosic compounds. In a study by Li et al.,[99] natural retting was conducted by sealing non-retted hemp fibres in a bag under a controlled condition of 60% relative humidity for certain periods of time at room temperature. In another separate experiment, the authors treated non-retted hemp fibres with white rot fungi. It can be seen that fungal treatments removed more lignin compared to natural retting treatments (Figure 7). The crystallinity index of the fibres increased from 66% to approximately 85%, due to the removal of non-cellulosic compounds from the fibres, which are generally amorphous. Figure 8 shows the tensile properties of single hemp fibre and randomly oriented hemp fibre reinforced polypropylene (PP) composites as a function of different types of treatments. Although the tensile strength of the fibres decreased when compared to neat hemp fibres, the composite strength improved by as much as 30% as a result of fungal treatment. This suggests improved fibre properties

(crystallinity index) and interfacial adhesion (surface roughness) between fibres and the matrix, which is confirmed by scanning electron micrographs. Natural retted fibres does improve the composite's tensile strength (due to the removal of non-cellulosic compounds) but the increment in the observed tensile strength is less than that of white rot fungi treated hemp fibres reinforced PP composites. This might be a direct result of poor single fibre tensile strength due to long retting time.

2.2.4 Coating natural fibres with nanocellulose

The previous three sections involved the treatment of removing substances from natural fibres. This section, however, describes a new modification which does not involve the removal but the *addition* of new material onto the surface of natural fibres. This type of modification involves the deposition of nano-sized cellulosic materials onto the surface of natural fibres to enhance the interfacial adhesion between the fibres and the matrix.[11-13, 103] By doing so, a hierarchical structure can be created. These works were inspired by nature. Nature maximises the efficiency of structural materials by defining a hierarchical structure; the arrangement of the constituents at every level, from the molecular level to the macroscopic level. By applying this concept, composites that possess a hierarchical structure with improved mechanical properties can be manufactured.
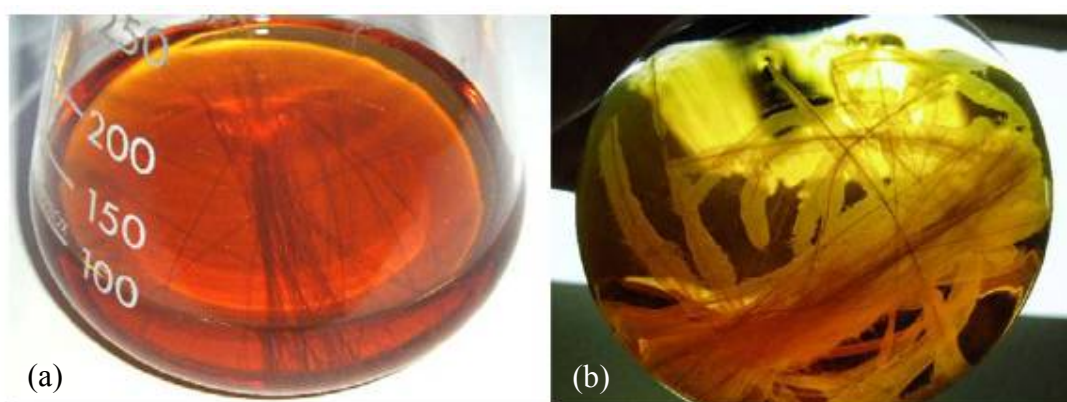
Figure 9: Images showing (a) natural fibres immersed in a culture medium of *Gluconacetobacter xylinum* before bacteria culturing (b) the culture medium after 2 days. Reprinted from Pommet et al., Biomacromolecules 2008 (9), 1643 with permission from ACS publication.
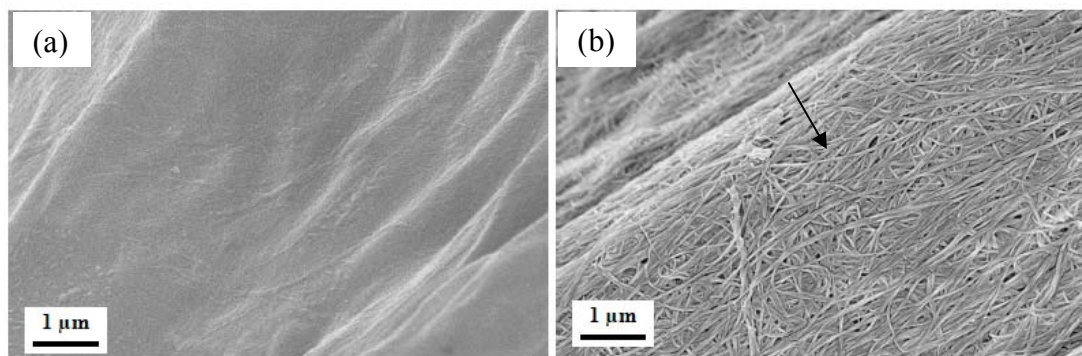
Figure 10: SEM images showing (a) neat sisal fibre (b) sisal fibre coated with bacterial cellulose. Reprinted from Pommet et al., Biomacromolecules 2008 (9), 1643 with permission from ACS publication.

In addition to plant derived cellulose, cellulose can also be synthesised by bacteria such as from the *Acetobacter* species. By culturing cellulose-producing bacteria in the presence of natural fibres in an appropriate culture medium, bacterial cellulose is preferentially deposited *in-situ* onto the surface of natural fibres. The introduction of bacterial cellulose onto natural fibres provides new means of controlling the interaction between natural fibres and polymer matrices. Coating of natural fibres with bacterial cellulose does not only facilitate good distribution of bacterial cellulose within the matrix, it also results in an improved interfacial adhesion between the fibres and the matrix. This enhances the interaction between the natural fibres and the polymer matrix through mechanical interlocking. Bacterial cellulose coated natural fibres introduced nanocellulose at the interface between the fibres and the matrix, leading to increased stiffness of the matrix around the natural fibres. Figure 9 shows the images of the culture medium and natural fibres immersed in the culture medium before and 2 days after culturing. A layer of bacterial cellulose (BC) pellicles can be seen growing away from the surface of the natural fibres. Scanning electron micrographs of the BC coated sisal fibres are shown in Figure 10. A layer of bacterial cellulose nanofibrils can be seen attached onto the surface of sisal fibres (Figure 10b). The coating of natural fibres with BC could also be a potential solution to the aforementioned shrinkage of natural fibres during thermal processing of the composites. Due to the low thermal expansion of BC (0.1×10^{-6} K^{-1}),[104] the BC coating could potentially bridge the gap that exists between the fibres and the matrix due to the high LCTE of natural fibres.

Simple weight gain measurements showed that approximately 5wt% to 6wt% of BC was deposited onto the surface of these natural fibres. However, the mechanical properties of the natural fibres after bacterial cellulose modification depend on the type of natural fibres used. The modification process did not change the mechanical properties of sisal fibres but the properties of hemp fibres were affected (see Table 6). The exposure of the hemp fibres to BC caused a drastic loss of fibre strength and Young's modulus. This might be due to a further separation of the bast fibres into smaller individual fibres making up the technical fibre as a result of the intrinsically non-cohesive structure of bast fibres. The interfacial shear strengths between sisal fibres and CAB and PLLA increased by 46% and 21%, respectively and the interfacial shear strength between hemp fibres and CAB increased by as much as 140% (Table 7). It should be noted that the increment seen in the interfacial shear strength between hemp fibres and CAB could also be due to the combined effect of BC coating and the disintegration of the fibres. This improvement seen in the interfacial shear strengths indicates enhanced stress transfer between the fibres and the matrix, which is a direct result of improved interfacial adhesion due to the bacterial cellulose coating applied to natural fibres.

Table 6: The mechanical properties of natural fibres modified with bacterial cellulose nanofibrils. Adapted from literature.[13]

Natural Fibres	Young's modulus (GPa)	Tensile strength (MPa)	Elongation at break (%)
Neat Sisal Fibre	15.0 ± 1.2	342 ± 33	2.9 ± 0.1
Bacterial cellulose modified sisal fibre	12.5 ± 1.0	324 ± 33	4.5 ± 0.4
Bacterial cellulose modified sisal fibre with purification*	12.0 ± 0.9	310 ± 32	4.1 ± 0.5
Neat Hemp fibre	21.4 ± 2.0	286 ± 31	2.0 ± 0.2
Bacterial cellulose modified hemp fibre	8.8 ± 0.7	171 ± 11	2.9 ± 0.2
Bacterial cellulose modified hemp fibre with purification*	8.0 ± 0.6	130 ± 12	2.9 ± 0.2

* Purification indicates the extraction of post-bacterial cellulose modified sisal fibres with NaOH at 80°C.

Table 7: Interfacial shear strengths between modified natural fibres and CAB or PLLA. Adapted from literature.[11, 13]

Natural fibres	Interfacial shear strength to CAB (MPa)	Interfacial shear strength to PLLA (MPa)
Neat sisal fibre	1.02 ± 0.06	12.1 ± 0.5
Bacterial cellulose modified sisal fibre	1.49 ± 0.03	14.6 ± 1.2
Neat hemp fibre	0.76 ± 0.06	-
Bacterial cellulose modified hemp fibre	1.83 ± 0.12	-

Table 8: Mechanical properties of bacterial cellulose modified hemp and sisal fibres reinforced CAB and PLLA composites. Adapted from literature.[12]

Composites	Neat Fibre		Modified Fibre		Improvements	
	σ (MPa)	E (GPa)	σ (MPa)	E (GPa)	σ	E
CAB/Hemp*	98.1±12.7	8.5±1.3	86.7±13.6	5.8±0.5	-12%	-35%
PLLA/Hemp*	110.5±27.2	11.8±4.2	104.8±9.1	7.9±1.2	-5%	-33%
CAB/Sisal*	92.9±9.3	5.5±0.5	100.4±7.0	8.8±1.4	8%	59%
PLLA/Sisal*	78.9±14.7	7.9±1.3	113.8±14.0	11.2±1.2	44%	42%
CAB/Hemp§	15.8±2.2	1.9±0.1	13.4±1.4	0.6±0.2	-15%	-69%
PLLA/Hemp§	13.4±3.6	3.2±0.2	13.3±2.5	2.3±0.3	-1%	-28%
CAB/Sisal§	10.9±1.7	1.6±0.1	14.4±3.7	1.8±0.3	32%	15%
PLLA/Sisal§	10.0±3.1	2.1±0.1	16.8±4.1	3.1±0.2	68%	49%

* The loading direction is parallel (0°)to the fibres.
* The loading direction is perpendicular (90°) to the fibres

Bacterial cellulose modified sisal and hemp fibres have also been used to produce unidirectional natural fibre reinforced CAB and polylactide (PLLA) model composites.[12] The mechanical properties of bacterial cellulose coated sisal fibre reinforced polymers showed significant improvements over neat polymers (Table 8). The tensile strength and modulus for sisal/PLLA composites improved by as much as 68% and 49%, respectively. However, improvements were not observed for composites containing BC coated hemp fibres. The tensile strength and modulus decreased by as much as 15% and 69%, respectively for hemp/CAB composites. One should note that the fibres were damaged during bacteria culture and their tensile strength were only one third of the original fibres. The use of BC coated sisal fibres has also led to some improvements in short fibre reinforced PLLA

composites.[103] It was shown that the crystallinity of the matrix, the tensile and flexural properties improved through the addition of bacterial cellulose coated sisal fibres to PLLA. The tensile and flexural properties of these composites were found to be higher than that of commercial polypropylene used in the automotive industry. This indicates the potential of hierarchical composites for applications in the automotive industry.

2.3 Conclusion

Natural fibres have significant advantages over conventional glass fibres. These include low cost, low density, high specific strength and most importantly, biodegradability (this might however results in problems if the fibres degrade within inside the matrix). They are the prime candidates for the manufacturing of truly green composites. However, the extremely hydrophilic nature of these natural fibres often leads to poor compatibility between conventional thermoplastics, such as polylactide. Modification to the matrix is one of the possible solutions to this problem. Surface treatments of natural fibres to enhance the interface between the fibres and the matrix might be a viable solution. Chemical treatments have been explored extensively in this context but it is not the most desirable method; hazardous chemicals are often involved in the chemical treatment of natural fibres. Solvent waste disposal after chemical treatment is another problem associated with surface chemical treatment of natural fibres.

New and greener methods of surface treatment are emerging. Plasma treatments have been shown to be effective in increasing the critical surface tension of natural fibres, thereby improving the wettability between the fibres and the matrix. Enzyme retting and treatments are also another emerging method to extract or treat natural fibres. Non-cellulosic compounds such as pectin, lignin and hemicellulose can be removed by specific enzymes, exposing the main cellulose backbone of natural fibres, which was shown to result in increased surface tension. Enzyme retting is favourable when compared to conventional water retting and dew retting methods. Water retting produces vast amounts of fermentation waste whilst dew retting has the disadvantage of producing fibres that possess lower quality compared to enzyme retting due to the inherent difficulties in controlling the retting parameters. However,

enzyme retting is limited to pilot scale only due to its high operating and capital cost when compared to water- and dew-retting methods.

White rot fungi have been shown to be effective in lignin removal. It has been used to remove non-cellulosic compounds from natural fibres, exposing the underlying cellulose and hemicellulose. A combination of alkali and fungal treatments showed the most improvement in the composites' mechanical properties. The surface of natural fibres can also be modified by coating them with a layer of bacterial cellulose nanofibrils, which allows the production of hierarchical composites. This can be done by immersing natural fibres in a culture medium containing cellulose-producing bacteria, such as the *Acetobacter* species. By using natural fibres as a substrate for cellulose producing bacteria, the bacteria will deposit their cellulose preferentially onto the surface of natural fibres. This increases the effective area of the interface, enhances the interfacial adhesion through mechanical interlocking and improves the wettability of the fibres by the matrix, as bacterial cellulose possesses higher surface tension than natural fibres. The resulting polymers reinforced with bacterial cellulose coated natural fibres have comparable properties with commercial polypropylene used in the automotive industry, indicating the potential of such surface treatment.

Public's demand for more environmental friendlier products and environmental legislations should motivate the composites industry (at least in parts) to move away from conventional polymeric materials such as synthetic glass fibres and polypropylene to greener materials such as natural fibres and biodegradable polymers. A combination of natural fibres as the reinforcing agent, greener surface treatments to enhance the interface and biodegradable polymers as the matrix should enable the production of truly green composite materials. The *ideal* truly green composite materials are as follow: When the material is not at the end of its lifetime, it should be recyclable without significant loss of mechanical properties. When the material is at the end of its life cycle, it can be triggered to biodegrade in composting condition. Therefore, the next challenge in green composites would be the production of green composites with triggered biodegradability and good recyclability.

Chapter 3 – Surface *only* modification of bacterial cellulose nanofibres with organic acids

Summary

Bacterial cellulose (BC) nanofibres were modified only on their surface using an esterification reaction with acetic acid, hexanoic acid or dodecanoic acid. This reaction rendered the extremely hydrophilic surfaces of BC nanofibres hydrophobic. The hydrophobicity of BC increased with increasing carbon chain length of the organic acids used for the esterification reaction. Streaming (zeta-) potential measurements showed a slight shift in the isoelectric point and a decrease in $\zeta_{plateau}$ was also observed after the esterification reactions. This was attributed to the loss of acidic functional groups and increase in hydrophobicity due to esterification of BC with organic acids. A method based on hydrogen/deuterium exchange was developed to evaluate the availability of surface hydroxyl groups of neat and modified BC. The thermal degradation temperature of modified BC sheets decreased with increasing carbon chain length of the organic acids used. This is thought to be a direct result of the esterification reaction, which significantly reduces the packing efficiency of the nanofibres because of a reduction in the number of effective hydrogen bonds between them.

3.1 Introduction

A research area that has been receiving much attention recently is the modification of cellulose for the development of bio-based materials and composites.[105-108] Cellulose is a linear macromolecule consisting of a repeat unit comprising two D-anhydroglucose rings linked by β (1→4) glycosidic bonds. It is the most abundant organic homopolymer on earth. Cellulose has found numerous industrial applications; in the pharmaceutical and cosmetic industries,[109] paper industry[110] and more recently in composites for the production of so-called 'green' (nano)composite materials.[11-13, 20, 111-113] Unfortunately, the major challenge of utilising (ligno)cellulosic materials, such as natural fibres, in composite applications

is its extremely hydrophilic nature,[114] high linear coefficient of thermal expansion (LCTE)[52] and poor transverse properties.[50] Due to the high LCTE of natural fibres, the residual stresses exerted on natural fibres by the matrix in a composite will be lowered, leading to low interfacial shear stresses between the fibres and a polymeric matrix, as the interfacial shear stress is the product of residual stress and static coefficient of friction of the fibres. As a result, the compatibility between natural fibres and hydrophobic thermoplastics (such as polypropylene and polylactic acid) is often poor.[13, 78] To overcome this challenge, nanocellulose can be coated onto the surface of natural fibres[11-13] (thereby creating "hairy natural fibres") to bridge the gap between the natural fibres and the matrices caused by the high LCTE of natural fibres. However, nanocellulose itself is still hydrophilic in nature and cellulose modification is therefore needed to improve the compatibility between cellulose and hydrophobic (renewable) thermoplastics.[39, 64]

In addition to plant sources, cellulose can also be derived from bacteria, such as from the *Acetobacter xylinum* species.[115] Bacterial cellulose (BC) is being currently explored for/or used already in biomedical applications,[116] the production of high quality papers,[115] diaphragms for electroacoustic transducers,[117] optically transparent films[105, 106] and nowadays as reinforcements for polymers.[118] Such extensive use of BC is due to the fact that the material has the advantage of being free of wax, hemicellulose, lignin and pectin, which are present in most plant based cellulosic materials,[115] with cotton as the exception.[5] In addition to this, BC is inherently nano-sized; with individual fibres having diameters ranging from 24 to 86 nm and are several micrometres in length.[119] This feature differs from plant based natural fibres, which have to be homogenised or fibrillated to obtain nanofibres (microfibrillated or nanofibrillated cellulose).[106] X-ray diffraction (XRD) has also revealed that BC has a very high degree of crystallinity of about 90%.[120] In terms of its mechanical properties, Hsieh et al.[6] have determined the Young's modulus of single bacterial cellulose nanofibres using Raman spectroscopy. They found that bacterial cellulose nanofibres possess a Young's modulus of 114 GPa, with a theoretical Young's modulus of between 130 to 160 GPa depending on its crystal form.[121, 122] Moreover, BC also has a very low thermal expansion coefficient of 0.1×10^{-6} K^{-1}.[104] All these properties are highly favourable for using BC as a nanofiller/reinforcement in green nanocomposite materials.

As already mentioned, the hydrophilic nature of cellulose will often result in poor compatibility between cellulose and hydrophobic polymer matrices. This will then lead to poor stress transfer efficiency between the matrix and the reinforcement. In order to utilise the full potential of BC as nanofiller for composites, a reliable surface-*only* modification is needed to tailor the surface properties of BC without affecting its bulk properties by turning it, for example into a cellulose ester, such as cellulose acetate. This will mean that the compatibility between BC and hydrophobic polymer matrices such as polylactide can be improved.[123] Grafting of polymers[124] or adsorptions of surfactants[125] onto cellulose surface have been investigated in order to functionalise and compatibilise cellulose with a matrix. However, the process of polymer grafting suffered from a lack of control, which prevents the design of well-defined materials. Moreover, although polymer grafting enhances the interaction with polymers, it limits the use of polymer-*graft*-BC for matrices consisting either of the grafted polymer or polymers the grafted polymer is miscible with, which are limited. On the other hand, in order to fully cover the surface of cellulose with surfactants, large quantities of surfactants are needed, usually 4 times the mass of cellulose.[125] This results in the increase in the raw material cost.

Heterogeneous esterification of cellulose nanofibres with organic acids usually resulted in significant bulk modification, characterised by loss of crystallinity and high degree of substitutions.[105, 107, 126] BC has also been esterified homogeneously in ionic liquids to produce cellulose acetate but the crystal structure of modified cellulose once regenerated is destroyed.[127] By restricting the modification *only* to the surface of BC nanofibres, the highly crystalline bulk structure of BC can be retained, while the surface is rendered hydrophobic. In this present work, the heterogeneous surface esterification of BC nanofibres with various organic acids, namely acetic, hexanoic and dodecanoic acid, is investigated. In a recent study[123] it was demonstrated that significant improvements in thermo-mechanical as well as mechanical properties over the neat poly(L-lactic acid) (PLLA) by using these esterified BC nanofibres as a reinforcement for polylactic acid-based nanocomposites. This current work will investigate and characterise the surface and bulk properties of BC as a result of organic acids modification.

3.2 Experimental

3.2.1 Materials

Acetic acid (analaR, purity $\geq$ 99.8%), methanol (GPR, purity $\geq$ 99%), ethanol (GPR, purity $\geq$99%) and pyridine (analaR NORAMPUR, purity $\geq$ 99.7%) were purchased from VWR. Hexanoic acid (purity $\geq$ 99.5%), dodecanoic acid (purity $\geq$ 98%), and *p*-toluenesulfonyl chloride (purity $\geq$ 99%), dimethyl carbonate (purity $\geq$ 99%) and deuterium oxide (purity $\geq$ 99.99 atom% D) were purchased from Sigma-Aldrich. Sodium hydroxide (purum grade, pellets) was purchased from Acros Organics. All the materials were used without any further purification. Bacterial cellulose was extracted from commercially available *Nata-de-coco* (CHAOKOH gel in syrup, Ampol Food Processing Ltd, Nakorn Pathom, Thailand).

3.2.2 Extraction and purification of bacterial cellulose

Bacterial cellulose was extracted from 10 jars of *Nata-de-coco*.[103] Firstly, *Nata-de-coco* was rinsed with de-ionised water (3 × 10 dm^3) to wash away the sugar syrup. The washed *Nata-de-coco* was then blended for 1 min using a laboratory blender (Waring Blender LB20EG, Christison Particle Technologies, Gateshead, UK). This BC blend was then homogenised (Polytron PT 10-35 GT, Kinematica, Lucerne, Switzerland) for 2 min and centrifuged at 14,000g to remove the excess water. To further purify BC, the centrifuged material was re-dispersed in de-ionised water (10 dm^3). Sodium hydroxide (40 g, 1 mol) was added into this mixture and heated to 80°C for 20 min, whilst stirring to remove any soluble polysaccharides.[128] The purified BC was then successively centrifuged and homogenised back to neutral pH using de-ionised water (4 × 10 dm^3).

3.2.3 Surface *only* modification of bacterial cellulose

In order to modify the surfaces of BC nanofibres, the purified material (2 g, 12.3 mmol†) was solvent exchanged from water through methanol (3 × 600 cm^3) into pyridine (2 × 600 cm^3). This mixture was then homogenised at 20,000 rpm for at least 1 min at each stage to completely disperse BC in the solvent§. BC was retained

---

† This value was obtained by using the molecular weight of the glucose-repeating unit in cellulose ($C_6H_{10}O_5$).
§ Although starting the reaction with freeze-dried BC is possible, which allows for the re-dispersion of BC in the reaction medium, its modification results in significant bulk modification of BC.

through centrifugation at 14,000g at each stage before re-dispersing it in the subsequent solvent. Another solvent exchange step was performed to adjust the final concentration of BC in pyridine to 0.5% (g cm^{-3}). The BC-pyridine mixture was then poured into a 1 dm^3 3-neck round bottom flask and stirred using a magnetic stirrer. *p*-Toluenesulfonyl chloride (92 g, 0.48 mol) was added into this BC-pyridine mixture and an equimolar amount of organic acid (0.48 mol) was added into the reaction vessel after the addition of *p*-toluenesulfonyl chloride. The reaction was conducted for 2 h at 50°C under nitrogen flow to create an inert atmosphere such that water vapour present in the atmosphere does not affect the esterification reaction. The reaction medium was then quenched with ethanol (1.5 dm^3). The modified BC was then washed with ethanol again (3 × 800 cm^3) using the previously described homogenisation-centrifugation step. The product was solvent exchanged from ethanol back to water (3 × 800 cm^3). In order to use the bacterial cellulose in later stages, the neat and modified BC nanofibres were dispersed in water (500 cm^3) and dimethyl carbonate (500 cm^3), respectively and subsequently freeze-dried (Edwards Modulyo freeze dryer, West Sussex, UK). The BC nanofibres modified with acetic, hexanoic and dodecanoic acids were termed C$_2$-BC, C$_6$-BC and C$_{12}$-BC, respectively.

3.2.4 Characterisation of neat and modified BC

3.2.4.1 Attenuated Total Reflection Infrared spectroscopy (ATR-IR)

ATR-IR spectra were recorded using a Spectrum One FTIR-spectrometer (Perkin Elmer, Massachusetts, USA). The spectra were collected at a resolution of 2 cm^{-1}, in the range of 600 cm^{-1} and 4000 cm^{-1}. A total of 16 scans were used to obtain each spectrum.

3.2.4.2 Preparation of sheets of (modified) bacterial cellulose (paper)

In order to aid the characterisation of modified BC, paper-like BC sheets made from (modified) BC suspensions were prepared. Initially the (modified) BC water dispersions were centrifuged and the wet centrifuged cake (the sediment) of BC was placed on a plate, spread with a spatula to a circular wet mass and finally placed into a hot press (George E Moore and Sons, Birmingham, UK) held at 110°C. Once the moisture from BC has been evaporated, the dried BC was then compressed at a pressure of 5 t for 5 min at the same temperature, to produce a flat BC sheet. Such

sheets made from neat or modified BC suspensions were used for Raman spectroscopy, X-ray diffraction and contact angle measurements.

3.2.4.3 Water/air contact angle measurements

In order to determine the hydrophobicity of modified BC, water/air contact angles were measured on BC sheets/paper made from (modified) BC suspensions. Advancing θ_a and receding θ_r water/air contact angles on the (modified) BC sheets were measured using the sessile drop method (DSA 10 Mk 2, Krüss GmbH, Hamburg, Germany) at room temperature. Images of the sessile drops were processed using DSA software version 1.80.1.12. At least 5 measurements were taken for each sample.

3.2.4.4 Streaming-potential measurements

The ζ-potentials of neat and modified BC were measured using an electrokinetic analyser (EKA, Anton Paar, Graz, Austria) based on the streaming potential method. In order to exclude any overlaying effects due to swelling (for BC) or extraction of water-soluble components from the samples, the pH dependency of ζ-potential was measured only after a time dependent ζ-potential measurement was completed. During the $\zeta = f(t)$ measurement, the streaming potential was generated by applying a steady pressure increase to 250 mbar across a channel, which was created by stacking the previously mentioned (modified) BC sheets in between a PTFE film The pH dependency of the ζ-potential was then measured by changing the pH of the electrolyte solution through the titration of 0.1 N HCl or KOH into KCl solution, using a titration unit (RTU, Anton Paar, Graz, Austria).

3.2.4.5 Determination of the degree of surface substitution of cellulose using Dynamic Vapour Sorption (DVS)

In order to determine the degree of surface substitution of modified BC by organic acids, a method based on hydrogen/deuterium (H/D) exchange was developed following on from early work reported in literature.[129] This measurement was carried out using DVS (DVS-Advantage, Surface Measurement Systems Ltd, Alperton, UK). Approximately 30 mg of freeze dried BC was placed in the sample pan and it was pre-conditioned at 0% relative humidity (RH) of deuterium oxide

(D$_2$O) for 5 h at room temperature to remove any adsorbed water molecules. The RH of D$_2$O was increased to 90% for 2 h to allow for the adsorption of D$_2$O molecules and hence, the H/D exchange with the accessible hydroxyl groups of BC. The RH was then reduced to 0% for 2 h to allow the D$_2$O molecules to desorb. This cycle was repeated 10 times such that the H/D exchange can occur on all accessible hydroxyl groups. A short adsorption time of 2 h was employed to avoid bulk sorption of BC, as only the accessible hydroxyl groups were of interest. The sample was then post-conditioned at 0% RH for 5 h to remove any residual adsorbed D$_2$O molecules. As the deuterium atom is one neutron heavier than hydrogen, the mass increase after the post-conditioned BC was measured *in situ* by an ultra-sensitive microbalance (with an accuracy of $\pm$ 0.05 μg) and the amount of accessible hydroxyl groups available was back calculated from this mass increase:

$$\Delta m = \frac{OH \times m_i \times A \times m_n}{162140} \hspace{3cm} (3.1)$$

where Δm = mass change after hydrogen-deuterium exchange (mg), OH = accessible hydroxyl groups, m_i = initial mass of sample (mg), A = Avogadro's number and m_n = mass of a neutron (in mg). The number 162140 represents the molecular mass of a single glucose unit having the unit of mg mol^{-1} ($C_6H_{10}O_5$). The derivation of this equation can be found in appendix A.

3.2.4.6 X-ray diffraction (XRD) to determine crystallinity of neat and modified BC

The XRD pattern of neat and modified BC was characterised on sheet samples using an X-ray diffractometer (PANalytical X'Pert 1, PANalytical Ltd, Cambridge, UK) using a 1.79 Å cobalt X-ray source. Measurements were taken from $2\theta = 10°$ to $45°$ at a step size of $0.04°$. In order to calculate the crystallinity of BC, Segal's method[130] was used. This equation is an empirical equation for estimating the degree of crystallinity in cellulose.

$$\chi_c = \frac{I_{002} - I_{amorphous}}{I_{002}} \times 100\% \hspace{3cm} (3.2)$$

where I_{002} is the intensity of the 002 reflection plane and $I_{amorphous}$ is the intensity of the amorphous plane. As a comparison, the crystallinity of the (modified) BC was also calculated based on the area under the XRD spectrum using equation:

$$\chi_c = \frac{A_c}{A_c + A_a} \times 100\% \qquad (3.3)$$

where A_c and A_a are the total crystalline area and total amorphous area, respectively, between 10° and 45°. Scherrer's equation,[131]

$$L_{(002)} = \frac{K\lambda}{\beta \cdot \cos\theta} \qquad (3.4)$$

where β is the full width at half maximum of the 002 reflection, θ is the Bragg's angle in degrees and $K = 0.91$, was used to determine the crystallite size ($L_{(002)}$), and hence, the structural order of 002 reflection.

3.2.4.7 Thermal stability of BC: Thermo Gravimetry Analysis (TGA)

The thermal degradation behaviour of neat and modified BC in nitrogen was investigated using high resolution modulated TGA (TGA 2950, TA Instruments, Crawley, UK). A sample size of approximately 1 mg was used. The samples were heated from 25 to 550°C at a heating rate of 10°C min^{-1}.

3.3 Results and discussions

3.3.1 ATR-IR Spectra

Figure 11 shows the ATR-IR spectra of neat BC and BC that was modified with organic acids in dispersion. The spectra were normalised against the intensity of the absorption band corresponding to the (C-O-C) link of cellulose,[132] which is located around 1158 cm^{-1}. The appearance of an absorption band characteristic for carbonyl bonds (C=O) around 1750 cm^{-1} can be seen. This is a direct result of the introduction of hydrophobic esters onto BC via the esterification reaction. The hydroxyl group absorption (-OH) around 3300 cm^{-1} did not seem to decrease significantly with the modification (C$_2$-BC is the exception). This result suggests that the modification

occurred essentially only on the surface of the nanofibres or in the amorphous fraction of the cellulose. The more intense 1750 cm^{-1} adsorption band in C$_2$-BC is caused by the higher reactivity of acetic acid compared to hexanoic and dodecanoic acid; in analogy to the lipase-catalysed esterification reaction of fatty acids with disaccharides.[133] Therefore, more ethanoate ester bonds form readily on BC. This is also accompanied by increases in the absorption band intensities around 900 cm^{-1}, 1280 cm^{-1} and 1360 cm^{-1}. These absorption bands correspond to the -CH vibrations[132] arising from the methyl groups. C$_2$-BC also showed a peak around 1650 cm^{-1}, which can be attributed to the symmetric deformation vibration of adsorbed water molecules.[134] Due to the more hydrophilic nature of C$_2$-BC as compared to C$_6$-BC and C$_{12}$-BC (see section 3.3.2), the full elimination of adsorbed water molecules proved to be difficult for acetic acid modified cellulose samples.[134, 135]
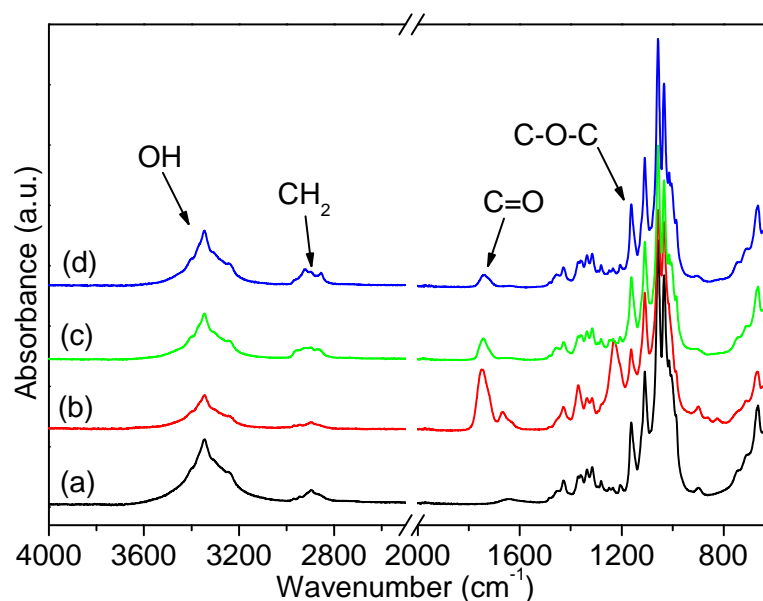
Figure 11. ATR-IR spectra of modified bacterial cellulose. (a) Neat BC, (b) C$_2$-BC, (c) C$_6$-BC, (d) C$_{12}$-BC.

3.3.2 Wettability of bacterial cellulose and modified bacterial cellulose

In order to obtain qualitative information about the hydrophilicity/hydrophobicity of modified BC nanofibres, the water/air contact angle as measure of the wettability of modified BC was determined using the sessile drop method on paper-like BC sheets made from (modified) BC nanofibres. It can be seen that both advancing θ_a and receding θ_r water contact angles increased with increasing carbon chain length of the

organic acid used to modify the BC nanofibre surface (Table 9). The esterification reaction introduced hydrophobic groups onto the surface of BC. The longer the length of the hydrocarbon chain with which the BC nanofibres were modified, the more hydrophobic was the BC surface leading to the observed increase in water contact angles on BC sheets. It must be noted however that the contact angles presented here are not equilibrium contact angles of BC nanofibres, as the roughness of the BC sheets cannot be easily taken into account. The roughness effect will cause the water droplet(s) to (i) follow the actual microtexture induced by surface roughness (corresponding to the Wenzel state) or (ii) contact only the top asperities, entrapping air below and so create a composite (Cassie-Baxter) wetting state. Both wetting states exaggerate the hydrophilicity and hydrophobicity.[136] The difference between these limiting (advancing and receding) contact angles is referred to as contact angle hysteresis ($\Delta\theta = \theta_a - \theta_r$). This hysteresis can be attributed to surface chemical heterogeneity, roughness or kinetic effects such as swelling or hydrophobic recovery.[137] The large $\Delta\theta$ observed suggests a Wenzel state. Removing water from such rough surface will make water contact itself (as a result of water leftover in the microtexture), yielding low receding contact angles.

Table 9. Advancing θ_a and receding θ_r water/air contact angles, contact angle hysteresis ($\Delta\theta$), isoelectric point (iep), ζ-potential plateau value ($\zeta_{plateau}$), hydroxyl group availability (-OH) and the degree of surface substitution (DSS) of neat and modified BC

Sample	θ_a (°)	θ_r (°)	$\Delta\theta$ (°)	iep (pH)	$\zeta_{plateau}$ (mV)	-OH [*,†]	DSS (%)
Neat BC	19 ± 3	12 ± 2	7	3.7 ± 0.1	-7.5 ± 0.2	1.24	0
C_2-BC	75 ± 1	35 ± 2	40	3.8 ± 0.1	-21.1 ± 0.1	0.01	98.9
C_6-BC	92 ± 1	45 ± 1	47	3.9 ± 0.1	-21.7 ± 0.3	0.52	58.5
C_{12}-BC	133 ± 4	80 ± 4	53	3.8 ± 0.2	-21.8 ± 0.5	0.60	51.9

[*]The –OH groups availability has a maximum value of 3 as there are 3 –OH groups per glucopyranose unit in cellulose.
[†]Due to the sensitivity of the ultra microbalance used in DVS, the error arising from the measurement was statistically insignificant between samples.

3.3.3 ζ-potentials of (modified) BC sheets

Measured ζ-potentials reflect the composition of the electric double layer on a substrate. It is used to approximate the electrostatic potential at the beginning of the diffusive part of the double layer.[138] The $\zeta = f(pH)$ of neat and modified BC (Figure 12) shows that neat and modified BC possess acidic surface groups (-OH groups) giving rise to a low isoelectric point (iep), where $\zeta=0$, and a plateau region in the

alkaline pH range. The plateau observed at high pH is a result of the full dissociation of acidic functional groups and, therefore, the surface is negatively charged. Lowering the pH of the electrolyte solution decreased the magnitude of ζ-potential due to the repression of the dissociation of acidic functional groups on the surface of (modified) BC. Ultimately, the ζ-potential changes sign to a positive value as a result of proton (H_3O^+) adsorption. The iep and $\zeta_{plateau}$ are tabulated in Table 9. Neat BC has an iep at pH 3.7 and a $\zeta_{plateau}$ of -7.5 mV. This measurement is in agreement with ζ-potentials measured by Blaker et al.[139]. A slight shift in iep (although it is within error) and a decrease in $\zeta_{plateau}$ can be observed for organic acid modified BC. This is not surprising as the modification of BC with organic acids does affect its surface properties, such as wettability and ζ-potentials. The surface modification of BC does not only increase the hydrophobicity of BC nanofibres but also the $\zeta_{plateau}$ values. The slight increase of the iep to higher pH for the modified BC is due the loss of acidic functional groups as a result of the esterification reaction. The dramatic decrease in $\zeta_{plateau}$ from -7.5 mV for neat BC to -22.8 mV for the modified BC could be attributed to the increase in hydrophobicity of the material. Due to the hydrophobic nature of the modified BC surfaces, water molecules could not adsorb as easily onto the surface, which resulted an increase of the concentration of electrolyte ions in the electrochemical double layer and, therefore, a smaller $\zeta_{plateau}$ was observed.
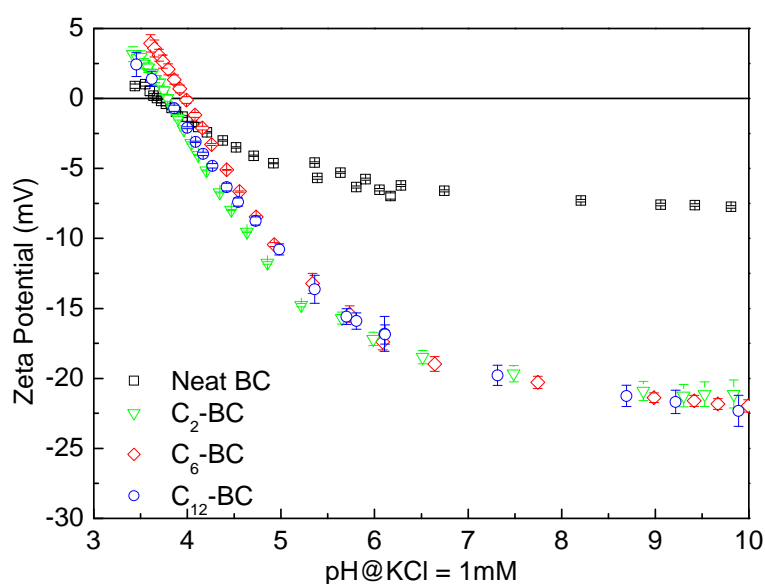
Figure 12: ζ-potentials of neat and modified BC sheets as function of pH measured in 1 mM KCl supporting electrolyte.

3.3.4 Degree of surface substitution (DSS) of modified BC or amount of accessible OH groups
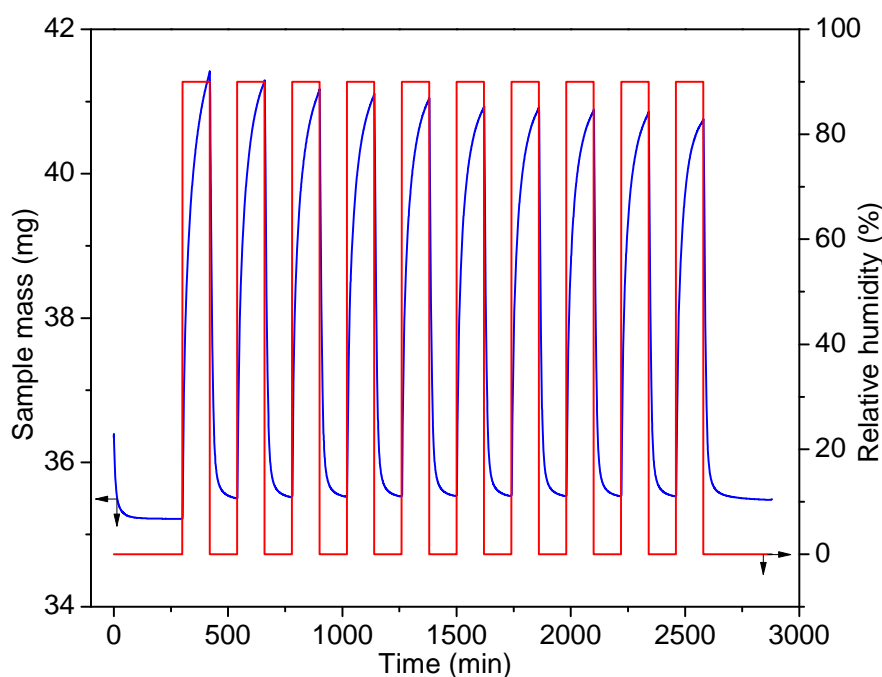
Figure 13. An example of D₂O adsorption on neat BC.

Figure 13 shows a typical example of the dynamic D_2O vapour sorption on neat BC. The amount of accessible hydroxyl groups and the degree of surface substitution are tabulated in Table 9. No bulk sorption of D_2O on bacterial cellulose was observed as only one plateau was seen when exposing neat BC to D_2O for 48 h at 90% RH (see Figure 14). Our results are also in agreement with results obtained by other researchers.[140] In order to access the bulk of bacterial cellulose, high temperature annealing of cellulose is required. Goussé et al.[141] have determined the amount of accessible hydroxyl groups of tunicin whiskers based on geometrical calculations. The authors arrived at a value of 1.5 (out of a maximum of 3). In this study, the amount of accessible hydroxyl groups of neat BC was found to be 1.24. This value is very close to the theoretical predictions of Goussé et al.[141] The discrepancy can be attributed to the difference in crystal structure between BC and tunicin whiskers (BC is rich in I_α,[142] while tunicin whiskers are thought to have a I_β structure[143]). In addition to this, the formation of hydrogen bonds between freeze-dried BC nanofibres can occur, which will lower the amount of accessible hydroxyl groups. As the carbon chain length of the organic acid used for the surface modification of BC nanofibres increases and its reactivity decreases, the amount of hydroxyl groups

present on the modified surface increases. In addition to this, packing efficiency between BC nanofibres will also be affected by the esterification. Hydrogen bonds between BC nanofibres arise from the presence of large amounts of OH groups on the surface of neat BC. However, the packing efficiency reduces as a result of the grafted long chain hydrocarbon. It is thought that the longer the grafted hydrocarbon chain, the lower the packing efficiency. Therefore, the effective hydrogen bonds between the BC nanofibres will no doubt decrease.
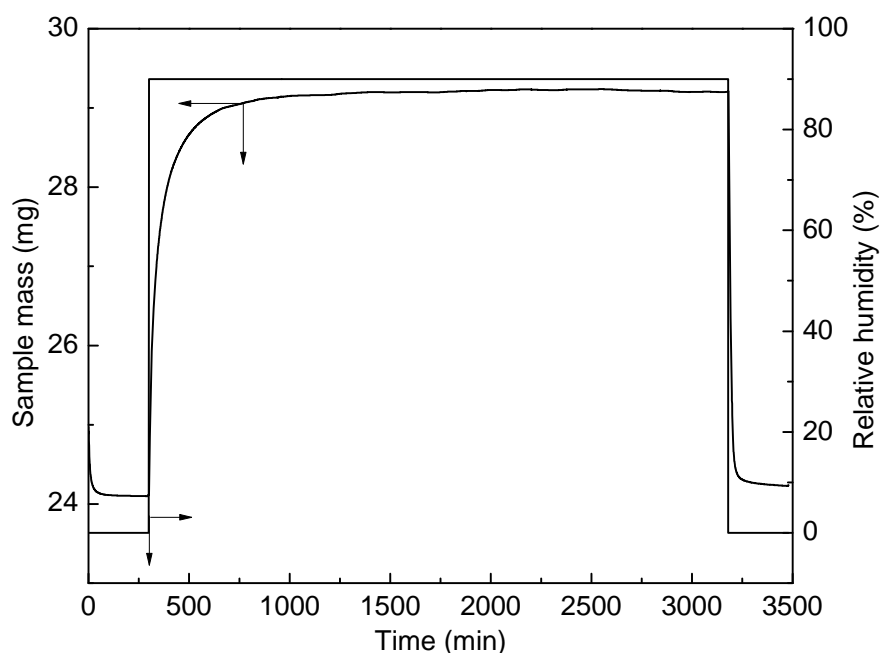
Figure 14. DVS of neat BC exposed to D_2O for 48 h at 90% relative D_2O humidity

3.3.5 XRD of neat and modified BC

Crystallographically, BC has a cellulose-I structure.[115] Its X-ray diffraction pattern is shown in Figure 15. The peaks shown correspond to the diffraction planes of 101, $10\bar{1}$, 002 and 040, respectively.[144] No peak shifting or appearance of new peaks was observed (Figure 15). This is further evidence to suggest that the surface modification of BC with organic acids occurred essentially only on the surface of or in the amorphous region of BC. The crystallinity of neat and modified BC as determined using the Segal-equation is tabulated in Table 10. It can be seen that the acetic acid modification led to a slight decrease in the BC crystallinity. This can be explained by the high reactivity of acetic acid compared to hexanoic and dodecanoic acids.[133] As already mentioned, the high reactivity of acetic acid can lead to more ester bond formation on BC. This result is also in agreement with the ATR-IR

spectra of C_2-BC, where the intensity of the adsorption band for carbonyl bonds is significantly higher than for C_6-BC and C_{12}-BC. As a comparison, the degrees of crystallinity of the (modified) BC were also calculated based on the crystalline and amorphous areas. Discrepancies of the crystallinity values can be seen between Segal's method and the crystallinity calculated based on the area under the XRD spectra. Similar results were also presented in the literature.[145] The original work by Segal et al.[130] was based on cotton cellulose, which is also pure cellulose. This aspect is very similar to bacterial cellulose, which is pure crystalline cellulose without other impurities. Since this current work compares cellulose from the same source (similar to Segal et al.[130] have conducted), it can be assumed that crystallinity based on Segal's method is preferred and valid for this work.
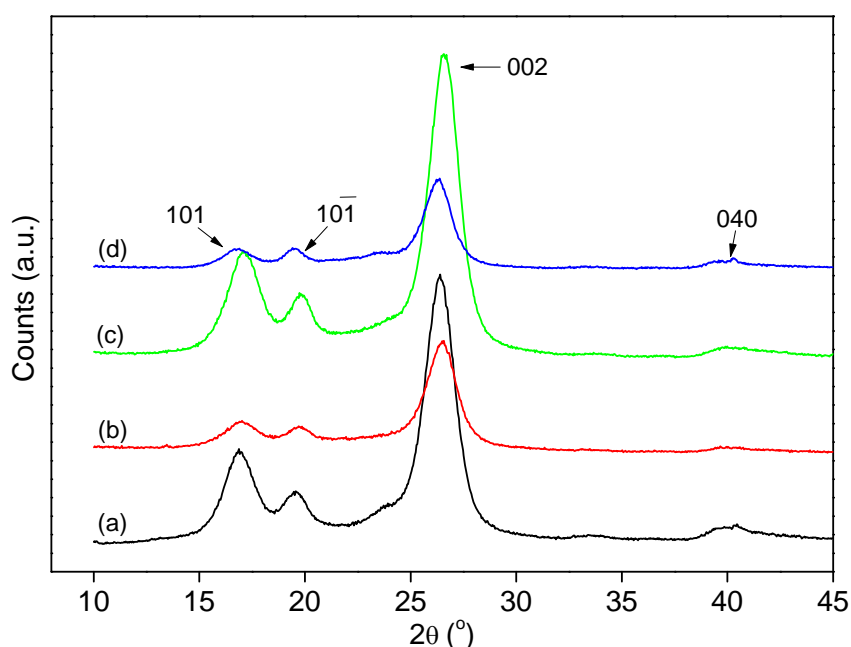
Figure 15. X-ray diffraction pattern of (a) Neat BC, (b) C_2-BC, (c) C_6-BC, (d) C_{12}-BC with the 101, 10$\bar{1}$, 002 and 040 reflections identified.

Table 10. Degree of crystallinity (χ_c), full width at half maximum (FWHM) of the 002 diffraction peak at $2\theta = 22.5°$, crystallite size of 002 reflection ($L_{(002)}$) and the calculated interlayer distance ($d_{(002)}$) for neat and modified BC.

Sample	χ_c (%)[§]	FWHM (°)	$L_{(002)}$ (Å)	$d_{(002)}$ (Å)	χ_c (%)[&]
Neat BC	90.2 ± 0.2	1.71 ± 0.02	60.81 ± 0.54	7.85 ± 0.01	74.4 ± 0.2
C_2-BC	83.2 ± 0.2	1.73 ± 0.01	60.40 ± 0.39	7.81 ± 0.01	59.6 ± 0.8
C_6-BC	89.7 ± 0.5	1.70 ± 0.02	61.26 ± 0.52	7.79 ± 0.02	70.6 ± 2.4
C_{12}-BC	85.1 ± 0.9	1.60 ± 0.01	64.93 ± 0.24	7.87 ± 0.01	69.3 ± 5.7

§ Crystallinity calculated based on Segal's method.

& Crystallinity calculated based on integrated area of XRD spectrum.

3.3.6 Thermal degradation behaviour of neat and modified BC
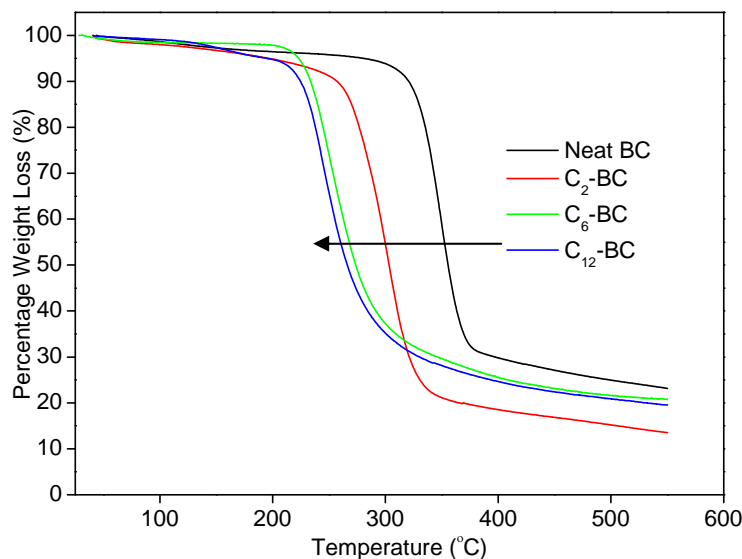
Figure 16. Percentage weight loss as a function of temperature for neat and modified BC.

Figure 16 shows the thermal degradation behaviour of neat and modified BC. All the samples underwent single step degradation. It can also be seen that the onset of degradation (defined as temperature at which 10% mass loss occurred) shifted to lower temperature with increasing carbon chain length of organic acids attached to the surface of BC (Table 11). Similar results were also obtained by Jandura et al.,[146] who modified pulp fibres with oleic and stearic acids. By increasing the carbon chain length, the temperature at which the maximum rate of weight loss (the peak of the derivative curves) decreased. This is thought the due to the reduced number of effective hydrogen bonds between BC nanofibres, as the nanofibres can then not be closely packed. In addition to this, as the amount of hydroxyl groups decreased due to the esterification reaction, the number of potential hydrogen bonds that can be formed decreased too. This results in the reduction of hydrogen bonds formation between nanofibres, which further reduces the thermal stability when compared to neat BC.

Table 11. The onset degradation temperature of neat and modified BC.

Samples	Onset degradation temperature (°C)
Neat BC	319
C_2-BC	259
C_6-BC	233
C_{12}-BC	225

3.4 Conclusions

The hydrophilic surface of BC was rendered hydrophobic via an esterification reaction with organic acids (acetic, hexanoic and dodecanoic acids). It was found that the degree of hydrophobicity of BC can be tailored by the carbon chain length of the organic acids used to modify BC. The amount of accessible hydroxyl groups on the surface of BC was determined using a H/D exchange method implemented using dynamic vapour sorption of D_2O and it was found to be 1.24 (out of a maximum of 3). In addition to this, the degree of surface hydroxyl group substitution decreases with increasing carbon chain length of the organic acids used. The esterification reaction did not alter the crystallinity of BC significantly, with C_2-BC being the exception. The decrease in the crystallinity of C_2-BC was attributed to the higher reactivity of acetic acid as compared to hexanoic and dodecanoic acid, which led to higher degree of modification. The thermal behaviour of neat and organic acid modified BC sheets decreased with increasing carbon chain length of the organic acids used. This is evidence of low packing efficiency, arising from the grafted hydrocarbon chains and, therefore, the reduced overall interaction between the nanofibres. As a result of the modification, the hydrophobic BC can easily be dispersed in hydrophobic PLLA and the compatibility (interfacial adhesion) to PLLA could be improved. Therefore, the mechanical properties of the resulting (modified) BC reinforced PLLA nanocomposites was improved (see chapter 4).

Chapter 4 – Heterogeneous modification of bacterial cellulose: Why do cellulose nanofibres behave differently when modifying freeze-dried or never-dried bacterial cellulose?

Summary

The susceptibility of (i) never-dried and (ii) freeze-dried bacterial cellulose (BC) with towards organic acid esterification is reported in this work. When never-dried BC (BC that was solvent exchanged from water through methanol into pyridine) was modified with hexanoic acid, it was found that the degree of substitution (DS) was significantly lower than that of modified freeze-dried BC. The crystallinity of freeze-dried BC hexanoate was found to be significantly lower compared to neat BC and never-dried BC hexanoate. This result, along with the high DS indicates that significant bulk modification occurred during the esterification of freeze-dried BC. Such results were not observed for never-dried BC hexanoate. All these evidence point towards to fact that freeze-dried BC was more susceptible to organic acid esterification compared to never-dried BC. A few hypotheses were proposed to explain the observed behaviour and further investigated to elucidate our observation; the effect of residual water in cellulose, the accessibility of hydroxyl groups and the crystal structure of never-dried and freeze-dried BC on the susceptibility of cellulose fibrils to the esterification, respectively. However, the investigation of these hypotheses raised more questions and the main question still remains; why do BC nanofibres behave differently when modifying freeze-dried BC or never-dried BC?

4.1 Introduction

Cellulose is the most abundant organic homopolymer on earth. It is a macromolecular polymer consisting of two D-anhydroglucose rings linked by β (1→4) glycosidic bonds.[147] Cellulose is used in numerous industries; the pulp and paper industry,[110] the pharmaceutical and cosmetic industry[109] and more recently

as reinforcement for polymers.[118, 148-150] Due to the rapid advancement and interest in nanotechnology, significant effort has been poured into the utilisation and isolation of nano-sized cellulose to produce nanocellulose for various applications. Nanocellulose can be obtained via two approaches; the top-down or bottom-up approaches. The top-down approach involves the disintegration of plant cellulose, such as wood fibres, using high shear forces[151, 152]. The bottom-up approach, on the other hand, utilises the biosynthesis of cellulose by bacteria, such as from the *Acetobacter* species.[153]

Although nanocellulose can be produced using the two approaches, the quality of bacterial cellulose (BC) was found to be superior over wood-derived nanocellulose.[154] This can be attributed to the high purity and water-absorbing capability of BC. Additionally, no further processing is required to obtain nano-sized cellulose. In addition to this, BC possesses a high degree of crystallinity of up to 90%.[120] Hsieh et al.[6] determined the mechanical properties of a single BC nanofibre using Raman spectroscopy. The authors estimated that a single BC nanofibre possesses a Young's modulus of 114 GPa. It was also predicted that cellulose crystals should possess a theoretical Young's modulus of between 130 and 160 GPa depending on the crystal form.[121, 122] These properties are highly favourable for the utilisation of nanocellulose as filler for composites. However, the hydrophilic nature of cellulose often resulted in poor interfacial adhesion between the cellulose and hydrophobic polymer matrices [13, 155], such as polypropylene and polylactic acid. Surface modification of nanocellulose is often performed to improve the compatibility and, therefore, the stress transfer between the cellulose and the matrix to produce nanocomposites with improvements in both modulus and strength.[123, 148, 156]

The chemical modification of BC presents an interesting scenario. Since BC is produced through the biosynthesis of bacteria in a culture medium, BC stays hydrated and so is never-dried. The successful surface-only modification of never-dried BC with organic acids has been reported.[123, 157] The procedure involved the solvent exchange of never-dried BC from water through methanol into pyridine. Attempts were made to reduce the laborious solvent exchange step by freeze-drying the BC from water and disperse freeze-dried BC, which does not hornify, directly

into pyridine to carry out the same esterification with organic acids. In this study, evidence is provided that freeze-dried BC is much more susceptible towards esterification with organic acid compared to never-dried BC. Possible hypotheses of the observed susceptibility of freeze-dried BC towards organic esterification are presented and have been further investigated in this study.

4.2 Experimental procedure

4.2.1 Materials

Methanol (GPR, purity $\geq$ 99%), ethanol (GPR, purity $\geq$ 99.7%), benzene (analaR NORAMPUR, purity $\geq$ 99.9%) and pyridine (analaR NORAMPUR, purity $\geq$ 99.7%) were purchased from VWR. Hexanoic acid (Aldrich, purity $\geq$ 99%), *p*-toluenesulfonyl chloride (Aldrich, purity $\geq$ 99%), dimethyl carbonate (Aldrich reagent plus, purity $\geq$ 99%), deuterium oxide (Aldrich, purity $\geq$ 99.99 atom% D), cellulose acetate (Aldrich, 39.7 wt% acetyl content) and cellulose triacetate (Aldrich, 43-49 wt% acetyl content) were purchased from Sigma-Aldrich. Sodium hydroxide (purum grade, pellets) was purchased from Acros Organics. All the materials were used as received without further purification. BC was extracted and purified from commercially available *Nata-de-coco* (CHAOKOH gel in syrup, Ampol Food Processing Ltd, Nakorn Pathom, Thailand) following previously described work.[139]

4.2.2 Hexanoic acid esterification of BC

In order to modify never-dried BC, which was always kept in water, 2 g (on dry weight basis) of the purified BC was solvent exchanged from water through methanol (3 × 600 cm^3) and into pyridine (2 × 600 cm^3) to ensure the complete removal of water and methanol. The mixture was homogenised using a homogeniser (Polytron PT 10-35 GT, Kinematica, CH) at 20,000 rpm for at least 1 min during each solvent exchange step to completely disperse the BC in the solvent. BC was retained through centrifugation at 14,000g for 15 min. The excess solvent was decanted prior to re-dispersion in the subsequent solvent. This homogenisation/centrifugation step was repeated three times. After the second solvent exchange step into pyridine, another solvent exchange step was performed to adjust the final concentration of BC in pyridine to 0.5% (g mL^{-1}). This BC-pyridine mixture was then poured into a 1 L 3-neck round bottom flask and stirred using a

magnetic stirrer. 92 g of *p*-toluenesulfonyl chloride was added into this BC-pyridine mixture and hexanoic acid was added at an equimolar concentration relative to *p*-toluenesulfonyl chloride into the same reaction vessel after the addition of *p*-toluenesulfonyl chloride. The reaction was conducted under nitrogen flow to create an inert atmosphere for 2 h at 50ºC. After 2 h, the reaction was quenched with 1.5 L of ethanol. The product was washed three times with 800 mL of ethanol using the previously described homogenisation-centrifugation steps.

In a separate experiment, the never-dried BC was homogenised in water at a concentration of 0.4% (g mL^{-1}), flash frozen in a Petri dish and subsequently freeze-dried (Edwards Modulyo freeze dryer, West Sussex, UK). This BC is termed freeze-dried BC throughout this study. 2 g of freeze-dried BC was dispersed into 400 mL (0.5 % (g mL^{-1})) of pyridine directly in a 1 L 3-neck round bottom flask and the reaction was conducted as previously described. After 2 h, the hexanoic acid modified freeze-dried BC was purified following the procedure described above. In order to characterise the hexanoic acid modified wet BC and freeze-dried BC, they were solvent exchanged from ethanol through water into dimethyl carbonate at a concentration of 0.4% (g mL^{-1}), flash frozen in a Petri dish and subsequently freeze-dried from dimethyl carbonate to obtain dry modified samples that were further characterised. The never-dried BC hexanoate and freeze-dried BC hexanoate are termed C$_6$-NDBC and C$_6$-FDBC, respectively.

4.2.3 Characterisation of the modified (never-dried and freeze-dried) BC
4.2.3.1 Attenuated Total Reflection Infrared spectroscopy (ATR-IR)
ATR-IR spectra were recorded using a Spectrum One FTIR-spectrometer (Perkin Elmer, Massachusetts, USA). The spectra were collected at a resolution of 2 cm^{-1}, in the range of 600 cm^{-1} and 4000 cm^{-1}. A total of 16 scans was used to collect each spectrum.

4.2.3.2 Degree of substitution of modified BC
The degree of substitution (DS) of C$_6$-NDBC and C$_6$-FDBC was determined using the procedure developed by Sassi and Chanzy.[158] The DS was calculated based on the ATR-IR spectra using the absorption band of the pyranose ring as an internal standard at a wavenumber of 1050 cm^{-1}. A calibration master curve was established,

relating the ratio of the absorbance intensities of the carbonyl bonds (1750 cm^{-1}) and pyranose ring's to the known DS for cellulose acetates and cellulose triacetates. By comparing the ratio of the intensities between 1750 cm^{-1} and 1050 cm^{-1} of C$_6$-NDBC and C$_6$-FDBC to the calibration master curve, the DS of the modified BC was obtained.

4.2.3.3 Crystallography of hexanoic modified BC

Structural information of modified BC was obtained using X-ray diffractography. The X-ray diffraction (XRD) pattern was obtained using a PANalytical X'Pert PRO X-ray diffractometer (PANalytical Ltd, Cambridge, UK) . The diffractograms were taken from 2θ = 10º to 45º at a step size of 0.02º using a Ni filtered Cu Kα$_1$ (1.541 Å) as the X-ray source. Segal's method[130] was used to calculate the crystallinity of (modified) BC (see equation 4.1):

$$\chi_c = \frac{I_{002} - I_{am}}{I_{002}} \times 100\%$$
(4.1)

where χ_c is the crystallinity of the cellulose, I_{002} and I_{am} are the intensity of the 002 (2θ = 22.5º) and amorphous (2θ = 18º) reflections, respectively. This is an empirical equation for estimating the degree of crystallinity of pure cellulose materials.

4.2.3.4 Scanning electron microscopy (SEM)

SEM was performed using a high-resolution field emission gun scanning electron microscope (LEO Gemini 1525 FEG-SEM, Oberkochen, Germany). It was used to characterise the morphology of BC nanofibres after esterification with hexanoic acid. The accelerating voltage used was 5 kV. Prior to SEM, the samples were mounted to SEM stubs using carbon tabs and coated with Cr (K550 sputter coater, Emitech Ltd, Ashford, Kent, UK) for 1 min at 75 mA.

4.2.4 Characterisation of neat never-dried and freeze-dried BC

In order to mimic never-dried BC in pyridine prior to hexanoic acid esterification reaction, the never-dried BC was solvent exchanged from water through methanol into benzene using the previously described concentration and homogenisation-

centrifugation steps. Once the never-dried BC was dispersed in benzene, it was subsequently freeze-dried to obtain a dry sample hopefully representative of never-dried BC in pyridine. Benzene was chosen as it is structurally related to pyridine and its ability to be freeze-dried.

4.2.4.1 Determining the residual water content of never-dried and freeze-dried BC

Esterification of cellulose with carboxylic acids is a reversible reaction and the presence of water will affect the conversion of cellulose to cellulose esters. The residual water content of freeze-dried BC was determined using dynamic vapour sorption (DVS-Advantage, Surface Measurement Systems Ltd, Alperton, UK). 30 mg of freeze-dried BC was loaded into the chamber of DVS held at 0% relative humidity (RH) for 5 h. During this period, the mass change was measured *in-situ* inside the chamber. The residual water content was obtained from the difference between the initial and final mass of the sample.

The residual water content in never-dried BC after successive solvent exchange steps was estimated from the solvent exchange efficiency. To determine the solvent exchange efficiency, 2 g (on a dry weight basis) of never-dried BC was dispersed in 600 cm^3 of methanol following the previously described homogenisation step and centrifuged at 14,000g for 15 min after which the supernatant was removed. The water content in this supernatant was determined using Karl-Fischer titration (DL32 Coulometer Titrator, Mettler Toledo, Leicester, UK). The homogenisation-centrifugation-titration step was repeated 5 times (the number of solvent exchange steps in this work). The efficiency of water removal for solvent exchange was calculated using:

$$R_w = \frac{W_{i+1} - W_i}{W_i} \times 100\%$$
(4.2)

where R_w, W_{i+1} and W_i are the water removal efficiency, the water content in solvent exchange step $i+1$ and step i, respectively.

4.2.4.2 Determining the hydroxyl group availability of never-dried and freeze-dried BC

In order to study the difference between the hydroxyl group availability for the esterification reaction of the different starting BC, a method based on hydrogen/deuterium (H/D) exchange was utilised following our previous work.[157] This measurement was carried out using dynamic vapour sorption (DVS-Advantage, Surface Measurement Systems Ltd, Alperton, UK). A sample mass of approximately 30 mg of BC was placed in the sample pan and the sample chamber was pre-conditioned at 0% RH of deuterium oxide (D_2O) for 5 h at room temperature to remove adsorbed water molecules. The RH of D_2O was increased to 90% for 2 h to allow for the adsorption of D_2O and for H/D exchange with accessible hydroxyl groups to occur. The RH was then reduced to 0% for 2 h to allow the D_2O molecules to desorb. This cycle was repeated 10 times such that the H/D can occur on all accessible hydroxyl groups on BC. A short adsorption-desorption cycle was utilised to avoid bulk sorption of BC, as only the accessible hydroxyl groups were of interest. After 10 adsorption-desorption cycles, the sample was post-conditioned at 0% RH for 5 h to remove any residual adsorbed D_2O molecules. As deuterium is one neutron heavier than hydrogen, the mass increase after post-conditioning of BC was measured *in-situ* by an ultra-sensitive microbalance and the amount of accessible hydroxyl groups was back calculated from this mass increase.

4.2.4.3 Specific surface area measurement of never-dried and freeze-dried BC

Nitrogen adsorption/desorption isotherms were performed to determine the specific surface area of never-dried and freeze-dried BC using a surface area and porosity analyser (TriStar 3000, Micrometrics Ltd, Dunstable, UK). The specific surface area was calculated using the Brunauer-Emmett-Teller (BET) equation. Prior to the measurement, the samples were degassed at 80°C overnight to remove adsorbed water molecules.

4.2.4.4 Allomorphs of never-dried and freeze-dried BC

The different allomorphs of crystalline cellulose were evaluated using an empirical mathematical function developed by Wada et al.[159] This mathematical function is supposed to discriminate cellulose I_α, which is triclinic, from cellulose I_β, which is

monoclinic, based on the XRD pattern of the cellulose of interest. The discrimination factor, Z, is related to the d-spacings of the cellulose via:

$$Z = 1693 \times d_1 - 902 \times d_2 - 549 \qquad (4.3)$$

where $Z > 0$ represents I_α-rich cellulose and $Z < 0$ represents I_β-rich cellulose. d_1 (nm) and d_2 (nm) represent the d-spacing of the reflection planes at Bragg's angle of 14° and 16°, respectively.

4.3 Results and Discussion

4.3.1 Degree of substitution of (hexanoic acid modified) BC
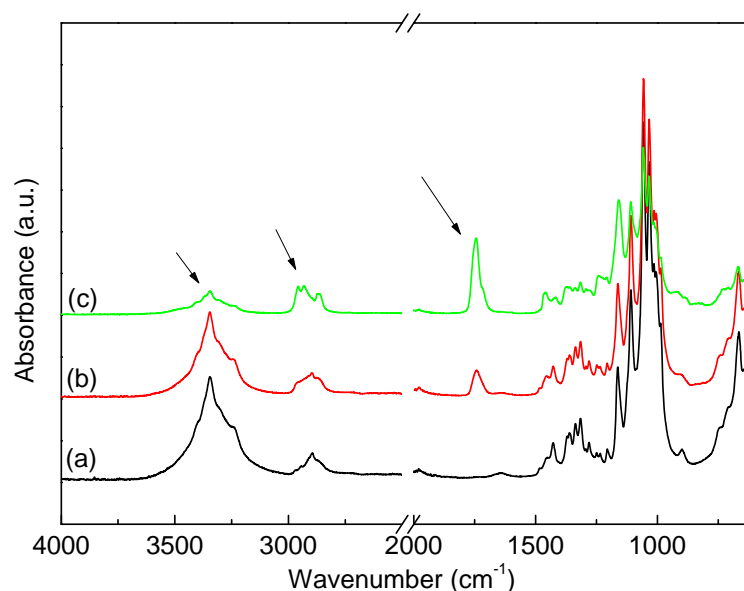
Figure 17: ATR-IR spectra of neat and hexanoic acid modified BC. (a) Neat BC, (b) C6-NDBC and (c) C6-FDBC.

ATR-IR was used to study the chemical characteristics of neat and hexanoic acid modified BC. The spectra are shown in Figure 17. The spectra were normalised against the intensity of the absorption band corresponding to the C-O-C link in cellulose molecules, which is around 1160 cm^{-1}.[132] The appearance of an absorption band around 1750 cm^{-1} for hexanoic acid modified BC can be attributed to carbonyl bonds (C=O), which formed during the esterification of BC with hexanoic acid. Additional peaks can also be seen around 2900 cm^{-1}, which correspond to the absorption of methyl (-CH$_3$) or methylene (-CH$_2$-) groups. It can be seen from these spectra that the intensity of 1750 cm^{-1} is higher when freeze-dried BC was used as

the starting material. In addition to this, the esterification of freeze-dried BC with hexanoic acid resulted in a significant decrease in the intensity of the hydroxyl groups (-OH) around 3300 cm^{-1}. When never-dried BC was used as the starting material for the esterification reaction, the intensity of the carbonyl absorption band was much lower than that of C_6-FDBC. This is due to the higher degree of substitution when freeze-dried BC was used as the starting material compared to never-dried BC (see Table 12).

4.3.2 XRD patterns of BC hexanoate
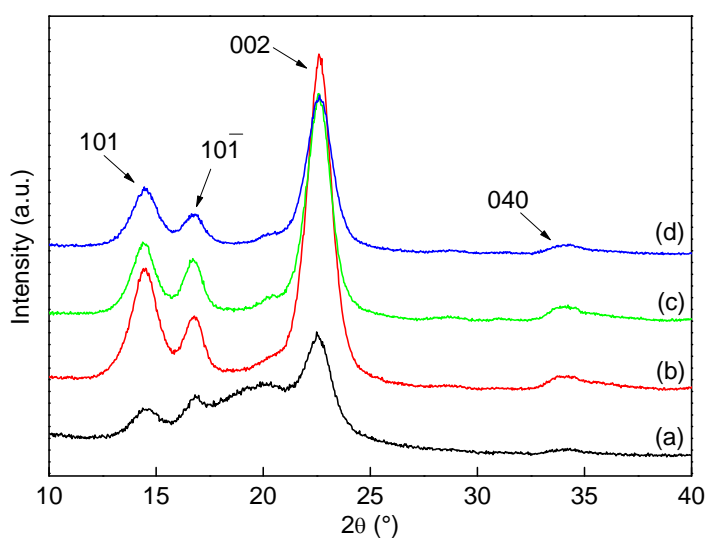
Figure 18: XRD spectra of (hexanoic acid modified) BC. (a) C6-NDBC, (b) C6-FDBC, (c) never-dried BC and (d) freeze-dried BC.

The XRD pattern of BC hexanoate is shown in Figure 18a-b and their crystallinity calculated from the Segal's equation in Table 12. Crystallographically, BC possess a cellulose I structure.[160] The characteristic peaks shown in Figure 18 correspond to the diffraction planes of 101, 10$\bar{1}$, 002 and 040, respectively for cellulose I$_\alpha$.[144] The crystallinity of C_6-NDBC is in good agreement with the crystallinity of neat BC of approximately 90%.[120] This implies that the modification of never-dried BC results in the *surface-only* modification of BC.[157] When freeze-dried BC was modified with hexanoic acid using identical reaction conditions, the XRD pattern of C_6-FDBC showed a significant reduction the intensities of all the diffraction planes. The crystallinity of C_6-FDBC dropped to only 53%, which is an indication that the cellulose loses its crystal structure and becomes more amorphous. These results are in good agreement with the ATR-IR spectra and DS of C_6-FDBC shown previously,

which points towards significant bulk modification of cellulose when freeze-dried BC was used as the starting material.

Table 12: Degree of substitutions and crystallinity (χ_c) of hexanoic acid modified BC.

Sample	Degree of substitution	χ_c (%)
C_6-NDBC	0.36 ± 0.01	91 ± 3
C_6-FDBC	1.87 ± 0.02	53 ± 4

4.3.3 Morphology of BC hexanoate
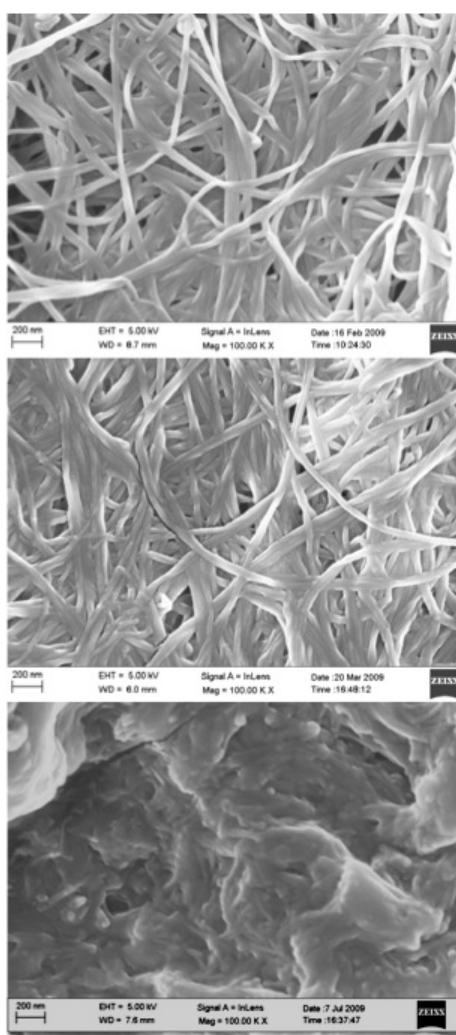
Figure 19: Scanning electron micrographs showing the morphology of neat and modified BC. Top: Neat BC, middle: C6-NDBC and bottom: C6-FDBC.

The morphology of BC before and after hexanoic acid esterification is shown in Figure 19. It can be seen that neat BC possesses a fibrous structure, approximately 50 nm in diameter and several micrometres in length. When BC was modified with hexanoic acid using never-dried BC as the starting material (C_6-NDBC), the fibrous structure of BC is retained (see Figure 19). This result corroborates with the low DS,

high crystallinity (Table 12) and low absorbance intensity at 1750 cm^{-1} in the ATR-IR spectra of C$_6$-NDBC (Figure 17). However, when BC was modified with hexanoic acid using freeze-dried BC as a starting material (C$_6$-FDBC), the original fibrous structure of BC was lost. No fibrous structure can be observed in Figure 19 (bottom). Instead, the modified cellulose resembles a semicrystalline cellulose ester polymer. Similar observations were also reported by Barud et al.,[161] who produced cellulose acetate by the acetylation of BC. This observation is consistent with the high DS and intensity of carbonyl bonds in the ATR-IR spectra, which points towards significant bulk modification during the esterification reaction.

4.4 Hypotheses for the bulk modification of freeze-dried BC and *surface-only* modification of never-dried BC

4.4.1 Could the adsorbed water in cellulose affect the equilibrium of the esterification reaction?

The esterification reaction of cellulose with a carboxylic acid is reversible with cellulose esters and water being the product of the reaction. According to Le Chatelier's principle, the removal of water from the reaction will shift the equilibrium of the reaction to favour the production of more cellulose esters. It has also been reported that the starting form of cellulose (never-dried, partially dried or fully dried) affects the dissolution of cellulose in ionic liquid as the water molecules in the never-dried cellulose reduce the solvent quality.[162] Therefore, it can be anticipated that never-dried BC should result in higher DS, as the presence of water shifts the esterification reaction to the left, producing more cellulose esters. The estimated residual water content for both types of BC is tabulated in Table 13. It can be seen that the efficiency of water removal was much greater through solvent exchange method compared to the direct freeze-drying of BC. This can be attributed to the hydrophilic nature of BC, which absorbs water from the atmosphere. The water removal efficiency of the solvent exchange method was found to be 58 ± 14 (wt/wt)%. Through solvent exchange, wet BC is thoroughly mixed with a solvent, which is miscible with water, and the liquid phase is displaced by centrifugation and then decanted. By repeating this process, the water in wet BC is constantly removed and reduced to a minimum. However, this result contradicts with the DS of the modified BC, which showed freeze-dried BC (with higher residual water content) underwent severe bulk modification but never-dried BC (with lower residual water

content) underwent surface modification only. The reason for this observation is not clear but it implies that the presence of water is not solely responsible for the observed different behaviour of freeze-dried and never-dried BC.

Table 13: A table summarising the estimated residual water content, accessible –OH groups, and specific surface area (S), respectively of never-dried and freeze-dried BC.

Types of BC	Residual water (mg/g cellulose)	Accessible OH group[†]	S (m^2 g^{-1})
Never-dried	13 ± 4	1.12 ± 0.04	92.2 ± 0.1
Freeze-dried	23 ± 6	1.24 ± 0.01	44.6 ± 0.1

[†] maximum value of 3.

4.4.2 Could the accessibility of hydroxyl groups be different between freeze-dried and never-dried BC?

The accessible hydroxyl groups (-OH) of both freeze-dried and never-dried BC is tabulated in Table 13. Never-dried BC and freeze-dried BC were found to possess an accessible –OH group availability of 1.12 and 1.24, respectively out of a maximum of 3. The difference in accessible –OH groups availability is about 10 ± 1%. This difference can be attributed to the different dispersing medium (either water or benzene) when preparing BC. Water is known to swell cellulose, exposing more cellulose –OH groups[163] but non-polar molecules, like benzene, have been shown to reduce the accessibility of the hydroxyl groups of cellulose.[164] As a result, BC freeze-dried from water possesses more accessible hydroxyl groups. Nonetheless, 10% more accessible hydroxyl groups of freeze-dried BC compared to never-dried BC is not significant and does not explain the observed severe modification of freeze-dried BC.

4.4.3 Could the exposed surface area of never-dried and freeze-dried BC affect the severity of the esterification reaction?

There is significant evidence in the literature that freeze-drying cellulose from solvents other than water resulted in a significant increase of the surface area of the nanocellulose.[165-167] Similar results were also found in this work. When BC was solvent exchanged into benzene and freeze-dried (never-dried BC), the surface area is twice as large as BC freeze-dried from water (see Table 13). This implies that the

exposed surface area of never-dried BC in a solvent is higher than that of freeze-dried BC. The larger surface area in an organic solvent is a result of the low surface tension of the solvent. Merchant[168] observed that the surface area of cellulose increases with decreasing surface tension of the organic solvent in which the cellulose was dispersed in. Although no exact reason was given at the time of this work, it can be postulated that better wetting can be expected between high surface energy BC and low surface tension liquids. This results in better dispersion of cellulose fibrils in the solvent and therefore the observed high surface area in low surface tension liquids. Nonetheless, our surface area results contradict the observation of severe bulk modification of freeze-dried BC, which possesses a lower surface area.

4.4.4 Could the crystallography of BC change as a result of drying from different solvents?

Cellulose is a semi-crystalline composite of two different crystalline structures, namely Iα and Iβ, respectively.[169] Cellulose Iα possesses a triclinic structure whereas Iβ has a monoclinic crystalline structure.[142] It was found that cellulose Iβ is the more thermodynamically favourable structure and cellulose Iα can readily be converted to Iβ via routes such as hydrothermal treatment.[170] In addition to this, at equivalent hydroxyl group accessibility, cellulose Iα was found to be more reactive towards acetylation compared to cellulose Iβ.[171] Wada et al.[159] derived an empirical equation (see equation 4.3) providing the ratio of Iα to Iβ based on two equatorial d-spacings of cellulose and these results are tabulated in Table 14, along side with the crystallinities and d-spacings of never-dried and freeze-dried BC. It can be seen from this table that the crystallinities of the two types of BC are the same (~90%), indicating that the significant bulk modification of freeze-dried BC could not be the direct result of differences in the crystallinity of BC.

The XRD patterns of never-dried and freeze-dried BC are shown Figure 18c-d. The two diffraction peaks, d_1 and d_2, are in fact composites of Iα and Iβ reflections.[159] d_1 corresponds to Iα 100 and Iβ $1\bar{1}0$ reflections, respectively whereas d_2 corresponds to Iα 010 and Iβ 110 reflections, respectively. From the calculated d-spacings for the two types of cellulose, the Z value (which discriminates between Iα-rich and Iβ-rich)

can be computed. Based on the calculated Z value, never-dried BC is rich in cellulose Iβ whereas freeze-dried BC is cellulose Iα dominant. Combining this result with the –OH group accessibility of freeze-dried BC, which is 10% higher than that of never-dried BC, it implies that freeze-dried BC is more susceptible to esterification compared to never-dried BC. This is consistent with our observations. However, this raises the next question; why should BC, which is known to be cellulose Iα, have a cellulose Iβ structure when dried from an organic solvent? There was significant evidence that points towards the fact that the surface tension of dispersing medium affects the exposed surface area of cellulose [166-168]. It was also speculated by Merchant[168] that the crystal structure of cellulose would be different when dried from different solvents due to the difference in polarity of the solvents.

Table 14: The crystallinity (χ_c), d-spacings of the reflection at 14° (d_1), 16° (d_2) and the discriminant value between Iα and Iβ (Z), respectively of never-dried and freeze-dried BC

Types of BC	χ_c (%)	d_1 (nm)	d_2 (nm)	Z value
Never-dried	90 ± 4	0.611	0.614	− 0.78 (Iβ-rich)
Freeze-dried	89 ± 3	0.528	0.531	13.87 (Iα-rich)

4.5 Conclusions

This study observed that BC freeze-dried from water is more susceptible towards organic acid esterification than never-dried BC. It was found that freeze-dried BC underwent significant bulk modification with degree of substitution of 1.87 compared to never-dried BC of only 0.36. The crystallinity of the freeze-dried BC decreased to only 53% (from the original of 90%) after the modification whilst the crystallinity of never-dried BC did not change significantly with modification. A few hypotheses to explain the observed behaviour were explored; the effect of residual water, accessibility of –OH groups and crystal structure of the cellulose, respectively. These results were found to be in disagreement with experimental observations. Never-dried BC, which was solvent exchanged from water through methanol into pyridine, was found to contain less residual water compared to freeze-dried BC. This implies that significant bulk modification should occur in never-dried BC as the lack of water should shift the equilibrium of the esterification reaction to the right, producing more cellulose esters. However, it was freeze-dried BC, which has higher water content, that underwent significant bulk modification. Freeze-dried

BC was found to possess 10% more accessible –OH groups compared to never-dried BC. However, 10% more –OH groups is very unlikely to result in an 80% increase in the degree of substitution of modified cellulose. XRD pattern show that freeze-dried BC is cellulose $I\alpha$-rich and never-dried BC is cellulose $I\beta$-rich. It has been shown that cellulose $I\alpha$ is more susceptible to acetylation compared to cellulose $I\beta$. It was postulated that it is this combination of more exposed –OH groups and the cellulose $I\alpha$ structure of freeze-dried BC that resulted in significant bulk modification of the cellulose compared to never-dried BC under identical reaction conditions. However, the main question that needs to be raised is why does never-dried BC, which was obtained by freeze-drying from an organic solvent is found to possess a cellulose $I\beta$ structure while it is well accepted that BC possesses a cellulose $I\alpha$ structure?

Chapter 5 – Surface functionalisation of bacterial cellulose as the route to produce green polylactide nanocomposites with improved properties

Summary

The effect of surface functionalisation of bacterial cellulose nanofibrils (BC) and their use as reinforcement for polylactide (PLLA) nanocomposites was investigated. BC was functionalised with various organic acids via an esterification reaction. This rendered the otherwise hydrophilic BC hydrophobic and resulted in better compatibility (interfacial adhesion) between PLLA and BC. A direct wetting method, allowing the determination of the contact angle of polymer droplets on a single BC nanofibre, was developed to quantify the interfacial adhesion between PLLA and functionalised BC. It was found that the contact angle between PLLA droplets and functionalised BC decreased with increasing chain lengths of the organic acids used to hydrophobise BC. A novel method to compound BC with PLLA based on thermally induced phase separation (TIPS) to yield a dry form of pre-extrusion composite was also developed. The mechanical properties of the surface functionalised BC reinforced PLLA nanocomposites showed significant improvements when compared to neat PLLA and BC reinforced PLLA. The thermal degradation and viscoelastic behaviour of the nanocomposites were also improved over neat PLLA.

5.1 Introduction

Recent interest in greener polymeric materials for general applications such as packaging and the public's growing demand for environmentally friendlier products have sparked the development of green composite materials.[108] One of the most extensively studied renewable reinforcements in this field is cellulose. Cellulose is the most abundant natural polymer, found in plant cells walls, and synthesised by

some bacteria and animals. The use of cellulosic materials in the production of green composites is well established. Numerous studies have focussed on the use of natural fibres in the production of composite materials.[4, 10, 12, 14-16] More recently, Juntaro et al.[11] and Pommet et al.[13] have successfully deposited bacterial cellulose onto natural fibres, thereby creating hierarchical composites with improved mechanical properties. Extensive research in the field of natural fibre reinforced composite materials is not surprising as natural fibres have many distinct advantages over conventional glass fibres. These include low cost, low density, high toughness, biodegradability and most importantly, carbon neutrality.[20, 21] As a matter of fact, major automotive companies in Germany such as Mercedes Benz and BMW have started to replace their glass fibre based composites with natural fibre reinforced plastics for their door panel and boot linings.[172] Rieter Automotive won the JEC Composites Award in 2005 for their development in natural fibre reinforced thermoplastic for an under-floor module with integrated aerodynamic, thermal and acoustic functions.[23]

Cellulose derived from bacteria such as from the *Acetobacter* species[115] has the advantage of being free from wax, lignin, hemicellulose and pectin, which are present in plant-based cellulosic material. BC is highly crystalline, with a degree of crystallinity of about 90%.[120] This highly crystalline structure of BC is a property that is favourable for composite production as it provides a high Young's modulus value to BC. It was found that BC possesses high Young's modulus of about 114 GPa and a theoretical Young's modulus of between 130 GPa to 145 GPa depending on the crystallinity.[6] This value is comparable to man-made glass fibres (~70 GPa) and aramid fibres (~67 GPa), considering that BC has a lower density (1.25 g cm^{-3}) than glass fibres (2.5 g cm^{-3}). Natural fibres, on the other hand, possess much lower Young's moduli; cotton (12.6 GPa), jute (26.5 GPa), flax (27.6 GPa) and sisal (22 GPa), respectively.[5] Unlike natural fibres, which has to be microfibrillated to produce cellulose strands in the order of 1-100 nm in diameter,[173] BC exists naturally as a nano-sized material (between 24-86 nm in diameter and several micrometres in length)[115, 119] and it has a surface area of about 150 m^2 g^{-1}.[174] Such properties are highly advantageous for the production of composite materials as this implies that for the same amount of material, the interface between the matrix and the reinforcement will be larger for BC compared to micrometre-scale natural fibres.

However, these interesting properties of BC do come with a price as BC is extremely hydrophilic in nature. As a result, BC will often have poor interfacial adhesion between hydrophobic polymer matrices such as polylactide.[13] Therefore, it can be anticipated that the highly crystalline structure of BC can be retained when functionalisation with hydrophobic groups is performed only on the surface of BC. By preserving the crystalline structure of BC, the Young's modulus will not be affected much and by combining it with a biodegradable polymer, truly green nanocomposites can be produced.

Poly(L-Lactic Acid) (PLLA) is a biodegradable, hydrophobic aliphatic thermoplastic polyester, derived fully from renewable resources such as corn, starch or sugarcane. It belongs to the family of poly(α-hydroxy acids) and is degraded principally via hydrolysis and to a lesser extent either though enzymatic attack.[4, 175] PLLA has been used in biomedical applications but its application is somewhat limited by its inherently poor properties such as poor impact strength, low thermal stability and narrow processing windows.[176] Modifications to PLLA are necessary such that it can compete with the conventional "big four" (PP, PE, PS, PVC) and engineering polymers.

In this work attempt were made to produce green nanocomposites using functionalised BC to improve the interfacial adhesion between BC and hydrophobic PLLA. BC was functionalised using various organic acids (acetic acid, hexanoic acid and dodecanoic acid). A direct wetting method was developed to determine the contact angle of PLLA on these surface functionalised BC. A method based on thermally induced phase separation (TIPS) was adapted from the literature[177] to produce composite microspheres which enables the compounding of dry BC in the polymer using conventional extrusion. The mechanical properties, thermal behaviour and viscoelastic properties of the nanocomposites were also characterised.

5.2 Experimental
5.2.1 Materials
PLLA was purchased from Biomer (L9000, MW $\geq$ 150 kg mol^{-1}, D-content $\approx$ 1.5%) and was used as the matrix for the production of nanocomposites. 1,4-Dioxane (Sigma-Aldrich, ACS Reagent, $\geq$ 99% purity) was used as the solvent for PLLA.

Pyridine (analaR NORAMPUR, ≥ 99.7% purity), methanol (GPR, ≥ 99% purity), ethanol (GPR, ≥99% purity) and acetic acid (analaR, ≥ 99.8% purity) were purchased from VWR. Hexanoic acid (Aldrich, ≥ 99.5% purity), dodecanoic acid (Aldrich, ≥ 98% purity), dimethyl carbonate (Aldrich Reagent Plus, ≥ 99% purity) and *p*-toluenesulfonyl chloride (Aldrich, ≥ 99% purity) were purchased from Sigma-Aldrich. Sodium hydroxide (purum grade, pellets) was purchased from Acros Organics. All the purchased materials were used as received without further purification. BC was extracted from commercially available *Nata-de-coco* (CHAOKOH coconut gel in syrup, Ampol Food Processing Ltd, Nakorn Pathom, Thailand).

5.2.2 Extraction and purification of BC

BC was extracted from *Nata-de-coco* in batches of 5 jars (of net weight 500 g each). For each batch of 5 jars, the coconut gels content was rinsed 3 times with 5 L of de-ionised water and blended for 1 min using a laboratory blender (Waring Blender LB20EG, Christison Particle Technologies, Gateshead, UK). The blended BC was then homogenised at 20,000 rpm in 5 L of water for 2 min using a homogeniser (Polytron PT 10-35 GT, Kinematica, Switzerland) and centrifuged at 14,000g to remove excess water. In order to purify the BC, the centrifuged BC was re-dispersed in 5 L of de-ionised water and boiled in 0.1 M NaOH solution at 80°C for 20 min to remove any remaining microorganisms and soluble polysaccharides.[128] The purified BC was then successively centrifuged and homogenised to neutral pH.

5.2.3 Surface functionalisation of BC

A functionalisation protocol, developed for the modification of natural fibres was adapted from the literature[146, 178] and modified for the derivatisation of BC. A dry weight equivalent of 2 g of the purified bacterial cellulose (wet) was solvent exchanged from water through methanol into pyridine at a concentration of 0.3% (g mL^{-1}) to ensure the complete removal of water and methanol. The mixture was homogenised at 20,000 rpm for at least 1 min at each stage to completely disperse BC in the solvent. BC was retained through centrifugation at 14,000g for 15 min prior re-dispersion in the subsequent solvent. The solvent exchange method was used in this case due to the inability of (vacuum) dried BC to re-disperse in any medium because of the strong hydrogen bonds formed between the nanofibrils. In the final

solvent exchange step, the concentration of BC in pyridine was adjusted to 0.5% (g mL^{-1}). From the authors' experiences, this is the concentration at which the mixture can be stirred properly. At higher concentrations, the mixture becomes too viscous to stir. This BC-pyridine mixture was poured into a 1 L 3-neck round bottom flask and stirred using a magnetic stirrer. 92 g (0.48 mol) of *p*-toluenesulfonyl chloride was added into the reaction vessel and an equimolar amount of organic acids was added into the vessel after the addition of *p*-toluenesulfonyl chloride. The reaction was conducted for 2 h at 50°C under nitrogen flow to create an inert atmosphere such that water vapour does not affect the esterification reaction. After the reaction, the reaction medium was subsequently quenched with 1.5 L of ethanol and washed 3 times with 800 mL of ethanol using the previously described homogenisation-centrifugation steps. The product was solvent exchanged from ethanol to water using this method. In order to use the BC in later stages, the product was freeze-dried. Neat and functionalised BC were dispersed in water and dimethyl carbonate respectively at a concentration of 0.4% (g mL^{-1}), flash frozen in Petri-dishes by immersion in liquid nitrogen and subsequently freeze-dried (Edwards Modulyo freeze dryer, West Sussex, UK). The BC functionalised with acetic acid, hexanoic acid and dodecanoic acid were termed C$_2$-BC, C$_6$-BC and C$_{12}$-BC, respectively.

5.2.4 Direct wetting measurement of functionalised BC

In order to investigate the wettability of individual functionalised BC by PLLA melts, a method developed to study the wetting of carbon nanotube by polymers was adapted from the literature.[179] Approximately 4.4 mg of PLLA was dissolved in 5 mL of chloroform (0.06 wt%). The solution was left overnight to ensure PLLA fully dissolved in the solvent. Another suspension was prepared by dispersing 3.7 mg of BC in 5 mL of chloroform (0.05 wt%). This suspension was homogenised for 2 min at 20,000 rpm. The polymer solution was then added into this suspension and the resulting mixture homogenised again for 2 min at 20,000 rpm followed by ultrasonication for 1 h in a low powered ultrasonic bath to ensure adequate nanofibril dispersion. The mixture of PLLA and BC was added drop wise slowly into a 200 mL hexane/chloroform non-solvent bath (80:20 by weight) under magnetic stirring to precipitate PLLA onto individual cellulose nanofibrils. Precipitates were filtered using a PTFE membrane (47 mm diameter, 0.2 μm pore size, Sartorius Stedium Biotech, UK). The filter cake was heated for 30 min at 180°C while it is still on the

PTFE membrane to melt to polymer. This filter cake was then investigated using a high-resolution scanning electron microscope (LEO Gemini 1525 FEG-SEM, Oberkochen, Germany). The contact angles of the polymer droplets on the cellulose nanofibrils were determined using the generalised height-length method described in literature.[180]

5.2.5 Preparation of composite microspheres with 2 wt% and 5 wt% BC loading

Most BC reinforced polymer composites fabrication methods in the literature are based on solution casting method.[20, 105, 181, 182] Whereby, dry BC sheets are immersed in the polymer solutions and a composite is obtained by evaporation of the polymer solvent. In this work, a novel method based on TIPS[177] to produce composite microspheres was exploited. This method enables the homogeneous dispersion of dry BC in a polymer melt using conventional extrusion processes at later stages. 153 mg (2 wt%) and 395 mg (5 wt%) of freeze-dried BC were added into 90 mL of 1,4-dioxane, respectively and homogenised at 20,000 rpm to disperse them in the 1,4-dioxane. PLLA pellets (7.5 g) were added into each mixture and left to dissolve overnight at 60°C under magnetic stirring. The resulting mixture was then poured into a 50 mL syringe and added drop wise into a bath of liquid nitrogen to rapidly induce the phase separation. The precipitates were collected in a 500 mL round bottom flask and subsequently freeze-dried to yield porous composite microspheres.

5.2.6 Processing of composite microspheres and the production of nanocomposite films

The produced composite microspheres were fed into a twin-screw micro-extruder (5 cm³ micro-extruder, DSM research BV, NL) kept at a melt temperature of 180°C and a screw rotational speed of 10 rpm. After the addition of all the microspheres, the screw speed was increased to 40 rpm for 30 min to promote mixing of BC in the polymer melt. Finally, the polymer melt was extruded at a screw rotation speed of 20 rpm. These extrudates were pelletised and compression moulded into films using a hot press (George E Moore and Sons, Birmingham UK) at 180°C and a pressure of 20 kN for 2 min. The resulting films were left to cool down to room temperature naturally. Neat PLLA films were processed similarly.

5.2.7 Characterisation of bacterial cellulose nanofibrils and its PLLA nanocomposites

5.2.7.1 Scanning electron microscopy (SEM)

SEM was performed using a high resolution field emission gun scanning electron microscope (LEO Gemini 1525 FEG-SEM, Oberkochen, Germany). It was used to characterise the composite microspheres, filter cakes from the direct wetting measurement and the morphology of the functionalised BC. The accelerating voltage used was 5 kV. To enable observation of the microsphere's interior, the microspheres were frozen in liquid nitrogen and bisected using a scalpel. Prior to the SEM, all the samples were fixed onto SEM stubs using carbon tabs and Cr coated for 1 min at 75 mA.

5.2.7.2 Mechanical testing of the nanocomposite films

Nanocomposite and neat PLLA films, were cut into dog-bone shaped samples using a Zwick cutter (Zwick GmbH and Co. KG, Ulm, Germany). These dog bone shaped samples had an overall length of 75 mm, gauge length of 30 mm, thickness of 0.2 mm, the narrowest part of the sample was 4 mm. Tensile tests were conducted in accordance to BS EN ISO 527: 1996 using an Instron universal material testing machine (Instron 4502, Instron Corporation, Massachusetts, USA). The testing speed and load cell used were 1 mm min^{-1} and 1 kN, respectively.

5.2.7.3 Effect of functionalised BC on the molecular weight of PLLA

The effect of the extrusion process with and without functionalised BC on the molecular weight of PLLA was investigated using gel permeation chromatography (GPC). The weight-averaged molecular weight (M_w) and polydispersity of the polymer were evaluated using conventional GPC with a refractive index detector and a PLgel 10 μm mixed bed-B column. Chloroform was used as the effluent at 30°C (flowrate was 10 mL min^{-1}). Prior to the injection, the nanocomposite and neat PLLA samples were dissolved in 10 mL of chloroform overnight and the solutions were filtered through a glass fibre pre-filter and a 0.2 μm polyamide membrane.

5.2.7.4 Differential scanning calorimetry (DSC) study of the nanocomposites

The crystallisation and melting behaviour of the BC reinforced PLLA nanocomposites and neat PLLA were investigated using DSC (DSC Q2000, TA Instruments, West Sussex, UK) under He atmosphere. A sample mass of approx. 6 mg was used for each sample. A heat-cool-heat regime was applied in this measurement and the second heating curve used for thermal analyses. The sample was heated from room temperature to 210°C at a heating rate of 10°C min^{-1} before cooling it down to room temperature using a cooling rate of 50°C min^{-1}. The sample was then re-heated to 210°C again at a heating rate of 10°C min^{-1}. The crystallinity of the nanocomposites produced was obtained from:

$$\chi_c(\%) = \frac{\Delta H_m}{\Delta H_m^\circ \times w} \times 100\% \qquad\qquad (5.1)$$

where χ_c is the crystallinity, w is the loading fraction of PLLA by weight, ΔH_m is the melting enthalpy from DSC and ΔH_m° is the melting enthalpy of pure crystalline PLLA (93.7 J g^{-1}).[113]

5.2.7.5 Thermal gravimetry analysis (TGA) of the nanocomposites

The thermal degradation behaviour of the nanocomposites and neat PLLA was characterised using TGA (TGA Q500, TA Instruments, West Sussex, UK). A sample size of approx. 5 mg was used and the sample was heated from room temperature to 500°C at a rate of 10°C min^{-1}. A nitrogen atmosphere was used for this characterisation to provide an inert atmosphere.

5.2.7.6 Dynamic mechanical analysis (DMA) of the nanocomposites

The viscoelastic behaviour of the nanocomposites was characterised using DMA (Tritec 2000, Triton Technology Ltd, Keyworth, UK). DMA was performed in single beam cantilever bending mode with a gauge length of 10 mm. The sample has a width of 4 mm and an average sample thickness of 0.3 mm. The storage modulus, loss modulus and tan delta (tan δ) were measured from 30°C to 120°C using a heating rate of 5°C min^{-1}, with a frequency of 1 Hz.

5.3 Results and Discussions

5.3.1 Morphology of surface functionalised BC
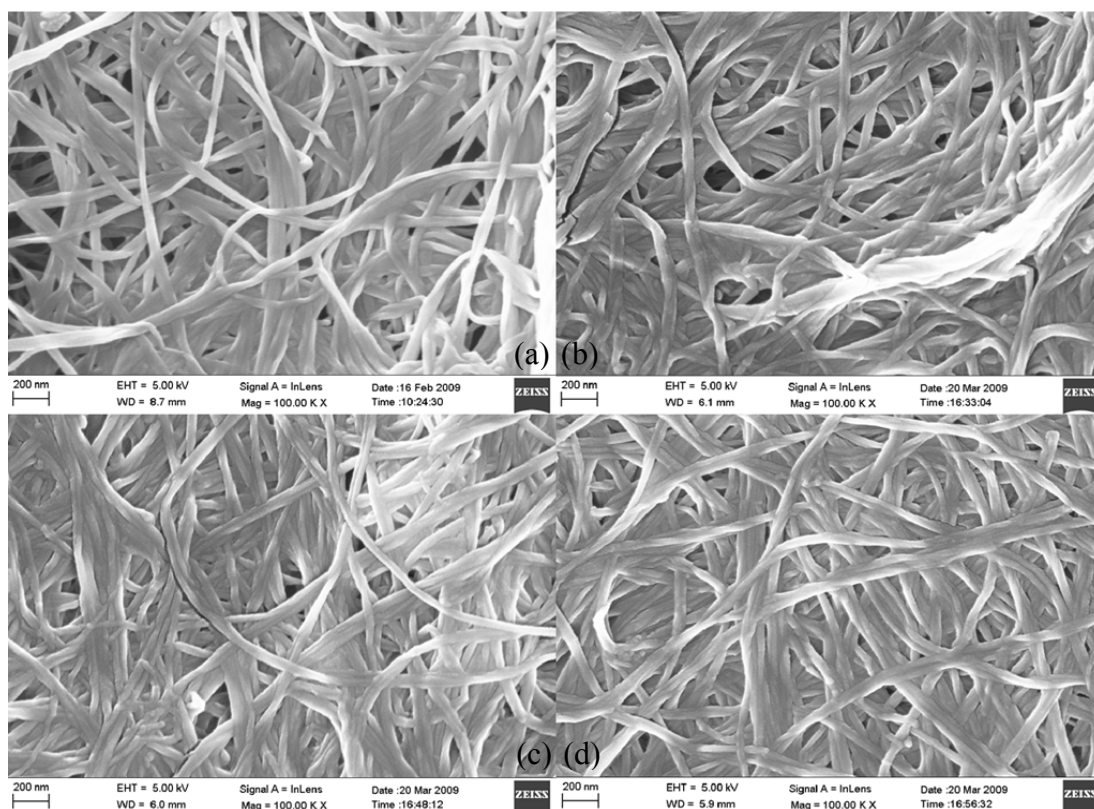
Figure 20: Scanning electron micrographs of (a) Neat BC, (b) C$_2$-BC, (c) C$_6$-BC, (d) C$_{12}$-BC

Figure 20 shows the SEM images of the functionalised and neat BC. It can be seen that the BC nanofibrils were about 50 nm in width and several micrometres long. The functionalisation reaction did not seem to change the morphology of these nanofibrils. C$_2$-BC, C$_6$-BC and C$_{12}$-BC still possessed the same fibrous structure as seen in neat BC. This is an indication that the functionalisation occurred essentially on the surface but not the bulk of the nanofibrils. If the functionalisation occurred in the bulk (i.e.: higher degree of substitution), the surface of the nanofibrils should not be smooth and damages to the fibre surface should be observed.[144]

In addition to this, attenuated total reflection infrared (ATR-IR) spectroscopy (see chapter 3) showed the appearance of new carbonyl bonds (C=O) around 1750 cm^{-1}. This is a direct result of the esterification of BC. The absorbance band of hydroxyl groups (-OH) around 3300 cm^{-1} did not seem to decrease significantly. This suggests the reaction occurred on the surface of the bacterial cellulose nanofibrils instead of the bulk. X-ray diffractography (XRD) of BC (shown in chapter 3) also support this

result as no significant decrease was observed in the crystallinity of BC. Therefore, it was concluded that the functionalisation reaction essentially occurred on the surface of the nanofibrils.

5.3.2 Direct wetting measurements on functionalised BC
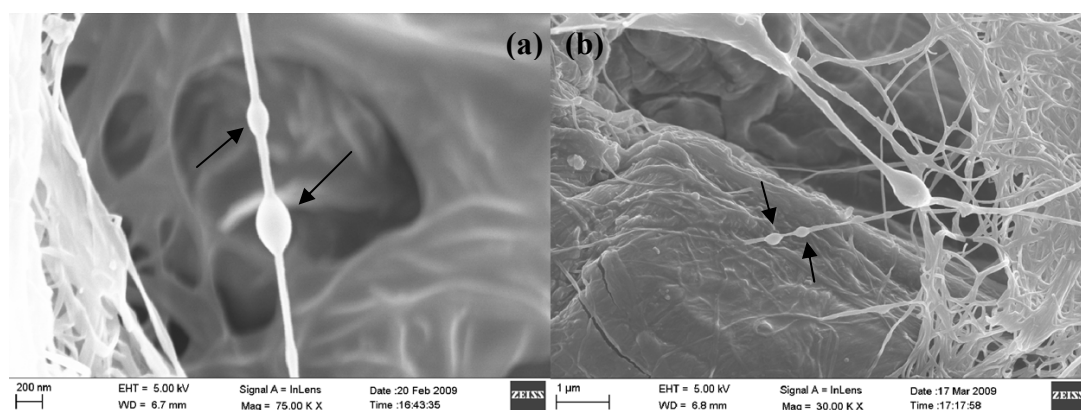
Figure 21: Examples of the SEM images showing PLLA melt droplets on BC nanofibre. (a) Neat BC (b) C_{12}-BC.

The direct wetting method was used as a simple means to determine the wettability of functionalised and neat BC nanofibrils by PLLA melts and thereby, quantifying the interfacial adhesion (thermodynamically) between a single bacterial cellulose nanofibre and PLLA melts. Figure 21 shows examples of typical SEM images of a drop of PLLA melt on single bacterial cellulose nanofibre. The contact angles measured between the polymer and the nanofibrils are given in Table 15. From the measured contact angles, it can be seen that as the chain length of the organic acid used to functionalise BC increased, the wettability between PLLA and the nanofibre increased. This is due to the fact that the esterification reaction introduced hydrophobic groups onto the surface of BC. The longer the hydrocarbon chain, the more hydrophobic the surface will become (advancing water-air contact angle of BC and C_{12}-BC is 19°±7° and 133°±9°, respectively). The decrease in the contact angle between PLLA and BC indicates an increase in the interfacial adhesion between the polymer and the functionalised BC. From Young-Dupre's equation,[183] it can be inferred that if the surface tension of the wetting liquid remains constant and the contact angle decreases, the work of adhesion increases. This will lead to a better interface between the liquid (polymer melt) and the substrate (functionalised BC). It is also worth mentioning that this direct wetting method is in fact measuring the receding contact angle rather than the advancing contact angle as the polymer was

first precipitated onto the nanofibre and then melted. This led to the de-wetting of the polymer from the surface of the nanofibre.

Table 15: Wettability of functionalised bacterial cellulose nanofibrils

Sample Name	Contact Angle (°)
Neat BC	35.4 ± 0.8
C_2-BC	29.5 ± 2.9
C_6-BC	27.7 ± 2.0
C_{12}-BC	20.8 ± 2.5

5.3.3 The use of composite microspheres for extrusion
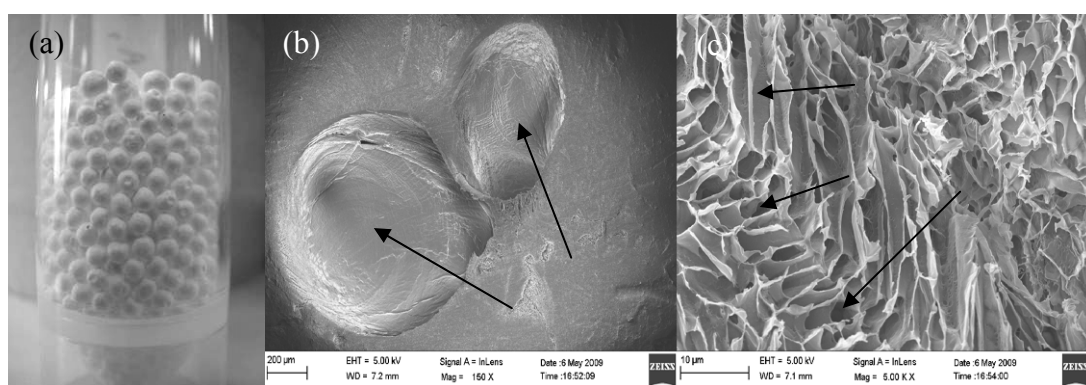
Figure 22: Images showing the morphology of the composite microspheres. (a) The microspheres (b) SEM image of the microsphere at low magnification (c) SEM image of the microsphere at high magnification.

As mentioned earlier, composite microspheres were produced to allow dry processing of BC reinforced polymer nanocomposites using conventional extrusion process. Another main advantage of using this method is that it enables the dispersion of dry BC in the polymer melt. This method is also intrinsically scalable. In terms of the morphology of the composite microspheres, they were about 2.5 mm in diameter (Figure 22a). The diameter of these microspheres is highly dependent on the internal diameter of the tip of the syringe used. These microspheres possess a porosity of approximately 94 vol.-% (calculated from the polymer to solvent ratio). The porous spheres are shown in Figure 22b and their internal structure can be observed from the SEM image, Figure 22c. Voids can be observed in the microspheres (Figure 22b). This was due to the entrapment of air during the drop-wise addition of polymer solution into the liquid nitrogen bath. Similar observations have been reported in the literature.[177, 184] Figure 22c shows the structure of the composite microspheres at high magnification. The composite microspheres possess a channel-like structure. This can be attributed to the solvent freezing from the

outside towards the centre of the microsphere. These channels represent the three-dimensional fingerprint of the solvent rich phase, which crystallised (froze) during phase separation. The structure of the composite microspheres was highly anisotropic (radially and axially), which is a characteristic of solid-liquid phase separation induced by TIPS process.[185]

5.3.4 Mechanical properties of nanocomposites

The tensile modulus of all the nanocomposites increased when compared to neat PLLA (Table 16). The tensile modulus increased by as much as 50%, as seen in PLLA/C_{12}-BC (5 wt%). Based on the "rule of mixtures" for nanocomposites,[186] the elastic modulus of a nanocomposite is the weighted mean of the elastic moduli of the polymer matrix and the reinforcement, depending only on the volume fractions and the orientation of the reinforcement. Since BC possesses a higher modulus compared to the polymer matrix, the elastic modulus of the nanocomposites increases as expected when BC is incorporated into the polymer matrix.

It can also be seen from Table 16 that the tensile strength of the nanocomposites improved by as much as 15% (PLLA/C_{12}BC 5 wt%). As a comparison, Huda et al.[187] have investigated the mechanical properties of recycled newspaper cellulose fibre (RNCF) reinforced PLLA composites. A fibre loading of 30 wt% was required to improve the tensile strength of the matrix by 15%. Such differences can be attributed to the large surface area of BC compared to RNCF. The improvements observed in the tensile strengths of the nanocomposites reinforced with functionalised BC could also be ascribed to the good dispersibility of functionalised BC in the polymer (the nanocomposites are transparent, Figure 23) and the intimate adhesion between functionalised BC and the polymer matrix. Due to the hydrophilic nature of neat BC, the dispersibility of the nanofibrils in the hydrophobic polymer melt and the interfacial adhesion between BC and PLLA are poor.[188] Such effects reduce the ability to transfer stress from the matrix to the reinforcement and thereby limit the tensile strength of the nanocomposites. The surface hydrophobisation of BC improved the dispersibility of BC in the polymer melt as well as the interfacial adhesion between BC and PLLA. As a result, the tensile strength of C_6-BC and C_{12}-BC reinforced nanocomposites showed significant improvements when compared to neat BC reinforced PLLA nanocomposites.

Table 16: Mechanical properties of cellulose nanofibrils reinforced PLLA nanocomposites

Sample	Tensile Modulus (GPa)	Tensile Strength (MPa)	Elongation at break (%)	M_w (kDa)
Neat PLLA	1.34 ± 0.04	60.7 ± 0.8	3.59 ± 0.07	157
PLLA/BC (2 wt%)	1.75 ± 0.05	57.5 ± 1.4	2.85 ± 0.12	147
PLLA/BC (5 wt%)	1.89 ± 0.02	60.9 ± 0.5	2.41 ± 0.08	146
PLLA/C_2BC (2 wt%)	1.71 ± 0.06	53.0 ± 1.4	2.23 ± 0.07	116
PLLA/C_2BC (5 wt%)	1.70 ± 0.03	60.1 ± 0.9	2.62 ± 0.07	135
PLLA/C_6BC (2 wt%)	1.63 ± 0.04	66.1 ± 2.4	3.12 ± 0.09	157
PLLA/C_6BC (5 wt%)	1.79 ± 0.02	65.1 ± 0.9	2.87 ± 0.03	153
PLLA/C_{12}BC (2 wt%)	1.66 ± 0.05	63.0 ± 1.2	3.21 ± 0.04	149
PLLA/C_{12}BC (5 wt%)	1.98 ± 0.04	68.5 ± 1.5	2.69 ± 0.06	157
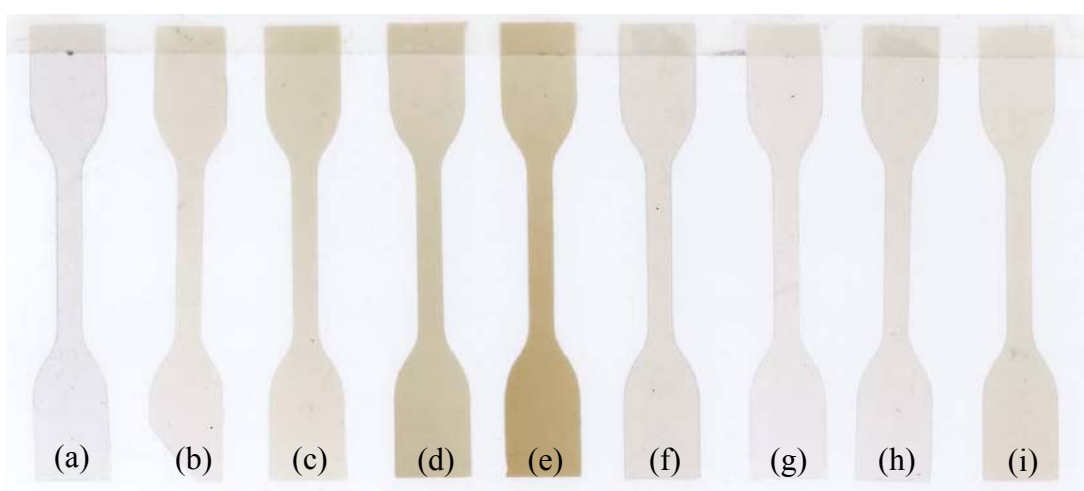
Figure 23: The nanocomposites samples. (a) Neat PLLA, (b) PLLA/BC (2 wt%), (c) PLLA/BC (5 wt%), (d) PLLA/C_2BC (2 wt%), (e) PLLA/C_2BC (5 wt%), (f) PLLA/C_6BC (2 wt%), (g) PLLA/C_6BC (5 wt%), (h) PLLA/C_{12}BC (2 wt%), (i) PLLA/C_{12}BC (5 wt%).

Although the direct wetting measurements showed lower contact angle (better interfacial adhesion) between PLLA droplets and C_2-BC compared to neat BC, PLLA/C_2-BC nanocomposites exhibited lower tensile properties compared to PLLA/BC nanocomposites. Visually, PLLA/C_2–BC nanocomposite samples were brown in colour as compared to other nanocomposites, which are optically transparent (Figure 23). PLLA/C_2-BC nanocomposites also suffered from serious embrittlement when compared to the rest of the nanocomposite samples, including PLLA/BC. This might be due to the hydrolysis of the polymer matrix due to the incorporation of C_2-BC nanofibrils. The relative hydrophilic nature of C_2-BC (advancing water/air contact angle of $75°\pm3°$) compared to other functionalised BC and therefore, the presence of water might cause the hydrolysis of the ester bonds in C_2-BC during the extrusion at 180°C. The produced acetic acid will initiate the acid

catalysed hydrolysis of PLLA,[175] leading to a decrease in the molecular weight of the matrix, which was confirmed by GPC (Table 16). This low molecular weight led to the lower tensile properties and the embrittlement of the nanocomposites. Due to the hydrophobic nature of C_6-BC (advancing water/air contact angle of 92°±2°) and C_{12}-BC (advancing water/air contact angle of 133°±9°), less water will be absorbed by the nanofibrils and the hydrolysis of ester bonds will be negligible. Hence, the matrix still possessed high molecular weight.

5.3.5 Crystallisation and melt behaviour of the nanocomposites

The DSC curves are shown in Figure 24 and the characteristic temperatures such as glass transition temperature, crystallisation temperature and melt temperature are tabulated in Table 17, along with the degrees of crystallinity of the nanocomposites. From Table 17, it can be concluded that the degree of crystallinity of the polymer was not significantly affected by the addition of BC into the matrix. The addition of cellulose nanofibrils into the matrix did however have a profound impact on the crystallisation behaviour of PLLA (Figure 24). It can be observed that the crystallisation temperature of the matrix decreased from 120°C to about 100°C in the presence of BC. This implied that the presence of BC aided the crystallisation of the matrix. A similar effect has been reported in the literature.[189]

Table 17: Glass transition temperature (T_g), crystallization temperature (T_c), melt temperature (T_m), the crystallinity (χ_c) and the onset thermal degradation temperature (T_d) of PLLA nanocomposites reinforced with functionalised cellulose nanofibrils

Sample	T_g (°C)	T_c (°C)	T_m (°C)		χ_c (%)	T_d (°C)
Neat PLLA	59	118	165	170	47.5	256
PLLA/BC (2 wt%)	59	102	168		46.0	275
PLLA/BC (5 wt%)	59	99	167		47.4	279
PLLA/C_2BC (2 wt%)	59	104	168		46.2	262
PLLA/C_2BC (5 wt%)	59	105	168		44.9	270
PLLA/C_6BC (2 wt%)	59	106	169		43.4	270
PLLA/C_6BC (5 wt%)	59	106	168		43.8	276
PLLA/C_{12}BC (2 wt%)	59	105	169		44.7	271
PLLA/C_{12}BC (5 wt%)	59	97	167		46.6	268

The glass transition temperature and the melt temperature of the nanocomposites on the other hand were not affected when compared to neat PLLA. This signifies that the cellulose nanofibrils did not affect the chain mobility of the polymer. The appearance of two melt peaks in neat PLLA is not surprising; annealing of a

crystallisable PLLA will often produce two melt peaks.[190] An exotherm around 150°C was also observed prior to the melting of PLLA in the nanocomposites samples. This exotherm is consistent with the solid-solid crystal transformation of α' form to α form of PLLA.[191] However, this exotherm was not observed in neat PLLA. This is because α' form is only crystallised below 120°C,[192] which was the case for all the nanocomposites.
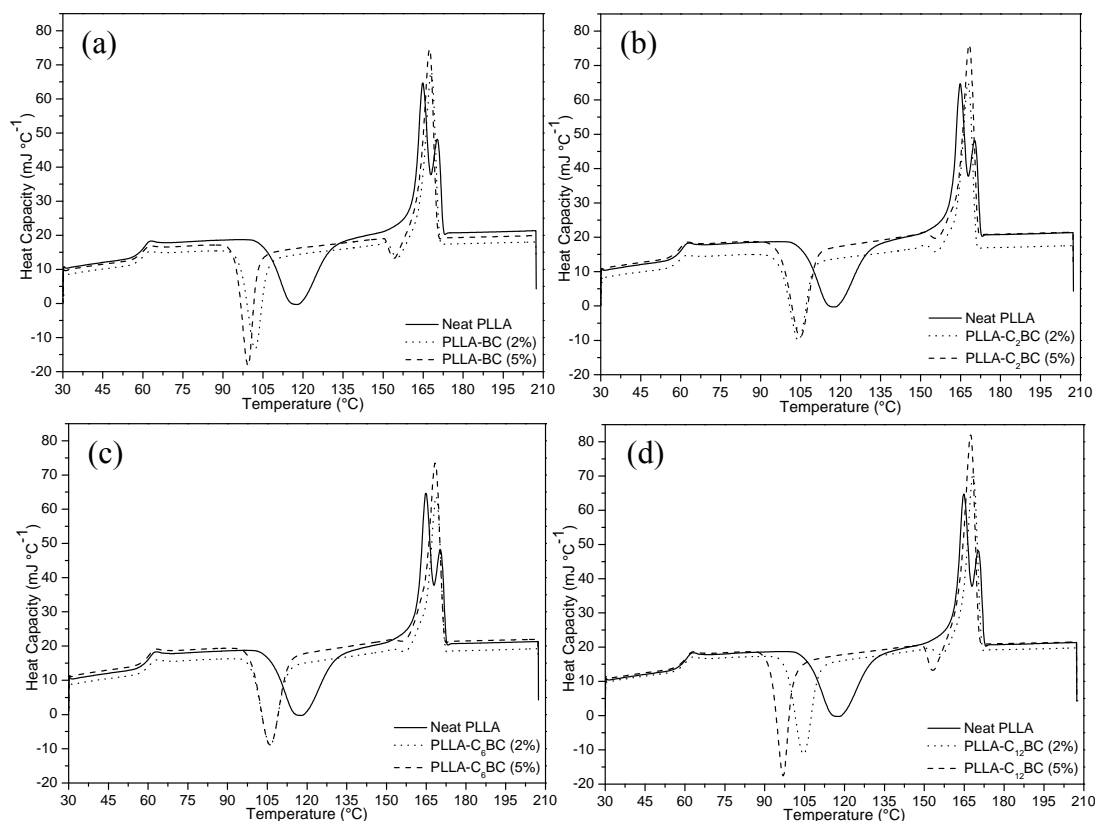
Figure 24: DSC plots of (a) PLLA/BC, (b) PLLA/C$_2$BC, (c) PLLA/C$_6$BC and (d) PLLA/C$_{12}$BC nanocomposites.

5.3.6 Thermal degradation behaviour of the nanocomposites

The onset thermal degradation temperature (T_d) and the TGA curves of the neat polymer and its nanocomposites are shown in Table 17 and Figure 25, respectively. It can be seen from Table 17 that T_d increased for all the nanocomposites. All the composites underwent single step degradation (Figure 25). This increment in T_d and the improvements in the thermal stability of the nanocomposites indicated that the presence of BC does affect the thermal stability of the nanocomposites. Such results can be attributed to the interaction between nanofibrils and the matrix.[46] The low T_d observed in PLLA/C$_2$-BC (2 wt%) nanocomposite sample might be a direct result of

the lower molecular weight of the polymer matrix, which in turn reduced the thermal stability of the nanocomposites.
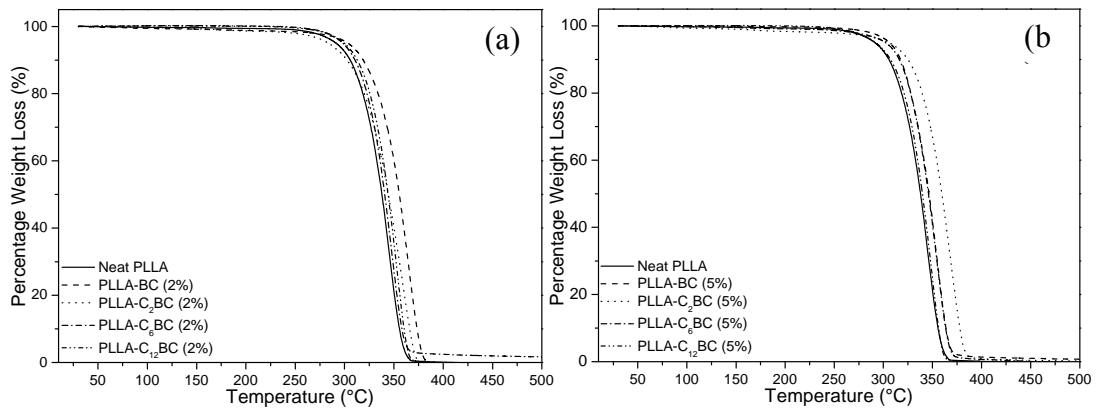
Figure 25: TGA curves of neat PLLA and its nanocomposites. (a) 2 wt% loading (b) 5 wt% loading.

5.3.7 Viscoelastic behaviour of the nanocomposites
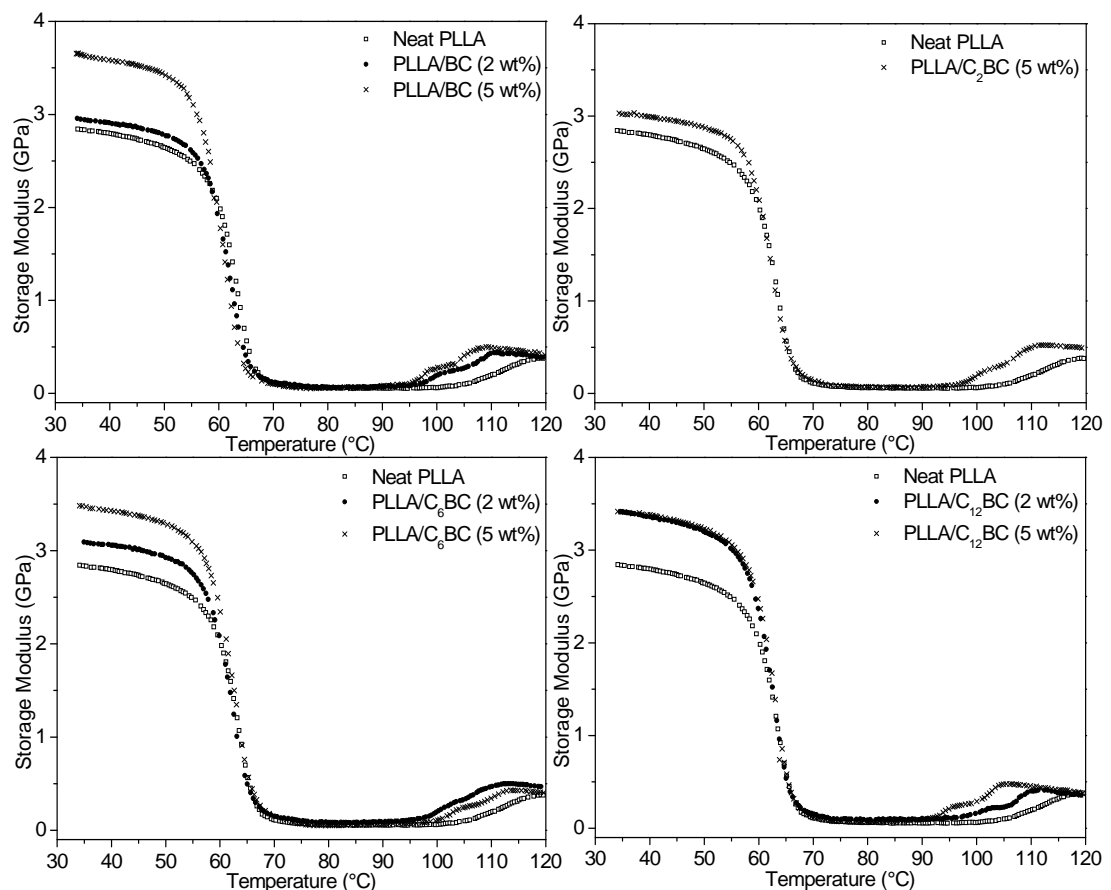
Figure 26: Storage modulus of neat PLLA and the nanocomposites with different functionalised BC nanofibrils and loading fractions.

Figure 26 and Figure 27 show the storage modulus and tan δ of the BC reinforced PLLA nanocomposites as a function of temperature. It is worth mentioning that these figures do not contain the DMA results for PLLA/C_2-BC (2 wt%). This is due to the brittleness of PLLA/C_2-BC (2 wt%). The sample failed repeatedly during the DMA runs (a total of 5 tries were made). Although the increment in storage moduli differs from sample to sample (Figure 26) it can be seen that generally, the storage moduli of the nanocomposites are higher than that of neat PLLA. The use of cellulose nanofibrils to reinforce PLLA matrix resulted in a much stiffer material compared to the neat polymer. This is a direct result of the reinforcing ability induced by BC. There are two possible contributions to the increment in the storage moduli;[187] (i) intramolecular bonds between BC and PLLA and (ii) rigid structure of BC.
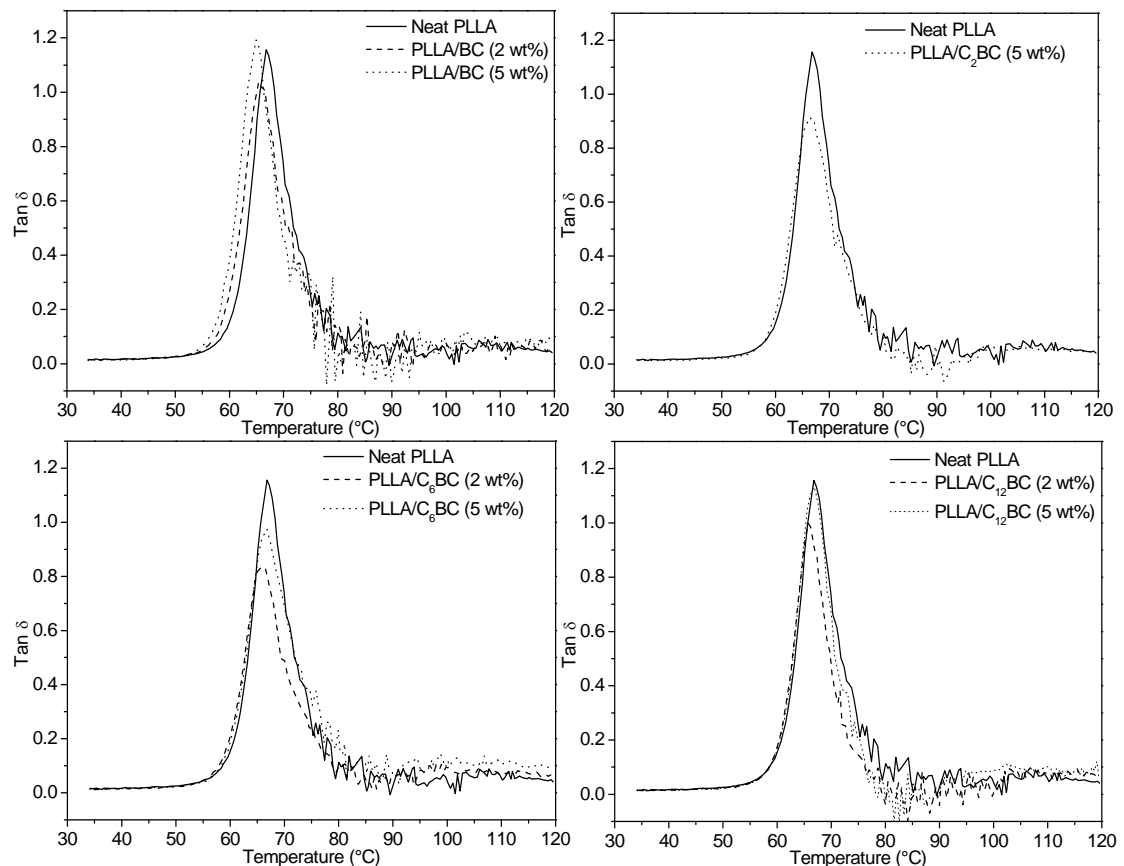
Figure 27: Energy dissipation factor of the nanocomposites.

The storage modulus of PLLA/C_2-BC (5 wt%) is significantly lower than other composites at 5 wt% loading fraction. This low value of storage modulus might be a direct consequence of the (degraded) low molecular weight matrix (Table 16). It can also be seen that the storage moduli of the nanocomposites are higher than neat

PLLA beyond its glass transition temperature at around 59°C (Figure 26). This is due to the early crystallisation of the polymer matrix. Such results corroborate the DSC results. The crystallisation temperature was found to be 120°C for neat PLLA compared to lower temperatures (by ~15°C) for the nanocomposites.

Table 18: Mechanical Tg, storage modulus (G') at 40°C, and the storage modulus imparted by the addition of BC nanofibrils

Sample	Mechanical T_g (°C)	G' @ 40°C (GPa)	G' @ 40°C imparted by nanofibrils (%)
Neat PLLA	67	2.79	-
PLLA/BC (2 wt%)	65	2.90	4
PLLA/BC (5 wt%)	65	3.58	28
PLLA/C$_2$BC (5 wt%)	66	2.99	7
PLLA/C$_6$BC (2 wt%)	66	3.06	9
PLLA/C$_6$BC (5 wt%)	67	3.42	23
PLLA/C$_{12}$BC (2 wt%)	66	3.35	20
PLLA/C$_{12}$BC (5 wt%)	67	3.38	21

The tan δ of the neat polymer and nanocomposites as a function of polymer is shown in Figure 27. Tan δ is related to the amount of energy dissipated as heat or the relaxation of polymer chains in the nanocomposites. The tan δ peak was not significantly affected by the addition of BC. One reason might be the loading fraction was too low to have a profound impact on the mobility of the polymer chains. These results are in agreement with the absence of significant changes in the glass transition temperatures of the nanocomposites as measured by DSC. The mechanical glass transition temperature (T_g) can be determined from the peak of tan δ or the point at which the storage modulus changes sharply. In this study, the mechanical T_g was taken as the peak of tan δ (Table 18). It can be seen that the mechanical T_g is about 8°C higher than the glass transition temperature determined by DSC. However, the changes in the mechanical T_g is not significant. This suggests the mobility of the polymer chains was not affected by the addition of BC. Such results are not surprising as high loading fraction of reinforcement[187] or high crystallinity of the polymer matrix[189] is usually required to have a significant impact on the polymer chain mobility. The storage modulus increased by as much as 28% upon incorporation of BC (Table 18). Generally, the higher the loading fraction of BC, the larger the increment in the storage modulus, with the exception of C$_{12}$-BC reinforced nanocomposites. The exception seen in C$_{12}$-BC reinforced nanocomposites might be due to the good contact between the polymer and the

reinforcement, which provides good stress transfer from the matrix to the nanofibrils regardless of the loading fraction. However, the increase of storage modulus by C_{12}-BC reinforced PLLA nanocomposites was not as high as neat BC reinforced nanocomposites. One explanation is that the crystallinity as measured by XRD of the BC is higher for neat BC compared to C_{12}-BC.

5.4 Conclusions

The hydrophilic surface of BC was rendered hydrophobic by organic acid functionalisation. The degree of hydrophobicity can be tailored by the length of the organic acid (C_2 to C_{12}). The incorporation of organic acid functionalised BC into PLLA led to an improvement in both tensile modulus and tensile strength of the C_6-BC and C_{12}-BC reinforced nanocomposites (by as much as 50% and 15%, respectively). However, the PLLA nanocomposites reinforced by C_2-BC seemed to undergo acid catalysed hydrolysis during extrusion and this led to a decrease in the molecular weight of the PLLA, which in turn affected the mechanical properties of the resulting material. An increase in the thermal degradation temperature by 15°C was also observed for the nanocomposites compared to neat PLLA. The nanocomposites also exhibit higher storage moduli compared to neat PLLA. This is evidence of improved interfacial adhesion between the polymer matrix and the functionalised BC. This result was also confirmed by direct wetting measurement of cellulose nanofibrils by PLLA droplets. Therefore, it can be concluded that PLLA nanocomposites with overall improved properties can be fabricated through the surface functionalisation of BC.

Chapter 6 – Carbohydrate derived copoly(lactide) as the compatibiliser for bacterial cellulose reinforced polylactide nanocomposites

Summary

A novel, entirely bio-derived copolymer is reported and applied as a compatibiliser, to produce composites of poly(L-lactide) (PLLA) reinforced with bacterial cellulose (BC), showing improved mechanical properties. The bio-derived copolymer is prepared by the random ring opening copolymerisation of a carbohydrate lactone (acetic acid 5-acetoxy-6-oxo-tetrahydro-pyran-2-yl methyl ester, monomer **1**) with *L*-lactide (LLA). Contact angle measurements of copolymer droplets on a single BC nanofibre showed that the copolymer possessed higher affinity towards BC compared to PLLA. The mechanical properties were also studied; the copolymer possessed a comparable Young's modulus, but lower tensile strength than PLLA. A bio-derived composite of BC and PLLA is prepared, using 5 wt.-% compatibiliser and 5 wt.-% BC, using solution impregnation followed by injection moulding. The composites showed improved mechanical properties, including a higher Young's modulus and tensile strength, compared to either pure PLLA or PLLA-BC composites (i.e. without compatibiliser). The application of the novel bio-derived copolymer as a compatibiliser enables preparation of 100% bio-based nanocellulose composites, showing improved properties and without the need for any chemical modification of cellulose nanofibres.

6.1 Introduction

Over the past few years, significant research effort has been focussed on the production of polymer nanocomposites. A major impetus for this research has been the potential to significantly improve the mechanical properties of the nanocomposites with very low nanofiller contents.[193] In the context of green

materials development, nanocellulose is often used as the filler in the preparation of polymeric nanocomposites.[118] It is attractive due to its high crystallinity, which results in high fibres stiffness. In addition to this, the stiffness of cellulose crystals, measured using X-ray diffraction[194] or estimated via numerical simulations,[121] has been determined to lie the range 100-160 GPa. This value is higher than that of some glass fibres (~70 GPa for E-glass fibres). The polymer matrix also needs to be a bio-derived material and an attractive option is poly(lactide) (PLA). Polylactide is currently commercially produced on a large-scale in the US, Europe, Japan and China.[195, 196] It derives from high-starch content plants, including corn, via fermentation to lactic acid, formation of lactide and ring-opening polymerization.[197, 198] PLA is currently applied in a range of commodity plastics applications including packaging and fibre use,[199] as well as in more specialised medical applications, including wound-healing, regenerative medicine and controlled release.[200] Whilst PLA shows promise for various applications, there remain problems associated with its materials properties, including its strength and stiffness.[196] An interesting approach to modify and improve the polymer properties is to reinforce the polymer with fillers such as nanocellulose to produce green polymer nanocomposites.

Nanocellulose can be obtained either via a 'top-down' approach, whereby biomass are subjected to high shear forces in order to create nanofibrillar structures,[173] or via a 'bottom-up' approach, utilising the biosynthesis of cellulose producing bacteria, such as from the *Acetobacter* species.[153] An advantage of bacterial cellulose (BC) compared to extracting fibres from plants or biomass, is that it is inherently produced as a nanomaterials, thereby obviating complex processing and nanostructuring steps.[115] In addition, BC is a highly crystalline material (~90% crystallinity).[120] The Young's modulus of a single BC nanofibre, determined using Raman spectroscopy, has been reported to be 114 GPa.[6] These properties make BC an interesting reinforcing agent for green nanocomposites.

A major drawback of BC, or indeed any other (nano)cellulose, is their hydrophilicity, which results in poor adhesion to the hydrophobic polymer matrices, such as polylactide and PHA.[13, 201] As a result, the cellulose surface needs to be modified to improve compatibility of the nanofibrils/matrix. This is usually accomplished by grafting long chain fatty acids onto the surface of BC.[202, 203]

Polymers are also grafted "onto" or "from" the nanocellulose and yields nanocomposites with improved properties.[204, 205] Alternatively, the polymer matrix (for example, PLA) can, in some cases, be modified, for example incorporating or grafting maleic anhydride or methylene diisocynate moities onto the polymer backbone to enhance the nanofibre-matrix interface.[206-209] However, these compounds are derived from petroleum, and in some cases toxic, thereby reducing the bio-derived content of the composites.

Herein, the use of a carbohydrate-derived copolylactide as a compatibiliser to produce 100% bio-based PLLA nanocomposites, with improved mechanical properties is reported. The copolymer is prepared by the ring-opening copolymerisation of a carbohydrate derived lactone **1**, acetic acid 5-acetoxy-6-oxo-tetrahydro-pyran-2-yl methyl ester, monomer,[210] and *L*-lactide (for the chemical structure of compound **1**, see Figure 28). Monomer **1** is prepared from D-gluconolactone in two high yielding steps, as previously reported.[210] The ring-opening copolymerisation of **1** and *L*-lactide, using $Sn(OBu)_2$ as the initiator, enables the preparation of the random copolymer (RP**1**, M_n (GPC) = 68 800, PDI = 1.55, 7 mol-% of compound **1** in the copolymer determined by ^{1}H NMR).[211] In previous study, RP**1** showed lower water contact angle (film, 73°; fibre, 128°) comparing PLLA (film, 79°; fibre, 132°).[211] Given that RP**1** had already shown an improved hydrophilicity compared to PLA, of equivalent M_n/end groups, it is interesting to test RP**1** as a compatibiliser for PLA-BC. It is expected that RP**1** and BC should be more compatible than PLLA and BC due to its more hydrophilic nature. It was reasoned that the application of RP**1** as a compatibiliser should facilitate the production of nanocomposites with improved mechanical properties.
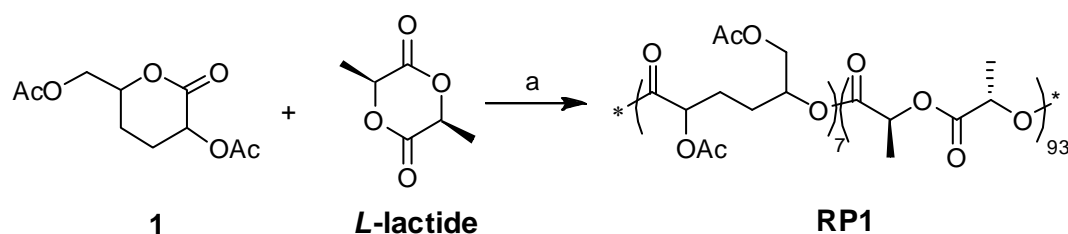
Figure 28: The synthesis of RP1 from monomer (1) and L-lactide. (a) Toluene, Sn(OBu)2:1:LLA = 1: 350:1650, 120 °C, 20 h.

6.2 Experimental Section

6.2.1 Materials

Poly(*L*-lactide) (PLLA), purchased from Biomer (L9000, $M_W \geq 150$ kg mol^{-1}, *D*-content = 1.5%), was used as the matrix polymer in the nanocomposites. 1,4-Dioxane (Sigma-Aldrich, ACS Reagent, $\geq 99\%$ purity) was used as the solvent for PLLA. The novel bio-derived compatibiliser (RP**1**) was prepared according to the previously published synthetic method.[211] Bacterial cellulose (BC) was kindly supplied by Forschungszentrum für Medizintechnik und Biotechnologie, GmbH, in wet pellicle form containing 94 wt.-% water. Prior to composite formation, the BC pellicle was blended, using a laboratory blender (Waring Blender LB20EG, Christison Particle Technologies, Gateshead UK), for 1 min and homogenised, at 20,000 rpm for 2 min, using a homogeniser (Polytron PT 10-35 GT, Kinematica, CH) at a concentration of 0.4% (mgL^{-1}) in water. This dispersion was flash frozen, in Petri dishes, by immersion into liquid nitrogen and subsequently freeze-dried (Edwards Modulyo freeze-dryer UK). The procedure enabled isolation of BC nanofibrils that are re-dispersible in the 1,4-dioxane.

6.2.2 Direct wetting measurements

The wettability of an individual BC nanofibre by either PLLA, RP**1** or a blend of RP**1** and PLLA was studied using a direct wetting method.[179, 202] The polymer (4.4 mg) was dissolved in CHCl$_3$ (5 mL, to prepare a 0.06 wt.-% solution). This solution was left for >20 h to ensure that the polymer had fully dissolved. Freeze-dried BC (3.7 mg) was suspended in chloroform (5 mL, so as to prepare an 0.05 wt.-% suspension). This suspension was homogenised for 2 min at 20,000 rpm. The polymer solution was then added into the suspension, and the resulting mixture was homogenised for a further 2 min at 20,000 rpm, followed by ultrasonication for 1 h in a low-power ultrasonic bath, to ensure adequate nanofibril dispersion. The mixture was added drop-wise into a magnetic stirred C$_6$H$_{14}$:CHCl$_3$ mixture (80:20 by weight, 200 mL), which caused the precipitation of the polymer onto individual BC nanofibres. The precipitate was filtered using a PTFE membrane (0.2 μm pore size, Sartorius Stedium Biotech, UK). The filtrate was heated (15 min at 180 °C) while it was still on the PTFE membrane to melt the polymer. The polymer coated BC was then investigated using a high-resolution scanning electron microscope (LEO

Gemini 1525 FEG-SEM, Oberkochen, D). The contact angles of the polymer droplets on the cellulose nanofibrils were determined for 5 different droplets using the generalised height-length method, described in literature.[180]

6.2.3 Preparation of the nanocomposite "pre-pregs" with 5 wt.-% BC loading

Freeze-dried BC (632 mg) was added into 1,4-dioxane (180 mL), followed by PLLA pellets (12 g) and the dispersion was stirred at 60 °C for 20 h. The resulting solution was then flash frozen, in liquid nitrogen, and subsequently freeze-dried (Edwards Modulyo freeze-dryer UK) to produce a nanocomposite "pre-preg". Nanocomposite "pre-preg" with RP**1** as compatibiliser was also prepared. RP**1** (0.6 g) and PLLA pellets (11.4 g) were added into the dispersion. This formulation contains 5 wt.-% RP**1,** relative to the total polymer content in the nanocomposite.

6.2.4 Processing of the polymers and nanocomposites

The previously produced nanocomposite "pre-pregs" were injection moulded using a piston injection moulder (Haake Minijet, Thermo Scientific, Hampshier, UK). The barrel temperature and the mould temperature were 190°C and 70°C, respectively. All the samples were injected with an injection pressure and time of 500 bar and 30 s, and a post-pressure and time of 200 bar and 30 s, respectively. The injection moulded tensile test specimens possessed a dog-bone shape, in accordance to BS ISO 527: 1996 type V. These dog-bone test specimens had an overall length of 60 mm, a gauge length of 10 mm, thickness of 3 mm and the narrowest part of the specimen was 3 mm.

6.2.5 Characterisation of the polymers and BC reinforced nanocomposites
6.2.5.1 Characterisation of RP1

NMR spectra were collected using a Bruker AV500 instrument; ^{1}H NMR spectra were collected at 500 MHz. CDCl$_3$ was used as the NMR solvent and the reference component. Size exclusion chromatography (SEC) was performed on a Polymer Laboratories SEC 50 instrument with two Polymer Laboratories mixed D columns and CHCl$_3$, at a flow rate of 1 mL min^{-1}, as the eluent. Narrow molecular weight polystyrene standards (Polymer laboratories, mixed A and B) were used to calibrate the instrument.

6.2.5.2 Thermal characterisation the polymers and nanocomposites

The crystallisation and melt behaviour of the polymers were investigated using DSC (DSC Q2000, TA Instruments, West Sussex, UK) in a He atmosphere. Approximately 10 mg of each moulded sample was used for the measurement. A heat-cool-heat regime was employed. The sample was first heated from room temperature to 200 ºC at a heating rate of 10 ºC min^{-1}, then cooled to room temperature at a cooling rate of 50 ºCmin^{-1}. The sample was then re-heated to 200 ºC at a heating rate of 10 ºC min^{-1}. The crystallinity (based on the 1st heating curve to evaluate the crystallinity of the composites after thermal processing) of the composites was calculated using equation 6.1:

$$\chi_C = \frac{\Delta H_m - \Delta H_c}{\Delta H_m^o (1 - w)} \times 100\% \qquad\qquad (6.1)$$

where χ_c is the crystallinity of the composite, ΔH_m, ΔH_c, and ΔH_m^o are the melting enthalpy and cold crystallisation enthalpy determined from the DSC curves and the melting enthalpy of pure crystalline PLLA (75.57 J g^{-1}), respectively.[212] w indicates the weight fraction of BC in the nanocomposites.

6.2.5.3 Mechanical testing of the polymers and nanocomposites

The previously manufactured dog-bone shaped specimen of the polymers (neat PLLA and RP**1**) and nanocomposites were tested in tension, using an Instron universal material testing machine (Instron 4505, Instron Corporation, MA, USA) equipped with a 10 kN load cell. The test was conducted in accordance to BS ISO 527: 1996. Strain gauges (FLA-2-11, Techni Measure, Studley, UK) were glued onto the middle portion of the narrowest part of the dog-bone shaped test specimens using cyanoacrylate glue (EVERBUILD Building Products Ltd, Leeds, UK). The test was conducted at a crosshead speed of 1 mm min^{-1}. A total of 5 specimens were tested for each type of sample.

6.3 Results and Discussion

6.3.1 Direct wetting measurements on single BC nanofibres

The bio-derived copolymer, RP**1**, was synthesised according to the previously published method.[210] Briefly, this involved the random copolymerisation of a carbohydrate derived lactone (**1**) and L-lactide, using $Sn(OBu)_2$ as the initiator (Figure 28). SEC analysis showed that RP**1** had an M_n of 68.8 kg/mol and a polydispersity index of 1.55. ^{1}H NMR spectroscopic analysis of the random copolymer composition showed that it contained 7 mol-% of carbohydrate **1** (see Figure B1 in appendix B for ^{1}H-NMR spectrum of RP**1**). It was also previously established that RP**1** has a higher hydrophilicity than PLLA and hypothesised it might therefore be a suitable compatibiliser for BC-PLLA nanocomposites. It is postulated that the carbohydrate moieties/repeating units would preferentially adsorb onto the surface of BC due to its hydrophilic nature compared to neat PLLA. In order to assess its suitability as a compatibiliser, it was of interest to determine or quantify the wetting of BC nanofibrils by RP**1**. This was accomplished by the measurement of BC-polymer droplet contact angles (known as the direct-wetting method). The direct wetting method is a straightforward means to quantify the interfacial adhesion between BC nanofibrils and a particular polymer.[202] The method involves precipitating a polymer onto BC fibres, followed by heating to melt the polymer. The polymer droplets on a single fibre were observed using SEM and the contact angle is determined using generalised drop length height method. It should be noted that the direct wetting method measures, in fact, the receding contact angle rather than the advancing contact angle. This is because the polymer sample is first precipitated onto the nanofibre, followed by melting the polymer. This results in droplets forming from a receding motion. SEM images of characteristic droplets of either PLLA, RP**1**+PLLA (5 wt.-% RP**1**) and RP**1** on a single BC nanofibre can be seen in Figure 29.

Measured contact angles showed that RP**1** possesses a higher affinity (Table 19),[180] i.e. lower contact angle, towards BC nanofibres than PLLA. The contact angles decreased from 35.4° for PLLA to 14.9° for RP**1**. This decrease can be attributed to the higher hydrophilicity of RP**1** compared to PLLA.[211] Additionally, a polymer blend containing 5 wt.-% RP**1** in PLLA was studied; the contact angle was lower

than that of PLLA alone (see Table 19), indicating there is an improved adhesion between the polymer blend and BC. This provides evidence to support the notion that RP**1** acts as a compatibilising agent for BC and PLLA composites.
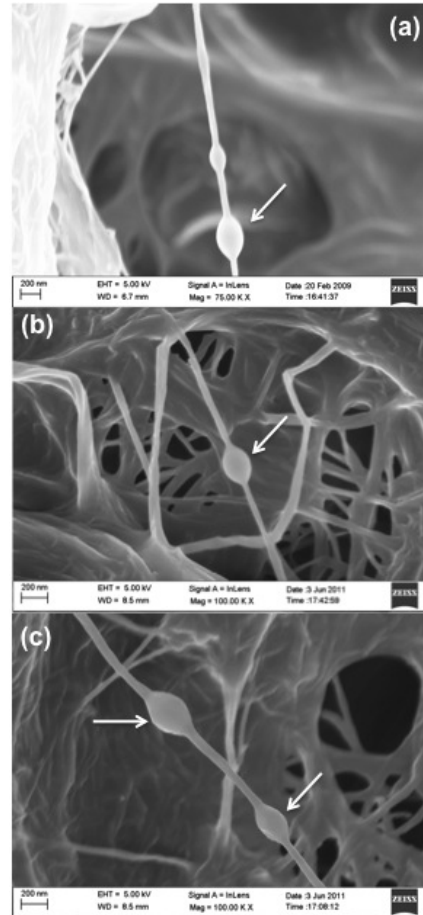
Figure 29: Typical example of SEM images showing a polymer droplet on a single BC nanofibre. Where the polymer is (a) PLLA, (b) PLLA and RP1 (5 wt-%) (c) RP1. The arrow indicates the polymer droplet on a single BC nanofibre.

Table 19: The wettability of the polymers, PLLA, RP1 and the blend, on BC nanofibrils.

Polymer	Contact angle (°)
PLLA	35.4 ± 1.6
PLLA-RP**1**	29.0 ± 2.7
RP**1**	14.9 ± 2.7

6.3.2 Crystallisation and melt behaviour of the polymers and nanocomposites

The glass transition (T_g) and crystallisation (T_c) temperatures of PLLA, RP**1**, PLLA-RP**1** blend and their nanocomposites are summarised in Table 20. No significant difference between the T_g of the polymers and their nanocomposites can be observed. This could be due to the low loading fraction of BC nanofibrils, which is

not significant enough to influence the molecular chain movements of the polymers. The T_c of the nanocomposites, however, decreased when compared to the polymers, indicating that BC aids polymer crystallisation. Indeed, BC was already found to act as nucleating agent for PLLA.[189] As a result, the nanocomposites possess higher crystallinity compared to the neat polymer. It can also be seen that RP**1** reduces the crystallisation kinetics of PLLA, probably due to the acetyl side chains on RP**1** as such substitution is known to decrease main chain crystallisation.[213]

Table 20: Glass transition temperature (Tg), crystallisation temperature (Tc), melt temperature (Tm) and crystallinity of the polymer and its nanocomposites.

Polymers	T_g (°C)*	T_c (°C)†	T_m (°C)§	χ_c (%)
PLLA	63 ± 3	113 ± 2	171 ± 2	18 ± 2
RP**1**	52 ± 4	119 ± 1	151 ± 3	6 ± 2
PLLA-RP**1** (5 wt.-%)	53 ± 2	113 ± 1	167 ± 4	5 ± 3
PLLA-BC (5 wt.-%)	58 ± 5	89 ± 4	167 ± 2	25 ± 5
RP**1**-BC (5 wt.-%)	45 ± 8	88 ± 2	146 ± 7	16 ± 6
PLLA-RP**1** (4.75 wt.-%) -BC (5 wt.-%)	57 ± 2	87 ± 3	166 ± 6	28 ± 2

* determined from half-C_p method.
† obtained from the peak of the exotherm.
§ obtained from the peak of the endotherm.

6.3.3 Mechanical performance of the polymers and nanocomposites

The tensile properties of both the polymers and BC reinforced nanocomposites were determined (Table 21). The data show that RP**1** has a low Young's modulus (E = 3.74 GPa) and low tensile strength (σ = 35.6 MPa) compared to PLLA (E = 4.08 GPa and σ = 63.1 MPa). The crystallinity of RP**1** (estimated from melting enthalpy compared to that of crystalline PLLA) was found to be only 6% (see Table 20). RP**1** is a random copolymer of monomer **1** and L-LA, it can be assumed that the reduced stiffness and strength, compared to PLLA, are due to the reduction in crystallinity, probably due to the two acetyl substituents.[214] Blending RP**1** with PLLA (at a loading of 5 wt.-%) resulted in an improvement in the tensile strength of the blend, which increased by 58% from 35.6 MPa (neat RP**1**) to 56.1 MPa. It is generally proposed that improvements in tensile strength of polymer blends result from an increase in the number of network chains per unit volume, formed by increased polymer entanglement and packing density.[215] The PLLA-BC (5 wt.-%) nanocomposite showed a higher Young's modulus, increasing by 12% (from 4.08

GPa to 4.55 GPa) compared to neat PLLA. The rule-of-mixtures for composite materials predicts that the introduction of a stiff filler/reinforcement (in this case, the stiff BC nanofibres) into a softer polymer matrix (in this case, PLLA) will improve the Young's modulus of the composite. However, the tensile strength of the PLLA-BC (5 wt-%) nanocomposite decreased by 10%, from 63.1 MPa for PLLA to 57.8 MPa for the composite. This result is consistent with our previous findings and is a result of insufficient interfacial adhesion between BC nanofibrils and PLLA.[202]

When BC nanofibres were used as filler (5 wt.-%) in RP**1,** the Young's modulus of the resulting nanocomposites increased from 3.74 GPa for neat RP**1** to 4.33 GPa for RP**1**-BC (Table 21). However, contrary to the results for PLLA, the tensile strength of the RP**1**-BC nanocomposite also improved from 35.6 MPa to almost 52 MPa. This improvement is attributed to the better affinity between BC nanofibrils and RP**1**, which enables efficient transfer of stress from the matrix to the reinforcing nanofibres. The direct wetting measurements corroborate the tensile properties of the nanocomposites (see Table 19). As already mentioned, the improved affinity between BC nanofibres and RP**1** is a direct result of the hydrophilic nature of RP**1**.[211] This result also implies that RP**1** has the potential to be used as a compatibiliser to produce BC reinforced PLLA nanocomposites.

To further investigate this hypothesis, BC reinforced PLLA nanocomposites with RP**1** as compatibiliser (5 wt.-% relative to the total polymer content) were prepared. The BC loading in the polymer was 5 wt.-%. It can be seen from Table 21 that the mechanical performance of PLLA-RP**1**-BC nanocomposites surpasses PLLA-RP**1**, neat PLLA and even PLLA-BC nanocomposites. The Young's modulus and tensile strength of the PLLA-RP**1**-BC nanocomposites improved by 26% and 20%, respectively compared to PLLA-RP**1**, and improved by 15% and 7%, respectively compared to neat PLLA. When comparing the mechanical performance of the PLLA-RP**1**-BC nanocomposite to the PLLA-BC nanocomposite, only a marginal increase in the Young's modulus was observed, but gratifyingly the tensile strength improved significantly, by 17% from 57.8 MPa to 67.4 MPa. These results indicate that RP**1** acts as an excellent compatibiliser for BC in PLLA. Thus, using only 5 wt.-% RP**1** as the compatibilising agent, enables improvement of both the Young's modulus and tensile strength of the nanocomposite. It was hypothesised that this

could be due to the higher affinity of RP1 for BC resulting in migration onto the surface of the BC nanofibrils. The enhanced wetting of RP**1** on BC nanofibrils (Table 19) improved the stress transfer between BC and the bulk polymer. The mechanical tests are in good agreement with the direct wetting measurement, which shows improved wetting.

Table 21: The mechanical properties of BC (5 wt-%) reinforced PLLA, with and without RP1 (5 wt-%) as the compatibiliser

Samples	E (GPa)	σ (MPa)
PLLA	4.08 ± 0.07	63.1 ± 2.0
RP**1**	3.74 ± 0.04	35.6 ± 1.9
PLLA-RP**1** (5 wt-%)	3.75 ± 0.05	56.1 ± 1.1
PLLA-BC (5 wt-%)	4.55 ± 0.03	57.8 ± 5.9
RP**1**-BC (5 wt-%)	4.33 ± 0.09	51.9 ± 0.5
PLLA-RP**1** (4.75 wt%)-BC(5 wt-%)	4.71 ± 0.13	67.4 ± 1.1

E and σ denote the Young's modulus and tensile strength, respectively.

6.4 Conclusions

The use of a bio-derived PLLA copolymer (RP**1**) as a compatibilising agent to produce BC reinforced PLLA nanocomposites with high stiffness and strength is reported in this chapter. Direct wetting measurements showed that RP**1** had a higher affinity for BC than PLLA. A polymer blend, containing 5 wt.-% RP**1** in PLLA, also showed an improved affinity for BC compared to PLLA. Nanocomposites were prepared, by dissolving all components in suitable solvents (1,4-dioxane) and were processed using injection moulding. The thermal characterisation of the polymer blend and the nanocomposites using DSC showed that BC aids the crystallisation of the PLLA, RP**1** and PLLA+RP**1** blend. In addition to this, the addition of RP**1** into PLLA does not have a negative impact on the T_g of the materials. Tensile tests on RP**1** alone established that RP**1** possesses low Young's modulus (3.74 GPa) and tensile strength (35.6 MPa). PLLA has a Young's modulus and tensile strength of 4.08 GPa and 63.1, respectively. The preparation of nanocomposites using either PLLA or RP**1** as the matrix, and 5 wt.-% BC as the reinforcement, resulted in the Young's modulus being improved by 12% and 16%, respectively, when compared to the either of the polymers alone. This is attributed to the presence of stiff BC nanofibrils in the matrix. Unfortunately, the tensile strength of the PLLA-BC

nanocomposite decreased by 8% vs. PLLA, due to poor compatibility between the matrix and reinforcement. However, the tensile strength of RP**1**-BC, improved by 46% compared to neat RP**1**, due to the improved compatibility. The preparation of nanocomposites using RP**1** as the compatibiliser, at just 5 wt-% loading, resulted in a improvement of both the Young's modulus (15% higher) and the tensile strength (7% higher) compared to the PLLA-BC composite. T_g of the nanocomposites did not change significantly compared to their respective neat polymers or polymer blend. However, the presence of BC reduced the T_c of the nanocomposites as BC is an effective nucleating agent. This is accompanied by an increase in the crystallinity of the nanocomposites compared to the neat polymer and polymer blend. The bio-derived copolymer enables enhanced fibre-matrix stress transfer leading to better performance. The approach is completely different to the conventional use of petrochemically derived compatibilisers, such as maleic anhydride grafted PLA, and highlights the potential to use bio-derived polymers to prepare fully renewable composite materials.

Chapter 7 – Comparing nanocellulose obtained top-down and bottom-up: Nanofibrillated cellulose versus bacterial cellulose

Summary

This work investigates the difference between nanofibrillated cellulose (NFC) and bacterial cellulose (BC). BC possesses higher critical surface tension of 57 mN m^{-1} compared to NFC (41 mN m^{-1}). The thermal degradation temperature of BC was also found to be higher than that of NFC, in both nitrogen and air atmosphere. These results are in good agreement with the higher crystallinity of BC based on area under the XRD spectra, measured to be 71% as compared to NFC of 41%. Both types of nanocellulose papers were found to possess similar tensile moduli and strengths of 12 GPa and 100 MPa, respectively. Nanocomposites were manufactured by infusing the nanocellulose paper with an epoxy resin using vacuum assisted resin infusion. The cellulose reinforced epoxy nanocomposites were found to possess a stiffness and strength of approximately ~8 GPa and ~100 MPa at an equivalent fibre volume fraction of 60 vol.-%. In terms of the reinforcing ability of NFC and BC in a polymer matrix, no significant difference between NFC and BC was observed.

7.1 Introduction

Cellulose is used in the paper,[110] pharmaceutical and cosmetic industry,[216, 217] and more recently it is explored as reinforcement for polymers.[218, 219] Numerous products are also derived from cellulose; technical textile fibres, such as viscose and Lyocell[220] and thermoplastic polymers, such as cellulose acetate. Currently, much research activity and attention focused on the isolation and production of nano-scale cellulose fibres. For comprehensive reviews on the production and application of nanocellulose, the readers are referred to publications by Klemm at al.[221] and Siró et al.[155] Interests in nanocellulose come from the fact that nano-scale cellulose combines the physical and chemical properties of cellulose, such as hydrophilicity

and the ability to be chemically modified by a broad range of reactions, with the features of nanomaterials – high specific surface area and aspect ratio.

Nanocellulose can be obtained by two approaches: top-down and bottom-up. The top-down approach involves the disintegration of (ligno)cellulose biomass, such as wood fibres into nanofibres. This technique was first reported by Herrick et al.[222] and Turbak et al.,[151] whereby wood pulp was fed through a high-pressure homogeniser to reduce the size of the fibres down to the nano-scale. A more recent method of producing nanocellulose from plant-based cellulosic fibres involves using of grinders,[173] whereby wood pulp is passed through the slit between a static and rotating grindstone. This high shear fibrillation process converts micrometre-sized cellulose into nanocellulose. Herein, these plant derived nano-scale cellulose is termed nanofibrillated cellulose (NFC).

Nanocellulose produced via the bottom-up approach utilises the fermentation of low molecular weight sugar using cellulose producing bacteria, such as from the *Acetobacter* species, to produce nanocellulose.[153, 216, 223, 224] These nanocellulose, herein termed bacterial cellulose (BC), is pure cellulose without the presence of pectin or lignin.[115] The cellulose is excreted by the bacteria into the aqueous culture medium as nanofibres, with a diameter ranging from 25 – 100 nm.[115, 223] These nanofibres makes up the pellicles in the culture medium.[223]

Utilising nanocellulose as filler in polymer matrices was first reported by Favier et al.[225] The authors reinforced latex (styrene-butyl acrylate copolymer) with cellulose nanowhiskers derived from tunicin to produce polymer nanocomposites. Since then, studies on utilising nanocellulose as filler in polymer matrices have increased significantly over the years. The major driver for this is the potential of exploiting the high stiffness of cellulose crystals. X-ray diffraction and numerical simulations estimated the stiffness of a cellulose crystal to be approximately 100-160 GPa,[121, 194] which is highly desirable as reinforcing filler for polymer matrices. However, it is not clear what is the true crystal modulus of cellulose nor its maximum attainable stiffness as reinforcing filler.[118] Nonetheless, nanocellulose has been shown to improve the mechanical performance of the resulting nanocomposites. Yano et al.[226] have obtained a tensile modulus and strength of up to 21 GPa and 325 MPa,

respectively, for a BC sheet reinforced epoxy resin with a nanocellulose loading of 70 wt.-%. However, the authors failed to explain why the tensile strength of the nanocomposites was 25% higher than that of the reinforcing BC sheets. Nevertheless, this study showed that high strength nanocomposites can be produced using BC sheets. Laminated BC-polylactide nanocomposites at a loading fraction of 18 vol.-% have also been studied.[227] The tensile modulus doubled and the strength tripled when compared to neat polylactide. NFC has also shown to improve the mechanical properties of the nanocomposites. Henriksson et al.[228] produced NFC sheet reinforced hexamethoxymethyl melamine-based nanocomposites; at a volume fraction of 55 vol.-%, a Young's modulus of 9.7 GPa and tensile strength of 108 MPa was achieved. The neat polymer possesses a Young's modulus and tensile strength of only 3.6 MPa and 6.1 MPa, respectively.

It is evident that BC and NFC have the ability to act as reinforcement for the production of high strength and stiffness materials. However, there are currently no systematic studies reporting the surface and bulk properties of NFC and BC, and the reinforcing capability of these two types of nanocellulose for composite materials. With nanocellulose gaining significant research interest, it is important to quantify the differences, if any, between NFC and BC. Therefore, the aim of this work is to elucidate the differences in terms of their wettability, ζ-potential, crystallinity, thermal degradation behaviour and mechanical properties of NFC and BC. This article also demonstrates and discusses the reinforcing ability of NFC and BC in nanocomposites applications.

7.2 Experimental section

7.2.1 Materials

n-Hexane (GPR RECTAPUR, purity ≥ 95%), dimethyl sulfoxide (analytical reagent, purity ≥ 99.5%) and water (HiperSolv CHROMANORM, purity ≥ 99.5%) were purchased from VWR. n-Dodecane (purity ≥ 99%) and formamide (purity ≥ 99.5%) were purchased from Acros Organics. Ethylene glycol (Aldrich, purity ≥ 99%) was purchased from Sigma-Aldrich. All these chemicals were used without purification for wicking rate measurement of NFC and BC. Ultra low viscosity epoxy resin (PRIME 20ULV, Gurit Ltd, Isle of Wight & Hamble, UK) was used as the matrix

for the nanocomposites. BC was kindly supplied by fzmb GmbH (Bad Langensalza, Germany) in wet pellicle form containing 94 wt.-% water. NFC was produced by grinding of never-dried bleached birch Kraft pulp (*Betula pendula*). The grinding of birch pulp was conducted using a Masuko Mass Colloider (Masuko Sangyo Co., Kawaguchi, Japan). The pulp was passed through the grinder seven times and the final consistency of the aqueous gel-like NFC was approximately 2 wt-%.

7.2.2 Large scale manufacturing of BC and NFC papers

BC and NFC papers with a grammage of 60 g m^{-2} were produced using a home-made vacuum assisted sheet former equipment designed by VTT in cooperation with Metso Paper. Firstly, the BC pellicles were cut into small pieces and blended for 2 min using a blender (Breville BL18 glass jug blender, Pulse Home Products Ltd, Oldham, UK) at a consistency of 0.1 wt.-%. The NFC suspension was adjusted to 0.4 wt.-% from 2 wt.-% consistency and blended for 2 min using the blender to produce a homogenous dispersion of nanocellulose in water. These nanocellulose suspensions were then vacuum filtered onto a filter. The filter cake was then wet pressed twice under a weight of 10 kg between bloating papers for 10 s. The partially dried nanocellulose sheets from the wet pressing steps were then sandwiched between bloating papers and metal plates under a weight of 10 kg during the drying process in the oven held at 55°C for at least 48 h to dry. This was to prevent the nanocellulose sheets from shrinking during the drying process. Shrinkage of cellulose sheets will induce flexibility in the fibre network and decrease the load bearing capability of the resulting sheets.[229]

7.2.3 Manufacturing of BC or NFC paper reinforced nanocomposites

The nanocellulose paper reinforced epoxy was produced using vacuum assisted resin infusion (VARI). A schematic diagram of the VARI lay-up is shown in Figure 30. A polyester porous flow medium (15087B, Newbury Engineer Textile, Berkshire, UK) was placed on top of the tooling side (a 460 mm x 920 mm heating plate with a temperature control unit), which consisted of a layer of polyester film (Melinex PW 122-50-RL, PSG group, London UK). 11 nanocellulose papers were laid up and sandwiched between two PTFE coated glass release fabrics (FF03PM, Aerovac, West Yorkshire, UK) and placed on top of the polyester porous flow medium.

Another polyester porous flow medium was then placed on top of the release fabric. The whole setup was covered with a vacuum bagging film (Capran 519 heat stabilised Nylon 6 blown tubular film, Aerovac, West Yorkshire, UK) and sealed using a vacuum sealant tape (SM5127, Aerovac, West Yorkshire, UK).
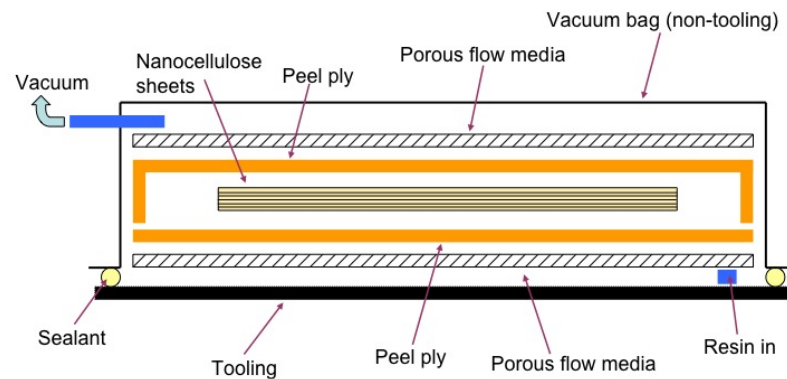
Figure 30: Schematic diagram of the VARI process.

Prior to the infusion, the epoxy and hardener were mixed thoroughly at a ratio of 100:19 by weight and degassed at room temperature under a reduced pressure of 75 mmHg for 5 min. This ensures that all air bubbles trapped during the mixing process were removed. The infusion process starts with an air removal step, whereby a vacuum was applied to the system via the tubing on the non-tooling side with the resin inlet tubing sealed off. When the maximum vacuum was reached (~15 mmHg), the VARI setup was left under this vacuum for 2 h to ensure that there was no leakage in the set up by constantly monitoring the pressure in the vacuum bag. Once the system was determined to be leakage-free, the liquid resin was fed at room temperature from the bottom of the polyester porous flow medium on the tooling side through the nanocellulose sheets and exit via the tubing on the non-tooling side. The inlet and outlet of the system were sealed off again when the resin fully impregnated the nanocellulose sheets. The resin was left to cure at room temperature for 24 h, followed by a post-curing step conducted at 50ºC for 16 h.

7.2.4 Characterisation of nanocellulose and its nanocomposites
7.2.4.1 Scanning electron microscopy (SEM)
SEM was used to study the morphology of NFC and BC nanofibres. It was performed using a high-resolution field emission gun scanning electron microscope (LEO Gemini 1525 FEG-SEM, Oberkochen). The accelerating voltage used was 5

kV. Prior to SEM, the nanocellulose was solution cast from water onto carbon tabs stuck on the SEM stubs, air dried and Cr coated (K550 sputter coater, Emitech Ltd, Ashford, Kent, UK) for 1 min at 75 mA.

7.2.4.2 X-ray diffraction (XRD) to determine the crystallinity of nanocellulose

The XRD pattern of NFC and BC nanofibres was measured using an X-ray diffractometer (PANalytical X'Pert Pro, PANalytical Ltd, Cambridge, UK) equipped with 1.54 Å Cu Kα X-ray source. Measurements were taken from $2\theta = 10°$ to $40°$ using a step size and scan speed of $0.05°$ and $0.2°$ s^{-1}, respectively. The crystallinity of the nanocellulose was calculated based on the area under the curve of the XRD diffraction pattern using:

$$\chi_c = \frac{A_c}{A_c + A_a} \times 100\%$$

(7.1)

where A_c and A_a are the total crystalline and amorphous areas, respectively, between the measured Bragg's angles.

Scherrer's equation,[131]

$$L_{002} = \frac{0.91 \times \lambda}{\beta \times \cos\theta}$$

(7.2)

where θ, β, and λ are the Bragg's angle (in degrees), full width at half maximum of the 002 reflection, and wavelength of the X-ray source used, respectively, was used to determine the crystallite size and hence, the structural order of the 002 reflection (L_{002}).

7.2.4.3 Determining the critical surface tension (γ_c) of NFC and BC nanofibres

γ_c of NFC and BC nanofibres were determined from wicking measurements.[230] The nanocellulose sheets were cut into rectangular strips of 5 mm × 20 mm. One end of the strip was mounted onto an ultra sensitive microbalance (Type 4505 MP8-1, Sartorius ultramicro, Göttingen, GmbH). The reservoir containing the test liquid is moved upwards towards the other end of the strip until it touches the sample, then

the movement of the reservoir was immediately stopped. This ensures that the mass gain of the sheets is only a result of the penetration of the test liquid into the nanocellulose strips due to capillarity. During the measurement, the mass gain of the strip was recorded as a function of time. A total of 5 strips were tested for each test liquid. These data was then evaluated using the Washburn equation for a single capillary,[231] which is derived from the combination of the Laplace and Hagen-Poiseuille equations for steady state, laminar flow through a capillary neglecting gravity:

$$\gamma_{lv} \cos\theta = \left[\frac{2}{A^2 r}\right]\left[\frac{\eta}{\rho^2}\right]\left[\frac{m^2}{t}\right] \tag{7.3}$$

where γ_{lv}, η, ρ, are the surface tension, viscosity and density of the test liquid, respectively, and m, A, r, θ and t are the mass gain due to capillarity, cross-sectional area of the capillary, radius of the capillary, contact angles and time, respectively.

However, for the case of these nanocellulose sheets, the geometry of the capillary is unknown. Therefore, the factor $\left[\frac{2}{A^2 r}\right]$ can be grouped as a factor $\left[\frac{1}{C}\right]$ and assuming the geometry of the capillary is constant[232] throughout the measurement, the following equation can be obtained:

$$C\gamma_{lv} \cos\theta = \left[\frac{\eta}{\rho^2}\right]\left[\frac{m^2}{t}\right] \tag{7.4}$$

By performing this measurement using a series of different test liquids with known γ_{lv}, the critical surface tension of the solid, γ_c, which corresponds to the maximum of the $\left[\frac{m^2}{t}\right]\left[\frac{\eta}{\rho^2}\right] = f(\gamma_{lv})$, can be determined.[230]

7.2.4.4 Electrokinetic behaviour of NFC and BC

The electrokinetic behaviour of the nanocellulose was evaluated using ζ-potential measurements using an electrokinetic analyser (EKA, Anton Paar, Graz, Austria) based on streaming potential method. In order to exclude any overlaying effects due

to the swelling of the nanocellulose or extraction of water-soluble components from the samples, the pH dependency of ζ-potential was measured only after a time dependent ζ-potential measurement in 1 mM KCl electrolyte was completed. During the $\zeta = f(t)$ measurement, the streaming potential was generated by applying a steady pressure increase to 250 mbar across a channel, which was created by stacking two nanocellulose sheets between a PTFE channel. The pH dependency of the ζ-potential was then measured by changing the pH of the 1 mM KCl electrolyte solution by adding 0.1 N HCl or KOH using a titration unit (RTU, Anton Paar, Graz, Austria).

7.2.4.5 Thermal stability of NFC and BC nanofibres: thermogravimetry analysis (TGA)

The thermal degradation behaviour of NFC and BC nanofibres was investigated using TGA (TGA Q500, TA Instruments, UK). Samples of 5 mg were heated from room temperature to 600ºC at a heating rate of 10ºC min^{-1} in nitrogen and air atmosphere.

7.2.4.6 Density of nanocellulose sheets and their nanocomposites

He pycnometry (AccuPyc 1330, Micromeritics Ltd, Dunstable, UK) was used to measure the true density of nanocellulose sheets and their nanocomposites. The volume fractions of nanocellulose in the composites are then back calculated from their respective densities. The thickness of the nanocellulose sheets was measured using a micrometer. With the thickness known, the bulk volume was calculated and the bulk density was determined by taking the ratio between the mass and the bulk volume of the evaluated sheet. The porosity (P) was then calculated using:

$$P(\%) = \left(1 - \frac{\rho_{bulk}}{\rho_{sheets}}\right) \times 100 \tag{7.5}$$

where ρ_{bulk} and ρ_{sheets} are the bulk and true density of the nanocellulose sheets, respectively.

7.2.4.7 Tensile properties of the nanocellulose sheets and nanocomposites

Nanocellulose sheets were cut into dog bone shape specimens using a Zwick cutter. The test specimen possesses an overall length of 35 mm and the narrowest part of the specimen is 2 mm. Prior to the test, the specimens were secured onto testing cards using a two-part cold curing epoxy resin (Araldite 2011, Huntsman Advanced Materials, Cambridge, UK). This was to prevent the clamp of the tensile testing equipment from damaging the test specimens. Tensile test was conducted using a TST350 tensile tester (Linkam Scientific Instruments, Surrey, UK). The load cell and crosshead speed used were 200 N and 1 mm min^{-1}, respectively. The sample thickness was determined using a digital micrometer. A total of 5 specimens were tested for each type of nanocellulose. The machine compliance was determined to be 7.19×10^{-3} mm N^{-1}.

The nanocomposites were tested in tension using an Instron universal material testing equipment (Instron 4505, Instron Corporation, MA, USA). The tensile test was conducted in accordance to ASTM D3039-00 using a load cell of 10 kN. The test specimens possessed dimensions of $100 \times 10 \times 1$ mm, with a gauge length of 40 mm. Prior to the test, woven glass fibre reinforced polyester end tabs with 1.6 mm thickness were glued onto the samples using a two-part cold curing epoxy resin (Araldite 2011, Huntsman Advanced Materials, Cambridge, UK). The distance between the end tabs were 60 mm. Strain gauges (FLA-2-11, Techni Measure, Studley, UK) were glued onto the middle portion of the test specimen using cyanoacrylate glue (EVERBUILD Building Products Ltd, Leeds, UK). Specimens were tested until failure at a crosshead speed of 1 mm min^{-1}. A total of 5 specimens were tested for each type of nanocomposites.

7.3 Results and discussions
7.3.1 Morphology of NFC and BC

The morphology of the two different forms of nanocellulose (solution cast from 0.05 wt.-% concentration) was studied using scanning electron microscopy (SEM) (see Figure 31). Both types of nanocellulose possess a fibrous structure with dimensions of approximately 50 nm in diameter and several micrometres in length. It

can also be seen that the diameter of the nanofibres are very uniform. This is not surprising for BC as its production is well-controlled by the biosynthesis of cellulose producing bacteria, whereby the nanocellulose is spun out by bacteria and assembled into the ribbon-shaped nanofibres.[233] The production of NFC, on the other hand, was through the shearing of wood pulp through a grinder. This repeated shearing and grinding actions ensure a uniform fibre diameter.[234] In addition to this, both the NFC and BC papers are also translucent (see Figure 32). This translucency is due to the lack of scattering of light by the nanofibres that made up the papers.[226] It appears that the BC sheet is less translucent compared to NFC sheets. This difference is attributed to the difference in the thickness between BC and NFC sheets.[235] BC and NFC sheets made from suspensions (grammage of 60 m^2 g^{-1}) were 79 μm and 64 μm thick, respectively.
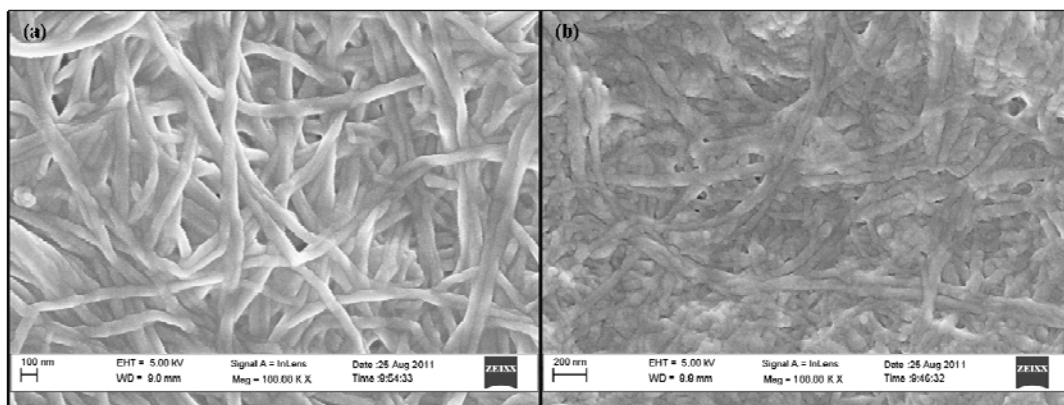
Figure 31: Scanning electron micrographs of (a) BC nanofibres and (b) NFC.

Figure 32: A comparison of the optical transparency of NFC and BC sheets. Left: BC sheet and right: NFC sheet.

7.3.2 X-ray diffraction (XRD) of NFC and BC

The XRD pattern of NFC and BC is shown in Figure 33. The diffraction pattern of BC exhibited the typical diffraction peaks of native cellulose at 14°, 16°, 22.5°, 34°, which corresponds to the diffraction plane of 101, $10\bar{1}$, 002 and 040, respectively.[159] The diffraction pattern of NFC showed two broad peaks around 15° and 22.5°. Similar diffraction patterns were also observed by Leppänen et al.;[236] native (cotton) cellulose exhibited two distinct peaks corresponding to 101, $10\bar{1}$ but Kraft pulp exhibited only one but broad peak at 15°. The absence of two distinct peaks around $2\theta = 14°$-16° can be attributed to the presence of non-cellulosic compounds such as hemicellulose in NFC and the difference in cellulose crystal structures of NFC.
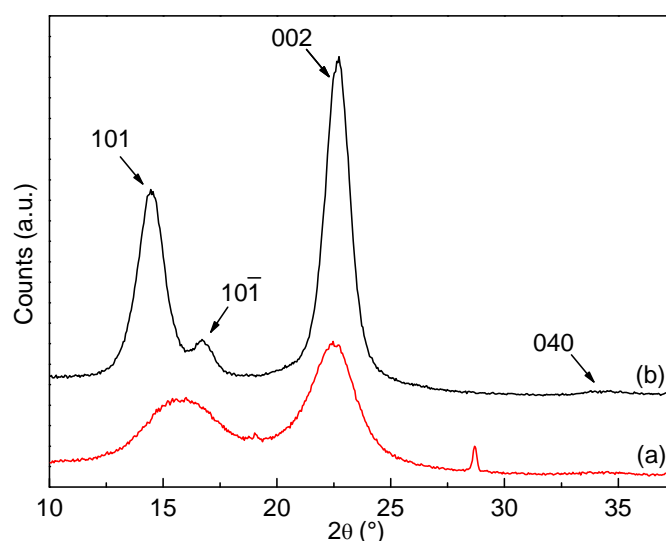
Figure 33: X-ray diffraction pattern of (a) NFC and (b) BC.

The crystallinity of all the samples were calculated based on the area under the curves of the diffraction pattern (see equation 7.1), instead of the more commonly used Segal equation.[130] These results are tabulated in Table 22. Segal's equation is a semi-empirical equation derived for native cellulose (cotton) without any impurities and therefore, the crystallinity obtained for NFC using this equation would not be accurate. BC possesses a higher crystallinity compared to NFC (see Table 22). BC also possesses a larger crystallite size and smaller d-spacing compared to NFC. This is due to the fact that NFC possesses high content of amorphous non-cellulosic compounds, such as hemicellulose and carbohydrates. The carbohydrate composition

of the pulp and the NFC produced from it are very similar. The composition is 73% glucose, 26% xylose and 1 % mannose.[237] The pulp contains also 0.2% residual lignin and 0.09% residual extractives.[238] In addition to this, the difference in the crystallite size and d-spacings of NFC and BC could be ascribed to the difference in crystal structures between the two types of cellulose. BC is predominantly cellulose-Iα whereas plant-based cellulose such as NFC is predominantly cellulose-Iβ.[159] This difference in the types of crystal structures result in the observed difference in crystallite size and d-spacings.[239]

Table 22: A comparison of the crystallinity (χ_c), d-spacing ($d_{(002)}$) and the crystallite size of the 002 reflection ($L_{(002)}$), critical surface energy (γ_c), onset degradation temperature in N_2 ($T_{d, N2}$) and air ($T_{d, air}$) of NFC and BC, respectively.

Types of nanocellulose	χ_c (%)	$d_{(002)}$ (Å)	$L_{(002)}$ (Å)	γ_c (mN m^{-1})	$T_{d, N2}$ (°C)	$T_{d, air}$ (°C)
NFC	41 ± 5	8.07 ± 0.01	31.82 ± 0.32	41.7 ± 0.8	247 ± 2	244 ± 1
BC	72 ± 1	7.99 ± 0.01	62.94 ± 0.15	57.0 ± 0.2	294 ± 1	289 ± 1

7.3.3 Critical surface tension of BC and NFC

Wicking of test liquids into nanocellulose paper was used to characterise the wetting kinetics of nanocellulose and to determine the surface energy. Typical wetting curves are shown in Figure 34. The initial slope is a result of capillary effect and the plateau is caused by the balance between capillarity and gravity.[230] By evaluating the initial slope of wetting curves, a plot of the normalised wetting rate (right hand side of equation 7.4 in the experimental section) against the surface tension of the test liquids can be produced (see Figure 35). This plot shows a maximum point, which is analogous to the Zisman's critical solid-vapour surface tension of the investigated nanocellulose.[230] The liquids with surface tension values to the left of the maximum will fully wet the nanocellulose whilst partial wetting is obtained with liquids having surface tension values to the right of the maximum. The data points shown in Figure 35 were fitted with a polynomial curve. The maximum point, corresponding to the critical surface tension of cellulose, which is equal to the surface tension of a liquid just wetting a solid completely, is summarised in Table 22. BC has a γ_c of 57 mN m^{-1} compared to NFC of 41.7 mN m^{-1}. The high γ_c value for BC could be ascribed to its high crystallinity[240, 241] and purity.[242] On the other hand, NFC is a composite material consisting of cellulose and hemicellulose and

both constituents will contribute to the overall solid surface tension of NFC. The surface tension of hemicellulose was found to be lower than that of cellulose.[242] This resulted in the observed lower surface tension of NFC compared to BC.
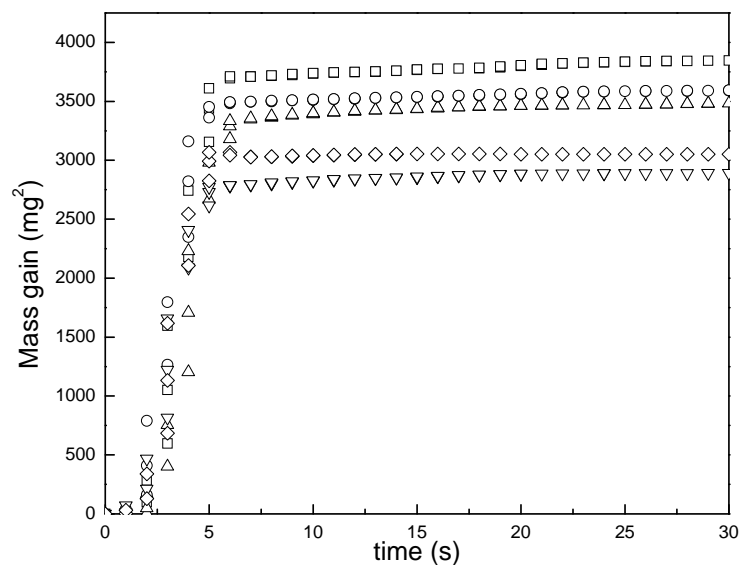
Figure 34: Typical wetting curves of BC by water.
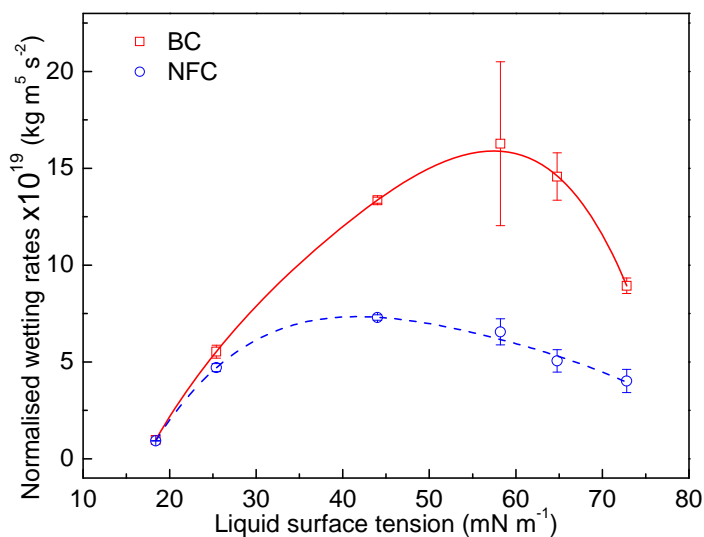
Figure 35: Normalised wetting rates as a function of the surface tension of test liquids for NFC and BC.

7.3.4 Streaming potential of NFC and BC sheets

ζ-potential provides information regarding the surface chemistry of a material and the formation and composition of the electrochemical double layer when this material is in contact with an aqueous electrolyte solution. Figure 36 shows the streaming ζ-potential of NFC and BC as a function of pH. The formation of the electrochemical double layer is predominantly due to the adsorption of electrolyte

ions onto the surface and the dissociation of Brønstedt acid/base groups. The ζ-potential shows a plateau at high pH, indicating that the surface is acidic as all dissociable functional groups, such as –OH group, are fully deprotonated. As the pH decreased, the ζ-potential becomes more positive due to (i) protonation of functional groups and (ii) adsorption of protons (H_3O^+) onto the surface. As the pH is decreased further, the ζ-potential reaches zero, which corresponds to the isoelectric point (iep) of the investigated surface. This is the point where no net charge is present on the surface. After iep, the decrease in pH resulted in the drastic increase in ζ-potential due to the adsorption of protons.
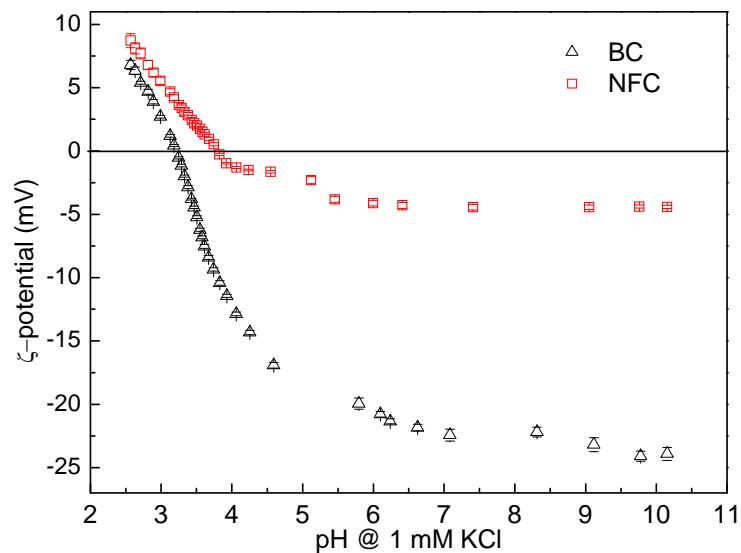
Figure 36: ζ = f(pH) of NFC and BC sheets.

Table 23 summarises the iep and the plateau values of ζ-potential ($\zeta_{plateau}$) of NFC and BC. NFC and BC possess iep of pH = 3.8 and 3.2, respectively. The iep is governed by the pK_a of all the dissociable functional groups present.[243] In the case of BC, the iep is due to dissociation of -OH groups in cellulose molecules, with pKa values of between 2.5 and 3.4 (estimated based on purified cotton cellulose).[244] On the other hand, the dissociable functional groups in NFC include the –OH and carboxyl (-COOH) groups present in the cellulose and hemicellulose, such as xylan and glucose, which possess pK_a values of 3.7[245] and 5.6,[246] respectively. The observed more negative value of $\zeta_{plateau}$ for BC compared to NFC can also be attributed to the low crystallinity and high hemicellulose content of NFC. Hemicellulose is known to swell in water.[247] The lower crystallinity of NFC also enhances the swelling effect due to the high water uptake.[248] This swelling of NFC

124

causes the transfer of the plane of shear into the electrolyte that excludes the diffusive part of the electric double layer from mechanical and electrical interaction.[249] This is also supported by the $\Delta\zeta$ obtained from $\zeta = f(t)$ measurement. The quotient $\Delta\zeta = (\zeta_\infty - \zeta_0) / \zeta_0$ provides indication of the degree of swelling of the investigated surface.[77] The larger $\Delta\zeta$ value of NFC (low crystallinity) indicates a higher degree of swelling compared to BC (high crystallinity), which possesses a lower $\Delta\zeta$ value. These results are in good agreement with the observed more negative $\zeta_{plateau}$ value for BC compared to NFC.

Table 23: The isoelectric point (iep), $\zeta_{plateau}$ and $\Delta\zeta$ of NFC and BC sheets.

Nanocellulose	iep (pH)	$\zeta_{plateau}$ (mV)	$\Delta\zeta = (\zeta_\infty - \zeta_0) / \zeta_0$
NFC	3.8 ± 0.1	-4.3 ± 0.1	0.125
BC	3.2 ± 0.1	-22.9 ± 0.9	0.064

7.3.5 Thermal degradation behaviour of NFC and BC
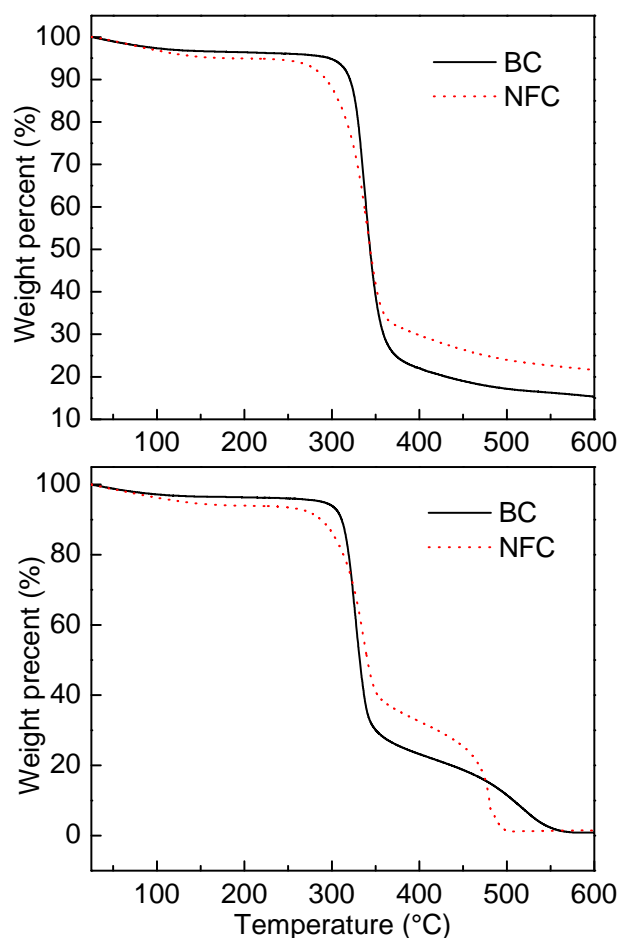
Figure 37: Thermal degradation behaviour of NFC and BC in nitrogen (top) and air (bottom), respectively.

The thermal degradation behaviour of NFC and BC is shown in Figure 37. The onset degradation temperatures in nitrogen and air are tabulated in Table 22. In nitrogen atmosphere, both the nanocellulose underwent a single step thermal degradation (see Figure 37, top). The initial weight loss in temperatures of 50 – 150°C is mainly due to removal of moisture from the cellulose. The thermal degradation occurring between temperatures of 250-400°C is attributed to the depolymerisation of hemicellulose (for NFC) and cleavage of glycosidic linkages of cellulose (for both NFC and BC).[250] In air, a two-step thermal degradation behaviour for NFC and BC was observed (Figure 37, bottom). The initial weight loss between 300-350°C is attributed to the decomposition of smaller molecular fragments of the sample and the second decomposition step (350-500°C) is attributed to the degradation of the six-member cyclic structure of cellulose (pyran).[251, 252] Even though the thermal degradation behaviour of NFC and BC are very similar in nitrogen and air atmosphere, the onset degradation temperature of NFC is lower than that of BC (see Table 22). The earlier onset degradation of NFC can be attributed to its lower crystallinity compared to BC.[253]

7.3.6 Tensile properties of sheets and nanocomposites

Both types of nanocellulose sheets possess a stiffness and strength of approximately 12 GPa and 110 MPa (see Table 24), respectively. These values are consistent with the mechanical properties of nanocellulose sheets studied by Henriksson et al.[228] and Iwamoto et al.[254] At first glance, it seems surprising that BC sheets, which have a much higher degree of crystallinity possess almost the same tensile properties as NFC. However, BC paper is more porous compared to NFC paper (see Table 25). The porosity of BC paper was found to be 52% compared to NFC paper of only 38%. It is postulated that the more crystalline nature of BC led to a decrease in the packing efficiency of the nanofibres. Nevertheless, it is quite remarkable that BC papers with such a high porosity possess good mechanical properties. In addition to the difference in porosity of the papers, the presence of hemicellulose also affects the mechanical properties of NFC papers. Hemicellulose aids the nanofibres to bonding together forming a composite.[254, 255] As a result, NFC with lower crystallinity and porosity possesses a similar strength and stiffness to BC (higher crystallinity and porosity). BC, on the other hand, has a higher strain-to-failure at 7.5% compared to

NFC of only 4.2%. The lower strain-to-failure of NFC papers could be due to fewer physical crosslink points between the nanofibres, which allows for the realignment of the fibres during tensile loading. This is accompanied by reduction in the strain-to-failure of the nanocellulose sheets. The tensile work of fracture (W_A, calculated from the area under the stress-strain curve) was also smaller for NFC papers compared to BC papers. This could be due to the higher strain-to-failure of BC papers, which allows for more energy to be absorbed during tensile loading.

Table 24: Mechanical properties and the properties of NFC and BC sheets. E_{sheet}, σ_{sheet}, ε_{sheet} and W_A indicate Young's modulus, tensile strength, elongation at break, true density of the sheet and work of fracture, respectively.

Types of nanocellulose	E_{sheet} (GPa)	σ_{sheet} (MPa)	ε_{sheet} (%)	grammage (g m^{-2})	W_A (MJ m^{-3})
NFC	12.8 ± 1.4	103 ± 13	4.2 ± 0.8	59.5 ± 0.4	3.8 ± 0.7
BC	12.0 ± 1.1	123 ± 7	7.5 ± 0.6	57.2 ± 3.2	5.8 ± 0.6

Table 25: The bulk density (ρ_{bulk}), true density (ρ_{sheet}) and porosity (%) of the nanocellulose sheets

Nanocellulose	ρ_{bulk} (g cm^{-3})	ρ_{sheet} (g cm^{-3})	P (%)
NFC	0.93 ± 0.01	1.51 ± 0.02	38.4 ± 0.7
BC	0.72 ± 0.02	1.54 ± 0.05	52.3 ± 2.2

A stack of 11 sheets of NFC and BC paper were resin infused with an ultra low viscosity epoxy resin. This resin was chosen to ensure that the liquid will impregnate the nanocellulose papers. The surface tension of the liquid epoxy resin (with hardener) was measured[§] to be 32.3 ± 0.1 mN m^{-1}. This liquid resin should fully wet both BC and NFC papers as the critical surface tension of the papers was higher than the surface tension of the resin. The manufactured nanocomposites possess different fibre volume fractions (v_f). In order to be able to compare between the nanocomposites, the Young's moduli of the nanocomposites were normalised to an equivalent fibre volume fraction of 60 vol.-% (see Table 26). Both NFC and BC exhibited excellent reinforcing ability when used in nanocomposites as paper form due to the presence of cellulose network in the reinforcing paper. The Young's

---

[§] Surface tension was measured using pendant drop method performed on Easydrop (DSA 15B, Krüss, Hamburg, GmbH) at 20°C.

modulus of the nanocomposites increased to 8 GPa compared to that of the neat resin of only 3 GPa. This increase is inline with the values calculated using the "rules-of-mixtures" for composites,[†] indicating that the maximum possible Young's modulus of the material was achieved. There is a slight difference in the reinforcing ability between NFC and BC when the tensile strength (σ) was compared. It seems that BC reinforced nanocomposites possesses higher σ compared to NFC reinforced nanocomposites, even when the former possesses slightly lower v_f. This is attributed to the higher surface energy of BC, which promotes better adhesion between the matrix and the reinforcing fibre

Table 26: Fibre volume fraction (v_f) and the mechanical properties of the nanocomposites. E, E_{norm}, σ and ε indicate the Young's modulus, normalised Young's modulus to 60 vol.-% and tensile strength of the nanocomposites, respectively.

Types of nanocellulose	v_f (vol.-%)	E (GPa)	$E_{norm} = (E / v_f) \times 0.6$ (GPa)	σ (MPa)
Neat resin[&]	0	3.0	-	71
NFC nanocomposites	58 ± 1	8.5 ± 0.2	8.8 ± 0.2	96 ± 1
BC nanocomposites	49 ± 2	7.1 ± 0.1	8.7 ± 0.2	102 ± 1

[&] Obtained from manufacturer's data.

7.4 Conclusions

Nanocellulose obtained top-down (NFC) or bottom-up (BC) was studied and compared in this work. SEM showed that both types of nanocellulose posses a fibrous structure of approximately 50 nm in diameter and several micrometre in length. BC had significantly higher degree of crystallinity (as measured by XRD) of 72% compared to NFC of 41%. The lower crystallinity of NFC is attributed to the presence of non-cellulosic compounds such as hemicellulose. NFC was derived from plant-based cellulose and possesses cellulose-Iβ structure whereas BC possesses a cellulose Iα structure. This difference in cellulose structures also resulted in difference in the cellulose crystallite size and d-spacings. The critical surface tension of NFC and BC was determined from the normalised wetting rates as determined by wicking rate measurements. It was found that BC possesses a γ_c of 57 mN m^{-1}. NFC, on the other hand, possesses lower γ_c of 41 mN m^{-1}. ζ-potentials indicate that both surfaces possess acidic characteristics. However, the more amorphous nature of NFC

[†] The moduli used in this calculation are 3 GPa for the matrix, 12.8 GPa for NFC and 12.0 GPa for BC, respectively.

also showed higher degree of swelling and therefore, less negative $\zeta_{plateau}$ compared to BC. In addition to this, the more crystalline nature of BC also resulted in higher thermal degradation temperature as studied by TGA compared to NFC.

Both the NFC and BC papers were found to possess similar tensile properties; a Young's modulus of ~12 GPa and tensile strength of ~110 MPa. When used as reinforcement in an epoxy matrix, the nanocomposites were found to possess a high stiffness and strength of approximately ~8 GPa and ~100 MPa, respectively at an equivalent fibre volume fraction of 60 vol.-%. However, no significant difference was observed between the reinforcing ability of NFC and BC in terms of the stiffness of the nanocomposites. The nanocomposites reinforced with BC papers, however, showed slightly higher tensile strength compared to NFC papers by approximately 6%. Nonetheless, the difference between the tensile strength of the nanocomposites reinforced by NFC and BC is not very significant. This implies that both NFC and BC will serve as excellent reinforcing material for the production of nanocomposites.

Chapter 8 – Creating hierarchical structures in short sisal fibre reinforced polylactide; short hairy fibre reinforced bacterial cellulose nanocomposites

Summary

Hierarchical sisal fibre reinforced bacterial cellulose (BC) polylactide (PLLA) nanocomposites were produced using a simple slurry dipping method to create "hairy" sisal fibres, which were then incorporated into PLLA. Neat sisal fibres were coated with BC to create (i) a dense BC coating around the fibres or (ii) "hairy" fibres, on which BC is oriented perpendicular to the fibre surface. The specific surface area of the BC coated fibres increased when compared to neat sisal fibres. This increased the surface roughness of the fibre resulted in enhanced mechanical interlocking between the fibres and the matrix. Single fibre tensile tests revealed no significant difference in the tensile modulus and tensile strength of "hairy fibres". However, when sisal fibres were coated with a dense layer of BC, the mechanical properties of the fibres decreased. This is due to the manufacturing process where the nano-sized BC nanofibrils were not activated (i.e. not restrained from shrinkage during the drying process) on the surface of sisal fibres. The tensile, flexural and visco-elastic properties of the hierarchical PLLA nanocomposites reinforced by both types of BC coated sisal fibres showed significant improvements over neat PLLA.

8.1 Introduction

There is growing demand nowadays for more environmental friendlier products, greener sustainable technology and materials. Combining these demands with the ever growing problem of global waste, rising oil prices, exhaustion of landfill sites[108] and environmental legislative pressures[148] has led to significant research effort being spent in utilising renewable sources in the polymer industry. Polymer manufacturers are forced to evaluate the life cycle and environmental impact of their

products throughout their products' lifetime. Research interest in utilising natural fibres as reinforcement for polymers is re-emerging in the field of engineering.[5] Natural fibres have the advantages such as high specific strength and modulus, low density, biodegradability and renewability compared to glass fibres.[4] As a result, numerous automotive companies, such as Mercedes-Benz, BMW, Audi and Daimler are replacing some glass fibre based composites with natural fibre reinforced polymers.[172]

However, natural fibres do come with some major drawbacks when used as fibre reinforcement in composite materials. One of the major issues associated with natural fibres is their inherent variability in dimensions and mechanical properties, even when extracted from the same cultivation. Another important factor that limits the use of natural fibres in composites is their low thermal stability. Wielage et al.[37] have shown that the tensile properties of natural fibres can decrease by as much as 60% when the fibres are processed for 60 min at 220ºC. Natural fibres are also inherently hydrophilic in nature due to the presence of large amounts of hydroxyl groups.[36] This is a major drawback for their utilisation in composite materials, often resulting in poor compatibility between hydrophobic polymer matrices, such as polypropylene or polylactide.[13] Numerous attempts have been made to improve the compatibility between hydrophilic natural fibres and hydrophobic polymer matrices.[40] These include silylation, acetylation, benzoylation, the use of maleated coupling agents, isocyanate treatment and polymer grafting of natural fibres. Even though the surfaces of natural fibres have been rendered more hydrophobic through these chemical treatments, large amounts of hazardous chemicals are involved and the chemical waste must be handled and disposed of appropriately. Moreover, chemical treatments of natural fibres do not always translate into composites with improved mechanical performance.[47, 256-259] A possible reason is the anisotropicity of natural fibres. To date, the anisotropicity of natural fibres have been commented on but received little attention.[260] One reason is the great challenge of characterising the transverse properties of natural fibres. Studies on the transverse properties of natural fibres have shown that the transverse moduli of natural fibres are an order of magnitude lower than their axial moduli; jute (axial: 38.4 GPa, transverse: 5.5 GPa),[50] flax (axial: 59 GPa, transverse: 8 GPa)[51] and sisal (axial: 11.5 GPa, transverse: 1.4 GPa).[261] Thomason[52] attributed the disappointment of natural fibres

to deliver good mechanical composite performance compared to glass fibre-reinforced composites to the linear thermal coefficient of expansion (LTCE) of natural fibres. Thermoplastic composites are generally moulded at high temperature and cooled to room temperature. The cooling process results in residual compressive stresses in the reinforcing fibres, as the LTCE of the polymer is often greater than of the fibre. Different types of reinforcing fibres however, do have different LTCE. The LTCE of glass fibres is approximately 15 times smaller than jute fibres.[52] As a result, the residual compressive stress on the reinforcing fibres is smaller for jute fibres compared to glass fibres, as jute fibres shrink more than glass fibres. This contributes to a poor interface between fibres and matrix and, therefore, reduced overall mechanical performance of the composites.

In this study, the aim is to address the challenge of poor interfacial adhesion of sisal fibres to thermoplastics by attaching nano-sized cellulose onto the fibre surfaces to produce natural fibre reinforced composites with improved properties. Bacterial cellulose (BC) is pure highly crystalline cellulose, with a degree of crystallinity of up to 90%.[120] This highly crystalline structure of BC results in a high Young's modulus, reported to be 114 GPa,[6] with a theoretical Young's modulus of up to 145 GPa depending on the crystal structure.[121] BC also possesses a LTCE of only 0.1×10^{-6} K^{-1}.[104] Nature maximises efficiency by defining multiple scales of length in a material; i.e. hierarchical structures. By creating a hierarchical structure in composites, it is possible to influence one of the most important elements in a composite structure, through improved mechanical interlocking and stiffening of the matrix around the fibre-matrix interface.[262] A recent review on various efforts to hierarchical structures can be found in literature.[148] Coating BC onto sisal fibres could be a potential solution to the aforementioned shrinkage of natural fibres during thermal processing of the composites. BC, with its low LTCE could potentially bridge the gap between the fibres and the matrix. It has been shown previously that it is possible to attach BC onto sisal fibres by culturing cellulose-producing bacteria with natural fibres in a bioreactor.[13] Incorporation of these BC coated fibres into a matrix resulted in improvements in the fibre-matrix interface and the mechanical properties of unidirectional composites.[11, 12] However, studies on BC coated short sisal fibre reinforced composites did not show improvements in the tensile and

flexural properties of the composites.[263] In this work, a simple and cost effective method to coat sisal fibres with nano-sized BC without the need of bioreactors is discussed. The mechanical performance of randomly oriented BC coated short fibre hierarchical composites, with and without BC dispersed throughout the matrix is also investigated. The thermal and the visco-elastic behaviour of the hierarchical composites is presented. This novel method of modifying the fibre-matrix interface provides a more cost effective method to produce greener composites with improved properties.

8.2 Experimental

8.2.1 Materials

Poly(L-lactic acid) (PLLA) was purchased from Biomer GmbH (L9000, MW ≥ 150 kDa, D-content ≈ 1.5%) and was used as the matrix for the production of hierarchical composites. 1,4-Dioxane (Sigma-Aldrich, ACS Reagent, ≥ 99% purity) was used as the solvent for PLLA. Sodium hydroxide (purum grade, pellets) was purchased from Acros Organics. Loose sisal fibres were kindly supplied by Wigglesworth & Co. Ltd. (London, UK). These fibres were grown in East Africa. The harvested crop was left in the field for approximately 3 to 4 weeks for dew retting in order to allow the combined action of temperature, humidity and bacteria to loosen the fibres. After this retting process, the fibres were processed with a rudimentary tool where the fibres were pulled out by hand, washed with water and sun-dried for one day. BC was extracted from commercially available *nata-de-coco* (CHAOKOH coconut gel in syrup, Ampol Food Processing Ltd, Nakorn Pathom, Thailand). The extraction and purification was conducted as previously described.[123] Briefly, the sugar was removed by washing the coconut gel with water and blended/homogenised in order to create a dispersion of BC nanofibres in water. This dispersion was then purified using 0.1 M NaOH and washed back to neutral pH prior to the utilisation of BC.

8.2.2 Coating sisal fibres with nano-sized BC nanofibres

A dispersion of 0.1 wt% BC was prepared by homogenising 0.3 g of freeze-dried BC (weight is given as the dry basis) in 300 mL of de-ionised water, to which, 0.5 g of sisal fibres were added and left for three days at room temperature. The fibres were then removed from the aqueous dispersion of BC and dried in two different ways to

create either (i) a dense (collapsed) BC coating or (ii) "hairy fibres", with a layer of BC coating oriented perpendicular away from the fibre surface. To create a dense layer BC coating on the fibres, the wet fibres were dried under vacuum at 80ºC overnight. "Hairy fibres" were created by pressing the wet fibres between two filter papers (qualitative filter paper 413, 125 mm in diameter, particle retention of 5–13 μm, VWR, UK) under a weight of 3 kg for 10 s to partially dry them. The partially dried "hairy sisal fibres" were then dried in an air oven held at 40ºC. The sisal fibres coated with a dense layer of BC are referred to as densely coated neat sisal (DCNS) fibres and the "hairy fibres" as "hairy neat sisal fibres" (HNSF).

8.2.3 Preparation of hierarchical short fibre composites

Two different types of hierarchical composites were prepared; (i) BC coated sisal fibre reinforced PLLA and (ii) BC coated sisal fibre reinforced PLLA-BC nanocomposites (see Figure 38 for a schematic diagram). The former composites contained BC on the surface of sisal fibres only and the latter composites contained BC both on the fibre surfaces and dispersed within the PLLA matrix. For hierarchical composites (i), 2.4 g of (BC coated) fibres, cut to approximately 10 mm in length, were added into 200 mL of 1,4-dioxane. 9.6 g of PLLA pellets were added into this mixture and left to dissolve overnight at 60ºC under magnetic stirring to eventually create 20 wt% fibre content PLLA "pre-preg". The resulting mixture was then poured into a Petri dish and dried under vacuum (Edwards Modulyo freeze dryer, UK) at room temperature to remove any remaining solvent. This process leads to sisal fibres-PLLA "pre-pregs". The solvent was captured by a cold trap and was re-used in the polymer dissolution process. Hierarchical composites with BC dispersed in the PLLA matrix were prepared by immersing 1.8 g of (BC coated) fibres in 200 mL of 1,4-dioxane, to which, 9.6 g of PLLA pellets were added. This mixture was left to dissolve overnight at 60ºC under magnetic stirring. 0.6 g of freeze-dried BC was added into 150 mL of 1,4 dioxane in a separate beaker and homogenised at 20,000 rpm for 2 min. This BC dispersion was then added into the PLLA solution containing sisal fibres and stirred gently to ensure homogeneous dispersion of BC in the fibre-polymer solution. This mixture was then vacuum dried at room temperature to remove any remaining solvent in order to create sisal fibres-BC-PLLA "pre-pregs".
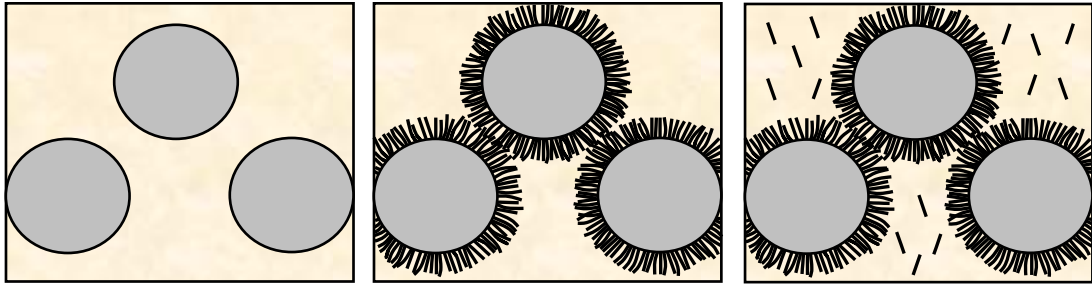
Figure 38: Schematic showing the different types of hierarchical composites. Left: conventional fibre reinforced polymer composites, middle: BC coated fibre reinforced hierarchical composites and right: BC coated fibre reinforced hierarchical nanocomposites.

8.2.4 Processing of hierarchical composites

The previously produced sisal fibres-BC-PLLA "pre-pregs" were injection moulded into flexural test bars with sample dimensions of 80 mm × 12 mm × 3.5 mm using a piston injection moulder (Haake Minijet, Thermo Scientific, Hampshire, UK). Tensile test specimens were injection moulded into dog bone shaped specimens, according to BS ISO 527:1996 type V. These dog bone test specimens had an overall length of 60 mm, a gauge length of 10 mm, thickness of 3 mm and the narrowest part of the specimens were 3 mm. The barrel temperature and the mould temperature were held at 190ºC and 70ºC, respectively. Neat PLLA was injection moulded with an injection pressure and time of 400 bar and 30 s and a post-pressure and time of 200 bar and 30 s, respectively. (BC coated) sisal fibre reinforced PLLA was injected at a pressure of 500 bar for 30 s and held at a post-pressure of 200 bar for a further 30 s. Due to the increase in viscosity of the polymer melt when BC was attached onto the surface of sisal fibres and dispersed in the PLLA matrix, the hierarchical composites with (BC coated) sisal fibre and BC dispersed in the matrix were injected at a pressure of 600 bar for 30 s and held at a post-pressure of 200 bar for 30 s.

8.2.5 Characterisation of BC coated sisal fibres and PLLA hierarchical composites

8.2.5.1 Scanning electron microscopy (SEM)

SEM was conducted to characterise both the surface morphology of neat and BC coated sisal fibres and the fracture surfaces of the hierarchical composites. SEM was performed using a high-resolution field emission gun scanning electron microscope (LEO Gemini 1525 FEG-SEM, Oberkochen, Germany). The accelerating voltage used was 5 kV. Prior to SEM, all the samples were fixed onto SEM stubs using

carbon tabs and coated with Cr for 1 min (K550 sputter coater, Emitech Ltd, Ashford, Kent, UK) using a coating current of 75 mA.

8.2.5.2 Specific surface area (BET) measurements

Nitrogen adsorption/desorption isotherms were conducted to determine the specific surface area of neat and BC coated sisal fibres. This measurement was performed using a surface area and porosity analyser (TriStar 3000, Micromeritics Ltd, Dunstable, UK). The specific surface area was calculated using the Brunauer-Emmett-Teller (BET) equation. Prior to the measurement, the fibres were degassed at 80ºC overnight to remove any adsorbed water molecules.

8.2.5.3 Single fibre tensile properties of neat and BC coated sisal fibres

Single fibre tensile tests were performed to investigate the effect of BC coating on the tensile properties of sisal fibres. The test was conducted at room temperature in accordance with ASTM D-3822-07, using a TST 350 tensile testing rig (Linkam Scientific Instrument Ltd, Surrey, UK) equipped with 200 N load cell. The gauge length and crosshead speed used were 20 mm and 1 mm min^{-1}, respectively. A single sisal fibre was fixed at either end of a testing card using cyanoacrylate glue. At least 20 fibres were tested for each fibre type to obtain a statistical average. The fibre diameter of each sample was evaluated using an optical microscope (Olympus BX 41 M reflective microscope, Essex, UK) and the tensile properties of the fibres were calculated based on the assumption of cylindrical fibre geometry.

8.2.5.4 Mechanical properties of neat PLLA and hierarchical composites

Tensile and flexural (3-point bending) properties of neat PLLA and (BC coated) fibre reinforced PLLA hierarchical (nano)composites were conducted in accordance with BS EN ISO 527: 1997 and BS EN ISO 178: 2003, respectively. The tests were performed using an Instron universal testing machine (Instron 4466, Instron Corporation, Massachusetts, USA) with a load cell of 10 kN at room temperature and 50% relative humidity. The testing speeds used for tensile and flexural tests were 1 mm min^{-1} and 20 mm min^{-1}, respectively. A span of 55 mm (span to thickness ratio of 16) was used for the flexural tests. A total of 5 samples were tested for each type of composite.

8.2.5.5 Differential scanning calorimetry (DSC) study of hierarchical composites

The crystallisation and melt behaviour of (BC coated) fibre reinforced PLLA hierarchical (nano)composites were investigated using DSC (DSC Q2000, TA Instruments, West Sussex, UK) in a He atmosphere. Approximately 20 mg of moulded sample was used for the measurement. A heat-cool-heat regime was employed. The sample was first heated from room temperature to 210°C at a heating rate of 10°C min^{-1}, then cooled to room temperature at a cooling rate of 50°C min^{-1}. The sample was then re-heated to 210°C at a heating rate of 10°C min^{-1}. The crystallinity (based on 1st heating curve to evaluate the crystallinity of the composites after thermal processing) of the composites produced was calculated using the equation:

$$\chi_C = \frac{\Delta H_m - \Delta H_c}{(1-f)\Delta H_m^o} \times 100\% \tag{8.1}$$

where χ_c is the crystallinity of the composite, ΔH_m, ΔH_c, f and ΔH_m^o are the melting enthalpy and cold crystallisation enthalpy determined from DSC curves, weight fraction of the reinforcing phase (20 wt%) and the melting enthalpy of pure crystalline PLLA (75.57 J g^{-1}),[212] respectively.

8.2.5.6 Dynamic mechanical analysis (DMA) of hierarchical composites

The viscoelastic behaviour of the composites was investigated using DMA (Tritec 2000, Triton Technology Ltd, Keyworth, UK). DMA was performed in single beam cantilever bending mode with a gauge length of 10 mm. The sample had a thickness and width of approximately 3 mm. The storage, loss modulus and energy dissipation factor (tan δ) were measured from 30°C to 100°C at a heating rate of 2°C min^{-1} at a frequency of 1 Hz.

8.3 Results and discussion

8.3.1 Morphology of the BC coated sisal fibres

Figure 39 shows the SEM images of neat sisal fibres, densely BC coated and "hairy" BC coated sisal fibres. The morphology of densely coated sisal fibres with BC

(Figure 39b and Figure 39c) resembles that of the BC coated fibres obtained by culturing *Acetobacter* in the presence of sisal fibres in a bioreactor.[13] It was also possible to obtain true "hairy" BC coated sisal fibres by employing a different drying regime (Figure 39d). The loading fraction of BC on sisal fibres was found to be 10 ± 1 wt%[‡]. Natural fibres when immersed into dispersions of BC in water will absorb water into the fibres, drawing in the water and BC nanofibril from the medium. Since BC nanofibrils are larger than water molecules, they are not able to penetrate into the sisal fibres. Instead, they are filtered against the surface sisal fibres, resulting in a BC coating of sisal fibres. The fast drying rate of the coated fibres under vacuum resulted in the collapse of BC nanofibrils onto the surface of sisal fibres (Figure 39b and Figure 39c). By pressing the wet BC coated sisal fibres between filter papers, the fibres were partially dried. It is hypothesised that during this process, the water containing the BC nanofibrils was drawn into the filter paper by capillary action. The combination of capillary action with the slow drying of the coated fibres (which prevents the collapse of the nanofibrils) results in a BC coating in which BC nanofibrils were oriented perpendicular to the sisal surface. The morphology resembles "hairy fibres".
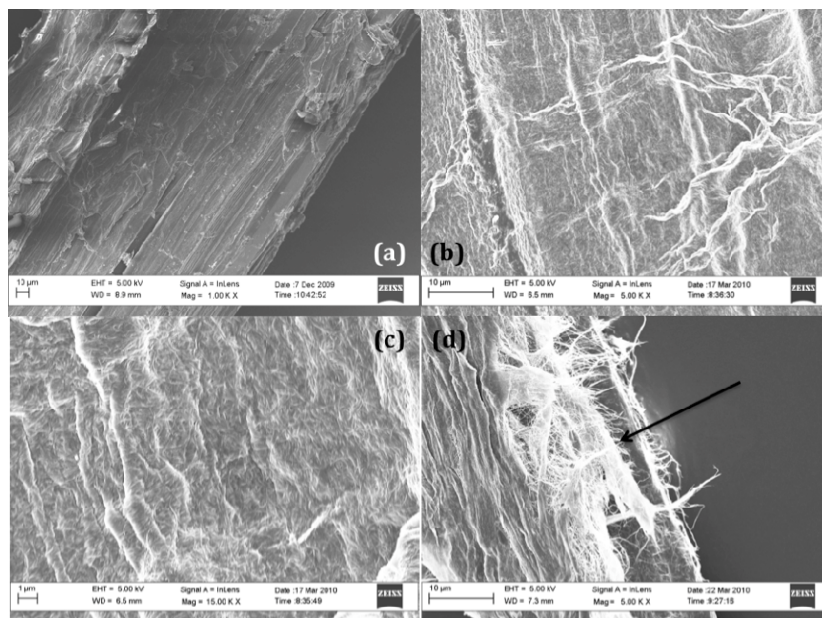
Figure 39: Scanning electron micrographs showing (a) neat sisal fibres, (b), densely BC coated sisal fibres at low magnification, (c) densely BC coated sisal fibres high magnification and (d) "hairy" BC coated sisal fibres. The arrow in (d) shows agglomeration of BC nanofibrils on sisal fibres.

[‡] BC loading fraction was determined by measuring the mass of dry sisal fibres before and after immersion in BC dispersion in both DCNS and HNSF.

8.3.2 BET surface area of BC coated sisal fibres

The measured BET surface area of the neat and BC coated sisal fibres is given in Table 27. The specific BET surface area of neat sisal fibres is relatively small ($\sim$0.1 m^2 g^{-1}), which is in line with previously reported BET surface areas for natural fibres.[5] In comparison, the surface area of BC coated fibres increased by as much as 8 times when compared to neat sisal fibres. It is also interesting that "hairy fibres" have a lower surface area than DCNS even though both types of fibres have a similar BC loading. This might be due to the agglomeration of BC nanofibrils on the "hairy sisal fibres" when they are pressed between the filter papers. This agglomeration (see Figure 39d) reduced the accessible area for nitrogen adsorption and, therefore, the observed reduced surface area. During the wet pressing of the fibres, the BC nanofibrils are pressed onto the fibres surface using filter papers and this forces the BC nanofibrils to agglomerate. On the other hand, the preparation of DCNS involves drying the wet fibres without restraining the BC nanofibrils on the surface. This allows the nanofibrils to collapse freely onto the surface of sisal fibres, which results in larger surface area. Even so, the surface area of HNSF is five times larger than that of neat sisal fibres.

Table 27: BET surface area, single fibre tensile modulus and tensile strength of neat and BC coated sisal fibres; dense layer and "hairy fibres", respectively.

Sample	BET surface area (m^2 g^{-1})	Single fibre tensile properties	
		Tensile modulus (GPa)	Tensile Strength (MPa)
Neat sisal fibres	0.097 ± 0.008	24.1 ± 3.1	535 ± 69
DCNS fibres	0.770 ± 0.030	12.5 ± 1.3	253 ± 27
HNSF fibres	0.485 ± 0.029	22.9 ± 2.2	456 ± 50

8.3.3 Tensile properties of neat and BC coated sisal fibres

The single fibre tensile properties of neat and BC coated sisal fibres are shown in Table 27. The tensile properties of neat sisal fibres reported here is in agreement with values obtained by other researchers in the literature.[5] When sisal fibres are coated with a dense layer of BC (DCNS), the tensile modulus and tensile strength of the fibres decreased by 40% and 45%, respectively. The tensile modulus of "hairy

fibres" (HNSF) remained unchanged and the tensile strength reduced only by 10% (but is still within the error of neat sisal fibres). This suggests that the drying process has an effect on the tensile properties of BC coated fibres. When BC nanofibril networks are wet pressed and dried under restraint without shrinkage, the flexibility of the fibre network will be removed and this will increase the load bearing capability of the BC network.[229] Indeed, when BC nanofibrils were wet pressed and dried effectively under restraint, a modulus of 9.7 GPa was achieved.[6] However, a modulus of only 1.4 GPa was measured when BC nanofibrils were dried freely, allowing the nanofibril network to shrink§. The procedure results in a dense coating layer of BC on sisal fibres (DCNS) does not restrain the BC nanofibril network during the drying process. This resulted in the poor tensile properties of the fibres as the force at break stayed constant but the fibre diameter increased due to the BC coating. "Hairy" neat sisal fibres (HNSF), on the other hand, were partially dried whilst being restrained during wet pressing. Therefore, their tensile properties did not change significantly when compared to neat sisal fibres even though the same increase in fibre diameter was observed.

8.3.4 Mechanical properties of neat PLLA and its hierarchical composites

In order to investigate the effect of BC coating on the mechanical properties of (BC coated) sisal fibre reinforced PLLA hierarchical (nano)composites, tensile and flexural tests were conducted. From the results summarised in Table 28, it can be seen that with (BC coated) sisal fibres as reinforcement, the tensile moduli for all samples increased. The increase in the tensile modulus of the hierarchical composites was enhanced when BC was additionally dispersed in the matrix (sisal-BC-PLLA, DCNS-BC-PLLA and HNSF-BC-PLLA). This is thought to be due to the stiffening of the matrix by BC. It has been shown that a PLLA matrix can be stiffened by as much as 40% if BC is dispersed in the matrix at a loading fraction of 5 wt%.[123] With BC dispersed in the matrix and attached to the fibres, both the matrix and the fibre-matrix interface could be reinforced (or stiffened). This led to the observed improvements in tensile modulus of DCNS-BC-PLLA by as much as

---

§ Such BC sheets were made by allowing the BC nanofibrils to dry freely without restrain before dry pressing. This was done by placing a wet filter cake of BC in a hot press to evaporate all the water at 110°C first before dry-pressing of the BC sheet.

72% when compared to neat PLLA and 30% in comparison to PLLA-sisal hierarchical composites.

Table 28: Summary of mechanical properties of neat PLLA and its composites. E_T, σ_T, E_F, σ_F indicate tensile modulus, tensile strength, flexural modulus and flexural strength, respectively.

Sample	E_T (GPa)	σ_T (MPa)	E_F (GPa)	σ_F (MPa)
Neat PLLA	0.97 ± 0.02	62.6 ± 1.0	3.70 ± 0.04	86.1 ± 6.9
PLLA-sisal	1.28 ± 0.03	58.7 ± 1.0	4.85 ± 0.10	105.6 ± 1.5
PLLA-DCNS	1.35 ± 0.03	57.3 ± 1.3	5.19 ± 0.07	99.2 ± 2.8
PLLA-HNSF	1.29 ± 0.03	57.8 ± 1.6	4.96 ± 0.16	102.0 ± 2.5
PLLA-sisal-BC	1.46 ± 0.02	60.9 ± 1.9	5.74 ± 0.05	100.0 ± 2.2
PLLA-DCNS-BC	1.63 ± 0.04	67.8 ± 1.2	6.19 ± 0.08	95.5 ± 2.3
PLLA-HNSF-BC	1.59 ± 0.05	69.2 ± 1.2	5.77 ± 0.13	96.8 ± 2.0

The tensile strength of the hierarchical composites showed a slightly different trend compared to tensile modulus. A decrease in tensile strength was observed when PLLA is reinforced with (BC coated) sisal fibres, with no BC dispersed in the matrix. Such a result could possibly be due to (i) the poor transverse properties of fibres or (ii) poor fibre-matrix interface. The poor tensile strength of PLLA-sisal could be attributed to the latter whilst that of PLLA-DCNS and PLLA-HNSF could be attributed to the former (see section 7.3.5 for more details). When the hierarchical composites were reinforced with BC in the PLLA matrix (HNSF-BC-PLLA) the tensile strength improved by as much as 11% when compared to neat PLLA and 21% when compared to DCNS-PLLA. This could be due to enhanced interfacial adhesion between BC coated fibres and BC reinforced PLLA matrix. With BC dispersed in the matrix, the matrix is stiffened.

Flexural modulus increased with fibre/BC reinforcement, as shown in Table 28. The flexural modulus of the hierarchical composites with BC dispersed in the matrix (DCNS-BC-PLLA) improved by as much as 67% when compared to neat PLLA and 40% when compared to hierarchical composites without BC dispersed in the matrix. As aforementioned, this is due to a matrix stiffening effect induced by nano-sized reinforcement in PLLA matrix. The flexural strength of all the composites increased when compared to neat PLLA. An increase in flexural strength by as much as 23%

was observed. It seems, however, that the BC coating on sisal fibres and/or in the matrix has no effect on the overall flexural strength of the composites. Due to the low fibre volume fraction of these composites, individual fibre failure is isolated and, therefore, microbuckle bands and kinkbands do not form.[264] It is proposed that the observed relatively constant flexural strength of the fibre-reinforced composites is a result of poor shear and transverse properties of sisal fibres.[52, 265]

8.3.5 Fractography of hierarchical composites

Typical example of a fracture surface of the composites failed in tension is given in Figure 40 and Figure 41. When PLLA is reinforced by sisal fibres, fibre debonding (Figure 40a) and fibre pull out can be clearly seen (Figure 40b). This is a direct result of poor interfacial adhesion between fibre and matrix, which results in poor stress transfer. This is attributed to the poor tensile strength of PLLA-sisal to this when compared to neat PLLA. When sisal fibres are coated with BC, the fibre-matrix adhesion improved as no fibre debonding was observed (Figure 40c-f). Single fibre pull out tests performed on BC-coated sisal made by the aforementioned *in situ* culturing method[13] showed the interfacial adhesion between BC coated fibres and PLLA was indeed enhanced. This can be attributed to the enhanced mechanical interlock as a result of BC coating and the increased surface energy of BC coated fibres,[13] which enhances wetting by polymers. In the case of PLLA-DCNS and PLLA-HNSF, no fibre debonding was observed but the tensile strengths decreased when compared to neat PLLA. Failure of short-fibre composites can be classified into two types; T-fibre fracture (crack plane oriented transverse to fibre orientation – high fracture energy) and L-fibre fracture (crack plane oriented parallel to fibre orientation – low fracture energy).[264] In general, short-fibre composites exhibit a combination of failures and fracture occurs along the weakest part of a composite. The overall fracture surface of PLLA-DCNS and PLLA-HNSF exhibited L-fibre fractured surface as the dominant mechanism. This explained the poor tensile strengths of these composites even though the fibre-matrix interface is enhanced through mechanical interlock. Through this mechanical interlock enhancement, the weakest region in the composite is no longer the fibre-matrix interface but the bulk of the polymer. This resulted in L-fibre fractured surface as the dominant failure mechanism. However, when BC is dispersed in the fibre reinforced PLLA composites, the overall fracture surface and hence, fracture mechanism, was

modified. No significant fibre debonding or fibre pull-out can be observed in sisal-BC-PLLA, DCNS-BC-PLLA and HNSF-BC-PLLA composites in Figure 41a-f. This is accompanied by the improved mechanical properties (both tensile strength and modulus) of hierarchical composites when compared to neat PLLA.
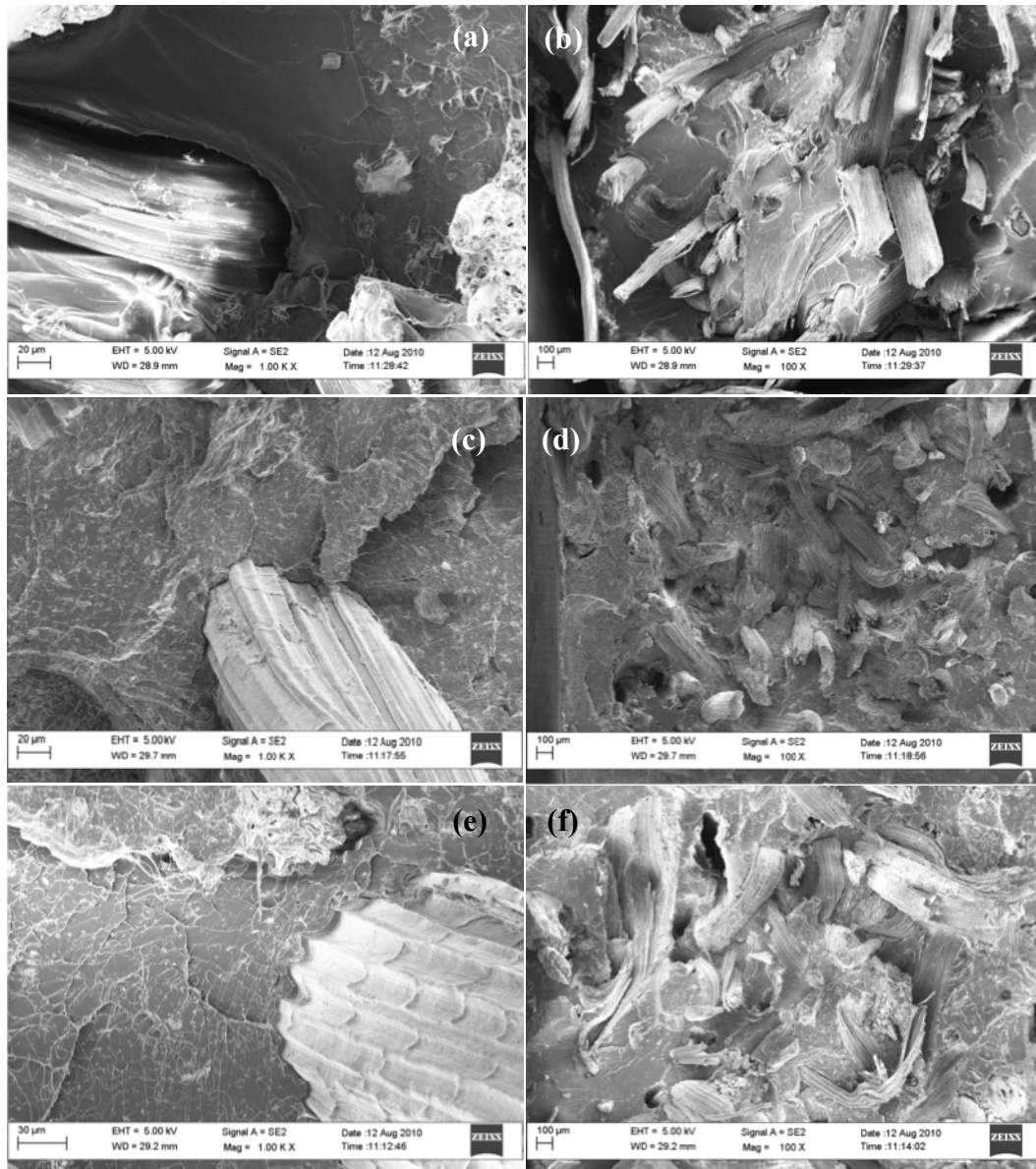
Figure 40: Fractured surface of fibre reinforced composites at fibre-matrix interface and overall fractured surface. (a) (b) are PLLA-sisal, (c) (d) are PLLA-DCNS and (e) (f) are PLLA-HNSF, respectively. (a), (c) and (e) are at higher magnification. (b), (d) and (f) are at lower magnification.
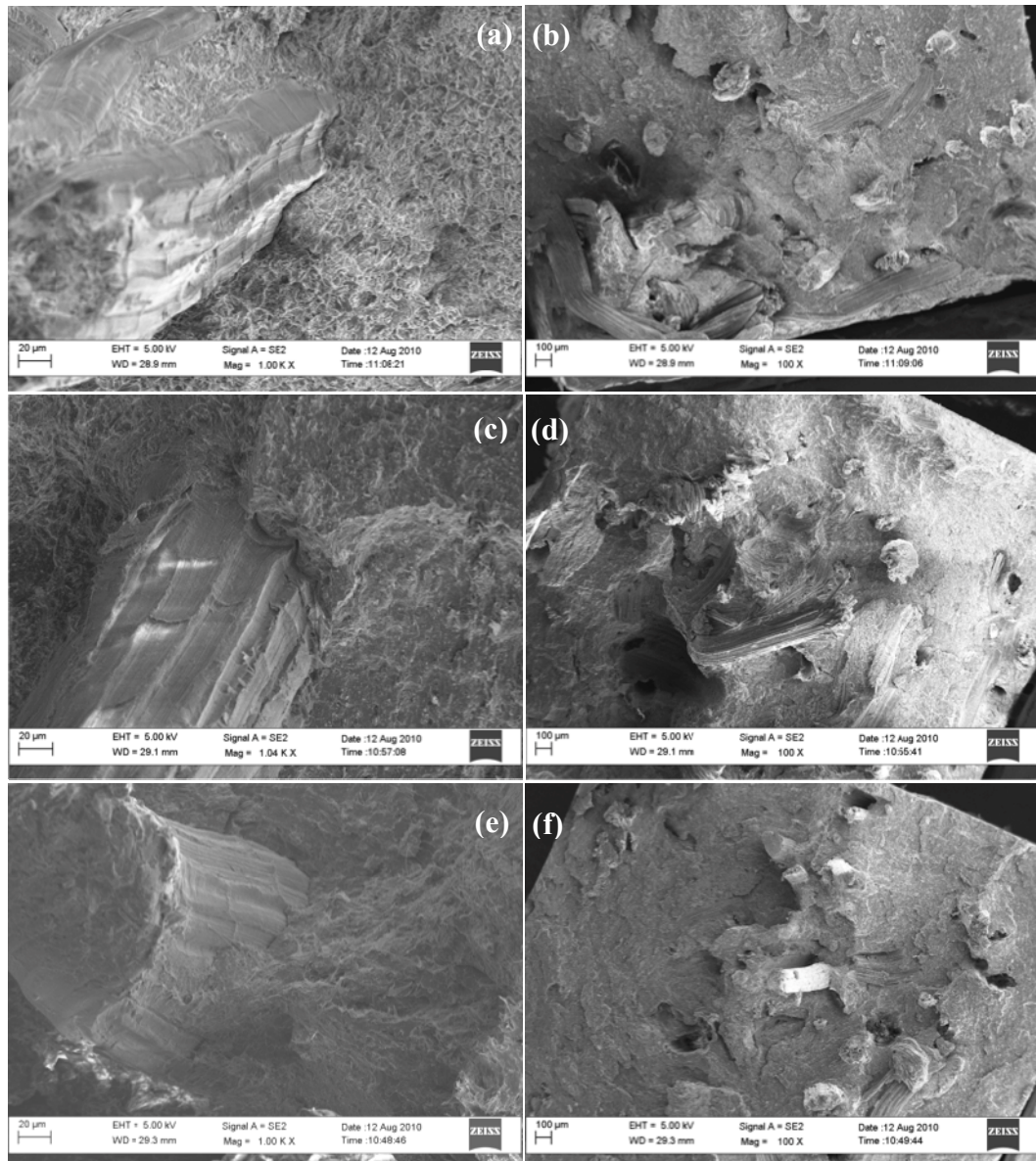
Figure 41: Fractured surface of fibre reinforced hierarchical composites at fibre-matrix interface and overall fractured surface. (a) (b) are PLLA-sisal-BC, (c) (d) are PLLA-DCNS-BC and (e) (f) are PLLA-HNSF-BC, respectively. (a), (c) and (e) are at higher magnification. (b), (d) and (f) are at lower magnification.

8.3.6 Crystallisation and behaviour of the hierarchical composites

The thermal behaviour of the composites was characterised by DSC and their characteristic temperatures such as glass transition temperatures (T_g), crystallisation temperatures (T_c) and melt temperature (T_m) of the first and second heating are tabulated in Table 29. The T_g of PLLA in the composites was slightly lower when compared to neat PLLA. This might be due to the plasticising effect of natural waxes leaching from the sisal fibres in PLLA.[266] The presence of wax will act to aid the polymer chain's mobility, in turn lowering the T_g. There are also no significant changes in T_m of the composites but the crystallisation behaviour of the composites

changed significantly compared to neat PLLA. A lowering of T_c can be observed in composites reinforced with sisal fibres. Cellulosic fibres are known to act as nucleation sites for PLLA crystallisation.[112] With BC coating on sisal fibres, T_c was lowered even further from 100°C to 90°C. BET measurements showed an increase in the surface area of coated fibres. This led to more nucleation sites for PLLA crystallisation and, therefore, the further decrease of T_c. It should also be noted that there are no T_g or T_c observed in the second heating of the hierarchical composites with a BC reinforced matrix. This might be due to the fact that during the first cooling step, cold crystallisation occurred even at a high cooling rate of 50°C min^{-1}. This implies that the high interface area of BC and PLLA enhanced the crystallisation of PLLA even more when compared to the case where BC was not dispersed in the matrix. A similar observation was also found by Lee et al.[123] when PLLA is reinforced by BC. However, crystallinity of the composites did not seem to be affected with the addition of sisal fibres and/or BC. This could be due to the fast cooling rate during the production of the composites. An exotherm was observed around 150°C (results not shown). This is consistent with the solid-solid crystal transformation of the α' form to the α form of PLLA.[191] Such an exotherm was not observed in neat PLLA as the α' form is only crystallised below 100°C, this was the case for all the composites tested, with neat PLLA being the exception.[192]

Table 29: Crystallisation and melt behaviour of neat PLLA and its fibre/BC reinforced hierarchical composites. T_g, T_c, T_m and χ_c are glass transition temperature, crystallisation temperature, melt temperature and crystallinity of the composites based on the 1st heating curve, respectively.

Sample	Heating	T_g (°C)	T_c (°C)	T_m (°C)	χ_c (%)
PLLA	1st	63	113	171	18 ± 2
	2nd	61	110	169	
PLLA-sisal	1st	57	100	168	21 ± 3
	2nd	59	103	168	
PLLA-DCNS	1st	57	88	168	20 ± 3
	2nd	62	93	169	
PLLA-HNSF	1st	57	94	166	18 ± 2
	2nd	57	94	166	
PLLA-sisal-BC	1st	55	83	165	23 ± 4
	2nd	-	-	168	
PLLA-DCNS-BC	1st	56	85	163	18 ± 3
	2nd			166	
PLLA-HNSF-BC	1st	54	81	165	24 ± 4
	2nd	-	-	167	

8.3.7 Viscoelastic behaviour of hierarchical composites

The viscoelastic properties of neat PLLA and (BC coated) PLLA hierarchical (nano)composites as a function of temperature are shown in Figure 42. The storage moduli of the hierarchical composites are markedly higher than that of neat PLLA. These results corroborate with the tensile and flexural moduli, which indicate that the (BC coated) sisal fibres have a strong influence on the viscoelastic properties of the resulting (nano)composites. The storage moduli stayed relatively constant until T_g, when a sharp decrease can be seen. This corresponds to the softening of the polymer. It can also be seen from Table 30 that by coating the surface of sisal fibres with BC or with BC dispersed in the polymer matrix that the storage modulus improved in comparison to neat PLLA (by at least 52%) or neat sisal reinforced PLLA composites (by at least 15%). The former is due to the enhanced fibre-matrix interface as a result of BC coating and the latter is thought to be due to the inclusion of rigid BC into the matrix.[123] DCNS-BC-PLLA showed the lowest E' increment among all the samples with BC dispersed in the matrix. This might be a result of poor DCNS fibre properties compared to neat sisal or HNSF fibres (see Table 27). Different viscoelastic behaviour between composites with and without BC dispersed in the matrix (Figure 42a-b) can also be observed beyond the mechanical T_g of the hierarchical composites. Crystallisation of the matrix occurred at lower temperatures when BC was dispersed in the matrix. This led to the observed higher storage moduli above its T_g compared to hierarchical composites with no BC dispersed in the matrix.

The tan δ for the composites as a function of temperature is shown in Figure 42c-d. Tan δ, a measure of the damping properties of the material, is also determined by the quality of fibre-matrix adhesion.[64] Large tan δ amplitude indicates a weak composite interface whereas small tan δ amplitude indicates a stronger interface.[267] The amplitude of tan δ is lower for BC coated sisal fibre reinforced PLLA and composites with BC dispersed in the matrix. This implies that the fibre-matrix interface of these composites is improved with BC coating/dispersion. Table 30 shows the mechanical T_g (taken as the peak of tan δ) and improvements in storage moduli as a result of BC and fibre reinforcement. The mechanical T_g of PLLA was determined to be 73°C and decreased with fibre reinforcement. This result also

corroborates the DSC results, showing a reduction in T_g. As aforementioned, this is a result of the plasticising effect from the waxes present on neat sisal fibres dissolving into PLLA. Nonetheless, DMA results show an improved fibre-matrix interface as a result of BC coating/dispersion.
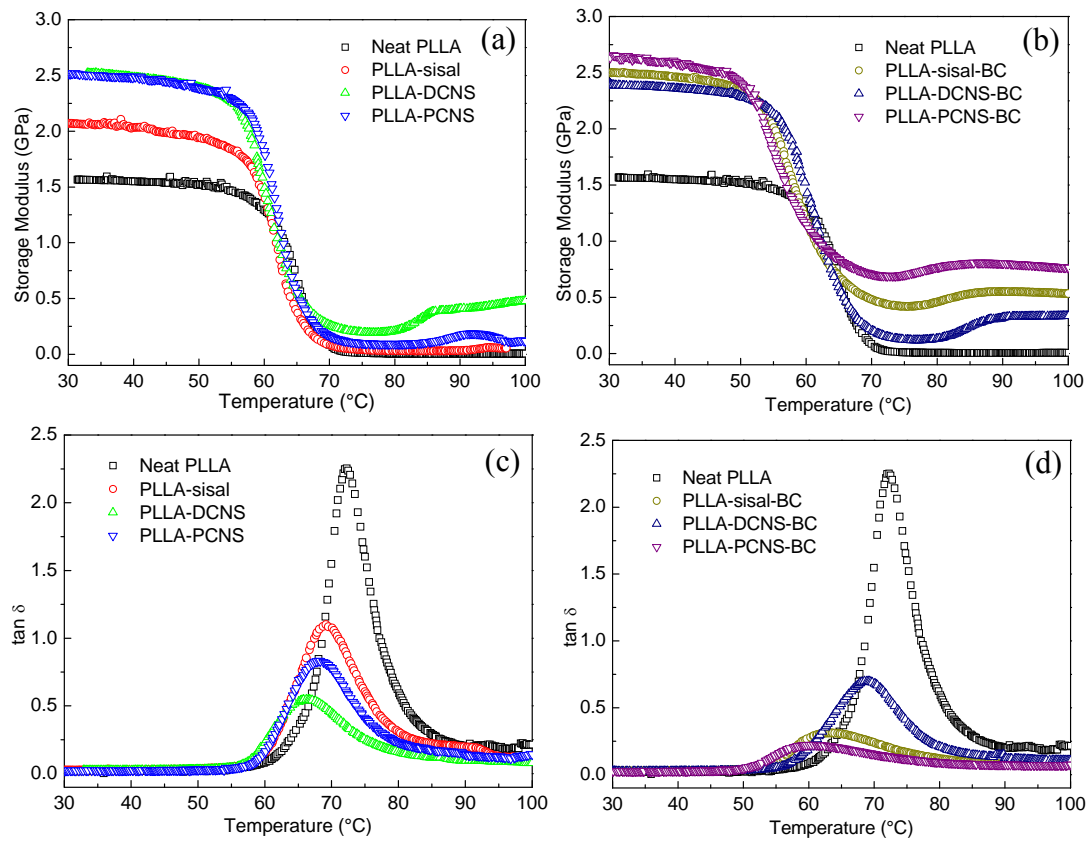
Figure 42: Graphs showing the temperature dependency of storage moduli and tan δ of neat PLLA and its hierarchical composites.

Table 30: Mechanical Tg (taken as the peak of tan δ), storage moduli (E') and improvements in storage moduli of the hierarchical composites.

Sample	Mechanical T_g (°C)	E' @ 30°C (GPa)	Improvements in E' over neat PLLA (%)
PLLA	73	1.57	-
PLLA-sisal	69	2.07	32
PLLA-DCNS	68	2.52	61
PLLA-HNSF	66	2.52	61
PLLA-sisal-BC	63	2.49	59
PLLA-DCNS-BC	69	2.39	52
PLLA-HNSF-BC	61	2.64	69

8.4 Conclusions

Randomly oriented bacterial cellulose coated short sisal fibre reinforced PLLA hierarchical composites with improved properties over neat PLLA were produced. A novel method based on slurry dipping to coat sisal fibres with nano-sized BC was developed as an alternative method to modify the surface of natural fibres. This method was also extended to produce either a dense BC coating layer on the surface of sisal fibres or BC coated hairy fibres, in which the BC is oriented perpendicular to the surface of the fibres. BET surface area measurements showed an increase in surface area of the fibres by as much as 800% when compared to neat sisal fibres. The use of BC coated sisal fibres in PLLA matrix showed an improvement in tensile modulus of nearly 40% but their tensile strengths decreased by as much as 10%. Not only was the fibre-matrix interface enhanced through the presence of the BC coating on sisal fibres, but also the fracture mechanism of the composites was modified; the fracture mechanism switched from a high fracture energy (T-fibre fracture) to a low fracture energy (L-fibre fracture) mechanism and hence resulted in decrease of the tensile strength of PLLA reinforced with BC coated fibres. When the BC coated fibre reinforced composites were further reinforced with BC by dispersing BC in the matrix, the tensile modulus and strength improved even more when compared to neat PLLA by as much as 72% and 11%, respectively. This is attributed to the enhanced fibre-matrix interface and stiffening of PLLA due to the incorporation of BC into the matrix. The flexural modulus of the hierarchical composites improved by as much as 67% and their flexural strength increased by 23% when compared to neat PLLA. DMA confirmed the increased storage moduli when compared to neat PLLA and also suggests an enhanced fibre-matrix interface (a reduction in the height of tan δ). These new types of short fibre composites offer a promising alternative to the industry as no chemical modifications or plasma treatments are required to produce biodegradable composites with improved properties.

Chapter 9 – Short sisal fibre performs for hierarchical bio-based poly(acrylated epoxidised soybean oil): Using bacterial cellulose as binder

Summary

A novel non-woven sisal fibre preform was manufactured using a papermaking process utilising bacterial cellulose (BC) as binder. It was found that BC provides significant mechanical strength to the sisal fibre preforms. This can be attributed to the high stiffness and strength of BC network. Truly green non-woven fibre preform reinforced hierarchical composites were prepared by infusing the fibre preforms with acrylated epoxidised soybean oil (AESO) using vacuum assisted resin infusion and cured using Luperox P as thermal initiator. Both the tensile and flexural properties of the hierarchical composites showed significant improvements over polyAESO and neat sisal fibre preform reinforced polyAESO. These results were corroborated by the thermo-mechanical behaviour of the (hierarchical) composites, which showed increased storage modulus and enhanced fibre-matrix stress transfer. By using BC as binder for short sisal fibres, added benefits such as the high Young's modulus of BC, enhanced fibre-fibre and fibre-matrix stress transfer can be utilised in the resulting hierarchical composites.

9.1 Introduction

Significant research effort has been poured into the manufacturing of sustainable materials due to public's growing demand for more environmentally friendly products, depletion of petroleum resources, the ever-growing problem of landfill of waste and heavy environmental legalisation.[268] Natural fibres have gained significant attention as potential replacement for glass fibres to produce greener composites. The advantages of natural fibres as reinforcement in composites include low density, wide availability and biodegradability.[21] In addition to this, natural

fibres possess specific mechanical properties that are comparable to some glass fibres.[4] However, natural fibres suffer from drawbacks such as poor compatibility with hydrophobic polymer matrices and its inherent variability in both fibre properties and dimensions, even within the same cultivation.[5] There is very little that can be done in terms of the variability in their properties and dimensions of the fibres. However, significant research effort has been poured into modifying the fibres to enhance the fibre-matrix interface.[40]

One method of modifying the fibre-matrix interface is to attach bacterial cellulose (BC) onto the surface of natural fibres.[11-13] BC is highly crystalline nano-sized cellulose (24-86 nm in diameter and several micrometres in length[115]) without impurities such as hemicellulose or lignin and possesses a degree of crystallinity of up to 90%.[120] The Young's modulus of a single BC nanofibre was reported to be 114 GPa,[6] with theoretical cellulose crystal modulus being as high as 160 GPa.[118] In addition to this, BC also possesses a linear thermal coefficient of expansion (LTCE) of only 0.1×10^{-6} K^{-1}.[104] By culturing cellulose-producing bacteria, such as from the *Acetobacter* species,[115] in the presence of natural fibres, BC is preferentially deposited *in-situ* onto the surface of natural fibres. The introduction of BC onto natural fibres provides a new mean of controlling the interaction between natural fibres and polymer matrices. Coating of natural fibres with BC does not only facilitate good distribution of BC within the matrix, it also results in an improved interfacial adhesion between the fibres and the matrix. This enhances the interaction between natural fibres and a polymer matrix. In addition to culturing cellulose-producing bacteria in the presence of natural fibres to coat the fibres, a method based on slurry dipping was developed recently to coat the surface of sisal fibres with BC.[269] This method utilises the water absorbing capability of natural fibres to absorb the water in BC dispersion, drawing along the nanocellulose in the dispersion onto the surface of the fibres.

In this work, the slurry dipping method was extended to create non-woven sisal fibre preforms for thermosetting matrices. Natural fibre can be stitched or stapled together using polymer fibres to produce non-woven fibre preforms.[270-273] In addition to this, fibre preforms can also be produced by spraying a polymer solution onto the fibre

mat followed by heat pressing to consolidate the polymer to bind the fibres together.[274] Natural fibres can be blended with a thermoplastic polymer and melt pressed to create the fibre preform.[275] To create composites, these polymeric binder based natural fibre preforms can then be impregnated with a thermosetting resin to produce natural fibre reinforced composites.[274, 276, 277] Natural fibre preform reinforced thermoplastic composites can also be produced using film stacking, whereby the fibre preforms are stacked between sheets of polymers in alternative sequence and consolidated.[19, 278]

Our current study focuses on using BC as binder to produce novel non-woven short sisal fibre preforms, moving away from the conventional polymer binders such as polypropylene, polyesters and epoxies.[279] These natural fibre preforms are infused with epoxidised and acrylated soybean oil (AESO) using vacuum assisted resin infusion (VARI) and cured to produce truly green hierarchical composites. Nature maximises the efficiency of structural materials by organising them hierarchically; the arrangement of the constituents at every level, from the molecular to the macroscopic level. By applying this concept, composites that possess a hierarchical structure should show enhancement in mechanical performance. Not only does the BC act as a binder for the loose fibres, it also simultaneously acts as nanofiller to further enhance the mechanical properties of the hierarchical composites due to its high stiffness and strength. The mechanical properties, thermal degradation and thermo-mechanical behaviour of the hierarchical composites were studied in this work.

9.2 Materials and methods

AESO (Aldrich, density = 1.04 g cm^{-3}, inhibited with 8500 ppm monomethyl ether hydroquinone) and *tert*-butyl peroxybenzoate, otherwise known as Luperox P (Aldrich, purity ≥ 98%), were purchased from Sigma-Aldrich and used as the thermosetting monomer and thermal initiator, respectively in this study. Loose sisal fibres were kindly supplied by Wigglesworth & Co. Ltd. (London, UK). These fibres were grown in East Africa. The harvested crop was left in the field for approximately 3 to 4 weeks for dew retting in order to allow the combined action of temperature, humidity and bacteria to loosen the fibres. After this retting process, the fibres were

processed with a rudimentary tool where the fibres were pulled out by hand, washed with water and sun-dried for one day. BC was kindly supplied by fzmb GmbH as wet pellicle containing 94 wt.-% water.

9.2.1 Manufacturing natural fibre preforms

The fibre preforms were manufactured using a papermaking process. Neat sisal fibre preforms were manufactured using 16 g of sisal fibres, cut to approximately 10 mm in length and soaked in 2 L of de-ionised water overnight. This dispersion of short sisal fibres was then filtered under vacuum onto a 125 mm diameter filter paper (VWR, Lutterworth, UK) using a Büchner funnel. The filter cake was wet pressed twice under a weight of 1 t for 2 min. This wet pressed filter cake was then further dried in an oven held at 60°C overnight under a weight of 10 kg. Short sisal fibres were used instead of long fibres because a more uniform dispersion of fibres in water can be obtained. The fibre preforms produced from short fibres were also more uniform.

In order to use BC as binder for the fibre preforms, 29.6 g of wet BC pellicles (equivalent dry mass of 1.78 g) were cut into small pieces and blended for 1 min using a blender (Breville BL18 glass jug blender, Pulse Home Products Ltd, Oldham, UK) and further homogenised (Polytron PT 10-35 GT, Kinematica, Lucerne, Switzerland) for 2 min in 2 L of de-ionised water to produce a uniform dispersion of nanocellulose. 16 g of sisal fibres, cut to approximately 10 mm in length, were soaked in this nanocellulose dispersion overnight. The fibre preforms were then manufactured following the previously described wet pressing followed by drying method. The weight fraction of BC in these sisal fibre preforms was 10 wt.-%. Herein, fibre preforms with neat sisal fibres only and sisal fibres with BC binder are termed sisal fibre preforms and BC-sisal fibre preforms, respectively.

9.2.2 Manufacturing of natural fibre preform reinforced (hierarchical) composites

The (hierarchical) composites were manufactured using VARI. A schematic diagram of the VARI setup is shown in Figure 43. A polyester porous flow medium (15087B, Newbury Engineer Textile, Berkshire, UK) was placed on top of the tooling side (a

460 mm x 920 mm heating plate with a temperature control unit), which was covered by a layer of polyester film (Melinex PW 122-50-RL, PSG group, London UK). The natural fibre preforms were sandwiched between two PTFE coated glass release fabrics (FF03PM, Aerovac, West Yorkshire, UK) and placed on top of the polyester porous flow medium. Another polyester porous flow medium was then placed on top of the PTFE glass release fabric. The whole setup was covered with a vacuum bagging film (Capran 519 heat stabilised Nylon 6 blown tubular film, Aerovac, West Yorkshire, UK) and sealed using vacuum sealant tape (SM5127, Aerovac, West Yorkshire, UK).
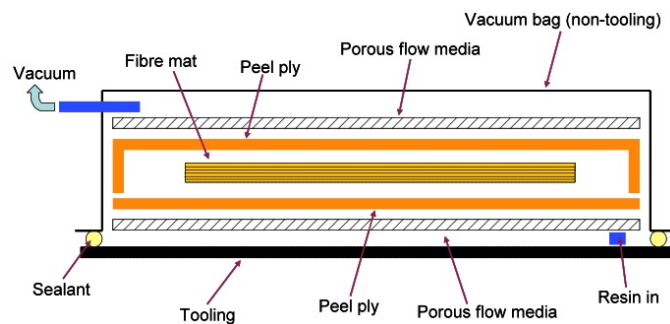
Figure 43: Schematic diagram of the VARI process.

Prior to the infusion of the resin, the previously prepared fibre preforms were further dried by hot-pressing the preforms at 120°C and 0.25 t for 15 min. This also reduced the porosity of the fibre preforms, resulting in an increased fibre volume fraction of the final (hierarchical) composites. AESO was heated to 80°C to reduce its viscosity and 5 wt.-% of Luperox P relative to the weight of AESO was mixed with the resin. This mixture was then de-gassed at a reduced pressure of 100 kPa at 80°C for 30 min prior to the infusion step in order to remove all air bubbles entrapped during the mixing of the resin and the initiator. The infusion process starts with an air removal step, whereby vacuum was applied to the system via the tubing on the non-tooling side with the resin inlet tubing sealed off. When the maximum vacuum was achieved (~20 kPa), the VARI setup was left under vacuum for 2 h to ensure that there was no leakage in the setup by constantly monitoring the pressure in the vacuum bag. Once the system was determined to be leakage-free, the liquid resin was fed at the same temperature from the bottom of the polyester porous flow medium on the tooling side through the fibre preforms and exited via the tubing on the non-tooling side. Both the VARI setup and the resin were heated to 80°C in order to reduce the

viscosity of AESO such that the resin flows readily during the infusion process. The inlet and outlet of the setup were sealed off again once the resin fully impregnated the fibre preforms. The resin was cured at 110°C for 2 h followed by a post-curing step at 130°C for 2 h. The VARI setup was cooled to room temperature prior to the removal of the manufactured (hierarchical) composites. The composites reinforced with sisal fibre preforms and BC-sisal fibre preforms are termed sisal-polyAESO and BC-sisal-polyAESO, respectively hereafter. Neat polymerised AESO was produced by pouring the resin into a mold with dimensions of $3 \times 15 \times 20$ mm and polymerised using the same reduced pressure and curing cycle as previously described.

9.2.3 Characterisation of the natural fibre preforms and (hierarchical) composites

9.2.3.1 Tensile properties of the natural fibre preforms

In order to investigate the effect of the BC binder on the mechanical properties of the fibre preforms, tensile tests were conducted on these preforms in accordance to BS EN ISO 9073-18:2008. Prior to the test, the fibre preforms were cut into dimensions of $3 \times 15 \times 100$ mm. Woven glass fibre reinforced polyester end tabs with a thickness of 1.6 mm were glued (Araldite 2011, Hunstman Advanced Materials, Cambridge, UK) onto the ends of the test specimens to prevent the clamping jaws of the test machine from damaging the test specimens. The distance between the end tabs and the distance between the clamps (the gauge length) were set to be 60 mm. Tensile tests were conducted using an Instron universal material testing equipment (Instron 4505, Instron Corporation, MA, USA) equipped with 1 kN load cell. The specimens were tested using a crosshead speed of 1 mm min^{-1}.

9.2.3.2 Density measurements of the fibre preforms and (hierarchical) composites

The density of the fibres, neat polyAESO and its (hierarchical) composites was measured using He pycnometry (AccuPyc 1330, Micromeritics Ltd, Dunstable, UK). The samples were weighed prior to placing them in the measuring chamber of the He pycnometer. As the pressure of He rises above the atmospheric value, it was expanded through a value and this expanded volume was measured. Due to the

expansion of He, the pressure inside the chamber will decrease to a steady-state value. With the mass of the sample known, the density ρ_m of the sample can then be calculated using the equation:

$$\rho_{\mathrm{m}} = \frac{m_{\mathrm{s}}}{V_{\mathrm{c}} - \dfrac{V_{\mathrm{E}}}{\dfrac{P_1}{P_2} - 1}} \tag{9.1}$$

where m_{s} is the sample mass, V_{c} is the volume of the chamber, V_{E} is the expanded volume of helium, P_1 and P_2 are the chamber's elevated pressure and steady-state pressure, respectively. The envelope density (ρ_e) of the fibre preforms was calculated from the mass and envelope volume of the preforms. The fibre volume fraction (v_f) of the (hierarchical) composites was calculated based on the densities of the fibre preforms and (hierarchical) composites, respectively.

9.2.3.3 Mechanical properties of the (hierarchical) composites

The (hierarchical) composites were tested in tension and flexural (3-point bending) mode using an Instron universal material testing equipment (Instron 4505, Instron Corporation, MA, USA) in accordance to ASTM D 3039-00 and D638-03, respectively. The tensile test specimens possessed dimensions of $3 \times 15 \times 100$ mm, with a gauge length of 30 mm. Prior to the test, woven glass fibre reinforced polyester end tabs with a thickness of 1.6 mm were glued onto the samples using a two-part cold curing epoxy resin (Araldite 2011, Huntsman Advanced Materials, Cambridge, UK). The distance between the end tabs was set to be 60 mm. Strain gauges (FLA-2-11, Techni Measure, Studley, UK) were glued onto the middle portion of the test specimen using cyanoacrylate glue (EVERBUILD Building Products Ltd, Leeds, UK). Tensile tests were conducted using a crosshead speed and load cell of 1 mm min^{-1} and 10 kN, respectively. The flexural test specimens possessed dimensions of $3 \times 15 \times 80$ mm. The span to thickness ratio and crosshead speed used in flexural test were 20 and 1 mm min^{-1}, respectively. A total of 5 specimens were tested in each test for each type of samples.

9.2.3.4 Thermo-mechanical behaviour of (hierarchical) composites

The viscoelastic behaviour of polyAESO and the (hierarchical) composites was characterised using dynamic mechanical thermal analysis (DMTA) (Tritec 2000, Triton Technology Ltd., Keyworth, UK). DMTA was conducted in single beam cantilever bending mode with a gauge length of 10 mm. The sample had a width and an average thickness of 4 mm and 3 mm, respectively. The storage modulus, loss modulus and energy dissipation factor (tan δ) were measured from -95°C to 180°C at a heating rate of 5°C min^{-1}, with a frequency of 1 Hz.

9.2.3.5 Thermal stability of (hierarchical) composites: Thermal gravimetric analysis (TGA)

The thermal degradation behaviour of sisal fibres, BC, neat polyAESO and its (hierarchical) composites was characterised using TGA (TGA Q500, TA Instruments, UK). Samples of 35 mg were heated from room temperature to 600°C in N_2 at a heating rate and N_2 flowrate of 5°C min^{-1} and 60 mL min^{-1}, respectively.

9.3 Results and discussion

9.3.1 Tensile properties of the natural fibre preforms

The mechanical performance of the fibre preforms under tension is shown in Table 31, along with the porosity of the fibre preforms. The tensile strength tabulated in this table is defined as the maximum load required to fail the sample per unit width of the specimen (15 mm) as the cross-sectional area of the fibre mat is not well defined. With BC as the binder, a tensile strength of 13.1 kN m^{-1} was achieved. However, the tensile strength of the neat sisal fibre preforms was not measureable. This is due to the fact that these sisal fibres are loose and held together only by friction between the fibres even after the wet pressing step to consolidate them into fibre preforms. The improved mechanical performance of BC-sisal fibre preforms can be attributed to the use of BC as the binder, which is also expected to promote fibre-fibre stress transfer. The nano-sized BC holds the otherwise loose sisal fibres together due to hornification (irreversible hydrogen bonding between the nanocellulose).[280] It was found that BC sheets have very high tensile strength of approximately 300 MPa (estimated to be approximately 17 kN m^{-1}).[281] The high tensile strength of the BC network, which formed in between the sisal fibres

provided the mechanical performance of the manufactured BC-sisal fibre preforms in this study (Table 31). The use of BC as binder also reduced the porosity of the fibre preforms as the hornified BC network held the fibres more tightly together. It can also be seen from Table 31 that the true density of BC-sisal preform is higher than that of neat sisal preform. This is due to the incorporation of 10 wt.-% BC nanofibres, which is denser, into the BC-sisal preforms. The true density of BC was measured to be 1.525 g cm^{-3} in this study.

Table 31: Properties of natural fibre performs: σ_w, ρ_m, ρ_e and P denote the tensile strength, true density, envelope density and porosity of the fibre preform, respectively.

Fibre preforms	σ_w (kN m^{-1})	ρ_m (g cm^{-3})	ρ_e (g cm^{-3})	P (%)
Sisal	Not measureable	1.298 ± 0.004	0.350 ± 0.018	73 ± 5
BC-sisal	13.1 ± 2.1	1.318 ± 0.004	0.514 ± 0.015	61 ± 3

9.3.2 Mechanical properties of the (hierarchical) composites

Both the tensile and flexural properties of neat polyAESO and its (hierarchical) composites are summarised in Table 32. The fibre volume fractions of sisal-polyAESO and BC-sisal-polyAESO were found to be 40 vol.-%, implying that direct comparisons between sisal-polyAESO and BC-sisal-polyAESO can be made. When sisal fibres were used as reinforcement for polyAESO, the tensile modulus improved from 0.4 GPa for neat polyAESO to 3.2 GPa for 40 vol.-% sisal fibre reinforced polyAESO composites. A further improvement from 3.2 GPa to 5.6 GPa in the tensile modulus of the composites was achieved when BC was used as the binder for the natural fibre preform. This is thought to be the stiffening of polymer matrix when the fibre preform contained a hornified network of BC was used. It has been shown that the stiffness of a polymer matrix can be improved by as much as 40% when BC, which has an estimated Young's modulus of 114 GPa,[6] at a loading fraction of only 5 wt.-% was used.[202]

A similar trend was observed for the tensile strength of the (hierarchical) composites. Neat polyAESO had a tensile strength of only 4.1 MPa. When neat polyAESO was reinforced with 40 vol.-% sisal fibres, the tensile strength increased to 18.4 MPa. A further improvement was achieved when 40 vol.-% of BC and sisal fibres in form of a preform, were used as reinforcement. The tensile strength of BC-sisal-polyAESO

increased by 71% and nearly 700% when compared to sisal-polyAESO and neat polyAESO, respectively. This significant improvement when BC-sisal fibre preforms were used to create hierarchical composites can be attributed to (i) the enhanced fibre-matrix interaction (see DMTA section) and (ii) enhanced fibre-fibre stress transfer. The use of BC as binder for the fibres resulted in the formation of continuous but hornified BC network, encasing sisal fibres bonding them together. It is postulated that this enhances the fibre-fibre stress transfer compared to sisal fibres only preforms, where the fibres are mostly isolated. In addition to this, it has been shown that using BC as binder enhances the tensile properties of the BC-sisal fibre preforms compared to sisal fibre preforms. This translates to the improved tensile strength of the manufactured BC-sisal-polyAESO.

Table 32: Mechanical properties of neat polyAESO and its (hierarchical) composites. v_f, E_T, σ_T, E_F, σ_F, denote the fibre volume fractions, tensile modulus, tensile strength, flexural modulus and flexural strength, respectively.

Sample	v_f (vol.-%)	E_T (GPa)	σ_T (MPa)	E_F (GPa)	σ_F (MPa)
Neat polyAESO	0	0.4 ± 0.1	4.1 ± 0.1	0.2 ± 0.1	9.0 ± 0.1
Sisal-polyAESO	40 ± 2	3.2 ± 0.2	18.4 ± 0.9	1.9 ± 0.2	28.9 ± 1.6
BC-Sisal-polyAESO	41 ± 3	5.6 ± 0.4	31.4 ± 0.5	4.6 ± 0.3	62.4 ± 3.0

The flexural modulus and strength of the (hierarchical) composites also increased when compared to neat polyAESO (see Table 32). When BC-sisal fibre preforms were used as reinforcement to create hierarchical composites, improvements over sisal-polyAESO of 142% and 116% were observed in the flexural modulus and strength, respectively. As aforementioned, the improvement in the flexural moduli of BC-sisal-AESO can be attributed to the inclusion of nano-sized BC, which is an effective stiffening agent, into the polymer matrix. This can be attributed to (i) enhanced mechanical performance of the BC-sisal preforms (see Table 31), (ii) rigid structure of BC and (iii) formation of a 3-dimensional network of rigid nanocellulose within the matrix.[202]

9.3.3 Thermo-mechanical behaviour of (hierarchical) composites

The viscoelastic properties of neat polyAESO and its (hierarchical) composites as a function of temperature are shown in Figure 44. The storage moduli of the (hierarchical) composites are markedly higher than that of neat polyAESO. These

results corroborate the tensile and flexural properties. The storage moduli stayed relatively constant in the glassy region until T_g, when they sharply decreased. As the temperature is increased further, the storage moduli decreased to a constant value independent of temperature as expected for a thermoset. The increment in the storage moduli at -95°C of the (hierarchical) composites is summarised in Table 33. When sisal preforms were used as reinforcement, only a 96% increase in the storage modulus was observed. When BC-sisal preforms were used instead, a remarkable 244% increase in the storage modulus was observed when compared to neat polyAESO. Improvements in the storage moduli of the (hierarchical) composites at 100°C were also observed (see Table 33).
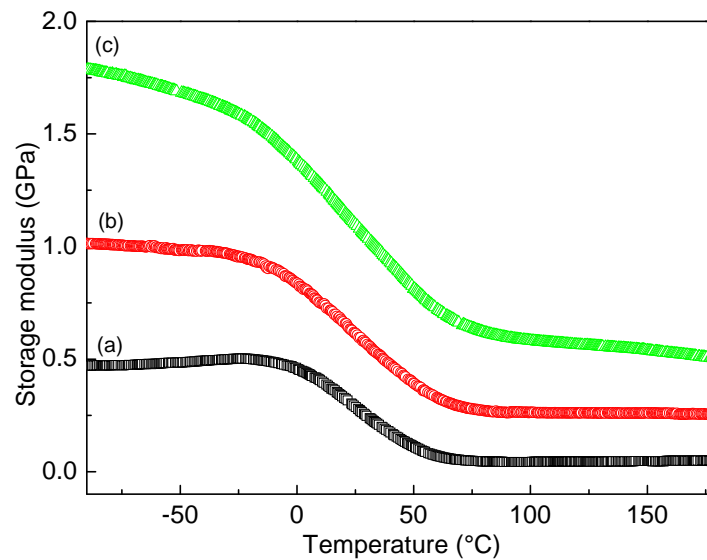
Figure 44: Visco-elastic behaviour of the (hierarchical) composites as a function of temperature. (a) Neat polyAESO, (b) Sisal-polyAESO and (c) BC-Sisal-polyAESO.

Tan δ = f(T) of neat polyAESO and the (hierarchical) composites as a function of temperature is shown in Figure 45. Tan δ is a measure of the damping properties of a material. It is also determined by the quality of the fibre-matrix interface in composites via the relationship:[282]

$$b = \frac{\left(1 - \dfrac{\tan\delta_c}{\tan\delta_m}\right)}{v_f} \tag{9.2}$$

where tan δ_c, tan δ_m, v_f and b represent the tan δ of the composite and neat polymer, fibre volume fraction and the fibre-matrix interfacial strength indicator, respectively.
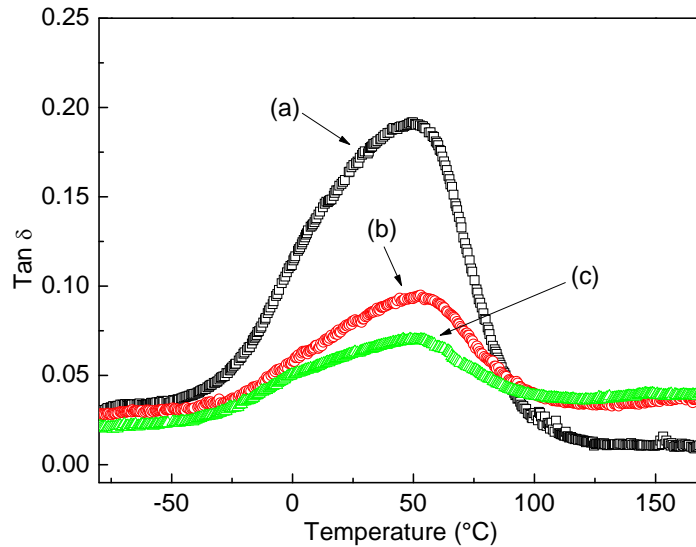
Figure 45: Tan δ as a function of temperature. (a) Neat polyAESO, (b) Sisal-polyAESO and (c) BC-Sisal-polyAESO.

Table 33: Visco-elastic properties of polyAESO and its (hierarchical) composites. G' and ΔG' denote the storage modulus and improvements in storage modulus over neat polyAESO, respectively.

Sample	G' at -95°C (GPa)	ΔG' at -95°C (%)	G' at 100°C (MPa)	ΔG' at 100°C (%)
Neat polyAESO	0.52 ± 0.01	-	43.4 ± 0.3	-
Sisal-polyAESO	1.02 ± 0.01	96 ± 1	263.3 ± 0.1	501 ±3
BC-Sisal-polyAESO	1.79 ± 0.01	244 ± 6	580.4 ± 0.6	1237 ± 9

This equation implies that a large tan δ amplitude indicates a weak fibre-matrix interface whereas a small tan δ amplitude indicates a stronger interface. It can be seen from Figure 45 that BC-sisal-polyAESO had the lowest amplitude of tan δ, which indicates that the sisal fibre-polyAESO interface was enhanced when BC was used as binder for the sisal fibres. The fibre-matrix interfacial strength indicator, b, is tabulated in Table 34. Larger b value was also observed for BC-sisal-polyAESO compared to sisal-polyAESO. These can be explained by coating the sisal surface with BC in the preforms. It has been shown that coating the surface of fibres with a layer of BC does enhance the fibre-matrix interface in polylactide and cellulose acetate butyrate composites.[11, 241] The surface energy of sisal fibres did increase

when BC was used, as BC possesses high surface energy[13, 241] due to its highly crystalline nature.[240] Higher surface energy should result in better wetting by the polymer. These two effects enhanced the fibre-matrix interaction in the hierarchical composites compared to sisal-polyAESO. These results also corroborate with the mechanical properties of the composites; BC-sisal-polyAESO had better tensile and flexural properties compared to sisal-polyAESO.

Table 34: The mechanical glass transition temperature (mechanical T$_g$), taken as the peak of tan δ and the quality of fibre-matrix interface (*b*) of the hierarchical composites.

Sample	Mechanical T$_g$ (°C)	*b*
Neat polyAESO	49 ± 2	-
Sisal-polyAESO	50 ± 3	1.26 ± 0.06
BC-Sisal-polyAESO	50 ± 2	1.54 ± 0.11

9.3.4 Thermal degradation behaviour of (hierarchical) composites
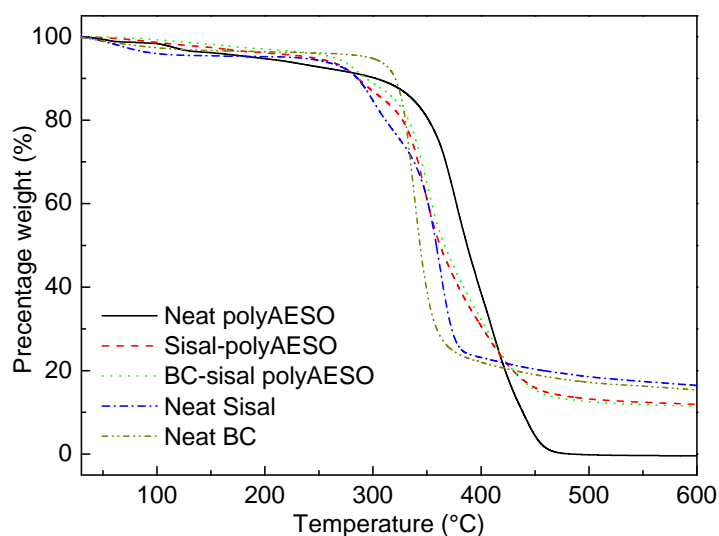
Figure 46: TGA of sisal fibres, BC, neat polyAESO and its (hierarchical) composites.

The thermal degradation behaviour of neat polyAESO and its (hierarchical) composites in N$_2$ atmosphere is shown in Figure 46, along with neat sisal and neat BC. It can be seen that neat polyAESO showed single step thermal degradation behaviour. Two-step degradation behaviour was observed for the (hierarchical) composites. The single step degradation of neat polyAESO is due to the random polymer chain scission occurring around 350-400°C.[283] On the other hand, the observed lower onset degradation temperature of the (hierarchical) composites is due to the presence of sisal fibres in the composites. The first step of degradation in the

(hierarchical) composites is a result of degradation of the fibres occurring around 250°C,[250] followed by a second step of degradation, which is the random chain scission of polyAESO around 350°C[283] and thermal degradation of crystalline BC. The residual weight of the (hierarchical) composites is approximately 10 wt.-%. This can be explained by the carbonisation of the natural fibres and BC.

9.4 Conclusions

A novel sisal fibre preform was manufactured using BC as binder, moving away from commonly used polymer binders. The BC-sisal fibre preforms possessed a tensile strength of 13.1 kN m^{-1}, whereas the sisal fibre preforms possess no measureable tensile strength. This implies that BC enhanced the mechanical properties and the fibre-fibre stress transfer of the natural fibre preforms. polyAESO reinforced with sisal fibre and BC-sisal fibre preforms was manufactured using VARI. The use of BC-sisal preforms improved both the tensile and flexural properties of BC-sisal-polyAESO when compared to sisal-polyAESO and neat polyAESO. The tensile modulus and strength of BC-sisal-polyAESO improved by 75% and 71%, respectively over sisal-polyAESO and 1300% and 600%, respectively over neat polyAESO. A similar trend was also observed for the flexural properties of the (hierarchical) composites. The flexural modulus and strength of BC-sisal-polyAESO improved by 142% and 116%, respectively over sisal-polyAESO and 2200% and 590%, respectively over neat polyAESO. DMTA confirmed the increase in storage moduli of BC-sisal-polyAESO compared to neat polyAESO and sisal-polyAESO. A decrease in the amplitude of tan δ of BC-sisal-polyAESO compared to sisal-polyAESO was also observed, indicating an enhanced fibre-matrix interface when BC was used as binder. These new types of natural fibre preform reinforced hierarchical composites offer promising alternative bio-based materials for the industry.

Chapter 10 – Bio-based macroporous polymer nanocomposites made by mechanical frothing of acrylated and epoxidised soybean oil

Summary

Mechanical frothing is one of the most commonly used methods to create gas-liquid foams. Until recently, the polymerisation of mechanically frothed gas-liquid foams was limited to quasi two-dimensional polymer structures, such as films. In this study three-dimensional bio-based polymer foams was created by microwave curing of gas-soybean oil foams created by mechanical frothing using peroxide as the radical initiator. It was found that the introduction of air during the mechanical frothing was necessary to create the three-dimensional polymer foams. The potential of using bacterial cellulose nanofibrils (BC) simultaneously as stabilisers by obstructing the flow of liquid from the lamella region for these gas-soybean oil foams and nano-filler in the polymer foam is also demonstrated. It was found that the stability of the gas-soybean oil foam templates and the mechanical properties of the polymer nanocomposite foams are enhanced upon the addition of BC foams.

10.1 Introduction

Polymer foams, which represent a group of lightweight materials, were a £7.5 billion industry in the year 2010 and are expected to reach £8.6 billion by the year 2015.[284] These very porous and low density foams makes them attractive materials for both science and engineering applications.[285] Generally, polymer foams can be classified into rigid or flexible foams, open- or closed-cell foams. Open-cell foams can be used as scaffolds for tissue engineering[286-288] or catalyst supports[289] whereas closed-cell foams have found application in sandwich structures[290] and thermal insulation.[291] Generally, the interconnected nature of open-cell foams provides better permeability while closed-cell foams offer low or zero permeability, which results in better insulating properties.[292]

Polymer foams can be produced in various ways; by using chemical or physical blowing agents,[293-295] thermally induced phase separation (TIPS),[296, 297] sintering of particles/microspheres[298, 299] or polymerising the continuous phase of suitable emulsion templates.[285, 300] A novel technique to produce foams has been reported by Murakami and Bismarck.[301] The authors utilised oligomeric tetrafluoroethylene (OTFE) particles to stabilise air bubbles in monomers and UV-polymerised this foam to produce macroporous closed cell polymers. A similar technique was also used to produce macroporous ceramics.[302] A wet foam was produced by mechanically frothing a suspension of hydrophobic alumina powder. The alumina powder serves as foam stabilisers. After a drying step to remove the water followed by sintering of the alumina, Gonzenbach et al.[302] were able to produce macroporous ceramics with porosities up to 88%. However, the polymerisation of mechanical frothed organic gas-monomer foams remain under studied. Marlin et al.[303] first studied macroporous polymers produced from mechanically frothed air-urethane foams. The authors mechanically frothed a mixture of isocyanate, polyols, surfactants and catalyst with air, followed by thermal polymerisation of the monomer to produce polymeric foams. However, the authors only managed to produce two-dimensional (2D) polymer foams of 6 mm in thickness. Greer and Wilkes[304] mechanically frothed a highly viscous oligomer solution, polymerisation was initiated using a 175 keV electron beam to produce 2D thin (0.5 mm thick) polymer foams. They also used the same technique to produce polymeric foams from surfactant stabilised low viscosity monomers. However, the use of a high-energy electron beam reduces the commercial value of this technology.

In this study, a soybean oil-derived renewable monomer was mechanically frothed to create foams. The foam was polymerised using microwave irradiation to produce macroporous three-dimensional (3D) polymers. Macroporous polymer nanocomposites was also produced by dispersing bacterial cellulose nanofibrils (BC) in the monomer phase. BC is produced by the *Acetobacter* species[153] and has the advantage of being free of wax, lignin, pectin and hemicellulose. It is highly crystalline in nature, with a degree of crystallinity of approximately 90%.[120] BC inherently has nanometre dimensions (24 − 86 nm in diameter), and unlike plant-based sources of cellulose, does not require nanofibrillation.[115] Hsieh et al.[6]

predicted that BC possesses a Young's modulus of 114 GPa. These properties make BC an attractive nanofiller to reinforce fine structures, such as fibres, foams[139] and the matrix of composite materials.[11, 13] Wu et al.[305] used chemical blowing agent to produce soybean oil-derived macroporous polymers but styrene and methyl methacrylate were used as the solvents to dilute the soybean oil derived monomer and surfactants were also used to stabilise the foam during polymerisation. Bonnaillie et al.[306] pressurised CO_2 to 60 bar and used it as the physical blowing agent to produce soybean oil-derived macroporous polymers. Our current study focuses on a solvent- and surfactant-free process that operates at atmospheric condition to produce polymer foams. By reinforcing soybean oil derived polymer foams with BC, a new type of green macroporous polymer nanocomposites can be manufactured via simple mechanical frothing of monomer.

10.2 Experimental

10.2.1 Materials

Epoxidised and acrylated soybean oil, AESO (Aldrich, density = 1.04 g cm^{-3}, inhibited with 8500 ppm monomethyl ether hydroquinone), was purchased from Sigma-Aldrich and used as the monomer in this study. Lauroyl peroxide, also known as dodecanoyl peroxide (Alfa Aesar, purity $\geq$ 97%), and ethanol (GPR, purity $\geq$ 99.7%) were purchased from VWR International UK. Lauroyl peroxide was selected as the thermal initiator for this study because of its low initiation temperature (10 h half-life at 65°C). De-ionised water was used throughout this study and was obtained by passing water through a reverse osmosis water filtration unit (Triple Red Laboratory Technology, Bucks, UK). BC nanofibrils were extracted from commercially available *nata-de-coco* (CHAOKOH coconut gel in syrup, Ampol Food Processing Ltd, Nakorn Pathom, Thailand) following previously described work[123, 139, 157] and used in its freeze-dried form in this work.

10.2.2 Macroporous polymer nanocomposites preparation

Polymer foams of neat AESO (polyAESO **1**) were prepared by polymerising the gas-AESO liquid foams (AESO **1**) using lauroyl peroxide as the radical initiator. Firstly, 1 wt.-% (2.5 mol.-%) of lauroyl peroxide (relative to the monomer phase) was mixed with AESO and air was introduced into the monomer by using a hand mixer

operating at its maximum power output (100 W) for 5 min. The resulting gas-AESO liquid foam (AESO **1**) was shaped into cylindrical glass vials (25 mm in diameter and 60 mm in height) using spatula and polymerised for 2 min using microwave irradiation, operating at a frequency and power output of 2.45 GHz and 700 W, respectively. After polymerisation of the gas-AESO foams, the samples were left to cool to room temperature before washing them with ethanol to remove the unreacted monomer, followed by de-ionised water. The polymeric foams were then dried at 40°C in an air oven overnight. Gas-AESO liquid foams with 0.5 wt.-% BC (AESO **2**) and 1 wt.-% BC (AESO **3**) were prepared by mixing BC and 1 wt.-% of lauroyl peroxide (relative to AESO) followed by the introduction of air into the BC-monomer dispersion using the hand mixer as previously described. The gas-AESO-BC liquid foams (AESO **2** and **3**) were then polymerised and washed following the previously described methods. The macroporous polymer nanocomposites of AESO **2** and **3** are termed polyAESO **2** and polyAESO **3**, respectively.

10.2.3 Characterisation of the gas-AESO liquid foams and macroporous polymer nanocomposites

10.2.3.1 Stability indices of gas-AESO liquid foams

The stability indices of gas-AESO liquid foams were assessed by monitoring the upward movement of the air-in-AESO boundary as a result of creaming at 20°C. The movement of the air bubbles in AESO boundary was visually monitored every 24 h. The stability index was calculated by taking the ratio between the creaming heights at the time of assessment and the initial height of the gas-AESO liquid foams.

10.2.3.2 Structure and morphology of the macroporous polymer nanocomposites

The internal structure and morphology of the macroporous polymers and nanocomposites were characterised using variable pressure scanning electron microscopy (SEM) (JSM 5610 LV, Jeol Ltd, Herts, UK) using an accelerating voltage of 10 kV. The macroporous polymer nanocomposites were cut using a scalpel into approximately 0.5 cm^3 pieces and stuck onto aluminium SEM stubs using carbon tabs. Prior to SEM, the samples were Au coated (K550 sputter coater, Emitech Ltd, Ashford, Kent, UK) for 2 min at 20 mA.

10.2.3.3 Density and porosity of the macroporous polymer nanocomposites

He pycnometry (AccuPyc 1330, Micromeritics Ltd, Dunstable, UK) was used to measure the matrix (true) density of the polymer. Prior to this measurement, the polymer foams were crushed into powder using pesto and mortar. The envelope (foam) density of the cylindrical macroporous polymer was calculated by taking the ratio between the mass and the volume of the macroporous polymer, which was determined from the diameter and the height of the material. The porosities of the macroporous polymer nanocomposites were calculated as follows:

$$P = \left(1 - \frac{\rho_e}{\rho_m}\right) \times 100\%$$
(10.1)

where P, ρ_e and ρ_m are the porosity of the macroporous polymer, envelope (foam) density and matrix (true) density, respectively. A total of 5 specimens were measured for each type of sample.

10.2.3.4 Thermal gravimetric analysis (TGA) of the macroporous polymer nanocomposites

The degradation behaviour of the macroporous polymers and nanocomposites was characterised using TGA (TGA Q500, TA Instruments, UK). A piece of a sample with an approximate mass of 20 mg was heated from room temperature to 800°C at a heating rate of 10°C min^{-1} in nitrogen atmosphere.

10.2.3.5 Compression properties of the macroporous polymer nanocomposites

The macroporous polymer nanocomposites were tested in compression using an Instron universal material testing machine (Instron 4505, Instron Corporation, MA, USA) equipped with a 1 kN load cell. The test was conducted in accordance to BS ISO 844: 2009. The cylindrical test specimens had the same diameter and height of 25 mm. Strain gauges (FLA-1-11, Techni Measure, Studley, UK) were glued onto the middle portion of the test specimens using cyanoacrylate glue (EVERBUILD Building Products Ltd, Leeds, UK). In order to avoid the flue filling the pores, only a very thin layer of glue was applied on the strain gauges. The samples were

compressed between two flat and parallel thick polished plates coated with Teflon. Specimens were tested at a crosshead speed of 1 mm min^{-1}. A total of 5 specimens were tested for each type of sample. The errors tabulated are standard deviations.

10.3 Results and discussion

10.3.1 Stability indices of the liquid foam

Figure 47: A photograph showing the gas-monomer liquid foam 5 min after mechanical frothing. Left: AESO 1 (0 wt.-% BC), middle: AESO 2 (0.5 wt.-% BC) and right: AESO 3 (1 wt.-% BC).

The stability of gas-AESO liquid foam templates is very important for the resulting polymer foams. The stability index of gas-AESO liquid foams was determined by tracking the movement of the air-monomer interface due to creaming visually. Photographs of the mechanically frothed gas-AESO and gas-AESO-BC liquid foams are shown in Figure 47. The ability of the gas-AESO and gas-AESO-BC liquid foams to flow under gravity is shown in Figure 48. It can be seen from Figure 48 that AESO **1** flows easier than AESO **2** and **3**. This is due to the viscosifying effect of BC in AESO. BC is known as a thickening agent, stabiliser and texture modifier.[307] The stability of the liquid foams as a function of time is shown in Figure 49. The neat liquid AESO foams without BC (AESO **1**) destabilised rapidly compared to the liquid AESO foams containing 0.5 wt.-% and 1 wt.-% of BC (AESO **2** and **3)**. In fact, AESO **2** and AESO **3** showed insignificant changes in terms of the liquid foam height even 70 days after the foams were prepared. In contrast to AESO **2** and **3**, the

liquid foam height of AESO **1** reduced to half of its original height just 5 days after preparation and was fully phase separated after 70 days.
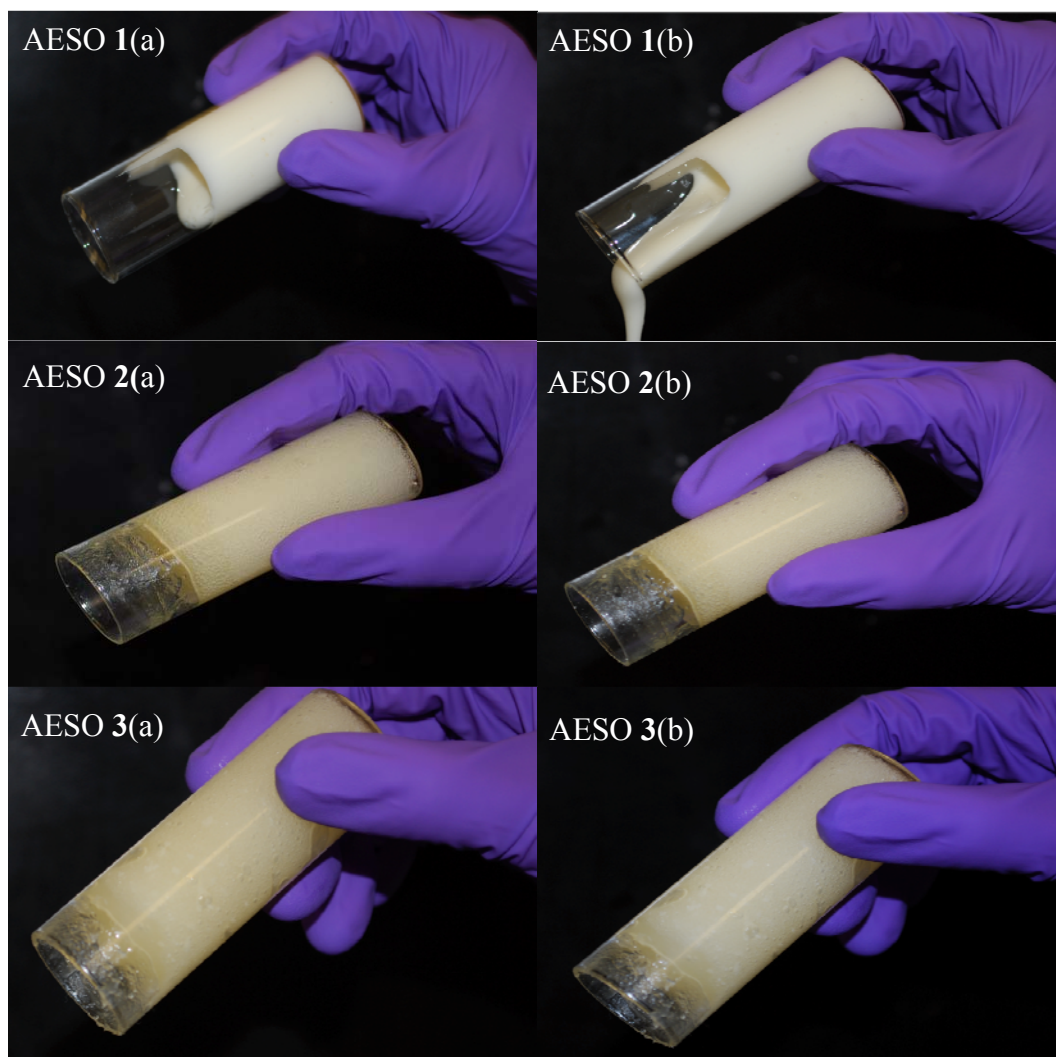
Figure 48: Images showing the capability of the gas-monomer liquid foam to flow. (a) Photographs taken after immediately (0 min) and (b) photographs taken 1 min after the liquid foam was tilted to this angle.

The stability of liquid foams is largely governed by the dynamics of the thin interfacial films, which formed between air bubbles approaching each other. Two main mechanisms are involved in liquid foam destabilisation; gravitational and capillary drainage.[308] The liquid foam will first undergo gravitational drainage, whereby two adjacent bubbles approach each other, resulting in the reduction of foam lamella thickness. The drained liquid will move to the edge of the planar foam lamella, known as the Plateau border. A second mechanism known as capillary drainage will become dominant when the pressure in the foam lamella is larger than the pressure in the Plateau border. As the monomer drains from the foam lamella to

the Plateau border, due to pressure differences, the air bubbles will approach each other resulting in bubble coalescence.[309] The foam AESO **1**, which does not contain BC, exhibited rapid destabilisation due to the expected fast kinetics of gravitational drainage, followed by capillary drainage, which ultimately resulted in the full phase separation of the foam by 70 days. When the monomer phase contains BC (AESO **2** and AESO **3**), the kinetics of destabilisation were significantly reduced. It has been proposed that nano-particles in the liquid phase of foams will aggregate in the Plateau border, obstructing the flow of the liquid from the lamella.[310] Ultimately, this liquid flow obstruction hinders the coalescence of bubbles in foams.
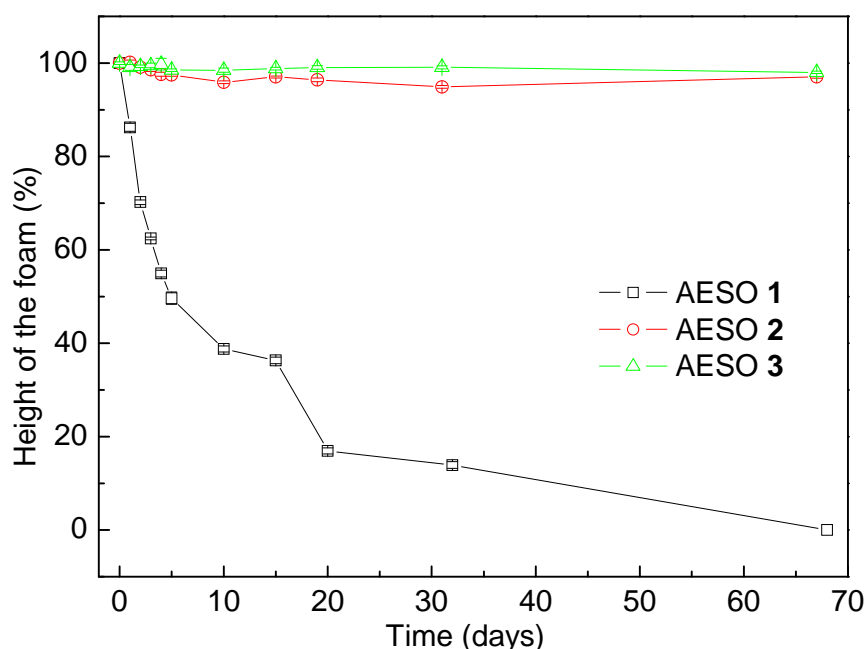
Figure 49: The stability index of the mechanically frothed gas-monomer liquid foams. AESO 1: 0 wt.-% BC, AESO 2: 0.5 wt.-% BC and AESO 3: 1 wt.-% BC.

10.3.2 Structure and morphology of the macroporous polymer nanocomposites

SEM images showing the internal structure and morphology of the polymerised AESO macroporous polymers (polyAESO) are shown in Figure 50. It can be seen from the SEM images that the pores are randomly oriented with pore shapes that are spherical, semi-ellipsoidal or highly irregular, both from the top and side views of the materials. Pore throats can be seen in the pores, indicating that the pores are interconnected. However, the pore size is highly non-uniform throughout the samples as seen in Figure 50. The pores in the macroporous polymer are formed by the polymerisation of the liquid monomer foam templates produced by mechanical frothing, with some contribution from the additional CO_2 released by the thermal

decomposition of the initiators (one mole of initiator produces two moles of CO_2). With increasing BC loading, the monomer phase became more viscous (Figure 48) and the expansion of the bubbles in the gas-monomer liquid foams could not reach its equilibrium state within the time frame of the polymerisation of AESO. This quasi-equilibrium state of the bubbles results in the randomly orientated ellipsoidal pores (polyAESO **1** and **2**). Increasing the BC concentration to 1 wt.-% (polyAESO **3**) increases the viscosity of the continuous phase even further and results in polymer foam structures with very irregular and ill-defined pores.

Top View   Side View
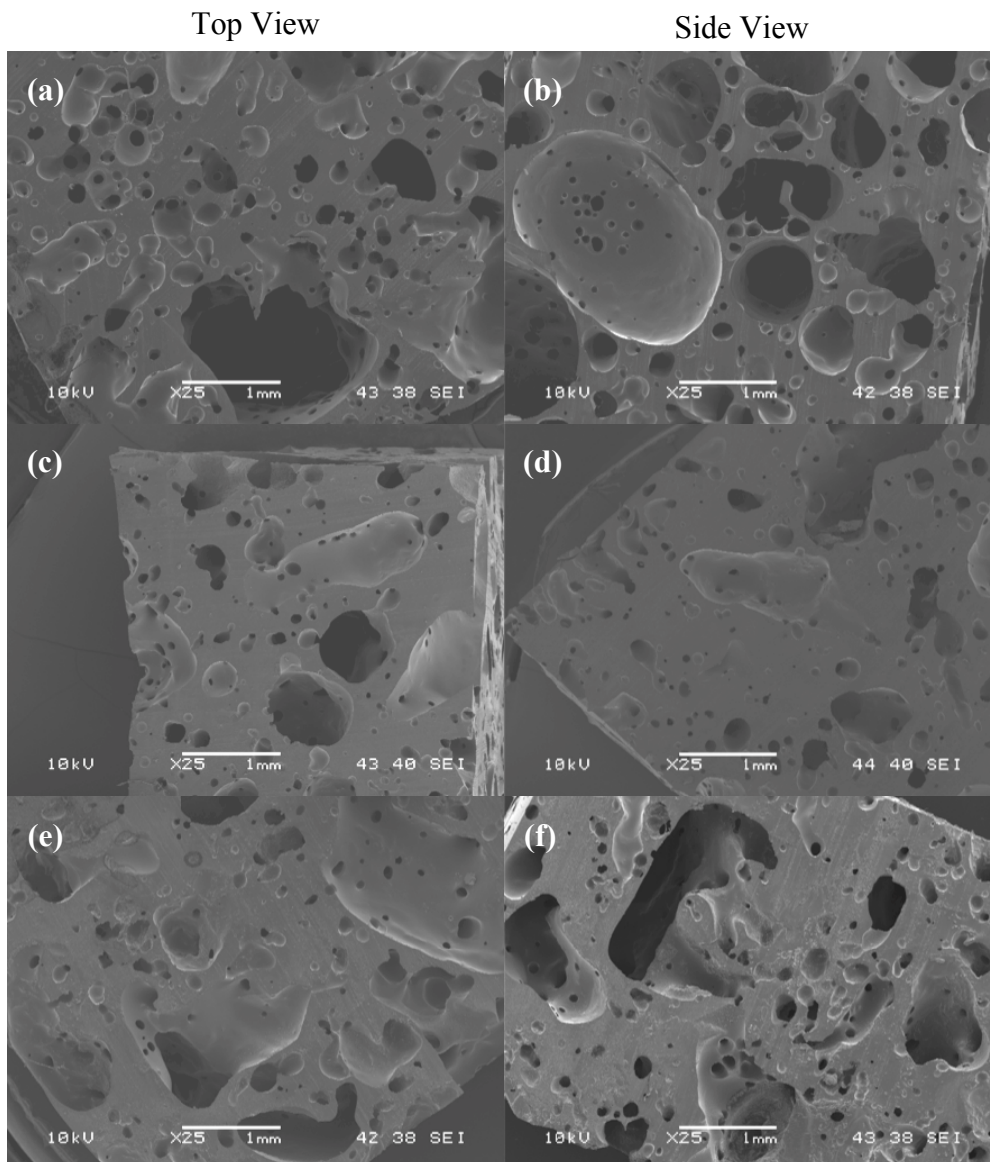
Figure 50: SEM images of the polyAESO. (a) and (b) are polyAESO 1 (0 wt.-% BC), (c) and (d) are polyAESO 2 (0.5 wt.-% BC), (e) and (f) are polyAESO 3 (1 wt.-% BC).

Figure 51: A comparison between non-mechanically frothed and air templated polyAESO. The photograph on the left shows polyAESO that was not mechanically frothed prior to its polymerisation and the image on the right shows the air templated polyAESO 1 (0 wt.-% BC).

10.3.3 Porosity of the macroporous polymer nanocomposites

Porosity is one of the important factors that govern the physical properties of macroporous polymers. Both the measured envelope and matrix densities along with the calculated porosity of the macroporous polymer and its nanocomposites are tabulated in Table 35. It can be seen that the envelope density increased from 0.44 g cm^{-3} to 0.58 g cm^{-3} and the porosity of the polyAESO decreases from 59% to 45% with increasing BC content. The introduction of BC into the monomer phase resulted in difficulties to mechanically froth the liquid at constant input of frothing energy. Even though the thermal degradation of the initiator could potentially contribute to the porosity (approximately 130 cm^3 of CO_2 produced per 100 mL of AESO used), the images shown in Figure 51 show otherwise. Polymerising AESO containing 1 wt.-% of initiator could potentially result in a theoretical porosity of 56%. However, the microwave irradiation also increased the temperature of the monomer to approximately 150°C[†]. At this temperature, the viscosity of the monomer phase is low enough for the CO_2 produced to rise to the air-monomer interface and escape from the monomer phase before it gels and cured. Therefore, non-frothed AESO did not polymerise into porous polymers (see Figure 51). By frothing the monomer phase, air bubbles are introduced. It is hypothesised that the CO_2 produced can

---

[†] This temperature was obtained by measuring the temperature of the microwave-irradiated monomer without thermal initiator immediately after irradiation.

escape from the monomer phase to the air-monomer interface at the top of the cylindrical vessel or into the air bubbles formed during mechanical frothing. The latter resulted in the expansion of the air bubbles during the polymerisation of the monomer. This might also explain why ellipsoidal pores are observed in polyAESO. The ellipsoidal pores could also be a result of buoyancy induced creaming.

Table 35: The envelope density, matrix density and porosity of the macroporous polymers. ρ_e, ρ_m and P correspond to the envelope density, matrix density and porosity of the macroporous polymers, respectively. The errors tabulated are the standard errors.

Sample	ρ_e (g cm^{-3})	ρ_m (g cm^{-3})	P (%)
polyAESO **1** (0 wt.-% BC)	0.44 ± 0.01	1.07 ± 0.01	59 ± 1
polyAESO **2** (0.5 wt.-% BC)	0.49 ± 0.01	1.08 ± 0.01	54 ± 1
polyAESO **3** (1 wt.-% BC)	0.58 ± 0.01	1.08 ± 0.01	45 ± 1

10.3.4 TGA of the macroporous polymer nanocomposites
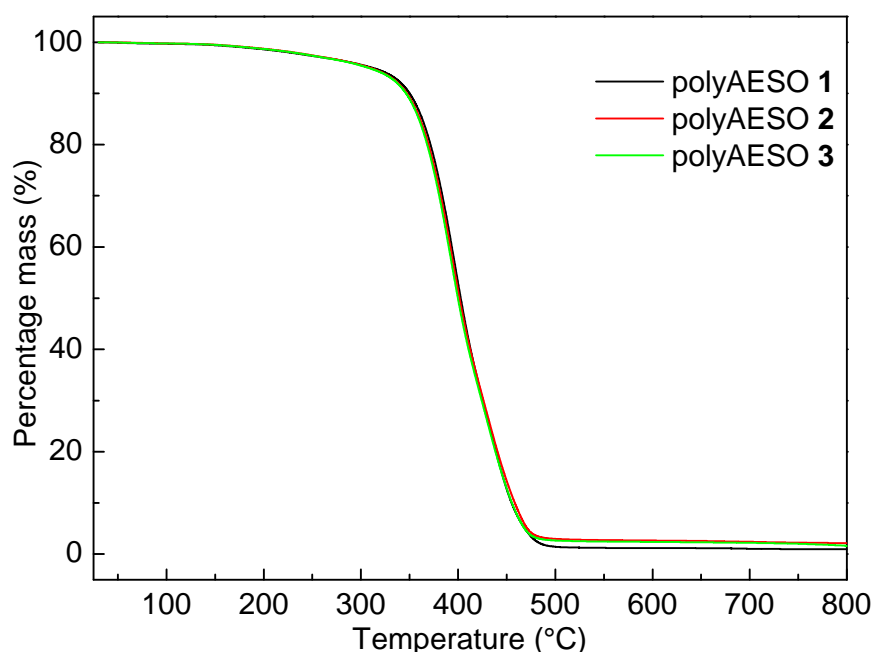
Figure 52: The thermal degradation behaviour of the macroporous polymer nanocomposites.

The thermal degradation behaviour of the macroporous polymer and its nanocomposites is shown in Figure 52. It can be seen that all the samples undergo single step degradation in nitrogen atmosphere. Random polymer chain scission occurred during the degradation of polyAESO.[283] The introduction of BC into the sample did not alter the degradation behaviour of polyAESO. This might be due to the low BC content in the sample. The onset degradation temperature determined from TGA analysis of the foams was found to be 380°C for all samples. In addition

to this, the residual carbon content for polyAESO **1** was found to be 0.98 wt.-% and approximately 2 wt.-% for both polyAESO **2** and **3**. The increase in the residual carbon content of polyAESO **2** and **3** compared to polyAESO **1** can be explained by the carbonisation of BC in the nanocomposites.

10.3.5 Compression properties of the macroporous polymer nanocomposites

The mechanical properties of the macroporous polymer nanocomposites determine their potential applications. The compressive modulus and strength, along with the specific compressive modulus and strength (absolute compressive properties divided by the envelope density of the material) of the macroporous polymer and its nanocomposites are summarised in Table 36 and characteristic load-displacement curves of the linear elastic region are shown in Figure 53. It should be noted that the polyAESO with different BC loadings possess different porosities and, therefore, this study compares only the specific compressive properties of the polyAESO. By adding 0.5 wt.-% of BC (polyAESO **2**), the specific modulus increased from 253 MPa kg^{-1} m^3 to 339 MPa kg^{-1} m^3. Even at such low nano-filler loading fraction, a 35% increase in the specific compression modulus was observed. This increase in stiffness of the foam can be attributed to the stiffness of BC, which has been estimated to possess a Young's modulus of 114 GPa.[6] However, when the nano-filler content was increased to 1 wt.-% BC (polyAESO **3**), the specific modulus decreased by 60% to 90.2 MPa kg^{-1} m^3 when compared to polyAESO **1**. This decrease in the compressive modulus of polyAESO **3** is thought to be due the ill-defined pore structure due to the inclusion of BC into the macroporous polymer (see Figure 50). The specific compressive strength of the polyAESO showed a different trend compared to the compressive modulus. It was observed that the compressive strength of the polyAESO decreased with increasing BC content (Table 36). The compressive strength of the polymer nanocomposite foams decreased by as much as 60% from 777 kPa kg^{-1} m^3 to 315 kPa kg^{-1} m^3 when the BC content was increased to 1 wt.-%. It is proposed that the poor specific strength of the nanocomposites is due to the poor compatibility and hence, poor stress transfer between BC and the polymerised AESO.
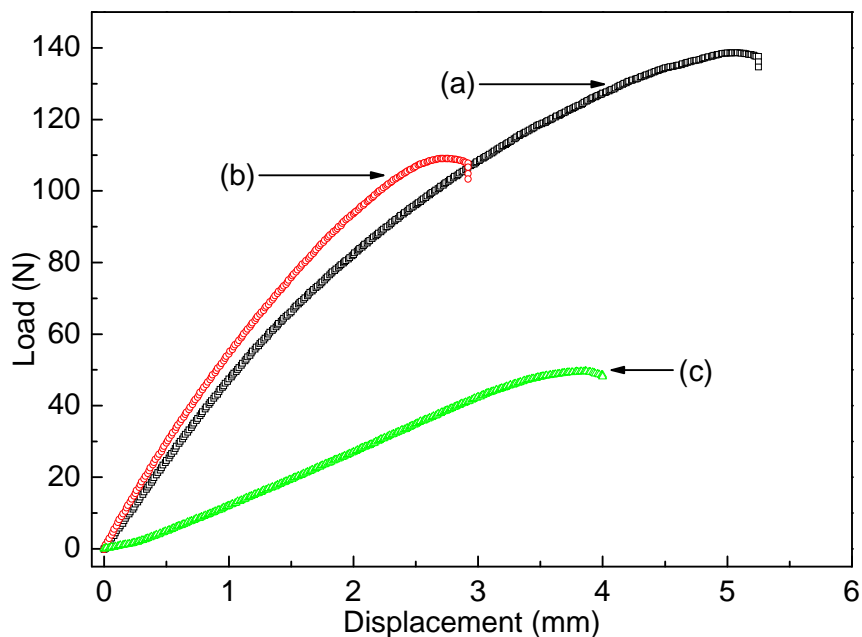
Figure 53: Characteristic load-displacement curves of the macroporous polymers. (a) polyAESO 1 (0 wt.-% BC), (b) polyAESO 2 (0.5 wt.-% BC) and (c) polyAESO 3 (1 wt.-% BC).

Table 36: Mechanical properties of the macroporous polymer. E_c, σ_c, E_c' and σ_c' denote compression modulus, compression strength, specific compression modulus and specific compression strength, respectively. The errors tabulated are the standard errors.

Sample	E_c (MPa)	σ_c (kPa)	E_c' (MPa kg^{-1} m^3)	σ_c' (kPa kg^{-1} m^3)
polyAESO **1** (0 wt.-% BC)	111 ± 11	343 ± 34	253 ± 25	779 ± 79
polyAESO **2** (0.5 wt.-% BC)	166 ± 33	254 ± 19	338 ± 68	519 ± 39
polyAESO **3** (1 wt.-% BC)	52 ± 9	183 ± 26	90 ± 15	315 ± 46

The presence of unreacted AESO in the macroporous polymers could also affect the mechanical properties by the plasticising action of the monomer.[311] It can be postulated that any unreacted monomer present only at the pore walls, where the monomer is exposed to oxygen during the polymerisation process. The oxygen-exposed surface will remain "tacky" as oxygen inhibits the surface polymerisation.[312] However, the macroporous polymers were washed with ethanol to remove any unreacted monomer prior to mechanical testing. In addition to this, the mechanical properties of porous materials are governed predominantly by cellular morphology and the properties of the base polymer.[313] Therefore, any

remaining unreacted AESO will not affect the mechanical properties measured in this study.

10.4 Conclusions

Studies on the mechanical frothing of liquid monomers to produce non-aqueous foam templates followed by their polymerisation to produce polymeric foams had been conducted in the 1970s. However, this technique was limited to the production of 2D foams, which might be due to the instability of the air-monomer foam. In this study however, macroporous polymers was produced through microwave heating of mechanically frothed gas-AESO liquid foams containing lauroyl peroxide as thermal initiator due to the high viscosity of the monomer phase and the obstruction of the flow into the Plateau border by BC. Through this route, 3D macroporous polymers can be produced. The resulting bio-based macroporous polymers possessed a porosity of approximately 60% but it was found that the stability of the gas-AESO liquid foam template was poor. This liquid foam destabilises within 7 days of preparation at room temperature. In order to enhance the stability of the gas-AESO liquid foams and the mechanical properties of the macroporous polymers, BC was added as a nano-filler to produce macroporous polymer nanocomposites. With the introduction of BC, the stability of the liquid AESO foams was significantly enhanced. No phase separation (e.g. creaming) was observed 70 days after the preparation of the liquid foams. This was thought to be due to the obstruction of the Plateau border in the presence of BC during capillary drainage of the monomer liquid foams. The incorporation of 0.5 wt.-% BC into the polymeric foams resulted in a significant increase of the specific compression modulus when compared to the neat polymer foams. This was attributed to the reinforcing effect of the highly crystalline and stiff BC. However, a further increase of BC to 1 wt.-% resulted in a decrease of the specific compression modulus when compared to the neat polymeric foams. This is thought to be due to the ill-defined cell structure of the macroporous polymer nanocomposites at 1 wt.-% BC loading. It was hypothesised that the poor compatibility between BC and polymerised AESO has resulted in the decrease of the compressive strength of the polyAESO with increasing BC content.

Chapter 11 – Conclusions and suggestions for future work

11.1 Summary of findings

Truly green (nano)composites are anticipated to be the next major step forward in the area of renewable composite materials for non-critical structural applications. The main aim of this work was to produce truly green, natural fibre-reinforced, nanocellulose renewable polymer composites and to demonstrate the scale of the resulting performance improvements. Numerous challenges have been addressed throughout the course of this work and novel composites manufacturing method have also been explored to produce renewable hierarchical composites. The achievements and findings of this work are summarised as follows:

11.1.1 *Surface-only* modification of bacterial cellulose (BC)

BC nanofibres were successfully modified only on their surface using an esterification reaction with organic acids of different chain length, i.e.: acetic acid, hexanoic acid or dodecanoic acid. This modification did successfully render the hydrophilic surfaces of BC nanofibres hydrophobic. It was found that the degree of hydrophobicity of BC can be tailored by the carbon chain length of the organic acids used to modify BC. The crystallinity of acetic acid modified BC reduced compared to neat BC but no reduction in the crystallinity of C_6- and C_{12}-BC was observed. A method based on hydrogen/deuterium exchange was developed in this work to evaluate the availability of surface hydroxyl groups of neat and modified BC. It was found that neat BC possesses hydroxyl group availability of 1.24 (out of a maximum of 3). With surface modifications of BC, the degree of surface hydroxyl group substitution decreased with increasing carbon chain length of the organic acids used. The thermal behaviour of neat and organic acid modified BC sheets decreased with increasing carbon chain length of the organic acids used. This is evidence of low packing efficiency, arising from the grafted hydrocarbon chains and, therefore, the reduced overall interaction between the nanofibres.

11.1.2 BC reinforced polylactide (PLLA) nanocomposites with improved mechanical properties

The previously described surface-modified BC was used as nano-reinforcement for PLLA. A direct wetting method, allowing the determination of the contact angle of polymer droplets on a single BC nanofibre, was developed to quantify the interfacial adhesion between PLLA and functionalised BC. It was found that the contact angle between PLLA droplets and functionalised BC decreased with increasing chain lengths of the organic acids used to hydrophobise BC. A novel method to compound BC with PLLA based on thermally induced phase separation (TIPS) to yield a dry form of pre-extrusion composite was also developed. The incorporation of organic acid functionalised BC into PLLA led to an improvement in both tensile modulus and tensile strength of the C_6-BC and C_{12}-BC reinforced nanocomposites by as much as 50% and 15%, respectively. However, the PLLA nanocomposites reinforced by C_2-BC seemed to undergo acid catalysed hydrolysis during extrusion and this led to a decrease in the molecular weight of the PLLA, which in turn affected the mechanical properties of the resulting material. The nanocomposites also exhibit higher storage moduli compared to neat PLLA. This is evidence of improved interfacial adhesion between the polymer matrix and the functionalised BC. This result was also confirmed by direct wetting measurement of cellulose nanofibrils by PLLA droplets.

A novel, entirely renewable copolymer of PLLA (RP**1**) was explored as a compatibiliser, to produce nanocomposites of PLLA reinforced with BC, showing improved mechanical properties. The renewable copolymer is prepared by the random ring opening copolymerisation of a carbohydrate lactone (acetic acid 5-acetoxy-6-oxo-tetrahydro-pyran-2-yl methyl ester) with *L*-lactide (LLA). Direct wetting measurements showed that RP**1** had a higher affinity for BC than PLLA. A polymer blend, containing 5 wt.-% RP**1** in PLLA, also showed an improved affinity for BC compared to PLLA. The preparation of nanocomposites using either PLLA or RP**1** as the matrix and 5 wt.-% BC as the reinforcement, resulted in the Young's modulus being improved by 12% and 16%, respectively, when compared to the either of the polymers alone. This is attributed to the presence of stiff BC nanofibrils in the matrix. Unfortunately, the tensile strength of the PLLA-BC nanocomposite decreased by 8% vs. PLLA, due to poor compatibility between the matrix and

reinforcement. However, the tensile strength of RP**1**-BC, improved by 46% compared to neat RP**1**, due to the improved compatibility. The preparation of BC reinforced PLLA nanocomposites using RP**1** as the compatibiliser, at just 5 wt-% loading, resulted in a improvement of 15% in the Young's modulus and 7% in the tensile strength compared to the PLLA composite. The renewable copolymer enables enhanced fibre-matrix stress transfer leading to better composite performance. The application of the novel renewable copolymer as a compatibiliser enables preparation of 100% renewable nanocellulose composites, showing improved properties without the need for any chemical modification of cellulose nanofibres.

11.1.3 The reinforcing ability of nanofibrillated cellulose (NFC) and BC for polymers

Chapter 6 compared NFC and BC. Scanning electron microscopy revealed that both types of nanocellulose possessed a fibrous structure of approximately 50 nm in diameter and several micrometre in length. BC had significantly higher degree of crystallinity (as measured by XRD) of 72% compared to NFC of 41%. The critical surface tension (γ_c)of NFC and BC was determined from the normalised wetting rates as determined by wicking rate measurements. It was found that BC possesses a γ_c of 57 mN m^{-1}. NFC, on the other hand, possesses lower γ_c of 41 mN m^{-1}. Both the NFC and BC papers were found to possess similar tensile properties; a Young's modulus of ~12 GPa and tensile strength of ~110 MPa. Nanocomposites were manufactured by infusing the nanocellulose paper with an epoxy resin using vacuum assisted resin infusion. When used as reinforcement in paper form for an epoxy matrix, the nanocomposites were found to possess a high stiffness and strength of approximately ~8 GPa and ~100 MPa, respectively, at an equivalent fibre volume fraction of 60 vol.-%. However, no significant difference was observed between the reinforcing ability of NFC and BC in terms of the stiffness of the nanocomposites. The nanocomposites reinforced with BC papers, however, showed slightly higher tensile strength and strain-to-failure compared to NFC papers by approximately 6%. Nonetheless, the difference between the tensile strength of the nanocomposites reinforced by NFC and BC is not very significant. This work shows that both NFC and BC will serve as excellent reinforcing material for the production of nanocomposites.

11.1.4 Heterogeneous chemical modification of freeze-dried or never-dried BC

The susceptibility of (i) never-dried and (ii) freeze-dried BC with towards organic acid esterification was reported in chapter 7. It was observed that BC freeze-dried from water is more susceptible towards organic acid esterification than never-dried BC. It was found that freeze-dried BC underwent significant bulk modification with degree of substitution of 1.87 compared to never-dried BC of only 0.36. The crystallinity of the freeze-dried BC decreased to only 53% (from the original of 90%) after the modification whilst the crystallinity of never-dried BC did not change significantly after the modification. A few hypotheses were proposed to explain the observed behaviour and further investigated to elucidate this observation; the effect of residual water in cellulose, the accessibility of hydroxyl groups and the crystal structure of never-dried and freeze-dried BC on the susceptibility of cellulose fibrils to the esterification, respectively. However, the investigation of these hypotheses raised more questions and the main question still remains; why do BC nanofibres behave differently when modifying freeze-dried BC or never-dried BC?

11.1.5 Fabrication of hierarchical (nano)composites with improved mechanical properties

Randomly oriented BC coated short sisal fibre reinforced PLLA hierarchical composites were discussed in chapter 8. A novel method based on slurry dipping to coat sisal fibres with nano-sized BC was developed as an alternative method to modify the surface of natural fibres. This method was extended to produce either a dense BC coating layer on the surface of sisal fibres or BC coated "hairy sisal fibres", in which the BC is oriented perpendicular to the surface of the fibres. The use of BC coated sisal fibres in PLLA matrix showed an improvement in tensile modulus of nearly 40% but their tensile strengths decreased by as much as 10%. Not only was the fibre-matrix interface enhanced through the presence of the BC coating on sisal fibres, but also the fracture mechanism of the composites was modified; the fracture mechanism switched from a high fracture energy (T-fibre fracture) to a low fracture energy (L-fibre fracture) mechanism and hence resulted in decrease of the tensile strength of PLLA reinforced with BC coated fibres. When the BC coated fibre reinforced composites were further reinforced with BC by dispersing BC in the matrix, the tensile modulus and strength improved even more when compared to neat PLLA by as much as 72% and 11%, respectively. This is attributed to the enhanced

fibre-matrix interface and stiffening of PLLA due to the incorporation of BC into the matrix. The flexural modulus of the hierarchical composites improved by as much as 67% and their flexural strength increased by 23% when compared to neat PLLA. DMA confirmed the increased storage moduli when compared to neat PLLA and also suggests an enhanced fibre-matrix interface (a reduction in the height of tan δ). These new types of short fibre composites offer a promising alternative to the industry as no chemical modifications or plasma treatments are required to produce biodegradable composites with improved properties.

11.1.6 Manufacturing of natural fibre performs using BC as binder

A novel non-woven sisal fibre preform was manufactured using a papermaking process utilising BC as binder. The BC-sisal fibre preforms possessed a tensile strength of 13.1 kN m^{-1}, whereas the sisal fibre preforms possess no measureable tensile strength. This implies that BC enhanced the mechanical properties and the fibre-fibre stress transfer of the natural fibre preforms. poly(acrylated epoxidised soybean oil) (AESO) reinforced with sisal fibre and BC-sisal fibre preforms was manufactured using vacuum assisted resin infusion. Both the tensile and flexural properties of the hierarchical composites showed significant improvements over polyAESO and neat sisal fibre preform reinforced polyAESO. These results were corroborated by the thermo-mechanical behaviour of the (hierarchical) composites, which showed increased storage moduli and enhanced fibre-matrix stress transfer. By using BC as binder for short sisal fibres, added benefits such as the high Young's modulus of BC, enhanced fibre-fibre and fibre-matrix stress transfer can be utilised in the resulting hierarchical composites.

11.1.7 BC as nano-filler and stabiliser for the manufacturing of macroporous polymers

Macroporous polymers were successfully produced through microwave heating of mechanically frothed gas-acrylated epoxidised soybean oil (AESO) liquid foams containing lauroyl peroxide as thermal initiator due to the high viscosity of the monomer phase and the obstruction of the flow into the Plateau border by BC. The resulting renewable macroporous polymers possessed a porosity of approximately 60% but it was found that the stability of the gas-AESO liquid foam template was

poor. This liquid foam destabilises within 7 days of preparation at room temperature. In order to enhance the stability of the gas-AESO liquid foams and the mechanical properties of the macroporous polymers, BC was added as a nano-filler to produce macroporous polymer nanocomposites. With the introduction of BC, the stability of the liquid AESO foams was significantly enhanced. No phase separation (e.g. creaming) was observed even 70 days after the preparation of the liquid foams. The incorporation of 0.5 wt.-% BC into the polymeric foams resulted in a significant increase of the specific compression modulus when compared to the neat polymer foams. This was attributed to the reinforcing effect of the highly crystalline and stiff BC.

11.2 Future work

The work discussed in this thesis opens new approaches to the engineering of novel green materials. Further developments of the discussed research work are as follows:

11.2.1 Optimising the carbohydrate content of the compatibiliser

The carbohydrate content used in the copolymer of PLLA was approximately 7 mol.-%. It can be anticipated that there should exist an optimum concentration whereby the carbohydrate content should result in good affinity towards BC (and hence significantly improved BC fibre-matrix interface) and the compatibiliser still possessed significant tensile properties of its own. By optimising this balance between BC affinity and mechanical properties of the compatibiliser, the tensile properties of the resulting nanocomposites should be able to be improved even further than what was reported in this thesis.

Another interesting direction of research utilising this compatibiliser would be its effect on the impact and heat deflection temperature of PLLA. The brittleness and low heat deflection temperature (~60°C) of PLLA has limited its wide spread usage in the industry. The use of this compatibiliser for the production of BC reinforced PLLA nanocomposites could improve the impact resistance and increase the heat deflection temperature of PLLA nanocomposites.

11.2.2 Unidirectional hierarchical (nano)composites manufacturing

The coating of BC onto the surface of sisal fibres is believed to be due to the absorption of water as a result of hydrophilic nature of the fibres. This drags along the BC in the dispersion and collapsed on the surface of the fibres. This approach can be extended to coat continuous regenerated cellulose fibres to produce unidirectional BC coated regenerated cellulosic fibre reinforced polymer nanocomposites. Regenerated cellulose fibres are hydrophilic in nature and the postulated coating mechanism should work with these fibres. Regenerated cellulose is of interested as it offers numerous advantages over natural fibres, such as minimal batch-to-batch variability in terms of the fibres properties.

The continuous production of unidirectional regenerated cellulose fibre reinforced composites can be achieved by dispersing a polymer powder and BC in a bath of water to create a suspension. The fibres are passed through the bath in a continuous fashion to pick up the BC and polymer powder in the bath. Prior to the consolidation into a pre-preg, the impregnated fibres can be dried in an oven to remove the water and further melt the polymer. Composite structures can be produced by laying up these laminates in various directions (i.e. $\pm 90°$ or $\pm 45°$) and followed by consolidation.

11.2.3 Further demonstration of value above the current state-of-the-art of the fibre preforms manufacturing technique

It has been demonstrated in this work that BC is an efficient binder for the manufacturing of sisal fibre preforms. The potential of BC as binder can be expanded to various types of fibres. These fibres could include high strength/stiffness natural fibres such as flax or hemp fibres, loose regenerated cellulose fibres and even possibly recycled paper. Apart from this, composite parts with curved surfaces are crucial for many structural designs and applications. Research efforts should also be directed towards identifying methodology of manufacturing fibre preforms with double curvature surfaces to increase the value of this fibre preforms manufacturing technique.

It can also be anticipated that the discussed fibre preform manufacturing technique can be adapted to produce fibre reinforced thermoplastic pre-pregs *in-situ* during the

production of the fibre-preforms. This could be achieved by dispersing BC and a thermoplastic polymer powder along with the fibre of interest in the same suspension, which is then subsequently vacuum-filtered and dried. This method of producing long fibre-reinforced thermoplastic is of interest because conventional extrusion-injection moulding cannot process very long fibres, without breaking the fibres.

References

[1] "Council Directive 1999/31/EC of 26 April 1999 on the Landfill of Waste", EU, Ed., 1999.

[2] "Directive 2000/53/EC of the European Parliament and of the Council of 18 September 2000 on End-of-life Vehicles", EU, Ed., 2000.

[3] "Directive 2002/96/EC of the European Parliament and of the Council of 27 January 2003 on Waste Electrical and Electronic Equipment (WEEE)", EU, Ed., 2003.

[4] A. K. Mohanty, M. Misra, G. Hinrichsen, *Macromol. Mater. Eng.* **2000**, *276*, 1.

[5] A. Bismarck, S. Mishra, T. Lampke, "Plant fibers as reinforcement for green composites", in *Natural fibers, biopolymers and biocomposites*, A.K. Mohanty, M. Misra, and L. Drzal, Eds., CRC Press, Boca Raton, 2005.

[6] Y. C. Hsieh, H. Yano, M. Nogi, S. J. Eichhorn, *Cellulose* **2008**, *15*, 507.

[7] M. A. R. Meier, *Macromol. Chem. Phys.* **2009**, *210*, 1073.

[8] V. Flaris, G. Singh, *J. Vinyl Addit. Technol.* **2009**, *15*, 1.

[9] W. Morton, J. W. S. Hearle, "*Physical properties of textile fibres"*, 3rd edition, The Textile Institute, Manchester, 1993.

[10] K. Oksman, M. Skrifvars, J. F. Selin, *Composites Science and Technology* **2003**, *63*, 1317.

[11] J. Juntaro, M. Pommet, G. Kalinka, A. Mantalaris, M. S. P. Shaffer, A. Bismarck, *Advanced Materials* **2008**, *20*, 3122.

[12] J. Juntaro, M. Pommet, A. Mantalaris, M. Shaffer, A. Bismarck, *Compos. Interfaces* **2007**, *14*, 753.

[13] M. Pommet, J. Juntaro, J. Y. Y. Heng, A. Mantalaris, A. F. Lee, K. Wilson, G. Kalinka, M. S. P. Shaffer, A. Bismarck, *Biomacromolecules* **2008**, *9*, 1643.

[14] K. L. Pickering, G. W. Beckermann, S. N. Alam, N. J. Foreman, *Composites Part A-Applied Sciencce and Manufacturing* **2007**, *38*, 461.

[15] T. Nishino, K. Hirao, M. Kotera, K. Nakamae, H. Inagaki, *Composites Science and Technology* **2003**, *63*, 1281.

[16] D. Plackett, T. L. Andersen, W. B. Pedersen, L. Nielsen, *Composites Science and Technology* **2003**, *63*, 1287.

[17] V. M. Castano, G. Vazquezpolo, M. A. Amador, F. Garciazetina, E. Martinez, U. Marquezamador, A. Altmamiranomeza, *J. Reinf. Plast. Compos.* **1995**, *14*, 866.

[18] A. K. Mohanty, M. Misra, *Polym.-Plast. Technol. Eng.* **1995**, *34*, 729.

[19] R. Heijenrath, T. Peijs, *Advanced Composites Letters* **1996**, *5*, 81.

[20] W. Gindl, J. Keckes, *Composites Science and Technology* **2004**, *64*, 2407.

[21] R. Karnani, M. Krishnan, R. Narayan, *Polym. Eng. Sci.* **1997**, *37*, 476.

[22] T. G. Schuh, "Renewable materials for automotive applications", Daimler-Chrysler AG, Stuttgart http://www.ienica.net/fibresseminar/schuh.pdf.

[23] "Ten Alps Communications Ltd t/a Sovereign Publications", Rieter Automotive Systems, 2008 http://www.sovereign.

[24] U. Riedel, J. Nickel, *Angew. Makromol. Chem.* **1999**, *272*, 34.

[25] D. N. Saheb, J. P. Jog, *Adv. Polym. Technol.* **1999**, *18*, 351.

[26] E. Sjostrom, "*Wood Chemistry: Fundamentals and Applications"*, Academic Press, California, 1981.

[27] P. J. H. Franco, A. Valadez-González, "Fiber-matrix adhesion in natural fiber composites", in *Natural fibers, biopolymers and biocomposites*, A.K. Mohanty, M. Misra, and L. Drzal, Eds., CRC Press, Boca Raton, 2005.

[28] B. Braun, J. R. Dorgan, J. P. Chandler, *Biomacromolecules* **2008**, *9*, 1255.

[29] D. R. Bloch, "Polymer Handbook 4th Edition Volume 2", J. Brandrup, E.H. Immergut, and R.A. Grulke, Eds., Wiley Interscience, 1999, p. VII/497.

[30] S. D. Zhu, Y. X. Wu, Q. M. Chen, Z. N. Yu, C. W. Wang, S. W. Jin, Y. G. Ding, G. Wu, *Green Chem.* **2006**, *8*, 325.

[31] A. L. Dupont, *Polymer* **2003**, *44*, 4117.

[32] P. O. Olesen, D. V. Plackett, "Perspectives on the performance of natural plant fibres", Plant Fibre Laboratory, Royal Veterinary and Agricultural University, Copenhagenhttp://www.ienica.net/fibresseminar/olesen.pdf.

[33] M. N. S. Kumar, A. K. Mohanty, L. Erickson, M. Misra, *J. Biobased Mater. Bioenergy* **2009**, *3*, 1.

[34] A. K. Mohanty, M. Misra, L. T. Drzal, *J. Polym. Environ.* **2002**, *10*, 19.

[35] Personal Communication, "Commercial documentation - No AQ.866 - 9 (September 2003)".

[36] C. A. S. Hill, A. Norton, G. Newman, *J. Appl. Polym. Sci.* **2009**, *112*, 1524.

[37] B. Wielage, T. Lampke, G. Marx, K. Nestler, D. Starke, *Thermochim. Acta* **1999**, *337*, 169.

[38] M. J. John, R. D. Anandjiwala, *Polym. Compos.* **2008**, *29*, 187.

[39] X. Li, L. G. Tabil, S. Panigrahi, *J. Polym. Environ.* **2007**, *15*, 25.

[40] S. Kalia, B. S. Kaith, I. Kaur, *Polym. Eng. Sci.* **2009**, *49*, 1253.

[41] A. Valadez-Gonzalez, J. M. Cervantes-Uc, R. Olayo, P. J. Herrera-Franco, *Compos. Pt. B-Eng.* **1999**, *30*, 321.

[42] G. Mehta, L. T. Drzal, A. K. Mohanty, M. Misra, *J. Appl. Polym. Sci.* **2006**, *99*, 1055.

[43] P. Ganan, S. Garbizu, R. Llano-Ponte, I. Mondragon, *Polym. Compos.* **2005**, *26*, 121.

[44] L. A. Pothan, S. Thomas, G. Groeninckx, *Compos. Pt. A-Appl. Sci. Manuf.* **2006**, *37*, 1260.

[45] V. Tserki, N. E. Zafeiropoulos, F. Simon, C. Panayiotou, *Compos. Pt. A-Appl. Sci. Manuf.* **2005**, *36*, 1110.

[46] K. C. M. Nair, S. Thomas, G. Groeninckx, *Composites Science and Technology* **2001**, *61*, 2519.

[47] S. Mishra, J. B. Naik, Y. P. Patil, *Composites Science and Technology* **2000**, *60*, 1729.

[48] J. George, R. Janardhan, J. S. Anand, S. S. Bhagawan, S. Thomas, *Polymer* **1996**, *37*, 5421.

[49] B. S. Kaith, S. Kalia, *Express Polym. Lett.* **2008**, *2*, 93.

[50] F. R. Cichocki, J. L. Thomason, *Composites Science and Technology* **2002**, *62*, 669.

[51] C. Baley, Y. Perrot, F. Busnel, H. Guezenoc, P. Davies, *Mater. Lett.* **2006**, *60*, 2984.

[52] J. L. Thomason, "Why are natural fibres failing to deliver on composite performance?", in *Conference Proceedings of the 17th International Conference of Composite Materials*, Edinburgh, 2009.

[53] A. Bismarck, W. Brostow, R. Chiu, H. E. H. Lobland, K. K. C. Ho, *Polym. Eng. Sci.* **2008**, *48*, 1971.

[54] A. Bismarck, M. E. Kumru, J. Springer, *J. Colloid Interface Sci.* **1999**, *210*, 60.

[55] K. K. C. Ho, G. Beamson, G. Shia, N. V. Polyakova, A. Bismarck, *J. Fluor. Chem.* **2007**, *128*, 1359.

[56] K. K. C. Ho, A. F. Lee, A. Bismarck, *Carbon* **2007**, *45*, 775.

[57] E. M. Liston, L. Martinu, M. R. Wertheimer, *J. Adhes. Sci. Technol.* **1993**, *7*, 1091.

[58] A. Bismarck, D. Righter, C. Wuertz, M. E. Kumru, B. Song, J. Springer, *J. Adhes.* **2000**, *73*, 19.

[59] A. Bismarck, J. Springer, "Wettability of materials: Plasma treatment effects", in *Encyclopedia of surface and colloids science 2nd edition*, 2nd edition, A. Hubbard and P. Somasundaran, Eds., Taylor and Francis, Boca Raton, 2006.

[60] J. Morales, M. G. Olayo, G. J. Cruz, P. Herrera-Franco, R. Olayo, *J. Appl. Polym. Sci.* **2006**, *101*, 3821.

[61] A. Schutze, J. Y. Jeong, S. E. Babayan, J. Park, G. S. Selwyn, R. F. Hicks, *IEEE Trans. Plasma Sci.* **1998**, *26*, 1685.

[62] A. Baltazar-Y-Jimenez, A. Bismarck, *Green Chem.* **2007**, *9*, 1057.

[63] L. Podgorski, B. Chevet, L. Onic, A. Merlin, *Int. J. Adhes. Adhes.* **2000**, *20*, 103.

[64] A. Baltazar-y-Jimenez, J. Juntaro, A. Bismarck, *J. Biobased Mater. Bioenergy* **2008**, *2*, 264.

[65] X. W. Yuan, K. Jayaraman, D. Bhattacharyya, *Compos. Pt. A-Appl. Sci. Manuf.* **2004**, *35*, 1363.

[66] X. W. Yuan, K. Jayaraman, D. Bhattacharyya, *J. Adhes. Sci. Technol.* **2004**, *18*, 1027.

[67] S. Zanini, C. Riccardi, C. Canevali, M. Orlandi, L. Zoia, E. L. Tolppa, *Surf. Coat. Technol.* **2005**, *200*, 556.

[68] E. Couto, I. H. Tan, N. Demarquette, J. C. Caraschi, A. Leao, *Polym. Eng. Sci.* **2002**, *42*, 790.

[69] X. W. Yuan, K. Jayaraman, D. Bhattacharyya, *J. Adhes. Sci. Technol.* **2002**, *16*, 703.

[70] S. Marais, F. Gouanve, A. Bonnesoeur, J. Grenet, F. Poncin-Epaillard, C. Morvan, M. Metayer, *Compos. Pt. A-Appl. Sci. Manuf.* **2005**, *36*, 975.

[71] X. Tu, R. A. Young, F. Denes, *Cellulose* **1994**, *1*, 87.

[72] E. Sinha, S. Panigrahi, *J. Compos Mater.* **2009**, *43*, 1791.

[73] C. W. Kan, K. Chan, C. W. M. Yuen, M. H. Miao, *J. Mater. Process. Technol.* **1998**, *83*, 180.

[74] P. P. Tsai, L. C. Wadsworth, J. R. Roth, *Text. Res. J.* **1997**, *67*, 359.

[75] M. Noeske, J. Degenhardt, S. Strudthoff, U. Lommatzsch, *Int. J. Adhes. Adhes.* **2004**, *24*, 171.

[76] M. J. Shenton, G. C. Stevens, *J. Phys. D-Appl. Phys.* **2001**, *34*, 2761.

[77] A. Baltazar-Y-Jimenez, A. Bismarck, *Cellulose* **2007**, *14*, 115.

[78] A. Baltazar-Y-Jimenez, M. Bistritz, E. Schulz, A. Bismarck, *Composites Science and Technology* **2008**, *68*, 215.

[79] R. B. Dodd, D. E. Akin, "Recent developments in retting and measurement of fiber quality in natural fibers: pros and cons", in *Natural fibers, biopolymers and biocomposites*, A.K. Mohanty, M. Misra, and L. Drzal, Eds., CRC Press, Boca Raton, 2005.

[80] H. S. S. Sharma, C. F. v. Sumere, *Genetic Engineer and Biotechnologist* **1992**, *12*, 19.

[81] Annonymous, "Harvesting, retting and fiber separation", USDA, 2009http://www.globalhemp.com/Archives/Government_Research/USDA/ages001Ee.pdf.

[82] D. E. Akin, J. A. Foulk, R. B. Dodd, D. D. McAlister, *J. Biotechnol.* **2001**, *89*, 193.

[83] B. E. Pallesen, *Ind. Crop. Prod.* **1996**, *5*, 65.

[84] G. Buschle-Diller, C. Fanter, F. Loth, *Text. Res. J.* **1999**, *69*, 244.

[85] W. R. Kenealy, J. Klungness, M. A. Tshabalala, M. Akhtar, E. Horn, R. Gleisner, G. Buschle-Diller, "Modification of the physical properties of lignocellulosic materials by laccase", in *225th National Meeting of the American-Chemical-Society*, 2003, p. 225/http://www.fpl.fs.fed.us/documents/pdf2003/kenea03b.pdf.

[86] J. E. G. v. Dam, "Optimisation of methods of fibre preparation from agricultural raw materials", Department of fibres and cellulose, Agrotechnological Research Institute, Wageningenhttp://www.ienica.net/fibresseminar/vandam.pdf.

[87] J. A. Foulk, W. Y. Chao, D. E. Akin, R. B. Dodd, P. A. Layton, *J. Polym. Environ.* **2004**, *12*, 165.

[88] J. A. Foulk, W. Y. Chao, D. E. Akin, R. B. Dodd, P. A. Layton, *J. Polym. Environ.* **2006**, *14*, 15.

[89] A. P. S. Adamsen, D. E. Akin, L. L. Rigsby, *Text. Res. J.* **2002**, *72*, 296.

[90] S. Ouajai, R. A. Shanks, *Macromolecular Materials and Engineering* **2009**, *294*, 213.

[91] "Scourzyme, Poroducts and Solutions", Novozyme (Bagsvaerd, Denmark), 2009http://www.novozymes.com/en/MainStructure/ProductsAndSolutions/Textile+mill/Bio.

[92] S. Ouajai, R. A. Shanks, *Macromol. Biosci.* **2005**, *5*, 124.

[93] S. Ouajai, A. Hodzic, R. A. Shanks, *J. Appl. Polym. Sci.* **2004**, *94*, 2456.

[94] K. L. Pickering, Y. Li, R. L. Farrell, M. Lay, *J. Biobased Mater. Bioenergy* **2007**, *1*, 109.

[95] A. Gutierrez, J. C. del Rio, M. J. Martinez, A. T. Martinez, *Trends Biotechnol.* **2001**, *19*, 340.

[96] R. Leone, C. Breuil, *Int. Biodeterior. Biodegrad.* **1998**, *41*, 133.

[97] M. J. Martinez-Inigo, A. Gutierrez, J. C. del Rio, M. J. Martinez, A. T. Martinez, *J. Biotechnol.* **2000**, *84*, 119.

[98] M. J. Martinez-Inigo, P. Immerzeel, A. Gutierrez, J. C. del Rio, R. Sierra-Alvarez, *Holzforschung* **1999**, *53*, 247.

[99] Y. Li, K. L. Pickering, R. L. Farrell, *Ind. Crop. Prod.* **2009**, *29*, 420.

[100] A. Schirp, F. Loge, S. Aust, P. Swarier, G. Turner, M. Wolcott, *J. Appl. Polym. Sci.* **2006**, *102*, 5191.

[101] D. Gulati, M. Sain, *J. Polym. Environ.* **2006**, *14*, 347.

[102] A. K. Clarke, D. H. G. S, W. X, H. C. J, *European Patent EP 1425440* **2004**.

[103] J. Juntaro, "Environmentally friendly hierarchical composites", in *Department of Chemical Engineering*, PhD Thesis, Imperial College London, London, 2009, p. PhD/207.

[104] T. Nishino, I. Matsuda, K. Hirao, *Macromolecules* **2004**, *37*, 7683.

[105] S. Ifuku, M. Nogi, A. Kentaro, H. Keishin, F. Nakatsubo, H. Yano, *Biomacromolecules* **2007**, *8*, 1937.

[106] M. Nogi, K. Abe, K. Handa, F. Nakatsubo, S. Ifuku, H. Yano, *Applied Physics Letters* **2006**, *89*, 233123.

[107] M. Suetsugu, M. Kotera, T. Nishino, "Cellulosic Nanocomposite Prepared by Acetylation of Bacterial Cellulose Using Supercritical Carbon Dioxide", in *Conference Proceedings of the 17th International Conference of Composite Materials*, Edinburgh, 2009.

[108] A. Bismarck, *Express Polym. Lett.* **2008**, *2*, 687.

[109] D. Klemm, B. Heublein, H. P. Fink, A. Bohn, *Angewandte Chemie - International edition* **2005**, *44*, 3358.

[110] A. Sczostak, *Macromolecular Symposia* **2009**, *280*, 45.

[111] A. N. Nakagaito, A. Fujimura, T. Sakai, Y. Hama, H. Yano, *Composites Science and Technology* **2009**, *69*, 1293.

[112] L. Suryanegara, A. N. Nakagaito, H. Yano, *Composites Science and Technology* **2009**, *69*, 1187.

[113] A. P. Mathew, K. Oksman, M. Sain, *Journal of Applied Polymer Science* **2005**, *101*, 300.

[114] D. J. Gardner, G. S. Oporto, R. Mills, M. A. S. A. Samir, *Journal of Adhesion Science and Technology* **2008**, *22*, 545.

[115] M. Iguchi, S. Yamanaka, A. Budhiono, *J. Mater. Sci.* **2000**, *35*, 261.

[116] W. K. Czaja, D. J. Young, M. Kawecki, R. M. Brown, *Biomacromolecules* **2007**, *8*, 1.

[117] Y. Nishi, M. Uryu, S. Yamanaka, K. Watanabe, N. Kitamura, M. Iguchi, S. Mitsuhashi, *Journal of Materials Science* **1990**, *25*, 2997.

[118] S. J. Eichhorn, A. Dufresne, M. Aranguren, N. E. Marcovich, J. R. Capadona, S. J. Rowan, C. Weder, W. Thielemans, M. Roman, S. Renneckar, W. Gindl, S. Veigel, J. Keckes, H. Yano, K. Abe, M. Nogi, A. N. Nakagaito, A. Mangalam, J. Simonsen, A. S. Benight, A. Bismarck, L. A. Berglund, T. Peijs, *Journal of Materials Science* **2010**, *45*, 1.

[119] E. Chanliaud, K. M. Burrows, G. Jeronimidis, M. J. Gidley, *Planta* **2002**, *215*, 989.

[120] W. Czaja, D. Romanovicz, R. M. Brown, *Cellulose* **2004**, *11*, 403.

[121] S. J. Eichhorn, G. R. Davies, *Cellulose* **2006**, *13*, 291.

[122] S. Reiling, J. Brickmann, *Macromol. Theory Simul.* **1995**, *4*, 725.

[123] K.-Y. Lee, J. J. Blaker, A. Bismarck, *Composites Science and Technology* **2009**, *69*, 2724

[124] D. Roy, M. Semsarilar, J. T. Guthrie, S. Perrier, *Chem. Soc. Rev.* **2009**, *38*, 2046.

[125] M. Samir, F. Alloin, A. Dufresne, *Biomacromolecules* **2005**, *6*, 612.

[126] S. Berlioz, S. Molina-Boisseau, Y. Nishiyama, L. Heux, *Biomacromolecules* **2009**, *10*, 2144.

[127] K. Schlufter, H. P. Schmauder, S. Dorn, T. Heinze, *Macromol. Rapid Commun.* **2006**, *27*, 1670.

[128] H. Toyosaki, T. Naritomi, A. Seto, M. Matsuoka, T. Tsuchida, F. Yoshinaga, *Bioscience Biotechnology and Biochemistry* **1996**, *59*, 1498.

[129] V. J. Frilette, J. Hanle, H. Mark, *Journal of the American Chemical Society* **1948**, *70*, 1107

[130] L. Segal, J. J. Creely, A. E. Martin-Jr, C. M. Conrad, *Textile Research Journal* **1959**, *29*, 786.

[131] A. L. Patterson, *Physical Review* **1939**, *56*, 978.

[132] L. M. Ilharco, R. R. Gracia, J. L. daSilva, L. F. V. Ferreira, *Langmuir* **1997**, *13*, 4126.

[133] N. R. Pedersen, R. Wimmer, J. Emmersen, P. Degn, L. H. Pedersen, *Carbohydr. Res.* **2002**, *337*, 1179.

[134] O. van den Berg, J. R. Capadona, C. Weder, *Biomacromolecules* **2007**, *8*, 1353.

[135] C. Radiman, G. Yulianil, *Polym. Int.* **2008**, *57*, 502.

[136] M. Callies, D. Quere, *Soft Matter* **2005**, *1*, 55.

[137] A. Olah, H. Hillborg, G. J. Vancso, *Appl. Surf. Sci.* **2005**, *239*, 410.

[138] R. J. Hunter, "*Introduction to modern colloid science*", Oxford University Press Inc. , New York, 1993.

[139] J. J. Blaker, K. Y. Lee, X. X. Li, A. Menner, A. Bismarck, *Green Chem.* **2009**, *11*, 1321.

[140] Y. Nishiyama, A. Isogai, T. Okano, M. Muller, H. Chanzy, *Macromolecules* **1999**, *32*, 2078.

[141] C. Gousse, H. Chanzy, G. Excoffier, L. Soubeyrand, E. Fleury, *Polymer* **2002**, *43*, 2645.

[142] J. Sugiyama, R. Vuong, H. Chanzy, *Macromolecules* **1991**, *24*, 4168.

[143] P. S. Belton, S. F. Tanner, N. Cartier, H. Chanzy, *Macromolecules* **1989**, *22*, 1615.

[144] C. S. R. Freire, A. J. D. Silvestre, C. P. Neto, M. N. Belgacem, A. Gandini, *Journal of Applied Polymer Science* **2006**, *100*, 1093.

[145] A. Thygesen, J. Oddershede, H. Lilholt, A. B. Thomsen, K. Stahl, *Cellulose* **2005**, *12*, 563.

[146] P. Jandura, B. Riedl, B. V. Kokta, *Polym. Degrad. Stabil.* **2000**, *70*, 387.

[147] D. Klemm, B. Philipp, T. Heinze, U. Heinze, W. Wagenknecht, "*Comprehensive cellulose chemistry*", Wiley VCH, Chichester, 1998.

[148] J. J. Blaker, K. Y. Lee, A. Bismarck, *J. Biobased Mater. Bioenergy* **2011**, *5*, 1.

[149] Y. Habibi, L. A. Lucia, O. J. Rojas, *Chem. Rev.* **2010**, *110*, 3479.

[150] D. J. Gardner, G. S. Oporto, R. Mills, M. Samir, *J. Adhes. Sci. Technol.* **2008**, *22*, 545.

[151] A. F. Turbak, F. W. Snyder, K. R. Sandberg, *Journal of Applied Polymer Science: Applied Polymer Symposium* **1983**, *37*, 459.

[152] F. W. Herrick, R. L. Casebier, R. I. Hamilton, K. R. Sandberg, *Journal of Applied Polymer Science: Applied Polymer Symposium* **1983**, *37*, 797.

[153] A. J. Brown, *Journal of the Chemical Society, Transations* **1886**, *49*, 172.

[154] D. Klemm, D. Schumann, F. Kramer, N. Hessler, D. Koth, B. Sultanova, *Macromolecular Symposia* **2009**, *280*, 60.

[155] I. Siro, D. Plackett, *Cellulose* **2010**, *17*, 459.

[156] A. J. de Menezes, G. Siqueira, A. A. S. Curvelo, A. Dufresne, *Polymer* **2009**, *50*, 4552.

[157] K.-Y. Lee, F. Quero, J. J. Blaker, C. A. S. Hill, S. J. Eichhorn, A. Bismarck, *Cellulose* **2011**, *18*, 595.

[158] J. F. Sassi, H. Chanzy, *Cellulose* **1995**, *2*, 111.

[159] M. Wada, T. Okano, J. Sugiyama, *Journal of Wood Science* **2001**, *47*, 124.

[160] D. L. Vanderhart, R. H. Atalla, *Macromolecules* **1984**, *17*, 1465.

[161] H. S. Barud, A. M. de Araujo, D. B. Santos, R. M. N. de Assuncao, C. S. Meireles, D. A. Cerqueira, G. Rodrigues, C. A. Ribeiro, Y. Messaddeq, S. J. L. Ribeiro, *Thermochim. Acta* **2008**, *471*, 61.

[162] M. Spinu, N. Dos Santos, N. Le Moigne, P. Navard, *Cellulose* **2011**, *18*, 247.

[163] A. Venkateswaran, W. P. Riemen, *J. Appl. Polym. Sci.* **1965**, *9*, 1139.

[164] E. A. Colombo, E. H. Immerguy, *Journal of Polymer Science Part C: Polymer Symposia* **1970**, *31*, 137.

[165] H. Jin, Y. Nishiyama, M. Wada, S. Kuga, *Colloids and Surfaces a-Physicochemical and Engineering Aspects* **2004**, *240*, 63.

[166] S. Kuga, D. Y. Kim, Y. Nishiyama, R. M. Brown, *Molecular Crystals and Liquid Crystals* **2002**, *387*, 237.

[167] O. Ishida, D. Y. Kim, S. Kuga, Y. Nishiyama, R. M. Brown, *Cellulose* **2004**, *11*, 475.

[168] M. V. Merchant, "A study of certain phenomena of the liquid exchange of water-swollen cellulose fibers and their subsequent drying from hydrocarbons", Lawrence College, Appleton, Wisconsin, 1957, p. PhD/124.

[169] F. Horii, A. Hirai, R. Kitamaru, *Macromolecules* **1987**, *20*, 2117.

[170] F. Horii, H. Yamamoto, R. Kitamaru, M. Tanahashi, T. Higuchi, *Macromolecules* **1987**, *20*, 2946.

[171] J. F. Sassi, P. Tekely, H. Chanzy, *Cellulose* **2000**, *7*, 119.

[172] B. C. Suddell, W. J. Evans, "Natural fiber composites in automotive applications", in *Natural Fibers, Biopolymers, and Biocomposites*, Crc Press-Taylor & Francis Group, Boca Raton, 2005, p. 231.

[173] S. Iwamoto, A. N. Nakagaito, H. Yano, M. Nogi, *Appl. Phys. A-Mater. Sci. Process.* **2005**, *81*, CP8.

[174] P. Terech, L. Chazeau, J. Y. Cavaille, *Macromolecules* **1999**, *32*, 1872.

[175] M. Mochizuki, M. Hirami, *Polym. Adv. Technol.* **1997**, *8*, 203.

[176] R. Bhardwaj, A. K. Mohanty, *J. Biobased Mater. Bioenergy* **2007**, *1*, 191.

[177] J. J. Blaker, J. C. Knowles, R. M. Day, *Acta Biomater.* **2008**, *4*, 264.

[178] P. Jandura, B. V. Kokta, B. Riedl, *J. Appl. Polym. Sci.* **2000**, *78*, 1354.

[179] M. Q. Tran, J. T. Cabral, M. S. P. Shaffer, A. Bismarck, *Nano Lett.* **2008**, *8*, 2744.

[180] B. H. Song, A. Bismarck, R. Tahhan, J. Springer, *J. Colloid Interface Sci.* **1998**, *197*, 68.

[181] Y. Kim, R. Jung, H. S. Kim, H. J. Jin, *Curr. Appl. Phys.* **2009**, *9*, S69.

[182] L. E. Million, G. Guhados, W. K. Wan, *J. Biomed. Mater. Res. Part B* **2008**, *86B*, 444.

[183] D. J. Shaw, "*Introduction to colloid and surface chemistry*", 4th Edition edition, Butterworth-Heinemann Ltd, 1992.

[184] V. Maquet, A. R. Boccaccini, L. Pravata, I. Notingher, R. Jerome, *Biomaterials* **2004**, *25*, 4185.

[185] C. Schugens, V. Maquet, C. Grandfils, R. Jerome, P. Teyssie, *Polymer* **1996**, *37*, 1027.

[186] G. G. Tibbetts, J. J. McHugh, *J. Mater. Res.* **1999**, *14*, 2871.

[187] M. S. Huda, L. T. Drzal, A. K. Mohanty, M. Misra, *Composites Science and Technology* **2006**, *66*, 1813.

[188] G. Siqueira, J. Bras, A. Dufresne, *Biomacromolecules* **2009**, *10*, 425.

[189] A. P. Mathew, K. Oksman, M. Sain, *J. Appl. Polym. Sci.* **2006**, *101*, 300.

[190] D. M. Bigg, *Adv. Polym. Technol.* **2005**, *24*, 69.

[191] T. Kawai, N. Rahman, G. Matsuba, K. Nishida, T. Kanaya, M. Nakano, H. Okamoto, J. Kawada, A. Usuki, N. Honma, K. Nakajima, M. Matsuda, *Macromolecules* **2007**, *40*, 9463.

[192] J. M. Zhang, K. Tashiro, A. J. Domb, H. T. Tsuji, *Macromolecular Symposia* **2006**, *242*, 274.

[193] F. Hussain, M. Hojjati, M. Okamoto, R. E. Gorga, *J. Compos Mater.* **2006**, *40*, 1511.

[194] M. Matsuo, C. Sawatari, Y. Iwai, F. Ozaki, *Macromolecules* **1990**, *23*, 3266.

[195] A. J. Ragauskas, C. K. Williams, B. H. Davison, G. Britovsek, J. Cairney, C. A. Eckert, W. J. Frederick, J. P. Hallett, D. J. Leak, C. L. Liotta, J. R. Mielenz, R. Murphy, R. Templer, T. Tschaplinski, *Science* **2006**, *311*, 484.

[196] S. Inkinen, M. Hakkarainen, A. C. Albertsson, A. Sodergard, *Biomacromolecules* **2011**, *12*, 523.

[197] R. H. Platel, L. M. Hodgson, C. K. Williams, *Polymer Reviews* **2008**, *48*, 11.

[198] R. H. Platel, A. J. P. White, C. K. Williams, *Chem. Commun.* **2009**, 4115.

[199] R. E. Drumright, P. R. Gruber, D. E. Henton, *Advanced Materials* **2000**, *12*, 1841.

[200] A. C. Albertsson, I. K. Varma, *Biomacromolecules* **2003**, *4*, 1466.

[201] I. K. Kang, S. H. Choi, D. S. Shin, S. C. Yoon, *International Journal of Biological Macromolecules* **2001**, *28*, 205.

[202] K. Y. Lee, J. J. Blaker, A. Bismarck, *Composites Science and Technology* **2009**, *69*, 2724.

[203] P. Tingaut, T. Zimmermann, F. Lopez-Suevos, *Biomacromolecules* **2010**, *11*, 454.

[204] B. Braun, J. R. Dorgan, *Biomacromolecules* **2009**, *10*, 334.

[205] A. L. Goffin, J. M. Raquez, E. Duquesne, G. Siqueira, Y. Habibi, A. Dufresne, P. Dubois, *Biomacromolecules* **2011**, *12*, 2456.

[206] H. S. Kim, B. H. Lee, S. Lee, H. J. Kim, J. Dorgan, *J. Therm. Anal. Calorim.* **2011**, *104*, 331.

[207] D. Plackett, *J. Polym. Environ.* **2004**, *12*, 131.

[208] A. Gregorova, V. Sedlarik, M. Pastorek, H. Jachandra, F. Stelzer, *J. Polym. Environ.* **2011**, *19*, 372.

[209] Z. Q. Li, X. D. Zhou, C. H. Pei, *Polym.-Plast. Technol. Eng.* **2010**, *49*, 141.

[210] M. Tang, A. J. P. White, M. M. Stevens, C. K. Williams, *Chem. Commun.* **2009**, 941.

[211] M. Tang, Y. X. Dong, M. M. Stevens, C. K. Williams, *Macromolecules* **2010**, *43*, 7556.

[212] O. Kantoglu, O. Guven, *Nucl. Instrum. Methods Phys. Res. Sect. B-Beam Interact. Mater. Atoms* **2002**, *197*, 259.

[213] W. Groenewoud, "*Characterisation of polymers by thermal analysis*", Elsevier Science BV, Amsterdam, 2003.

[214] A. Sodergard, M. Stolt, *Prog. Polym. Sci.* **2002**, *27*, 1123.

[215] J. R. Fried, W. J. Macknight, F. E. Karasz, *Journal of Applied Physics* **1979**, *50*, 6052.

[216] D. Klemm, B. Heublein, H. P. Fink, A. Bohn, *Angew. Chem.-Int. Edit.* **2005**, *44*, 3358.

[217] S. Kamel, N. Ali, K. Jahangir, S. M. Shah, A. A. El-Gendy, *Express Polym. Lett.* **2008**, *2*, 758.

[218] J. K. Pandey, S. H. Ahn, C. S. Lee, A. K. Mohanty, M. Misra, *Macromol. Mater. Eng.* **2010**, *295*, 975.

[219] K. G. Satyanarayana, G. G. C. Arizaga, F. Wypych, *Prog. Polym. Sci.* **2009**, *34*, 982.

[220] H. Harms, *Materialwiss. Werkstofftech.* **2003**, *34*, 267.

[221] D. Klemm, F. Kramer, S. Moritz, T. Lindstrom, M. Ankerfors, D. Gray, A. Dorris, *Angew. Chem.-Int. Edit.* **2011**, *50*, 5438.

[222] F. W. Herrick, R. L. Casebier, J. K. Hamilton, K. R. Sandberg, "Microfibrillated cellulose: morphology and accessibility", in *Proceedings of 9th Cellulose Conference*, A. Sarko, Ed., Wiley, New York, 1983, p. 37/797.

[223] R. Jonas, L. F. Farah, *Polym. Degrad. Stabil.* **1998**, *59*, 101.

[224] P. Ross, R. Mayer, M. Benziman, *Microbiol. Rev.* **1991**, *55*, 35.

[225] V. Favier, G. R. Canova, J. Y. Cavaille, H. Chanzy, A. Dufresne, C. Gauthier, *Polym. Adv. Technol.* **1995**, *6*, 351.

[226] H. Yano, J. Sugiyama, A. N. Nakagaito, M. Nogi, T. Matsuura, M. Hikita, K. Handa, *Adv. Mater.* **2005**, *17*, 153.

[227] F. Quero, M. Nogi, H. Yano, K. Abdulsalami, S. M. Holmes, B. H. Sakakini, S. J. Eichhorn, *ACS Appl. Mater. Interfaces* **2010**, *2*, 321.

[228] M. Henriksson, L. Fogelstrom, L. A. Berglund, M. Johansson, A. Hult, *Compos. Sci. Technol.* **2011**, *71*, 13.

[229] A. K. Vainio, H. Paulapuro, *Bioresources* **2007**, *2*, 442.

[230] J. Troger, K. Lunkwitz, K. Grundke, W. Burger, *Colloids and Surfaces a-Physicochemical and Engineering Aspects* **1998**, *134*, 299.

[231] J. Szekely, A. W. Neumann, Y. K. Chuang, *J. Colloid Interface Sci.* **1971**, *35*, 273.

[232] K. Grundke, T. Bogumil, T. Gietzelt, H. J. Jacobasch, D. Y. Kwok, A. W. Neumann, "Wetting measurements on smooth, rough and porous solid surfaces", in *Interfaces, Surfactants and Colloids in Engineering*, H.J. Jacobasch, Ed., 1996, p. 58.

[233] R. Malcolm Brown Jr, "Bacterial cellulose", in *Cellulose: Structural and functional aspects*, G.O. Phillips, J.F. Kennedy, and P.A. Williams, Eds., Ellis Horwood Limited, 1989, p. 145.

[234] S. Iwamoto, A. N. Nakagaito, H. Yano, *Appl. Phys. A-Mater. Sci. Process.* **2007**, *89*, 461.

[235] M. Nogi, S. Iwamoto, A. N. Nakagaito, H. Yano, *Adv. Mater.* **2009**, *21*, 1595.

[236] K. Leppanen, S. Andersson, M. Torkkeli, M. Knaapila, N. Kotelnikova, R. Serimaa, *Cellulose* **2009**, *16*, 999.

[237] P. Eronen, M. Osterberg, S. Heikkinen, M. Tenkanen, J. Laine, *Carbohydrate Polymers* **2011**, *86*, 1281.

[238] S. Asikainen, A. Fuhrmann, L. Robertsen, *Nordic Pulp & Paper Research Journal* **2010**, *25*, 269.

[239] H. Yamamoto, F. Horii, *Macromolecules* **1993**, *26*, 1313.

[240] E. Papirer, E. Brendle, H. Balard, C. Vergelati, *J. Adhes. Sci. Technol.* **2000**, *14*, 321.

[241] J. Y. Y. Heng, D. F. Pearse, F. Thielmann, T. Lampke, A. Bismarck, *Composite Interfaces* **2007**, *14*, 581.

[242] P. Luner, M. Sandell, *Journal of Polymer Science Part C* **1969**, *28*, 115.

[243] C. H. Sun, J. C. Berg, *Advances in Colloid and Interface Science* **2003**, *105*, 151.

[244] K. Stana-Kleinschek, V. Ribitsch, *Colloids and Surfaces a-Physicochemical and Engineering Aspects* **1998**, *140*, 127.

[245] B. Holmbom, A. Sundberg, A. Strand, "Surface-active compounds as forest-industry by-products", in *Surfactants from renewable resources*, M. Kjellin and I. Johansson, Eds., John WIley and Sons Ltd, Chippenham, 2010.

[246] J. van Wazer, "*Phosphorus and its compounds vol I*", Interscience Encyclopedia Inc, New York, 1958.

[247] N. M. L. Hansen, D. Plackett, *Biomacromolecules* **2008**, *9*, 1493.

[248] G. T. Pott, "Natural fibers with low moisture sensitivity", in *Natural fibers, plastics and composites*, F.T. Wallenberger and N. Weston, Eds., Kluwer Academic, Norwell, 2004, p. 105.

[249] A. N. Zhironkin, V. A. Volkov, *Colloid Journal of the Russian Academy of Sciences* **1992**, *54*, 470.

[250] U.S.D.A, "Thermal degradation of wood componenets", U.S. Department of Agriculture, Forest Service, Forest Laboratory Madison, 1970.

[251] M. Seifert, S. Hesse, V. Kabrelian, D. Klemm, *J. Polym. Sci. Pol. Chem.* **2004**, *42*, 463.

[252] K.-C. Cheng, J. M. Catchmark, A. Demirci, *J Bio Eng* **2009**, *3*.

[253] I. C. Um, C. S. Ki, H. Y. Kweon, K. G. Lee, D. W. Ihm, Y. H. Park, *Int. J. Biol. Macromol.* **2004**, *34*, 107.

[254] S. Iwamoto, K. Abe, H. Yano, *Biomacromolecules* **2008**, *9*, 1022.

[255] U. Molin, A. Teder, *Nordic Pulp & Paper Research Journal* **2002**, *17*, 14.

[256] S. Mishra, M. Misra, S. S. Tripathy, S. K. Nayak, A. K. Mohanty, *Polymer Composites* **2002**, *23*, 164.

[257] S. L. Favaro, T. A. Ganzerli, A. Neto, O. da Silva, E. Radovanovic, *Express Polym. Lett.* **2010**, *4*, 465.

[258] K. C. C. Carvalho, D. R. Mulinari, H. J. C. Voorwald, M. O. H. Cioffi, *BioResources* **2010**, *5*, 1143.

[259] M. Baiardo, E. Zini, M. Scandola, *Compos. Pt. A-Appl. Sci. Manuf.* **2004**, *35*, 703.

[260] J. L. Thomason, *Polymer Composites* **2010**, *31*, 1525.

[261] R. Ntenga, A. Beakou, J. A. Ateba, L. A. Ohandja, *J. Mater. Sci.* **2008**, *43*, 6206.

[262] H. Qian, E. S. Greenhalgh, M. S. P. Shaffer, A. Bismarck, *J. Mater. Chem.* **2010**, *20*, 4751.

[263] J. Juntaro, "Environmentally friendly hierarchical composites", in *Chemical Engineering and Chemical Technology*, Imperial College, London, 2009, p. PhD/207.

[264] E. S. Greenhalgh, "*Failure analysis and fractography of polymer composites*", Woodhead Publishing Ltd and CRC Press LLC, Cambridge, 2009, p. 608.

[265] J. Gassan, A. Chate, A. K. Bledzki, *J. Mater. Sci.* **2001**, *36*, 3715.

[266] V. L. Finkenstadt, C. K. Liu, R. Evangelista, L. S. Liu, S. C. Cermak, M. Hojilla-Evangelista, J. L. Willett, *Ind. Crop. Prod.* **2007**, *26*, 36.

[267] A. Afaghi-Khatibi, Y. W. Mai, *Compos. Pt. A-Appl. Sci. Manuf.* **2002**, *33*, 1585.

[268] S. Thomas, S. A. Paul, L. A. Pothan, B. Deepa, "Natural fibres: Structure, properties and applications", in *Cellulose Fibers: Bio- and Nano-Polymer Composites*, S. Kalia, B.S. Kaith, and I. Kaur, Eds., Springer-Verlang, Berlin, 2011, p. 3.

[269] K.-Y. Lee, P. Bharadia, J. J. Blaker, A. Bismarck, *submitted* **2011**.

[270] M. S. Salim, Z. A. M. Ishak, S. A. Hamid, "Effect of Stitching Density of Nonwoven Fiber Mat Towards Mechanical Properties of Kenaf Reinforced Epoxy Composites Produced by Resin Transfer Moulding (RTM)", in *Composite Science and Technology, Pts 1 and 2*, S.M. Sapuan, F. Mustapha, D.L. Majid, Z. Leman, A.H.M. Ariff, M.K.A. Ariffin, M.Y.M. Zuhri, M.R. Ishak, and J. Sahari, Eds., 2011, p. 987.

[271] D. S. Xue, M. H. Miao, H. Hu, *Journal of the Textile Institute* **2011**, *102*, 612.

[272] M. Z. Rong, M. Q. Zhang, Y. Liu, Z. W. Zhang, G. C. Yang, H. M. Zeng, *J. Compos Mater.* **2002**, *36*, 1505.

[273] W. Y. Tao, T. A. Calamari, L. Crook, *Text. Res. J.* **1998**, *68*, 402.

[274] Y. C. Du, J. L. Zhang, H. Toghiani, T. E. Lacy, Y. B. Xue, M. F. Horstemeyer, C. U. Pittman, *Forest Products Journal* **2010**, *60*, 289.

[275] G. N. Ramaswamy, T. Sellers, W. Y. Tao, L. G. Crook, *Industrial Crops and Products* **2003**, *17*, 1.

[276] D. Åkesson, M. Skrifvars, P. Walkenström, *Journal of Applied Polymer Science* **2009**, *114*, 2502.

[277] A. O'Donnell, M. A. Dweib, R. P. Wool, *Composites Science and Technology* **2004**, *64*, 1135.

[278] S. K. Garkhail, R. W. H. Heijenrath, T. Peijs, *Applied Composite Materials* **2000**, *7*, 351.

[279] B. Reck, J. Turk, *Angewandte Makromolekulare Chemie* **1999**, *272*, 5.

[280] J. Diniz, M. H. Gil, J. Castro, *Wood Sci. Technol.* **2004**, *37*, 489.

[281] Q. Zhou, E. Malm, H. Nilsson, P. T. Larsson, T. Iversen, L. A. Berglund, V. Bulone, *Soft Matter* **2009**, *5*, 4124.

[282] A. Afaghi-Khatibi, Y. W. Mai, *Composites A* **2002**, *33*, 1585.

[283] D. Behera, A. K. Banthia, *Journal of Applied Polymer Science* **2008**, *109*, 2583.

[284] C. Forman, "Polymeric foams (PLS008F)", BCC Research, MA, USA, 2001.

[285] V. O. Ikem, A. Menner, A. Bismarck, *Langmuir* **2010**, *26*, 8836.

[286] R. C. Thomson, M. J. Yaszemski, J. M. Powers, A. G. Mikos, *J. Biomater. Sci.-Polym. Ed.* **1995**, *7*, 23.

[287] J. M. Karp, P. D. Dalton, M. S. Shoichet, *MRS Bull.* **2003**, *28*, 301.

[288] L. Safinia, K. Wilson, A. Mantalaris, A. Bismarck, *Macromol. Biosci.* **2007**, *7*, 315.

[289] P. Ciambelli, V. Palma, E. Palo, *Catal. Today* **2010**, *155*, 92.

[290] A. Siriruk, Y. J. Weitsman, D. Penumadu, *Compos. Sci. Technol.* **2009**, *69*, 814.

[291] J. W. Kang, J. M. Kim, M. S. Kim, Y. H. Kim, W. N. Kim, W. Jang, D. S. Shin, *Macromol. Res.* **2009**, *17*, 856.

[292] L. J. Lee, C. C. Zeng, X. Cao, X. M. Han, J. Shen, G. J. Xu, *Compos. Sci. Technol.* **2005**, *65*, 2344.

[293] W. T. Zhai, S. N. Leung, L. Wang, H. E. Naguib, C. B. Park, *J. Appl. Polym. Sci.* **2010**, *116*, 1994.

[294] M. Mihai, M. A. Huneault, B. D. Favis, H. B. Li, *Macromol. Biosci.* **2007**, *7*, 907.

[295] D. J. Kim, S. W. Kim, H. J. Kang, K. H. Seo, *J. Appl. Polym. Sci.* **2001**, *81*, 2443.

[296] J. J. Blaker, V. Maquet, R. Jerome, A. R. Boccaccini, S. N. Nazhat, *Acta Biomater.* **2005**, *1*, 643.

[297] H. Y. Ma, J. A. Hu, P. X. Ma, *Adv. Funct. Mater.* **2010**, *20*, 2833.

[298] M. Singh, B. Sandhu, A. Scurto, C. Berkland, M. S. Detamore, *Acta Biomater.* **2010**, *6*, 137.

[299] I. Akartuna, E. Tervoort, J. C. H. Wong, A. R. Studart, L. J. Gauckler, *Polymer* **2009**, *50*, 3645.

[300] A. Menner, K. Haibach, R. Powell, A. Bismarck, *Polymer* **2006**, *47*, 7628.

[301] R. Murakami, A. Bismarck, *Adv. Funct. Mater.* **2010**, *20*, 732.

[302] U. T. Gonzenbach, A. R. Studart, E. Tervoort, L. J. Gauckler, *J. Am. Ceram. Soc.* **2007**, *90*, 16.

[303] L. Marlin, A. J. Durante, E. G. Schwarz, *Journal of Cellular Plastics* **1975**, *11*, 317.

[304] R. W. Greer, G. L. Wilkes, *J. Appl. Polym. Sci.* **1996**, *62*, 1115.

[305] S. P. Wu, M. Z. Rong, M. Q. Zhang, J. Hu, T. Czigany, *J. Biobased Mater. Bioenergy* **2007**, *1*, 417.

[306] L. M. Bonnaillie, R. P. Wool, *J. Appl. Polym. Sci.* **2007**, *105*, 1042.

[307] A. Okiyama, M. Motoki, S. Yamanaka, *Food Hydrocolloids* **1993**, *6*, 493.

[308] D. K. Sarker, D. Bertrand, Y. Chtioui, Y. Popineau, *J. Texture Stud.* **1998**, *29*, 15.

[309] P. Walstra, "Principles of foam formation and stability", in *Foams: Physics, chemistry and structure*, A.J. Wilson, Ed., Springer-Verlag Berlin, York, 1989, p. 1.

[310] F. Carn, A. Colin, O. Pitois, M. Vignes-Adler, R. Backov, *Langmuir* **2009**, *25*, 7847.

[311] S. Grishchuk, J. Karger-Kocsis, *Express Polym. Lett.* **2011**, *5*, 2.

[312] A. K. O'Brien, C. N. Bowman, *Macromolecules* **2006**, *39*, 2501.

[313] N. C. Hilyard, J. Young, "Introduction", in *Mechanics of Cellular Plastics*, N.C. Hilyard, Ed., Applied Science Publisher Ltd, Essex, 1982, p. 1.

Appendix A

The derivation of equation (3.1)

Average atomic mass of carbon = 12.0107 g mol^{-1}

Average atomic mass of hydrogen = 1.0079 g mol^{-1}

Average atomic mass of oxygen = 15.9994 g mol^{-1}

Average molecular mass of the molecule $C_6H_{10}O_5$ = 162.140 g mol^{-1} = 162140 mg mol^{-1}

$$moles\ of\ C_6H_{10}O_5 = \frac{m_i}{162140} \tag{A1}$$

$$\Rightarrow moles\ of\ accessible\ OH = \frac{[OH] \times m_i}{162140} \tag{A2}$$

The number of moles of accessible OH groups is equal to the number of moles of OD groups. Therefore,

$$\Rightarrow moles\ of\ accessible\ OD = \frac{[OH] \times m_i}{162140} \tag{A3}$$

The number of deuterium atoms exchanged with the hydrogen atoms on the cellulose sample is

$$\Rightarrow number\ of\ D\ atoms = \frac{[OH] \times m_i}{162140} \times A \tag{A4}$$

where A is the Avogadro's number.

This number of D atoms exchanged with hydrogen can be measured and back calculated from DVS measurements through the following equation:

$$\Rightarrow number\ of\ D\ atoms = \frac{m_f - m_i}{m_n} = \frac{\Delta m}{m_n} \tag{A5}$$

Equating (S4) and (S5), equation (3.1) can be obtained:

$$\therefore \frac{\Delta m}{m_n} = \frac{[OH] \times m_i}{162140} \times A \tag{3.1}$$

Appendix B

NMR spectra of RP**1**
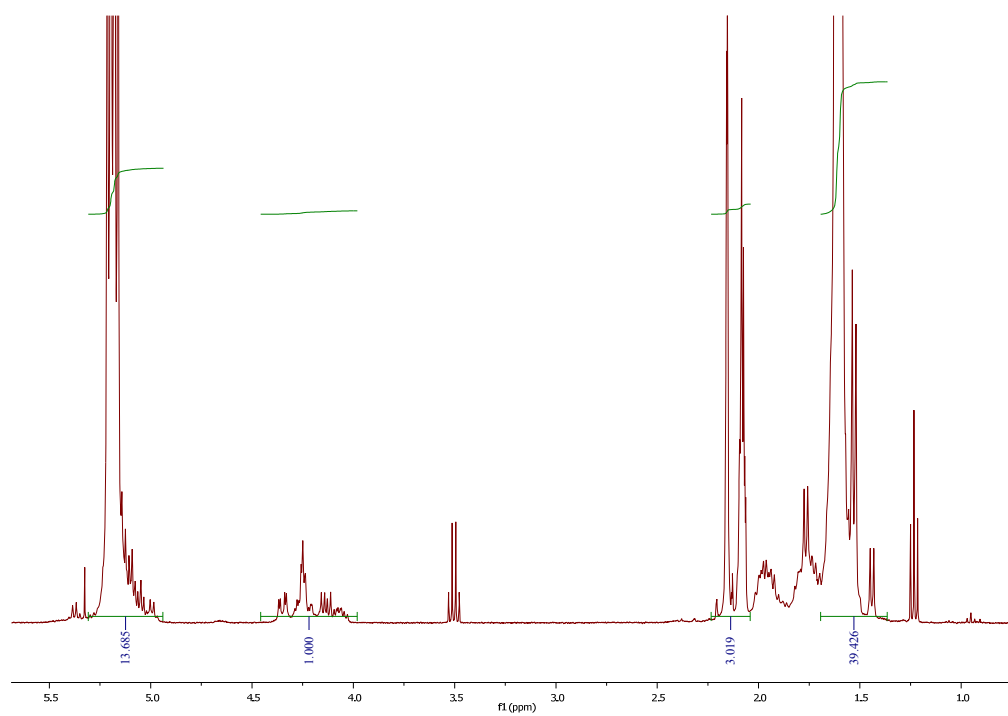

Figure B1: ^{1}H NMR spectrum of RP**1** in CDCl$_3$.